The Unique Reactions of Surface Bound H, Bulk H, and Gas Phase H Atoms with Acetylene, Ethylene, and Ethane on Ni(111)

by

Kerstin Leigh Haug

B.S. Chemistry
University of Wisconsin-Madison, 1993

Submitted to the Department of Chemistry
in Partial Fulfillment of the Requirements
for the Degree of

Doctor of Philosophy

at the
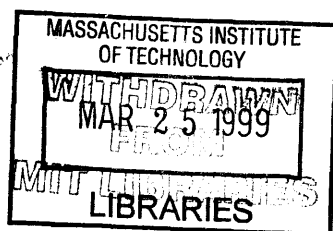Massachusetts Institute of Technology

February 1999

Signature of Author_____

Department of Chemistry
October 30, 1998
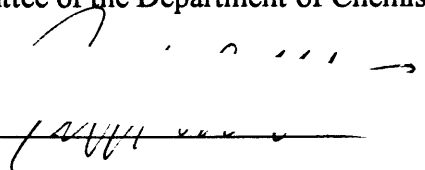
Certified by_____

Sylvia T. Ceyer
Professor of Chemistry
Thesis Supervisor

Accepted by_____

Dietmar Seyferth
Chairman, Department Committee
on Graduate Students

2

This thesis has been examined by a committee of the Department of Chemistry as follows:

Professor Jeffrey I. Steinfeld _____

Chair

Professor Sylvia T. Ceyer _____

Thesis Supervisor

Professor Moungi G. Bawendi _____

The Unique Reactivity of Surface H, Bulk H, and Gas Phase H with Acetylene, Ethylene, and Ethane on Ni(111)

by

Kerstin Leigh Haug

Submitted to the Department of Chemistry
on October 30, 1998 in partial fulfillment of the
requirements for the Degree of Doctor of Philosophy in Chemistry

Abstract

Hydrogenation of hydrocarbons over Ni catalysts is an important industrial process. Under catalytic conditions, two different hydrogen atom species exist, surface bound H atoms and H adsorbed in the bulk. The Horiuti-Polanyi mechanism asserts that surface bound H atoms add sequentially to C_2H_4 to form C_2H_6. However, on a Ni(111) surface in a well controlled environment, surface bound H does not react with C_2H_4 to form ethane. Instead, bulk H is the reactive species in ethane formation. The advantages of bulk H that lead to its reactivity are its approach along the rehybridized π bond of C_2H_4 and its energetics.

Acetylene has two sets of π orbitals, parallel and perpendicular to the surface. The parallel orbitals allow surface bound H atoms to react with acetylene, not to form C_2H_4 or C_2H_6, but to form the adsorbed product ethylidyne, CCH_3. The activation energy of this H addition is measured to be 8.8 to 16.7 kcal/mol, depending on coverage. The first step to make CCH_3 from C_2H_2 and surface H is presumed to be formation of a C-H bond, resulting in the vinyl, $CHCH_2$, intermediate. Ethylidyne is also formed during the bulk H reaction with C_2H_2. Presumably, bulk H adds to C_2H_2 to make $CHCH_2$, and then CCH_3.

Gas phase H atoms are special in that they are much more energetic than bulk or surface H atoms. This ability allows them to abstract a hydrogen from C_2H_4 to form $CHCH_2$. Indeed, CCH_3 is produced from the reaction of C_2H_4 and gas phase H atoms. Ethylidyne is also formed from the reaction of a gas phase H with C_2H_2 and C_2H_6.

The pattern of surface bound H, bulk H, and gas phase H reactions with C_2H_2, C_2H_4, and C_2H_6 illustrates the energy differences of the three H atom species, the importance of a low energy approach along the direction of an electron rich π orbital, and the energy difference between H addition and H abstraction. An argument is made for the presence of a $CHCH_2$ intermediate to CCH_3 formation. Preliminary spectroscopic evidence for $CHCH_2$ as an intermediate is presented.

Thesis Supervisor: Sylvia T. Ceyer
         Title: J.C. Sheehan Professor of Chemistry

Table of Contents

6

8

List of Figures

10

12

List of Tables

Acknowledgments

I would first like to thank my advisor, Sylvia Ceyer, who charmed me with the elegance and the apparent simplicity of her science before I even joined the group. As I began to develop a relationship with the ultra-high vacuum machine in lab, I then realized that to get a simple answer usually involves asking a complicated question. Our continued success in being able to ask complicated and relevant questions rests on the design of these extraordinary chambers as well as the collective knowledge that is the sum of what Sylvia brings, and what she creates from the continuous thread of graduate students and postdocs. We have all worked together to weave coherent strong stories.

The group is unique in that the projects on each machine truly span years if not a decade. The effort of those before us, as well as the present melding of ideas, and in practice whole lives, to keep the demanding stainless steel chamber healthy is amazing. I have been extremely fortunate to have learned both the mechanics and science initially from Ted Trautman, with gleanings from Art Utz and Sean Daley before they each left the group. When Thomas Bürgi joined Ted and I, our team was complete. There were disasters, but there was also hard work and good ideas that illuminated genuinely new chemistry. Thomas was both a good scientist and coworker. My appreciate to Michael Gostein is genuine for his contributions to our final efforts to understand the complex surface H and acetylene equilibrium, a system that at times seemed intransigent.

The host of people from the scattering chamber complete the group. David Pullman and Thanos Tsekouras were part of my first years in the group. David Gosalvez is a good natured Spainard- but we had to watch out for his high capacitance head when tuning the EELS. When Stacey Eckman joined the group she secured the cultural line in the lab between Minnesotans and Europeans (which has been further divided with the current strain of Texans), sitting firmly on the side of Minnesotans. Judson Holt (who introduced the Texas strain- in a big way), may the leak detector be with you. Massimo Bertino, life was rarely dull when you were around. I wish the best of luck to Matthew Tate in his thesis writing. I enjoyed his company as the other senior graduate student in a time when there were no

postdocs that shared our seniority. I appreciated his ear and thoughts very much through the end of this crazy process, where at time I was sure I would go insane.

Several things were lost during the renovations, including the door to 2-117, the fortune, "Ignorance never settled a question", the 74D key, and a sense of place- since each of us had four different desks over the span of a year.

My first year class deserves credit for making graduate school a supportive rather than an antagonistic environment. I wish Henry, Rose, Kevin, Dora, Dave, James, and Ken all the best as we go separate ways.

I own a tremendous amount to Fred, who not only did laundry, cooking and shopping during the prolonged period of writing and revisions, but was always there with support. We will be continuing our lives together with big changes - hold on, it should be an amazing adventure.

My parents and my sister also stood by me throughout this endeavor. Scientific steps forward do not just occur, they are taken by people. As a person, maintaining perspective and balance during the last five years has been the biggest challenge. All the people in my life, those mentioned above and others, played a vital role in this challenge.

Chapter 1

Introduction

Unsaturated hydrocarbon hydrogenation using heterogeneous catalysis occurs on a large scale in industry.[1] Ethylene is used as a model system to study these reactions. Hydrogenation requires a catalytic process because although hydrogen *molecules* are a readily available chemical species, they are not reactive with hydrocarbon molecules.[2,3] The advantage of heterogeneous catalysis is that the metal surface acts as an intermediary. H_2 is well known to dissociate to adsorbed H atoms on transition metal surfaces.[4] A H atom is bound to the surface with a significantly weaker bond than its bond to another H atom in H_2,[5] allowing it a higher probability to react with surface bound hydrocarbon species that also have weakened bonds due to their interactions with the surface. The advantage of heterogeneous catalysis is clear. The metal surface mediates changes in the bond strength and geometry of reactants, resulting in lower barriers to chemical reaction.

Hydrogen is not limited to dissociative adsorption on metallic surfaces. It is also possible for hydrogen to *ab*sorb into the bulk of the metal.[6] Raney nickel, the porous nickel used industrially in catalysis, readily absorbs hydrogen.[7,8,9] Hydrogen in the bulk could very

well play a role in many catalytic reactions. It is only recently that it has been possible to study

bulk H reactivity separately from surface H reactivity. For example, the hydrogenation of

$C_2H_4(ad) \rightarrow C_2H_6(g)^2$ and CH_3 (ad) $\rightarrow CH_4(g)^{10}$ on the Ni(111) surface both require bulk H

atoms to occur. These two reactants are inert in the presence of surface bound H atoms. Bulk

H atoms are beginning to demonstrate their uniquely different reactivity from surface H

atoms.[11]

There are large differences between surface bound H atoms and bulk H atoms in both

their energetics and geometry of approach. These factors distinguish the two types of H atoms

and also explain the differences in their reactivity. Bulk H atoms are up to 24 kcal/mol more

energetic than surface H atoms. This additional potential energy can be used to overcome

reaction barriers. The barrier to reaction of a hydrocarbon with surface bound H may also be

different from that with bulk H. The different barriers arise from the geometry of approach of

each H atom species. Bulk H atoms react with adsorbed hydrocarbons as they emerge from

the bulk. In the case of the hydrogenation of C_2H_4, it approaches the adsorbed C_2H_4 from

underneath the plane of the molecule. In the case of CH_3 hydrogenation, it approaches with

the correct tetrahedral geometry of the sp^3 transition state for CH_4 formation. Both of these

approaches of the bulk H atom are predicted to be the lowest energy pathway for H addition.

In contrast, surface adsorbed H atoms are restricted to motion in the surface plane. The

reaction barrier for the addition of surface H atoms in the plane is higher than the barrier for

bulk H for C_2H_4 and CH_3. Part of this higher reaction barrier is the result of steric hindrance

felt by the surface H atoms when they encounter the C-H bonds in the surface plane. The

advantages of the bulk H atom in both its energetics and geometry of approach over surface

adsorbed H is why bulk H is observed to react while surface H is not for the case of CH_3 and

C_2H_4 hydrogenation. Chapter 2 includes further discussion of the differences between bulk H

atoms and surface adsorbed H atoms.

Surface H addition to adsorbed C_2H_2 is seen, being driven by the π bond character of

C_2H_2 in the surface plane. The reactivity of surface bound H atoms with C_2H_2 is explored in

Chapter 3. The product of this surface H reaction is not gas phase hydrogenation species, but

an adsorbed species known as ethylidyne, CCH_3. The surface H study also investigates the

idea of an equilibrium surface reaction, measures the activation energy for this reaction, and

attempts to measure an equilibrium constant for this surface reaction. Bulk H is observed to

react with C_2H_2 to produce both gas phase hydrogenation products as well as adsorbed CCH_3,

as discussed in Chapter 4.

When the strong bond in the unreactive gas phase H_2 molecule is broken, H atoms are

formed. While gas phase H atoms are not reactants in heterogeneous catalysis, it is possible to

make gas phase H atoms and cleanly study the reactions between them and hydrocarbons

adsorbed on the surface under ultra-high vacuum conditions. The ability to make gas phase H

atoms gives us a third H atom species to explore as a reactant with adsorbed hydrocarbons.

Gas phase H atoms are energetic species with 63 kcal/mol more potential energy than surface

bound H. With this enormous potential energy difference, gas phase H atoms can readily

overcome barriers to chemical reactions and are observed to break and form C-H bonds easily.

The geometry of approach of a gas phase H atom to an adsorbed unsaturated hydrocarbon

species is favorable and includes the perpendicular approach that bulk H atoms have to the

adsorbed hydrocarbons. Details on the characteristics of gas phase H atoms are given in

Chapter 2.

The large energetic and geometric advantages of gas phase H atoms result in a wide

range of observed reactions with adsorbed C_2H_2, C_2H_4, and C_2H_6. Chapter 5 describes the gas

phase hydrogenation products as well as the adsorbed product, CCH_3, which is readily formed

from each hydrocarbon reactant. Time dependent surface carbon measurements give further

insight into the rates of each step in these reactions.

One larger question is what mechanism occurs in all of these different C-H bond

forming and C-H bond breaking reactions that make CCH_3? Arguments are made throughout

the thesis, but Chapter 6 is devoted to the experimental evidence and the case for a vinyl

intermediate as central in CCH_3 synthesis. Formation of a vinyl intermediate is expected to be

the rate limiting step in CCH_3 synthesis. When an elementary reaction step can be shown to be

responsible for a measured rate and activation energy, a significant step forward has been

made. If activation energies and rates were known for more surface reactions, it would be

possible to make reasonable predictions for reaction pathways and reaction products.

[1] C.N. Satterfield, *Heterogeneous Catalysis in Practice*, McGraw-Hill (1991)

[2] S.P. Daley, A.L. Utz, T.R. Trautman and S.T. Ceyer, J. Am. Chem. Soc. **116**, 6001 (1994)

[3] Z. Paál and P.G. Menon, *Hydrogen Effects in Catalysis*, Marcel Dekker (1988)

[4] K. Christmann, Surf. Sci. Reports **9**, 1 (1988)

[5] H-H bond is 104 kcal/mol, Ni-H bond 63 kcal/mol

[6] G. Alefeld and J. Völkl, *Hydrogen in Metals I and II*, Springer-Verlag (1978)

[7] J.I. Macnab and R.B. Anderson, J. Catal. **29**, 338 (1973)

[8] I. Nicolau and R.B. Anderson, J. Catal. **68**, 339 (1981)

[9] P. Fouilloux, Appl. Catal. **8**, 1 (1983)

[10] A.D. Johnson, S.P. Daley, A.L. Utz and S.T. Ceyer, Science **257**, 223 (1992)

[11] K.L. Haug, T. Bürgi, T.R. Trautman and S.T. Ceyer, J. Am. Chem. Soc. **120**, 8885 (1998)

20

Chapter 2

The Reactant Partner- Hydrogen Atom Species

1 Introduction

Molecular hydrogen, H_2, can be transformed into three different H atom species: gas

phase H atoms, surface bound H atoms, and absorbed bulk H atoms. The best way to

understand these different H atoms is to examine the potential energy surface for the hydrogen-

nickel system. This two-dimensional potential energy surface is presented in Figure 1. It is a

schematic diagram where the maxima and minima are derived from experimentally measured

quantities. Positive x values represent the distance of a H atom away from the Ni surface and

negative values represent its distance below the surface where x=0 represents the surface. The

y axis is energy. As a H_2 molecule approaches the surface, it experiences a small barrier of 1-2

kcal/mol to dissociative *ad*sorption and then a deep *ad*sorption well to form adsorbed surface

bound H atoms. The 11.5 kcal/mol well depth for adsorption is the measured heat of

dissociative adsorption of H_2 on Ni(111).[1] For H to be *ab*sorbed into the bulk, there is a much

higher energy barrier. Two thermodynamic quantities are used to determine the barrier to form

Hydrogen/Nickel potential energy surface

Solid Vacuum H(g)

52 kcal/mol

9 kcal/mol

4 kcal/mol

1/2 H₂(g)

11.5 kcal/mol

H H

H H H

H H

H
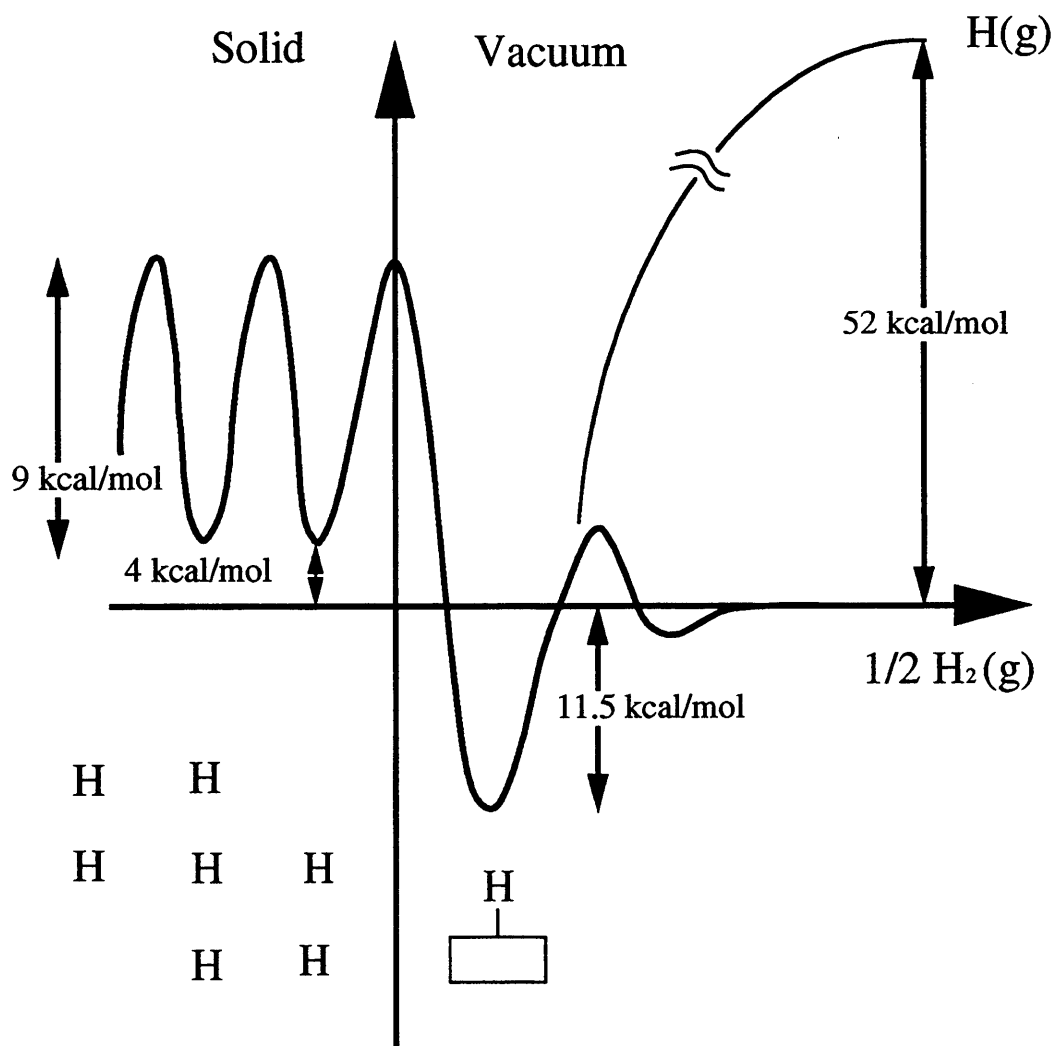
Figure 1 Schematic diagram of Hydrogen/Nickel potential energy surface. X-axis is distance from the Ni surface and y-axis is potential energy. 9 kcal/mol is the bulk diffusion barrier,[1] 4 kcal/mol is the heat of solution of H in Ni,[3,4] 11.5 kcal/mol is the binding energy of the H on Ni,[1] and 52 kcal/mol is half the dissociation energy of H₂.[2]

bulk hydrogen: the heat of solution of H in nickel which is 4 kcal/mol,[3,4] and the diffusion of H

in nickel which is 9 kcal/mol.[5] In order for a H atom, rigorously ½ H_2, to be dissociatively

absorbed into the bulk, it must overcome a 13 kcal/mol barrier representing the sum of these

two quantities. Since a single H atom at zero energy is fictitious, for the real H_2 species to

absorb into the bulk a 26 kcal/mol barrier must be crossed. A single surface H atom must have

24.5 kcal/mol to overcome the barrier to absorb into the bulk. Gas phase H atoms have 52

kcal/mol of potential energy. They can easily form both surface bound H and bulk H atoms.

The following discussion describes the properties of *ad*sorbed H atoms, bulk

(*ab*sorbed) H atoms and gas phase H atoms. The ultra-high vacuum (UHV) apparatus and the

various analytical techniques used in these studies are also described. The end of this chapter

details the methods used for synthesis, detection, and quantification of the three H atom

species used in these experiments.

2 Surface *Ad*sorbed Hydrogen

Surface bound H atoms are easily formed by the dissociative adsorption of H_2 on the

Ni(111) surface.[1] The saturation coverage of hydrogen is 1 monolayer (ML),[6,7] or 1 H atom

per surface Ni atom. H atoms adsorb in three-fold hollow sites on this surface of hexagonally

close-packed Ni atoms. At saturation coverage, hydrogen occupies half of all the three-fold

hollow sites, there being a total of 2 ML of three-fold sites on the surface. Two different types

of three fold hollow sites exist on the surface, hcp and fcc sites. The difference between these

sites is the arrangement of Ni atoms in the second layer of the metal. A nickel atom in the

second layer is centered below the hcp three fold hollow, whereas three nickel atoms are

centered below the fcc three-fold hollow site. Both types of sites are evenly

occupied at 0.5 ML coverage as shown by electron diffraction and vibrational spectroscopy,[7,8]

meaning that half of the H is bound to hcp sites and the other half is bound to fcc sites in an

ordered array. At saturation coverage of 1.0 ML the H atoms have rearranged and are

primarily on fcc sites.[9] A binding energy difference between these two sites of 0.001 kcal/mol

[10] is predicted by a theoretical calculation whereas another calculation predicted 0.3 kcal/mol,[11]

with the hcp site having the larger binding energy, and therefore the stronger H-Ni bond. The

agreement between these two calculations is not good, but the values are both small. In

addition to the difference in binding energy between hcp and fcc sites, there is an indirect long

range repulsion between H atoms that results in much larger energy differences between H

atoms on the surface. This repulsive interaction is the origin of the different desorption

features observed in thermal desorption measurements for hydrogen coverages over 0.5 ML,

as shown in the thermal desorption data in Figure 3. The magnitude of this long range

repulsive energy is between 1 and 3 kcal/mol.[7]

The processes of adsorption and recombinative desorption of H have been studied in

detail. The macroscopic picture is that the initial probability for dissociative adsorption of

thermal H_2 on a clean Ni(111) surface is quite low, $S_0 = 0.05$,[12,13,14] and drops by a half when the

H coverage increased to 0.15 ML.[15] This probability is much lower than that on other faces of

nickel where it is close to 1,[16] and is due to an activation barrier of 1-2 kcal/mol for

dissociative adsorption on the (111) face. After the H_2 molecule overcomes the activation

barrier, it dissociates into adsorbed H. This dissociation and adsorption is exothermic by 23

kcal/mol.[19]

A number of molecular beam experiments have been done that further probe the nature

of the barrier to H adsorption and desorption. They produce a coherent argument for a

mechanism of H processes on the Ni(111) surface.[14,17,18] Adsorption studies show little to no

dependence on the crystal temperature. The virtual independence of surface temperature on

adsorption shows that the surface precursor state is short lived and not able to exchange

energy. The dependence of the probability for dissociative adsorption on incident energy

displays normal energy scaling with incident angle which implies a one-dimensional activation

barrier.[19] There is a strong dependence on the energy of the impinging hydrogen molecules.

Energy in H_2 can efficiently be used to overcome the activation barrier. The energy of

desorbing molecules can also be measured using time of flight techniques. The average energy

of H_2 desorbing perpendicularly to the surface is the largest and decreases for the H_2 desorbing

at more glancing angles.[18] This behavior is the inverse of normal energy scaling for adsorption.

This shows that in both adsorption and desorption, energy is most effectively transferred when

it is in a direction perpendicular to the surface.

Other studies show that the probability of dissociative adsorption of H_2 varies with the

incident angle θ_i as $\cos^{3.5}\theta_i$. The desorption of H_2 shows a similarly strongly peaked angular

distribution which is best fit with a $\cos^{4.5}\theta_i$ function. The agreement between the angular

distributions for adsorption and desorption shows that the mechanism for these two processes

are the same. Highly peaked distributions like these observed for adsorption and desorption

arise from one-dimensional barriers. The mechanism of adsorption is that H_2

dissociates most efficiently when it approaches perpendicularly to the surface. In this

geometry, all of its energy is effective in overcoming the barrier, which is oriented normally to

the surface. This system has a direct reaction channel with an early barrier for adsorption. In

the desorption process, the molecule gains energy from falling down the adsorption barrier and

does not equilibrate with the surface before desorbing.

In considering the potential success of surface hydrogen as a reactant with adsorbed

hydrocarbon species, one very important question is the mobility of surface H. There are

several ways of answering this question. The diffusion constant of H on the Ni(111) surface

has been measured at different coverages, 0.08 to 0.6 ML, and temperatures, 77 to 125 K.[20] A

diffusion barrier of between 3 and 4 kcal/mol is measured, depending on coverage. The

diffusion coefficient below 100 K is independent of temperature and therefore is attributed to

tunneling. This tunneling diffusion gives an average diffusion rate of the order of 100 Å/sec,

and this rates increases above 100 K where non-tunneling diffusion is observed. This rapid

diffusion rate allows adsorbed H to readily interact with adsorbed hydrocarbons.

There is a second technique that shows high mobility of adsorbed H on Ni surfaces at

elevated temperature. Studies have been done on H covered Ni(111) surfaces using low

energy electron diffraction (LEED).[1,7] LEED experiments measure the long range order of the

surface. In the H/Ni(111) system with a constant surface temperature of 150 K, the strongest

intensity of the LEED (½ ½) order beam due to H is observed at 0.5 ML surface coverage.[7]

Temperature dependent intensity data measured at 0.5 ML coverage show a sharp drop in

intensity at a surface temperature of 270 K, with complete attenuation of signal above 310 K.

The loss of intensity with coverage could be due to loss of order occurring from antiphase

domains, island formation, diffusion, thermal vibrations or increased repulsive energy between

adsorbed H. A lattice gas model is used to describe the intensity behavior, the authors

reproduce the destruction of an ordered overlayer at the critical temperature of 270 K.

A third and final piece of experimental evidence that indicates that adsorbed hydrogen

is sufficiently mobile to interact with adsorbed hydrocarbons is the isotope exchange reaction

of D with C_2H_4 on Ni(111). [21,22] In this experiment, ethylene and deuterium are coadsorbed on

the Ni surface at low temperature and then the partial pressures of gas phase ethylene isotopes

are monitored as the crystal is heated. No new hydrocarbon is observed as a gas phase

product, but all of the possible isotopomers of ethylene are observed, including C_2D_4, at

surface temperatures between 200 and 240 K. This experiment confirms that surface bound H

is sufficiently mobile even at 200 K to interact with adsorbed hydrocarbons.

3 Bulk *Ab*sorbed Hydrogen

There is no dispute that hydrogen dissolves into nickel. Clear evidence that H resides

in the bulk is shown in a permeation experiment. In this experiment, the end of a tube is sealed

with a nickel disk and is placed in vacuum. The tube is then pressurized with H_2 gas and a rise

in the partial pressure of H_2 is observed in the vacuum chamber after an induction time. [23] A

schematic of this experiment is shown in Figure 2. The conclusion drawn is that if hydrogen is

first present on one side of the disk, and after some time is present on the other side, then it

must be dissolved in the bulk. The presence of H in the bulk is clear. Under typical
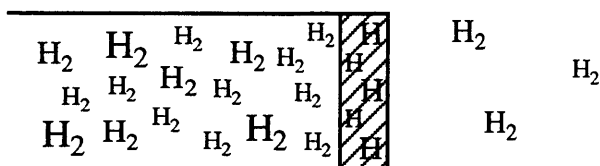
Figure 2 Schematic representation of permeation experiment.

hydrogenation conditions using a Raney nickel catalyst, bulk H is present,[24,25,26] but its role in catalysis as solely a source of surface H, an electronic structure modifier, or a reactant, is not clear. This is because it has not been previously possible to study the difference in reactivity between bulk and surface hydrogen under single collision conditions where their reactivity can be distinguished. The reason is that bulk hydrogen synthesis at the low pressures necessary for single collision conditions has not been possible due to a 26 kcal/mol barrier for H_2 dissociative *ab*sorption into the bulk. The recent capabilities of synthesis and spectroscopic identification[27,28,29] of bulk H in nickel under single collision conditions make it possible to study the reactivity of bulk H unambiguously. Further studies of the reactivity of bulk hydrogen will continue to clarify the role of this unique catalytic reactant.

Hydrogen in the Ni bulk occupies octahedral interstitial sites. Experiment[27] and theory[10,11] agree on this assignment. Unlike surface H, for which there are a limited number of adsorption sites, bulk H has an almost unlimited number of octahedral sites for absorption. This large number of potential sites allows many monolayer equivalences of hydrogen to be absorbed into the bulk. Absorbed bulk H has a lower binding energy than surface bound H. This lower binding energy of bulk H leads to a lower recombination and desorption temperature compared to surface H.

The energy characteristics of bulk hydrogen make it difficult to synthesize, with the

barrier to bulk H formation from H_2 being 26 kcal/mol and from surface H being 24.5

kcal/mol. The reason bulk H is not present under low pressure condition is that the average

energies of both an incident H_2 molecule and a surface bound H atom are much lower than the

barrier to form bulk H. Bulk H exists under high pressure conditions because, as the pressure

is increased, the flux of molecules in the high energy tail of the Boltzmann distribution that

have sufficient energy to overcome the barrier is proportionately increased. The eight-fold

increase in flux from 10^{-5} Torr under low pressure conditions to several atmospheres under

catalytic conditions is sufficient to produce bulk H. This difference in reactivity under low and

high pressure conditions in surface reactions in known as the pressure gap.

The large amount of energy that is necessary to form bulk H translates into the large

amount of energy bulk H has for reaction once it emerges from the bulk to the surface. As a

bulk H atom overcomes the barrier and emerges from the bulk to the surface it has up to 24.5

kcal/mol of energy available for reaction. The angular distribution of surface bound hydrogen

recombining and desorbing is highly peaked (discussed above) which is consistent with a small

one-dimensional barrier to desorption and adsorption. The angular distribution for bulk

hydrogen is quite broad, with a $\cos^{0.5}\theta_i$ dependence on polar angle.[30] The difference in the

angular distributions of bulk and surface H recombination and desorption suggests a significant

difference in the desorption process between these two species.

Stepping back to compare the reactivity of bulk hydrogen with surface hydrogen, it is

clear that there are several differences in both energetics and geometry. There is an energy

cost to make bulk hydrogen atoms, but this energy input creates an energetic

species when the hydrogen emerges from the bulk. Compared with the small thermal energy of

surface hydrogen, the bulk hydrogen emerges with as much as 24.5 kcal/mol of potential

energy. This is a significant amount of energy available to the bulk hydrogen to overcome

reaction barriers.

4 Gas Phase Hydrogen Atoms

Gas phase hydrogen atoms are very reactive species, due to their radical nature and

high potential energy. The dissociation energy of a H_2 molecule is 104 kcal/mol, which results

in each free H atom having 52 kcal/mol of potential energy, as shown in Figure 1. In

comparison with surface H and bulk H, gas phase H atoms have by far the largest amount of

potential energy. This large amount of energy leads to a multitude of reported reactions of

hydrogen atoms with surfaces. Gas phase H atoms can cross much higher reaction barriers

than surface or bulk hydrogen atoms due to its energy. It is observed that the initial sticking

coefficient of gas phase H atoms is between 0.9 and 1.0.[30,31]

There are several areas in which gas phase H atoms are regularly used. Gas phase H

atoms play a critical role in diamond film growth. They activate gas phase hydrocarbons by

abstracting a hydrogen atom from them, resulting in the formation of a hydrocarbon radical.

They also abstract H from a diamond surface, forming dangling bonds that act as the kernels

for further film growth.[32] Gas phase H atoms also convert both sp and sp^2 hydrocarbons to sp^3

hydrocarbons adsorbed on the surface,[33,34] and erode C:H films.[35]

However, hydrogen atom activity is not limited to diamond like C:H films. Addition

and abstraction reactions caused by gas phase hydrogen atoms have been observed on a

number of surfaces. Unsaturated hydrocarbons in organic films and adsorbed on silica are

hydrogenated to fully saturated hydrocarbons on reaction with gas phase H atoms.[36,37]

Additionally, hydrogenation by gas phase H of CO^{38} and alcohols[39] adsorbed on a surface

atoms have been observed. On metal surfaces gas phase H atom addition reactions that have

been observed are propane formation from cyclopropane,[40] cyclohexene hydrogenated to

cyclohexane on Ni(100),[41] as well as clear evidence of cyclohexene and cyclohexadiene

formation from benzene (with indications that straight chain hydrocarbons are also formed) and

ethylene hydrogenation on Cu(111)[42] and Cu(100).[43] H abstraction leads to dehydrogenation

products for cyclohexane reaction with gas phase H atoms on Cu(111), with the products

being cyclohexene, cyclohexadiene, and benzene.[44]

5 Experimental Methods

This section details methods for the synthesis and characterization of each type of

hydrogen. In addition, a step-by-step explanation of the vacuum chamber and the specific

analytical techniques used in these studies are presented.

5.1 The Instrument

All experiments were carried out in an ultra-high vacuum (UHV) molecular beam-

electron spectroscopy apparatus. Extensive detail on the design of this chamber can be found

elsewhere.[45,46,47] The main chamber of the apparatus houses the crystal and all analytical

Source   **1st** **2nd**   **Main Chamber**
                Stage **Stage**

Supersonic   **H ATOM**
Molecular   **SOURCE**
Beam
Nozzle

Skimmer   Shutter   Chopper   QMS

HREELS   Ni(111)

AUGER

Pumps
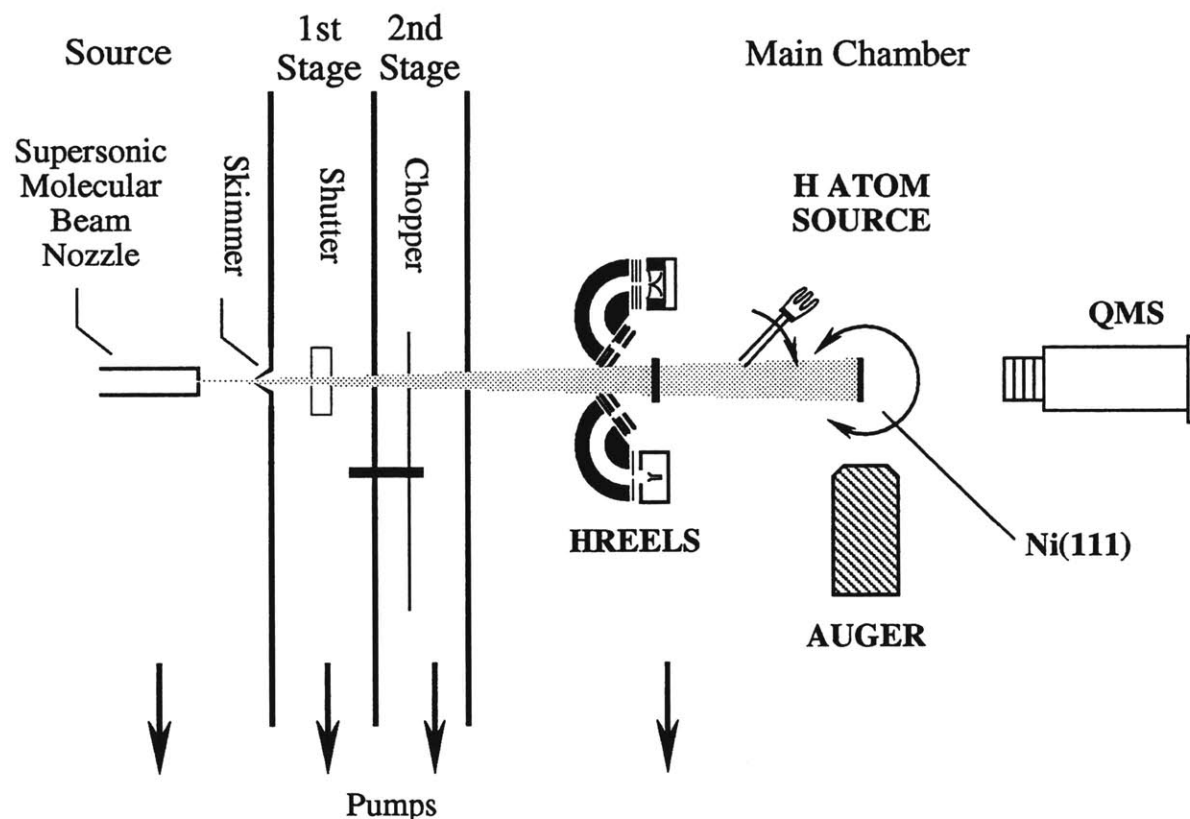
Figure 3 Schematic of ultra-high vacuum surface science apparatus with molecular beam source. Shows the two positions of the crystal in the main chamber and the analytical instruments accessible in the different positions.

instruments. It is precisely coupled to a differentially pumped molecular beam source consisting of three chambers, which are pictured in Figure 3. All chambers are pumped by diffusion pumps, with the main chamber and second stage (the last differential stage of the molecular beam source) having liquid nitrogen traps above the pumps to prevent oil contamination in these chambers. The base pressure in the main chamber of the apparatus is 5×10^{-11} Torr. This low pressure is attained by baking the main chamber at 120 °C for 48 hours after exposure to the atmosphere to remove water adsorbed on the chamber walls. It is critical to reach this low pressure so that the crystal stays clean for the duration of an experiment.

5.2 *The Crystal*

The Ni(111) face is the smoothest and most thermodynamically stable face of nickel. The almost oval-shaped crystal is 0.38" long and 0.37" wide and 0.04" thick. It has been oriented to within 0.2° of the 111 plane and mechanically polished. This precision of orientation should reduce the frequency of a step to one every 280 atoms at most. Over time, the crystal may develop waves around the edges and warp. The crystal must be replaced if this degradation of the surface can be seen by diffuse and multiple LEED diffraction spots. This degradation is also easily observed by reflection of a He/Ne laser beam from the crystal. An enlarged and non-uniform reflected image is a symptom of this crystal warping. The crystal is mounted concentrically on a manipulator with x and y degrees of freedom as well as rotational motion. The manipulator is mounted off-center on a rotatable lid that allows a total of seven inches horizontal displacement of the crystal within the main chamber. This motion allows the crystal to access analytical instruments at various locations in the chamber.

The Ni(111) crystal is mounted on the manipulator and cryostat by spot welds to two 0.020" diameter tungsten rods which are clamped into a copper block. This copper block is in thermal contact with the end of the cryostat, but is electrically isolated from it. The crystal can be heated in two ways. For lower temperatures (below 500 K), the crystal is heated radiatively by running current through a 0.010" thoriated tungsten filament positioned behind the crystal. Both the filament and crystal are held at ground potential. For higher temperatures (above 500 K), the crystal is heated with electron bombardment. In all high temperature heating the cryostat is cooled with either flowing air or liquid nitrogen. The crystal is biased to +600-700

V while the grounded rear filament produces electrons which heat the crystal by

dissipating their energy into it. It has been found that even though the filament is positioned

behind the crystal, the high energy electrons make their way to the front of the crystal and can

induce chemical changes in hydrocarbon adsorbates. Therefore, in any experiment where a

chemical change is observed that includes electron beam heating, the unique behavior is

confirmed to exist in the absence of the high energy electrons.

The crystal can be cooled by thermal contact with the cryostat which is filled with

either liquid nitrogen or liquid helium. The crystal is surrounded by a cryoshield to minimize

radiative heat loss from the crystal and cryostat.[48] The typical working temperature reached

with liquid nitrogen is 80 K. The manipulator is designed to reach a crystal temperature of 8 K

when using liquid helium in the cryostat.[48] However, for the work in this thesis not all thermal

connections were at their best, and this ultimate low temperature was not reached. The typical

crystal temperature using liquid helium coolant was 20 K. When measuring temperatures in

the liquid helium range, it is necessary to calibrate the thermocouple using an ice-point

reference. Unfortunately, the electronic thermocouple signal conditioner used in normal

operation was not calibrated properly for this low temperature region.

When an experiment is done, it is vital that the surface is free of contamination. The

major impurities encountered on nickel are sulfur, carbon and oxygen. There are two ways to

check for surface purity. The first is Auger spectroscopy, which is an elemental analysis

technique that detects the energy of core electrons as described below. The detection limit of

Auger is 0.01 ML.[49] The second method used to verify that the crystal is clean is high

resolution electron energy loss spectroscopy (HREELS). Contaminants have specific loss

features, the Ni-C stretch is observed at 300 cm^{-1}, the Ni-S stretch is observed at 400 cm^{-1}, and

the Ni-O stretch is observed at 550 cm^{-1}. After the crystal has seen atmosphere, extensive

cleaning is done using Auger spectroscopy to measure contaminants. After the crystal has

been established as clean, HREELS is sometimes used to verify the cleanliness of the surface

before starting experiments for the day.

Methods of cleaning the surface depend on the contaminant. For sulfur contamination,

which is the most common and persistent contaminant, argon ion sputtering is preferred. The

sputter gun produced a current of $3\text{-}4\times10^{-6}$ A of 1 keV Ar^{+} from an Ar partial pressure of

6×10^{-5} Torr. This beam is directed at the surface with the crystal at room temperature for

times of seconds to minutes. After sputtering, the crystal is annealed at 1000 K. Sometimes

sulfur will rise to the surface with continued annealing. A method used to drive sulfur out of

the near surface region is exposure of the crystal to hydrogen atoms. The H atoms penetrate

the bulk and either displace the sulfur out of bulk sites or attract sulfur towards the surface.

After a series of H atom exposures and subsequent argon sputtering, the crystal is then more

likely to stay free of sulfur.

Carbon contamination can usually be removed by heating the crystal above 935 K, at

which temperature the carbon dissolves into the bulk of the crystal. However, when the near

surface region is saturated, carbon dissolution into the bulk will no longer occur by heating the

crystal. Argon sputtering can be used, but a more effective method is oxidization of the crystal

by exposure to a molecular beam of O_2 with subsequent heating. The oxygen exposures

should be done with the crystal at room temperature or as the crystal is cooling

from 1000 K. The effectiveness of carbon removal can be measured by monitoring the CO and

CO_2 signal as the crystal is heated, once the O_2 exposure is complete. This process should be

repeated until little to no CO and CO_2 are observed. Oxygen contamination can be eliminated

by heating the crystal to 1000 K. If this procedure is not successful, the oxygen can be

transformed to H_2O and desorbed by exposure of the crystal to a beam of H_2 while the crystal

cools from 1000 K and subsequent annealing at 1000 K for 5 minutes.

In preparation for an experiment, the crystal is annealed until its surface is smooth. The

measure of smoothness is the temperature of the β_1 desorption feature of surface H. It is

known that this desorption temperature shifts with surface roughness.[15] The temperature of

the β_1 desorption feature must be at 335 K or higher before experiments are done. If the

temperature of the β_1 desorption feature is low and does not increase with additional

annealing, there could be oxygen contaminating the H_2 gas. A small amount of coadsorbed O

will depress the peak temperature in the recombination and desorption of H_2.[50]

5.3 Molecular Beam

The main chamber is precisely coupled to a supersonic molecular beam. In the

schematic in Figure 3, the three differential pumping chambers are shown. The source

chamber handles the bulk of the gas load from the expansion of between 40-100 psi of gas out

of the 0.001" diameter nozzle. The shutter in the first differential stage controls precisely the

time of the crystal exposure to the beam. In general, molecular beams are useful because they

produce a beam with a narrow translational energy distribution (typically $\Delta E/E=10\%$) that can

be tuned by either altering the composition of the mixture of gases in the beam or changing the

temperature of the nozzle. The gases expanded out of the nozzle are rotationally cooled.[51]

In these studies, the molecular beam is used for two types of applications. The first

application is to deliver precise hydrocarbon exposures to the crystal. All hydrocarbon species

are adsorbed on the crystal by exposure to a beam of a small percent of the specific

hydrocarbon seeded in an inert gas, typically argon. Any noble gas can be used, but Ar is a

good choice for C_2 hydrocarbons because it is a close match to the mass of a C_2 hydrocarbon

which eliminates acceleration or deceleration of the molecules. A dilute mixture (typically 1-

2%) of the hydrocarbon of interest coupled with the time control of the electronic shutter

allow partial monolayers of hydrocarbon to be deposited on the surface with precision. The

second application of the molecular beam in these studies uses the potential for producing

atoms or molecules with very high translational energies. For example, in synthesizing

exclusively bulk H, it is necessary to use very high energy noble gas atoms to sweep the

surface clean of surface bound H. The molecular beam is the key in this process, producing Xe

atoms with 144 kcal/mol of translational energy by expansion of a 0.25% Xe/He mixture from

the nozzle at 1000 K. This synthesis will be detailed below, but it would be impossible to

make such directed high energy species without the molecular beam, which in turn would make

it impossible to make bulk H atoms in the absence of surface bound H.

5.4 Auger Spectrometer

Auger spectroscopy is an elemental analytical technique that measures the binding

energy of core electrons in an atom. A 2 keV beam of electrons is directed at the surface

producing a current to the crystal of 0.5 µA. These high energy electrons eject

electrons from the core of the atom and in a process known as an Auger transition, an electron

in an outer shell drops down to fill the core hole. The energy generated in this transition is

converted to translational energy of a third electron ejected from the atom. A cylindrical

mirror electrostatic energy analyzer disperses the energy of ejected electrons, which are

detected by an electron multiplier. The Auger signal is recorded as a derivative signal to aid

observation of the Auger electrons which are observed on a high background of secondary

electrons. This derivative signal is proportional to the number of atoms in the exciting electron

beam.[52,53]

In these studies, Auger spectroscopy is used for two purposes. One purpose is to

check the crystal for contamination, with the major contaminants being sulfur at 152 eV,

carbon at 272 eV and oxygen at 550 eV. Some of these features occur in the same energy

region as nickel diffraction features, the strongest at 146, 166, 188, and 220 eV, which become

more intense at lower crystal temperatures. For this reason, the Auger spectrum of the crystal

is measured at room temperature. The detection limit of Auger spectroscopy is 0.01 ML.[49]

The other purpose for Auger spectroscopy in these studies is to measure the amount of

carbon on the surface, either after a known exposure of the crystal to a hydrocarbon so that the

exposure times and therefore coverage can be calibrated, or after a H atom exposure to see

how much carbon remains. In all measurements of carbon coverage, both the carbon and

nickel Auger signals are measured and the carbon coverage is reported as the C/Ni ratio. A

ratio is measured in order to eliminate error from drift in the absolute Auger intensities, since

the nickel signal is a constant regardless of carbon coverage. A detailed description of how

carbon Auger signals are analyzed is given in the below.

The most basic C/Ni Auger experiment is to measure the exposure time necessary to

saturate the crystal with the hydrocarbon of interest. A series of C/Ni measurements are made

after exposing the crystal to the hydrocarbon seeded beam for different times. An example of

such a data set is shown in Figure 6. The plot of the C/Ni ratio vs exposure time shows a

steady increase in the C/Ni ratio up to a time when the C/Ni ratio becomes constant. The

saturation time is defined as the exposure time in which the C/Ni ratio reaches a constant

value. However, this determination of the saturation time does not provide an absolute

coverage measurement. For ethylene, previous low energy electron diffraction (LEED)

measurements from this lab do allow determination of an absolute coverage. Diffraction from

a saturated surface showed a (2x2) unit cell.[48] This (2x2) structure of adsorbed C_2H_4 has been

studied in detail and corresponds to an absolute coverage of 0.25 ML.[54] In addition to

knowing the saturation coverage of C_2H_4, the coverage C_2H_2 is also important. The saturation

coverage of C_2H_2 is determined by comparing to the time necessary to achieve C_2H_2 saturation

with the time needed for C_2H_4 saturation. Using our molecular beam, the saturation exposure

time of C_2H_2 is similar to that of C_2H_4. Ordered acetylene layers are reported by LEED at 0.25

ML and 0.33 ML coverages, with corresponding exposures of 2L and 30-100L (Langmuir=

1×10^{-6} Torr/sec), respectively.[54] The saturation exposure of ethylene is reported to be 1.4 L.[54]

Since our exposure times for saturation of ethylene and acetylene are similar, and because

estimates of the flux of ethylene and acetylene from the beam are in the 1-2 L range, it is

concluded that the saturation observed for acetylene is 0.25 ML. The final

hydrocarbon used in these studies is C_2H_6. The saturation coverage of C_2H_6 is determined to

be 0.20 ML from comparison of the C/Ni ratio of a saturated layer of C_2H_6 to that of a

saturated layer of C_2H_4.

5.5 Measurement of Carbon Auger Signal

Using Auger as a technique for detecting impurities is straightforward. An impurity

signal is observed or it is not. On the other hand, quantitative measurements of carbon Auger

signals require care in proper spectral interpretation. The goal of this section is to detail clearly

the method for quantitatively measuring carbon coverage using Auger spectroscopy.

In all carbon coverage measurements, both carbon and nickel Auger signals are

recorded at 272 eV and 848 eV as derivative signals (dN(E)/dE). The amplitude of the

derivative signal is typically measured from the top of one peak to the bottom of second peak

as shown in Figure 4a.[55,56] However, the carbon signal is in a region of the energy spectrum

that has a sloping background, due to a nickel diffraction feature. This background is shown in

the top trace of Figure 5. Because of this sloping background, the peak-to-peak method of

measuring the carbon amplitude needs to be modified. This modification is necessary because

with increasing carbon coverage the peak-to-peak method does not measure a linear increase

in carbon coverage. Figure 5 shows a set of traces with increasing carbon coverage. The

peak-to-peak intensity of carbon in the 0.25 ML trace is easily measured between the features

at 258 and 276 eV. However, for the lowest carbon coverage trace at 0.07 ML carbon, there

is no discernible feature at 258 eV, and therefore the peak-to-peak intensity is measured to be
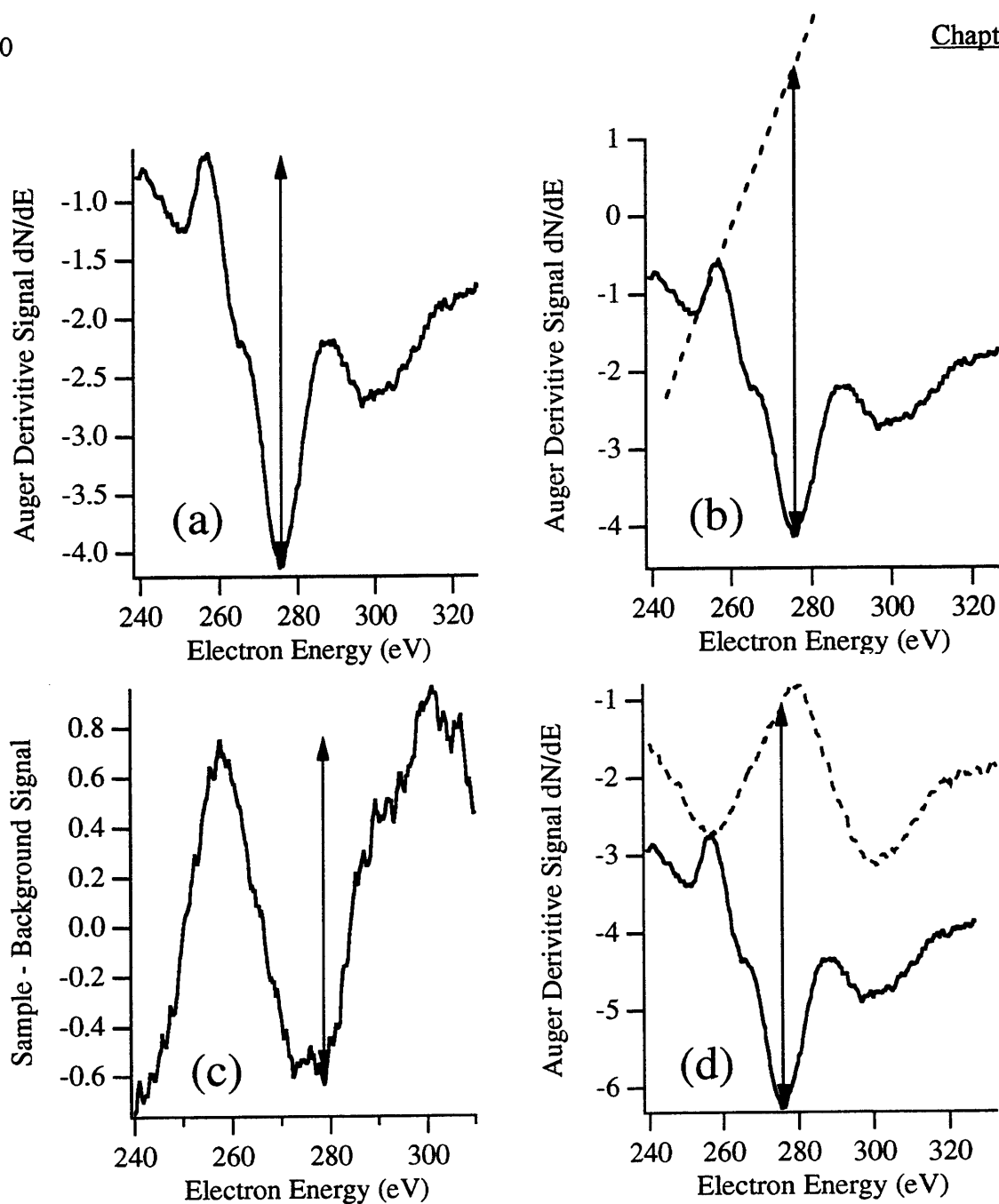
Figure 4 Representations of different Auger measurement schemes.

(a) Peak to peak measurement technique

(b) Linear extrapolation of the upward sloping background

(c) Point by point subtraction of the background from the signal, measured peak to peak

(d) Aligning measured sloping background with carbon data to measure carbon signal relative to the background
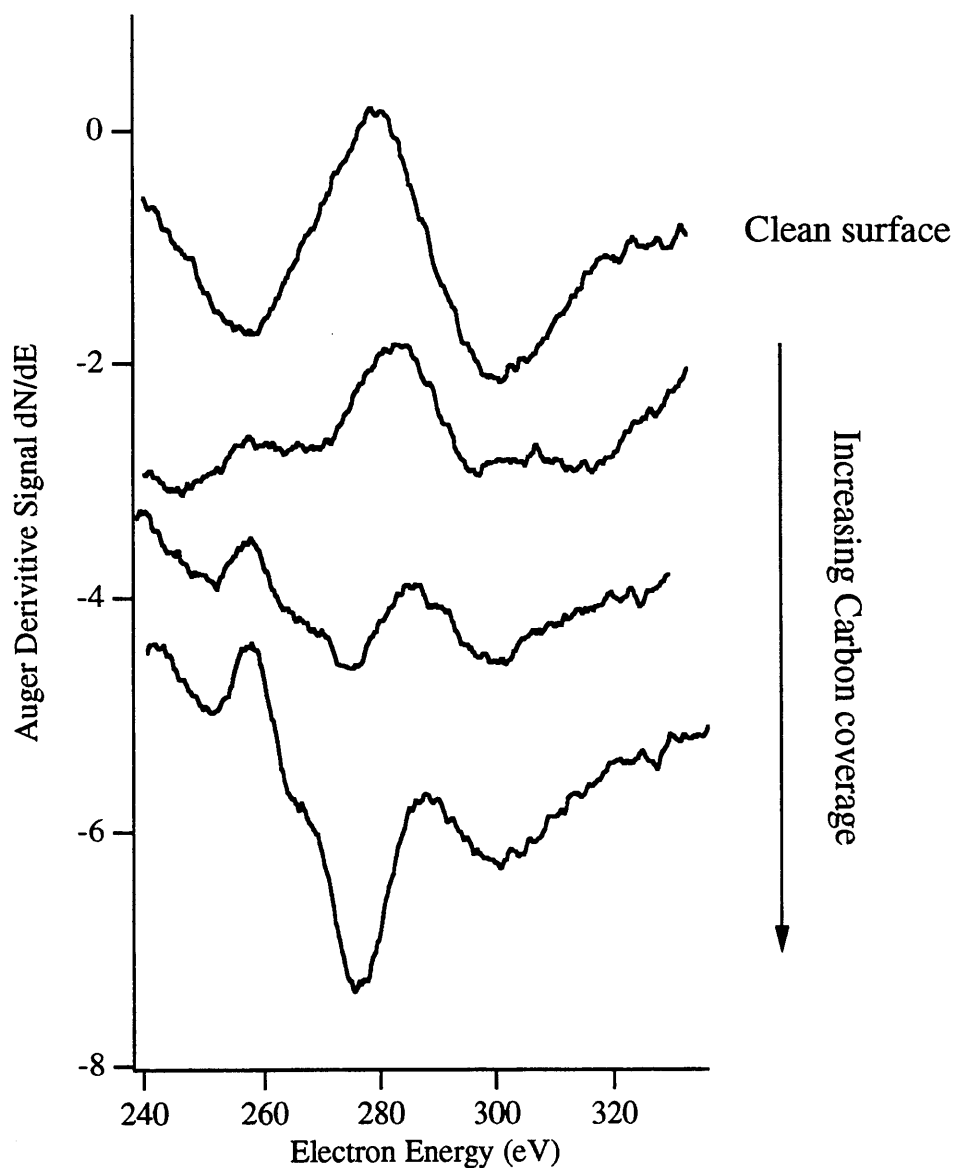
Figure 5 A set of Auger spectra in the region where carbon is observed. The top spectrum is the background from the clean surface with spectra of increasing carbon coverage 0.07, 0.14 and 0.25 ML. All scans taken at a crystal temperature of 85 K.

zero. The carbon intensity for this low coverage adds to the sloping background to flatten it, but does not produce the characteristic positive and negative peaks of the derivative signal.

The peak-to-peak measurement can give quantitative values for high carbon coverages, but this

technique systematically underestimates the amplitude of the carbon signal. A new method for quantitative measure of the carbon Auger signal is needed.

The observation of a sloping background in the energy range of the carbon signal is not new, but as the technology for recording and handling data has changed, the ability to correct for this background has improved. Because Auger data were collected in an analog mode and recorded on an x-y plotter prior to 1991, the correction of the Auger signal for the sloping background was carried out as shown in Figure 4b.[22] A line is drawn to continue the positive slope and the amplitude of the carbon signal is measured from this line to the bottom of the carbon valley. The goal of this method is that the line drawn represents the signal of a clean surface. The carbon amplitude is measured between this 'clean surface signal' and the actual carbon signal. This procedure gives satisfactory results for carbon coverage measurements.

Since 1991, Auger data has been collected digitally. An accurate analysis of the intensity of the Auger signal can be carried out on digital data by a point by point subtraction of the Auger signal of the clean crystal from that of a crystal covered with carbon. This yields a derivative signal with the background slope removed. The peak to peak distance of the carbon signal is then measured. Figure 4c is an example of this type of data analysis using the lowest carbon coverage data from Figure 5. This method is excellent in principle, since there is no ambiguity in measuring from the top of one peak to the bottom of the next. Unfortunately, this method is not easy in practice. From time to time there are small, but not insignificant, energy drifts in the Auger instrument. The measurement of the clean carbon signal is repeated every five or six measurements, to minimize any energy differences in the signal and the

background. These drifts require shifting the x energy axis before subtraction, so

the energy values are matched between the clean and carbon covered traces. This shifting is

possible by comparing the energy position of the nickel signal between the two data sets.

However, any energy shift makes this background subtraction method extremely labor

intensive.

Next is described a second technique that yields results as good as background

subtraction, but is much less time consuming. This second method is similar to the method

that was used with the analog x-y plotter data. The actual trace of the clean crystal is used,

instead of the straight line extrapolation, to measure the change in the carbon amplitude. In

this method the carbon amplitude is measured *between* the carbon Auger signal and the trace

of the clean crystal after aligning the clean crystal trace with the top of the positive slope in the

energy spectrum of the carbon signal (see Figure 4d). If the Auger stability is poor, and there

are energy drifts in the instrument, the energy drifts between the clean crystal and a specific

carbon coverage are measured using the Ni signals. Unlike the previous method, these shifts

can be taken into account easily when aligning the two signals. The most important part of this

measurement method is to line up the signal with the background in the proper manner. The

two traces must meet at an energy of ~257 eV. It is tempting to line up the clean crystal trace

with the slope between 240 and 250 eV or the higher energy background above 300 eV where

the shape is very similar between these two scans. However, changes in both of these energy

regions are seen with carbon coverage; there is also no firm physical reason to choose these
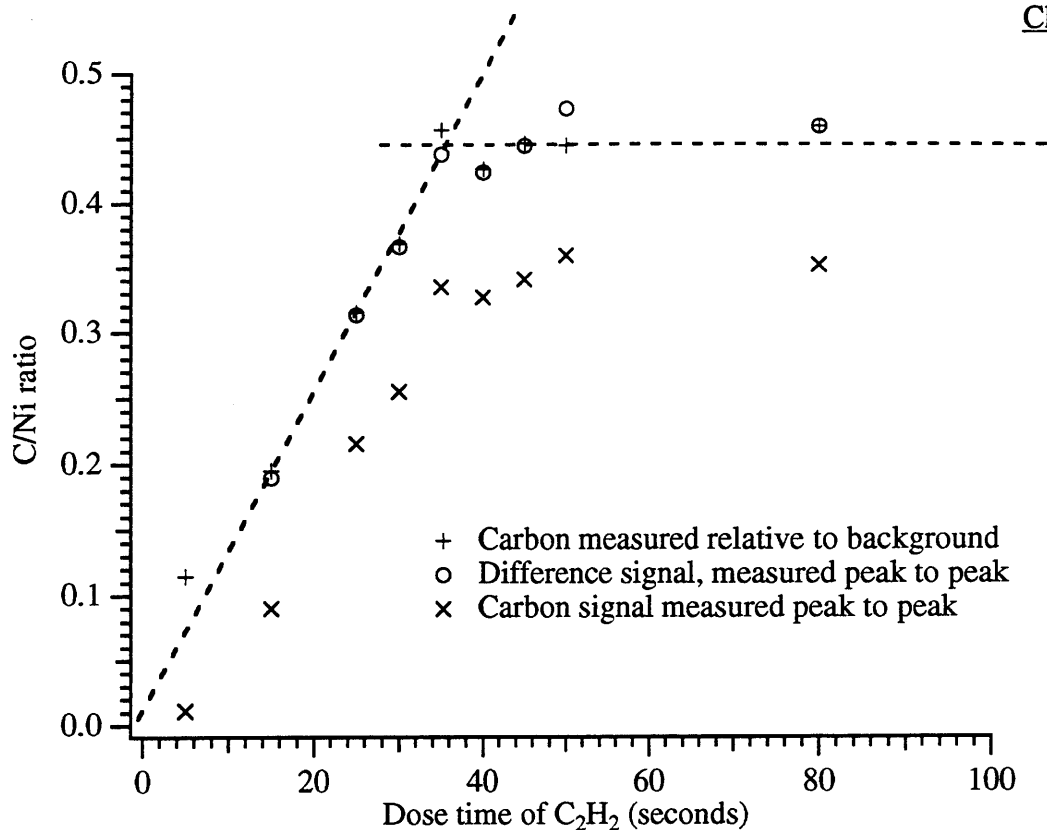
Figure 6 Auger calibration curve. Carbon to nickel Auger measurements analyzed in three different ways. Different dose times of an acetylene molecular beam taken to establish the saturation dose of acetylene. Dashed lines used to determine saturation.

+ carbon signal measured relative to background signal

o carbon signal measured peak to peak from the difference of carbon
   signal minus background

x carbon signal measured peak to peak

alternate overlap points.

In order to demonstrate the quality of each of these methods, Figure 6 shows a

calibration curve for acetylene. In this plot, the carbon to nickel ratio is measured as a function

of the time of exposure of the crystal to a beam of 2% acetylene seeded in Ar. Plotted on this

graph are three sets of carbon to nickel ratios analyzed from the same raw data; carbon

measured peak to peak with no attention paid to the sloping background, carbon measured

relative to the background, and carbon measured peak-to-peak after subtraction of the

background signal from the carbon signal. The first peak-to-peak measurement

predictably yields less carbon than the other measurements and does not extrapolate to pass

through the origin, which is physically expected since zero exposure should give zero carbon

Auger signal. The fact that the peak-to-peak data miss the origin undermines the accuracy of

this method. In contrast, the origin does fit with the data sets analyzed using the two methods

that account for the sloping background, which supports the accuracy of these methods. The

carbon intensity measured peak-to-peak from the difference signal and the carbon intensity

measured relative to the background agree very well. The agreement justifies the use of the

second method to measure all quantitative carbon Auger data.

5.6 Quadrupole Mass Spectrometer

The quadrupole mass spectrometer (QMS) is mounted on the molecular beam axis.

The mass spectrometer consists of an ionizer, quadrupole mass filter and channeltron electron

detector. The QMS is used to check the cleanliness of the chamber by measuring the masses

of the residual gases present. The residual gases with the largest concentrations are hydrogen

$m/e=2$ and CO ($m/e=28$). For a healthy vacuum, the ratio of the $m/e=28$ signal to $m/e=18$

(H_2O) should be greater than 2, the ratio of the $m/e=28$ to $m/e=32$ (O_2) signals should be

greater than 30, and the $m/e=12$ signal should be larger than the $m/e=14$ signal. A signal at

$m/e=14$ that is more intense that the $m/e=12$ signal indicates an air leak characterized by N_2.

The parent peak for nitrogen at $m/e=28$ is insensitive to small changes observed at the $m/e=14$

cracking fragment because it overlaps the CO peak. The QMS can be used to check for leaks

by observing the $m/e=4$ signal while spraying He around suspicious flanges.

Another use of the QMS is in thermal desorption spectrometry (TDS). TDS involves

heating the crystal at a constant rate of 2 K/sec and monitoring the partial pressure of the

molecular adsorbates or their fragments as they desorb. Desorbing molecules must be ionized

for mass selection and detection, during this dissociative ionization process fragments of many

different masses are produced. Each molecule dissociates into characteristic fragments when

ionized. The probability of ionization into all possible fragments is represented by the cracking

pattern of a molecule. When studying reactions that involve a mixture of ethane, ethylene and

acetylene, it is vital to know the cracking patterns of each species to distinguish between these

C_2 hydrocarbons. For this reason, the cracking patterns of ethylene and ethane were measured.

The cracking patterns include contributions from the natural abundance of ^{13}C labeled

hydrocarbons, which results in correction for ^{13}C contributions when the final analysis is

compete. For cracking pattern measurements, a mixture of 2% ethane in Ar or ethylene in He

was introduced into the main chamber using a leak valve so that a total pressure of 5×10^{-10} or

2.5×10^{-10} Torr, respectively, was attained. These two pressures are the same when corrected

for the difference in detection efficiency of Ar and He by the ionization gauge.[57] The increase

in partial pressure with introduction of the hydrocarbon is measured at the individual masses of

interest. The intensity of this increase is used to determine the cracking patterns shown in

Table 1. In assigning cracking intensities, a value of 1000 is given to the most intense mass

and the intensities of all other masses are given relative to this value of 1000. The published

acetylene cracking pattern that most closely matches the conditions of our system is also listed

in the table.[58] The column entitled "other masses" give the sum of cracking intensities for the

Mass/e	24	25	26	27	28	29	30	other masses	total signal
Acetylene (table[58])	50	194	1000	22	1			41	1305
Ethylene (measured)	*33*	130	628	637	1000	*19*		132	2579
Ethane (measured)	*5*	39	237	339	1000	191	224	83	2118

Table 1 Fragmentation pattern of acetylene, ethylene and ethane at ion energy=13.5 V and electron energy =70.7 V. The most intense fragment is defined to have signal of 1000 and other fragments are measured relative to this signal, values in italics are from liturature.[58] Other masses refers to the sum of the signals at values of m/e not reported here, the total signal is the sum of the signal at all values of m/e. Variation in measured fragmentation ratios is 5% (1σ error bar)

fragment not listed in the table. This table also includes the total cracking intensity, which is the sum of the cracking intensity of each fragment of a particular molecule. This total cracking intensity is important when TDS signals are adjusted to yield the absolute intensities of each species.

Another value necessary to compare the absolute intensity of one hydrocarbon species to another from TDS signals detected by a QMS is the ionization efficiency of each molecule. The ionization efficiencies for the hydrocarbons of interest have been measured by different research groups over the years. The average of the total ionization cross section (σ_{total}), which is the cross section for observing all of the fragments of a species are $5.83\pm0.4 \times 10^{-16}$ cm^2 for ethane,[59,60,61,62,63] $5.26\pm0.2 \times 10^{-16}$ cm^2 for ethylene,[61,63,64,65] and $4.38\pm0.3 \times 10^{-16}$ cm^2 for acetylene.[63,66,67] Ionization cross sections are measured relative to a standard, most frequently

Ar. The literature values of σ_{total} were adjusted if the standard total cross section for Ar,

$\sigma_{total}(Ar)$, was not the currently accepted value $(2.67\pm0.09 \times 10^{-16} \text{ cm}^2)$.[68] These ionization

cross section values will be used in analysis of QMS data.

5.7 High Resolution Electron Energy Loss Spectrometer

The heart of this apparatus is the high resolution electron energy loss spectrometer

(HREELS). The ability to record the vibrational spectrum of an adsorbate or mixture of

adsorbates proves to be a very powerful tool. A number of the species that are central to these

studies will not thermally desorb into the gas phase, so it is impossible to learn their identity

from a thermal desorption experiment. Auger spectroscopy allows the total carbon coverage

to be measured, but does not provide a method to distinguish between different adsorbed

carbon species. An HREEL spectrum is the best method available to identify molecular

adsorbates.

In HREELS, a monoenergetic 6.5 eV beam of electrons is formed by deflecting

electrons through a 127° energy sector. This monoenergetic beam is focused on the crystal

and both the elastically and inelastically scattered electrons are detected by a channeltron after

energy selection in a second 127° energy analyzer sector. The first sector is referred to as the

monochromator, while the second sector is referred to as the analyzer. In a typical spectrum,

the intensity of the elastically scattered electrons is large. Measuring electron intensity to

negative energies reveals small features that correspond to electrons that have given energy to

excitations of vibrational modes of the adsorbed species in multiples of hv. Vibrational spectra

are recorded at a specular angle with the incident beam 60° from the surface and are also

recorded at an off specular angle by rotating the crystal axis to change the incident

and scattered beam angle. Specific angles reported for off specular spectra are twice the angle

of the crystal rotation, because both the incident and scattering angles are changed.

Comparison of the specular and off specular spectra is important in determining the

excitation mechanism of different vibrational modes.[69] There are two different mechanisms by

which electrons lose energy to the surface adsorbates. These mechanisms for excitation have

different selection rules and therefore assist in assignment of the spectra. One mechanism is

dipolar excitation. As a molecule vibrates, it creates an oscillating dipole. If this dynamic

dipole is perpendicular to the surface, or has some component of its dynamic dipole

perpendicular to the surface, its intensity is amplified by its image charge in the metal. The

oscillating dipole creates a long range oscillating electric field that interacts with incoming

electrons at a distance of between 60 and 100 Å. Because this interaction is long range there is

a very small momentum change parallel to the surface so the electrons scatter with a narrow

angular distribution. Dipole scattering obeys strict selection rules since the mode must be

totally symmetric and have a dipole moment perpendicular to the surface. However, simply

because a vibrational mode is expected to have symmetric motion perpendicular to the surface

from symmetry arguments does not guarantee it will have a large enough dynamic dipole to be

observed as a dipole active vibration. The other mechanism for observing modes is impact

scattering. In this regime, incoming electrons interact with the molecular vibrations at a very

close range, on the order of 1 Å, and scatter from the surface with a broad angular distribution.

Symmetric modes with sufficient dynamic dipole motions can easily be identified by their large

drop in intensity, from the on specular to the off specular spectra. Non-dipole active modes

will have very similar intensities in the two spectra.

5.8 *Front Hydrogen Atom Source Filament*

.   An efficient way to make H atoms is the dissociation of H_2 over a hot filament. The

filament is a 0.010" tungsten wire bent into a grid shape and positioned 0.25" in front of the

crystal. The details of preparing filaments and the design of the front filament have been

documented previously.[29] The filament is rapidly heated in the presence of H_2 by placing a 3V

potential across the filament which results in a current of 3A and a filament temperature of

1600 K as measured by an optical pyrometer. H_2 molecules dissociate on the hot filament and

H atoms desorb and ultimately impinge on the crystal, as shown in Figure 7. The crystal

temperature rises due to radiative heating from the filament. With liquid nitrogen in the

cryostat, the crystal temperature rises from 80 to 120 K. With liquid helium in the cryostat,

the crystal temperature rises from 20 to 60 K. The flux of H atoms is determined by the
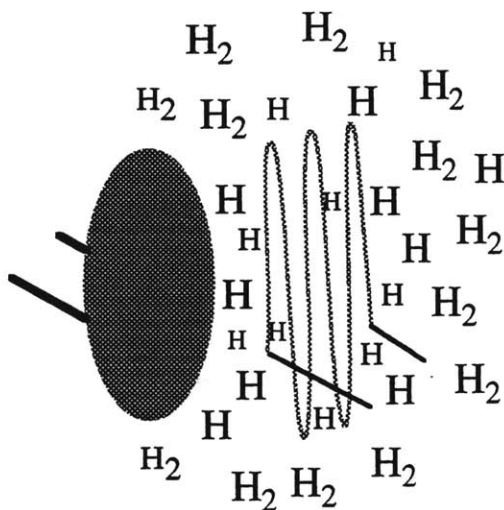
Figure 7 Representation of formation of H atoms from the hot front hydrogen atom source filament.

distance of the filament to the crystal, the pressure of H_2 in the chamber and the

temperature of the filament. The flux is not known for all conditions, but in a later section, a

measurement of the H atom flux for one specific condition will be presented. The front

filament assembly was modified from the original design[29] to allow the filament to be as far as

0.65" from the front face of the crystal. This modification allows H atom exposure with less

radiative crystal heating.

6 Synthesis and Characterization of Hydrogen Species

6.1 *Surface Hydrogen*

Synthesis of surface bound H is straightforward. A typical method for adsorbing

hydrogen on the Ni(111) surface is to raise the H_2 partial pressure to 2×10^{-5} Torr in the main

chamber for times varying from seconds up to 30 minutes, depending on the coverage desired.

The method used to measure H coverage is to take a thermal desorption spectrum and

integrate the m/e=2 signal. Comparison of this integrated signal to that from a crystal covered

with 1 ML of H,[22] the saturation coverage of H on Ni(111), gives an absolute coverage

Figure 8 shows a typical hydrogen TD measurement from 1 ML of H adsorbed on Ni(111).

Note the β_1 feature, which occurs due to the long range lateral interactions of the hydrogen

atoms on the surface. For coverages below 0.5 ML there is no β_1 feature. A β_2 feature is the

only feature observed. At this lower coverage the H atoms are far enough apart that the

repulsive lateral interactions do not affect the desorption.

Under typical synthesis of surface bound H, both the front and the back face of the

crystal are exposed to the same H_2 partial pressure, which leads to the question of whether
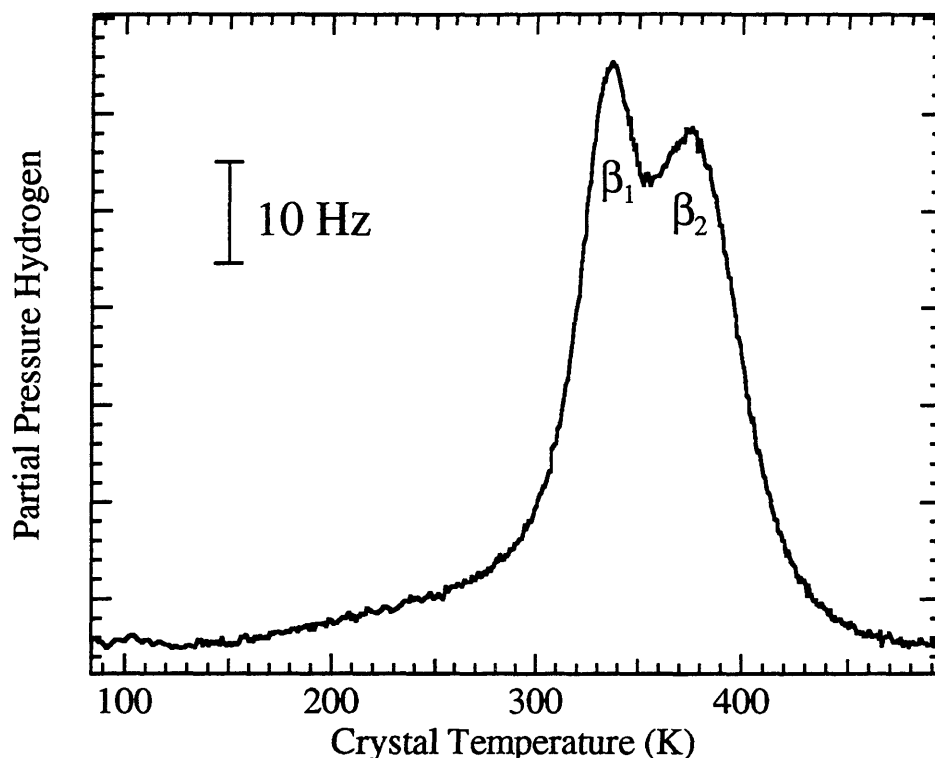
Figure 8 A thermal desorption spectrum of surface bound hydrogen desorbing from the crystal. Adsorbed layer formed by exposure of Ni to 2×10^{-5} torr H_2 for 2 min. with the crystal temperature between 560 K and 80 K. Surface H coverage is 0.8 ML.

there is any contribution in the integrated TD m/e=2 signal from the back of the crystal. This question can be resolved by measuring the integrated m/e=2 signal for a C_2H_4 saturated surface as the adsorbed hydrocarbon decomposes. The C_2H_4 exposure is done using the molecular beam. No C_2H_4 is adsorbed on the back of the crystal because the partial pressure of C_2H_4 at the back of the crystal is several orders of magnitude lower that on the front face. It is known that as the surface is heated at a rate of 2 K/s, 0.08 ML of C_2H_4 desorbs, leaving 0.17 ML of C_2H_4 on the surface.[22] This remaining C_2H_4 decomposes to C_2H_2 and surface bound H, and the C_2H_2 further decomposes to carbon and H above 450 K.[70] Therefore, the partial pressure of m/e=2 as the crystal is heated above 450 K arises from 4 H atoms desorbing from every

C_2H_4 molecule, leading to an integrated m/e=2 signal equal to 0.68 ML. The

agreement between the value of this integrated signal and the standard saturation exposure of

H^{22} confirm that no H adsorbs on the back of the crystal.

In addition to observation by TDS, surface H can also be observed by HREELS.

Figure 9 shows EEL spectra for saturated layers of hydrogen and deuterium. The two

fundamental modes for hydrogen (deuterium) at 950(700) cm^{-1} and 1150(850) cm^{-1} correspond

to motions parallel and perpendicular to the surface, respectively. The other features in these

spectra are unassigned as overtones of H(D). The vibrational spectra show a shift in frequency

of features at coverages under 0.5 ML.[8]

6.2 Bulk Hydrogen

Bulk H atoms are most easily synthesized by exposing the crystal to gas phase H

atoms. Bulk H can also be produced by collision induced absorption, but exposure of the

crystal to gas phase H atoms gives higher concentrations of bulk H more easily.[28,29] Gas phase

H atoms are generated by dissociation of $2x10^{-5}$ Torr H_2 over a hot tungsten filament. More

details of this method are given above. This procedure produces a flux of both H_2 molecules

and H atoms on the surface, as show in Figure 7. A thermal desorption spectrum of the crystal

after exposure to gas phase H atoms is shown in Figure 10. The difference between this

spectrum and the TDS spectrum of surface H in Figure 8 is a lower temperature feature

centered at 185 K. This low temperature feature is the signature of bulk H. Integration of this

thermal desorption spectrum allows determination of the number of equivalent monolayers of
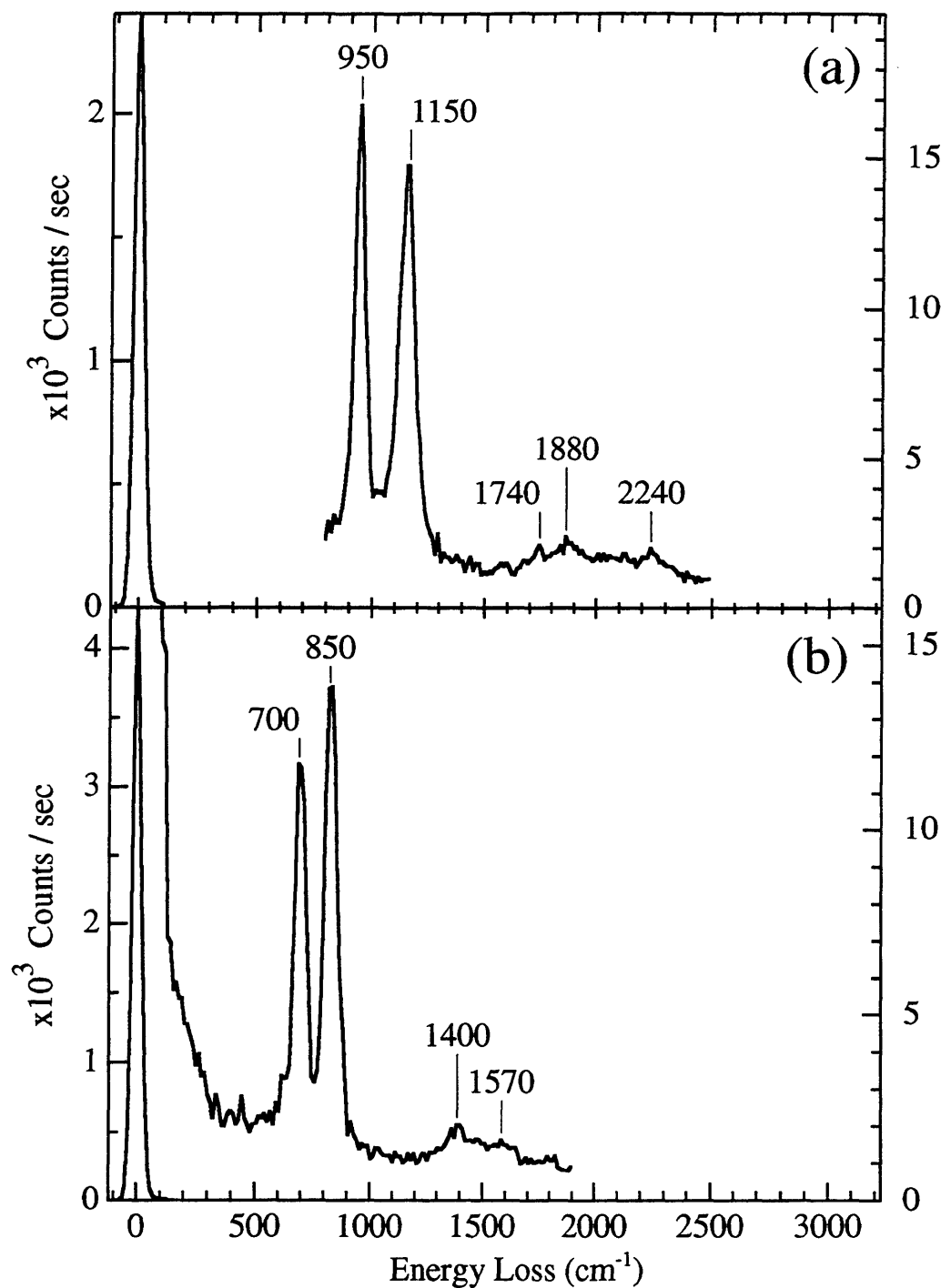
Figure 9 HREEL off specular spectra of saturated monolayers of H and D layers on the surface, panels (a) and (b) respectively. Spectra taken at 80 K, at 8° off specular with 6.5 eV electrons, ΔE_{fwhm} average 45 cm^{-1}.
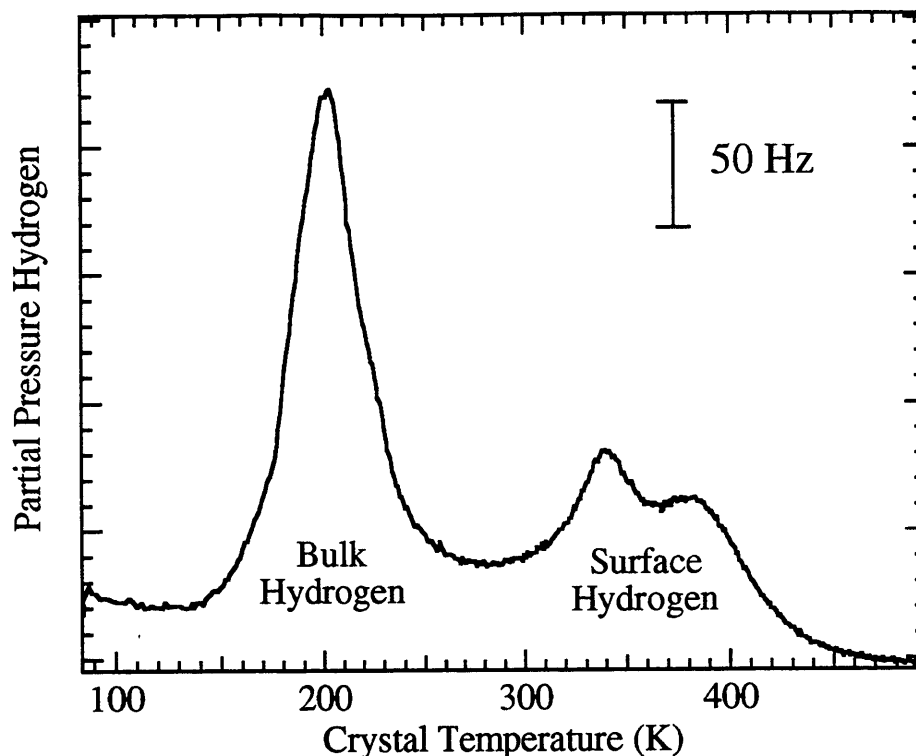
Figure 10 A thermal desorption spectrum of bulk and surface hydrogen desorbing from the crystal after exposure to gas phase H atoms. Low temperature feature is bulk H and high temperature feature is surface H. Hydrogen formed by exposure of Ni(111) to 3×10^{-5} torr H_2 for 2 min with front hydrogen atom source filament on.

absorbed hydrogen in the bulk. The integrated signal of the surface H features between 300 and 450 K provides a calibration for 1 ML because the surface remains saturated with H after the H moves out of the bulk. This 1 ML integral is then compared to the integrated signal between 150 and 300 K to provide the measure of the number of monolayers of H in the bulk.

Figure 11 shows that the bulk hydrogen feature is also observable in the HREELS with a unique frequency of 800 cm^{-1}. While EELS is typically thought of as a surface technique, the mean free path of the low energy electrons into the metal is long enough that the vibration of H atoms residing in the bulk can also be detected.[27]
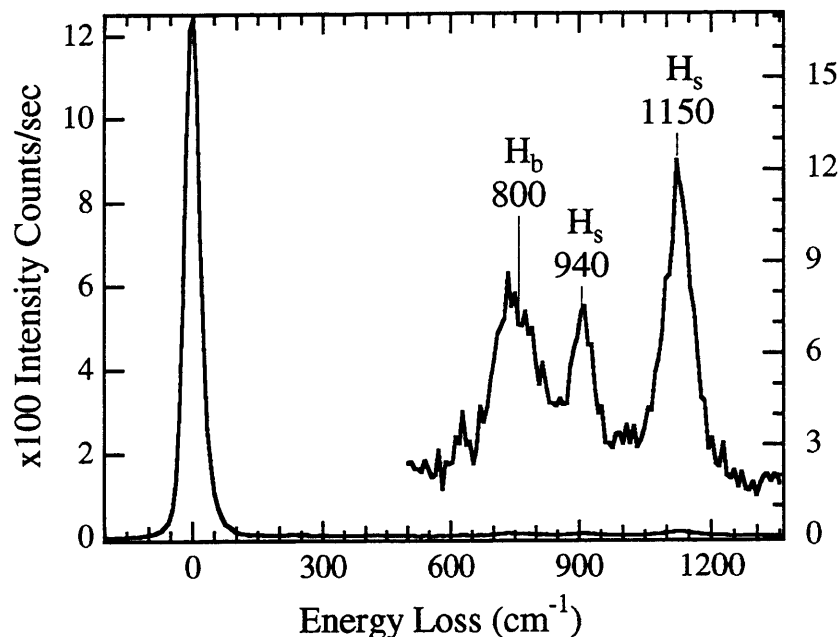
Figure 11 HREEL spectrum of bulk and surface hydrogen formed from exposure to $2x10^{-5}$ torr H_2 for 2 min with front hydrogen atom source filament on. 1.7 ML of H in the bulk and 1 ML of H on the surface. Spectrum taken at 80 K, at 12° off specular with 6.5 eV electrons, ΔE_{fwhm} 41 cm^{-1}.

Although bulk H is readily formed by exposure of nickel to gas phase H atoms, gas phase H atoms also adsorb on the surface. In order to probe the reactivity of bulk H, it is highly desirable to have *only* bulk H in the system. From the TDS result, it can be seen that it is not possible to remove only the surface H thermally, because bulk H desorbs at lower temperatures. The solution to this problem is to use a molecular beam technique called collision induced recombinative desorption.[71] Xenon atoms with a high translational energy are directed at the crystal with a 40° angle of incidence, crash into the lattice, and jostle the Ni atoms, causing the H on the surface to recombine and desorb. The bulk H atoms are not affected by this process. In this way, a clean surface with H in the bulk is produced.

6.3 *Gas Phase Hydrogen Atoms*

The production of gas phase H atoms has been described in the previous section, and in

the section on the hydrogen atom source filament. In experiments in which adsorbed

hydrocarbons are exposed to gas phase H atoms, the front H atom filament is placed 0.25"

in front of the crystal and is quickly heated to 1600 K by applying 3V across the filament with

5×10^{-6} Torr of H_2 in the chamber. The filament radiatively heats the crystal during the H atom

exposure.

One possible ambiguity with this method is that it is impossible to expose the crystal to

pure gas phase H atoms. As depicted in figure 7, exposure of the surface to gas phase H

atoms also results in exposure to H_2. However, because these two species are predicted to

have very different reactivities, due to their energetics, their coexistence should not create any

ambiguity in gas phase H chemistry. The large energy of the gas phase H atoms with 52

kcal/mol of potential energy and 4.8 kcal/mol of translational energy predicts that the gas

phase H atoms are most likely responsible for the observed reactivity. Comparison of the

observed chemistry with the filament on to the filament off will eliminate any doubt as to the

responsible reactive species.

In the reactions of hydrocarbons with surface H or bulk H to be described, an

integrated TD signal will yield the amount of H reacting in a system. It is desirable to also

have a measurement of the amount of gas phase H atoms reacting in a system. Unlike bulk H

and surface H, a TDS integral will not measure the amount of gas phase H in a system. Gas

phase H atoms are so reactive they abstract H from the surface[31,72,73] and from hydrocarbons

on the surface.[35,44] Gas phase H abstraction events will not be included in a TDS

measurement. For this reason, a measurement of the flux of gas phase H atoms is the only

reliable method to determine the amount of a gas phase H atom exposure.

6.4 H atom flux determination

The measurement of the gas phase H atom flux requires particular care. It is not

possible to measure directly H atoms with the mass spectometer because the H_2 molecules

crack to H atoms in the ionizer, producing an enormous background. The crux of this

measurement is to quantify the number of H and D atoms on the surface after exposure of a

partially covered D surface to H atoms. The incoming gas phase H atom either adsorbs on the

surface or abstracts a D atom from the surface. If an impinging H atom does not undergo

either of these two processes it is invisible. This measurement is therefore a lower limit on the

H atom flux. The assumption that every gas phase H atom either sticks or abstracts is

supported by the measured sticking coefficient for H on Ni(111) which is 1.0^{31} and the

measured probability of 0.25 for incoming H atoms to abstract a H atom from the nickel

surface to make gas phase H_2.[31,74] This method has been used by other researchers on different

metal surfaces.[31,73]

The initial coverage of adsorbed D atoms has two important purposes. First, it allows

abstraction to be measured easily. Loss of D coverage clearly arises from an abstraction event.

The initial coverage of D has a second unintended beneficial role. It prevents the background

H_2 from contributing to the adsorbed H signal. The adsorption probability of H_2 is 0.05 on a

clean surface, decreases by half at 0.15 ML, and decreases by an order of magnitude at 0.5 ML
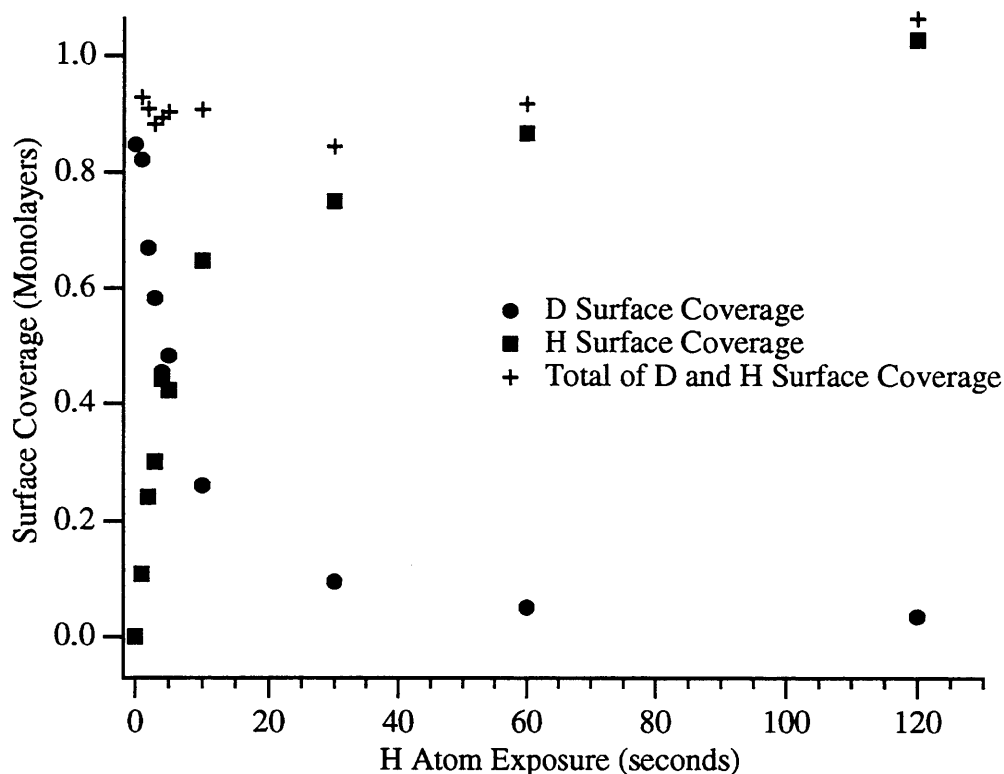
Figure 12 Hydrogen addition and abstraction from an initial coverage of 0.8
ML D at a surface temperature of 265 K.
● Integrated thermal desorption signal of D on the surface
■ Integrated thermal desorption signal of H on the surface
+ Sum of H and D integrated signals, total coverage of surface

of adsorbed H. [14,75] By starting with a partial monolayer of adsorbed D, and by using very

short gas phase H atoms exposures, the further adsorption of surface H from H_2 is vanishingly

small.

The measurement is done by preparing an initial coverage of 0.8 ML of deuterium. The

crystal is then exposed to H atoms for a specific time, on the order of seconds. After each

exposure, thermal desorption spectra are measured for m/e=2 (H_2), m/e=3 (HD) and m/e=4

(D_2). The TDS data are integrated and the total hydrogen and deuterium signals are generated

by adding half of the integrated HD signal to either the H_2 or D_2 integrated signal, respectively.

The H and D surface coverage as a function of time of gas phase H atom exposure is shown in

Figure 12. The decline in deuterium coverage is the result of H atom abstraction and the

increase in H coverage is the result of H atom adsorption. The initial slope of each of these

curves yields the initial rate of H abstraction and H adsorption. Figure 13a shows an example

of the lines fit to the data used to measure the initial rate of H abstraction and addition. The

total number of gas phase H atoms reacting with the surface is the number of H atoms

observed to abstract plus the number of H atoms that adsorb on the surface. Therefore, the

flux of gas phase H atoms on the surface at 265 K is the sum of the rate for abstraction plus

the rate for addition, 0.204 as shown in Table 2.

D coverage & crystal temp.	0.5 ML D 120 K	0.8 ML D 120 K	0.8 ML D 265 K
H addition rate (ML/sec)	0.150	0.080	0.096
D abstraction rate (ML/sec)	0.067	0.089	0.108
Total H flux (ML/sec)	0.217	0.169	0.204

Table 2 Adsorption rate, abstraction rate and the total H atom flux in ML/sec for three conditions of initial coverage and crystal temperature during H atom exposure.

The data for the total surface coverage in Figure 12 demonstrate why it is critical to

measure abstraction events. The total surface coverage is almost constant for H atom

exposures of many seconds and only begins to increase at long time exposures of 120 seconds,

which would indicate that gas phase H atoms add slowly to the surface. Comparing this

(a) 0.8 ML Deuterium   (b) 0.5 ML Deuterium
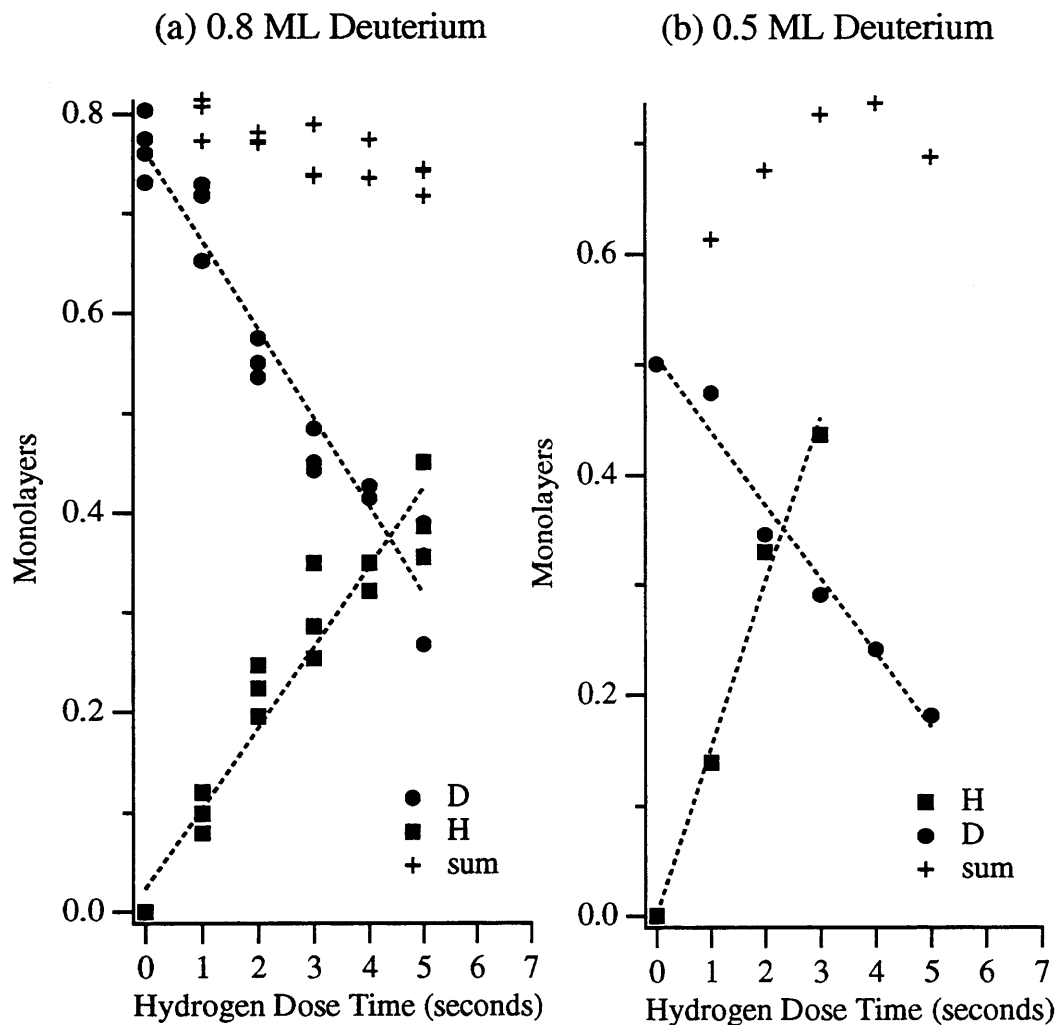
Figure 13 Hydrogen addition and abstraction at a surface temperature of 120 K at an initial coverage of (a) 0.8 ML and (b) 0.5 ML D, including H adsorption and D abstraction rate measurement fits.

● Integrated thermal desorption signal of D on the surface

■ Integrated thermal desorption of H on the surface

+ Sum of H and D integrated signals, total coverage of surface

observation with the rapid decrease of the D coverage shows that abstraction of surface D is indeed an important process to consider.

Two measurements of the H atom addition rate and D abstraction rate were done at a crystal temperature of 120 K with initial D coverages of 0.8 and 0.5 ML, as shown in Figure

13a and 13b, respectively. Comparison of the results for these two coverages probes the coverage changes that occur during an experiment. Differences of close to a factor of two are observed in the individual H adsorption rate and D abstraction rate. The trends in adsorption and abstraction are intuitive. A higher adsorption rate is observed when there is less D on the surface, and with more D on the surface, there is a higher abstraction rate. These differences cancel to some extent to give total H flux values of 0.217 to 0.169 ML/sec from the initial D coverages of 0.5 and 0.8 ML. These values are within 20-30% of each other. This flux determination is a lower limit, since any H which does not add or abstract is not measured. The goal of this flux determination is to have an approximation of the number of gas phase H atoms are involved in a reaction for comparison with the number of surface H and bulk H atoms. Knowing the number of H atoms to within 30% is acceptable.

The data displayed in Figure 12 are for an initial D coverage of 0.8 ML and a surface temperature of 265 K during the H atoms exposure. This second temperature was measured to gauge the surface temperature dependence of this H flux because gas phase H atoms are used from 60 to 300 K. The similarity between the H atom flux values with surface temperature confirms that H addition and D abstraction are not strongly surface temperature dependent.

[1] K. Christmann, O. Schober, G. Ertl and M. Neumann, J. Chem. Phys. **60**, 4528 (1974)

[2] *Handbook of Chemistry and Physics*, R. West, editor, Chemical Rubber Co. (1977)

[3] R.B. McLellan and W.A. Oats, Acta Metallurgica **21**, 181 (1973)

[4] F.G. Jones and R.D. Pehlke, Metal. Trans. **2**, 2655 (1971)

[5] G. Alefeld and J. Völkl, *Hydrogen in Metals I and II*, Springer-Verlag (1978)

[6] 1 ML = 1.9×10^{15} atom/cm^2

[7] K. Christmann, R.J. Behm, G. Ertl, M.A. Van Hove and W.H. Weinberg, J. Chem. Phys. **70**, 4168 (1979)

[8] Q.Y. Yang, Ph.D. Thesis, Massachusetts Institute of Technology (1989)

[9] K. Mortensen, F. Besenbacher, I. Stensgaard and W.R. Wampler, Surf. Sci. **205**, 433 (1988)

[10] S.E Wonchoba and D.G. Truhlar, Phys. Rev. B **53**, 11222 (1996)

[11] R. Baer, Y. Zeiri and R. Kosloff, Phys. Rev. B **55**, 10952 (1997)

[12] A. Winkler and K.D. Rendulic, Surf. Sci. **118**, 19 (1982)

[13] S_0 is sensitive to defect concentration H.P. Steinrück, K.D. Rendulic and A. Winkler, Surf. Sci. **154**, 99 (1985)

[14] H.J. Robota, W. Vielhaber, M.C. Lin, J. Segner and G. Ertl, Surf. Sci. **155**, 101 (1985)

[15] K.D. Rendulic, A. Winkler and H.P. Steinrück, Surf. Sci. **185**, 469 (1987)

[16] A. Winkler and K.D. Rendulic, Intnl. Reviews in Phys. Chem. **11**, 101 (1992)

[17] H.P. Steinrück, K.D. Rendulic and A. Winkler, Surf. Sci. **154**, 99 (1985)

[18] G. Comsa, R. David and B-J Schumacher, Surf. Sci. **85**, 45 (1979)

[19] K.D. Rendulic, G. Anger and A. Winkler, Surf. Sci. **208**, 404 (1989)

[20] T-S. Lin and R.Gomer, Surf. Sci. **255**, 41 (1991)

[21] S.P. Daley, A.L. Utz, T.R. Trautman and S.T. Ceyer, J. Am. Chem. Soc. **116**, 6001 (1994)

[22] S.P. Daley, Ph.D. Thesis, Massachusetts Institute of Technology (1994)

[23] W. Van Willigen, Phys. Lett. **28A**, 80 (1969)

[24] J.I. Macnab and R.B. Anderson, J. Catal. **29**, 338 (1973)

[25] I. Nicolau and R.B. Anderson, J. Catal. **68**, 339 (1981)

[26] P. Fouilloux, Appl. Catal. **8**, 1 (1983)

[27] A.D. Johnson, K.L. Maynard, S.P. Daley, Q.Y. Yang and S.T. Ceyer, Phys. Rev. Lett. **67**, 927 (1991)

[28] K.J. Maynard, A.D. Johnson, S.P. Daley, and S.T. Ceyer,. Faraday Discuss. Chem. Soc. **91**, 437 (1991).

[29] A.D. Johnson, Ph.D. Thesis, Massachusetts Institute of Technology (1991)

[30] H. Premm, H. Pölzl and A. Winkler, Surf. Sci. **401**, L444 (1998)

[31] G.Eilmsteiner, W. Walkner, and A. Winkler, Surf. Sci. **352-354**, 263 (1996)

[32] P. Deák, J. Giber and H. Oechsner, Surf. Sci. **250**, 187 (1991)

[33] A. Horn, J. Biener, A. Schenk, C. Lutterloh, and J. Küppers, Surf. Sci. **331-333**, 178 (1995)

[34] J. Biener, U.A. Schubert, A. Schenk, B. Winter, C. Lutterloh and J. Küppers, J. Chem. Phys. **99**, 3125 (1993)

[35] A. Horn, A. Schenk, J. Biener, B. Winter, C. Lutterloh, M. Wittmann and J. Küppers, Chem. Phys. Lett. **231**, 193 (1994)

[36] K. Hiraoka, K. Matsunaga, T. Shoda and H. Takimoto, Chem. Phys. Lett. **197**, 292 (1992)

[37] R.D. Gonzalez and R.J. Kokes, J. Phys. Chem. **70**, 2535 (1966)

[38] W.J. Mitchell, J. Xie, T.A. Jachimowski, and W.H. Weinberg, J. Am. Chem. Soc. **117**, 2606 (1995)

[39] J. Biener, C. Lutterloh, A. Schenk, K. Pöhlmann and J. Küppers, Surf. Sci. **365**, 255 (1996)

[40] K-A Son and J.L. Gland, J. Am. Chem. Soc. **118**, 10505 (1996)

[41] K-A Son, M. Mavrikakis and J.L. Gland, J. Phys. Chem. **99**,6270 (1995)

[42] M. Xi and B.E. Bent, J. Vac. Sci. Technol. B **10**, 2440 (1992)

[43] J-Y. Kim, Y-S. Park, and J. Lee, Surf. Sci **357-358**, 733 (1996)

[44] M. Xi and B.E. Bent, J. Phys. Chem. **97**, 4167 (1993)

[45] S.L. Tang, Ph.D. Thesis, Massachusetts Institute of Technology (1991)

[46] M.B. Lee, Ph.D. Thesis, Massachusetts Institute of Technology (1985)

[47] S.T. Ceyer, D.J. Gladstone, M. McGonigal, and M.T. Schulberg in *Physical Methods of Chemistry*, B.W. Rossiter and R.C. Baetzold, eds, Wiley (1993)

[48] J.D. Beckerle, Ph.D. Thesis, Massachusetts Institute of Technology (1988)

[49] J. Cazaux, Surf. Sci. **140**, 85 (1984)

[50] M. Hock and J. Kuppers, Surf. Sci. **188**, 575 (1987)

[51] R.E.Smalley, L. Wharton and D.H. Levy, Acct. Chem Res. **10**, 139 (1977)

[52] P.B. Needham, T.J. Driscoll, and N.G. Rao, Appl. Phys. Lett. **21**, 502 (1972)

[53]*Practical Surface Analysis Volume I Auger and X-Ray Photoelectron Spectroscopy*, D. Briggs and M.P. Seah, eds, John-Wiley and Sons (1990)

[54] L. Hammer, T. Hertlein and K Müller, Surf. Sci. **178**, 693 (1986)

[55] In the typical measurement technique measured signal $\propto n_i$

P.B. Needham, T.J. Driscoll, and N.G. Rao, Appl. Phys. Lett. **21**, 502 (1972)

[56] C.J. Powell and M.P. Seah, J. Vac. Sci. Technol. A **8**, 735 (1990)

[57] R.L. Summers, NASA Technical Note TND-5285 (1969)

[58] *Atlas of Mass Spectral Data*, E. Stehagen, S Abrahamsson and F.W. McLafferty, eds, Interscience Publishers (1969)

[59] H. Chatham, D. Hils, R. Robertson, and A. Gallagher, J. Chem. Phys. **81**, 1770 (1984)

[60] N. Duric, I. Cadez, and M. Kurepa, Intl. J. Mass Spec. Ion Proc. **108**, R1 (1991)

[61] J.A. Beran and L. Kevan, J. Phys. Chem **73**, 3866 (1970)

[62] V.Grill, G. Walder, P. Scheier, M. Kurdel, and T.D. Märk, Intl. J. Mass Spec. Ion Proc. **129**, 31 (1993)

[63] F.W. Lampe, J.L. Franklin and F.H. Field, J. Am. Chem. Soc. **79**, 6129 (1957)

[64] D. Rapp and P. Englander-Golder, J. Chem. Phys **43**, 1464 (1965)

[65] C. Tian and C.R. Vidal, Chem. Phys. Letters **288**, 499 (1998)

[66] A. Gaudin, R. Hagemann, J. Chim. Phys. **63**, 917 (1966)

[67] J.T. Tate and P.T. Smith, Phys. Rev. **39**, 270 (1932)

[68] H.C. Straub, P. Renault, B.G. Lindsay, K.A. Smith and R.F. Stebbings, Phys. Rev. A. **52**, 1115 (1995)

[69] H. Ibach and D.L. Mills, *Electron Energy Loss Spectroscopy and Surface Vibrations*, Academic Press (1982)

[70] P. Klimesch and M. Henzler, Surf. Sci. **90**, 57 (1979)

[71] A.D. Johnson, S.P. Daley, A.L. Utz and S.T. Ceyer, Science **257**, 223 (1992)

[72] C.T. Rettner, Phys. Rev. Lett. **69**, 383 (1992)

[73] W.H. Weinberg, Acc. Chem. Res. **29**, 479 (1996)

[74] Th. Kammler, S. Wehner and J. Küppers, Surf. Sci. **339**, 125 (1995)

[75] A. Winkler, and K.D. Rendulic, Surf. Sci. **118**, 19 (1982)

Chapter 3

Surface Hydrogen Reactivity

with Adsorbed C_2H_2

1 Introduction

Surface bound hydrogen is the most easily formed and the most common reactant of the three hydrogen species introduced in Chapter 2. Surface bound H has been designated as the reactant in many catalytic hydrocarbon reactions under high pressure conditions, such as the hydrogenation of adsorbed acetylene and ethylene, even though both surface H and bulk H are present. This chapter focuses on ultra-high vacuum experiments designed to probe the reactions of surface H with adsorbed acetylene in depth. The role of surface bound H in hydrogenation of the two hydrocarbons is clearly distinguishable from the role of bulk H which is discussed in Chapter 4.

2 Surface Hydrogen Reactions with Ethylene

Hydrogenation of hydrocarbons is done on a very large scale in industry. Historically, surface H has been considered the active H species in hydrogenation. The model system used to study hydrogenation is the smallest unsaturated hydrocarbon, ethylene. Horiuti and Polanyi proposed a mechanism for ethylene hydrogenation in 1934[1,2] in which the surface H atoms add in a step-wise fashion to adsorbed ethylene. This mechanism is known as the Horiuti-Polanyi mechanism, and is commonly put forth as the method for hydrocarbon hydrogenation on transition metal surfaces.[3] However, the body of work done under ultra-high vacuum single collision conditions does not support this mechanism of step-wise addition of surface H to ethylene. A brief description of previous work on the hydrogenation of ethylene on Ni(111) from our group follows, after which experiments carried out on other nickel faces are described and are found to be consistent with our findings.

The simplest experiment to test the Horiuti-Polanyi mechanism is to coadsorb surface H with ethylene at low temperature and then to look for ethane as the crystal temperature is raised to activate the reaction. In Figure 1, the partial pressure of molecules desorbing from a surface of coadsorbed surface H and C_2H_4 is shown as a function of the crystal temperature. It is quite apparent that no ethane is produced. If ethane were produced, there would be no question that it would be observed in the thermal desorption spectrum since it is very weakly bound to the surface. Figure 2 shows the results of a similar experiment with H absorbed in the bulk and ethylene adsorbed on the surface. When the crystal is heated, the H atoms move out of the bulk. There is clear evidence for ethane production at the same temperature that the
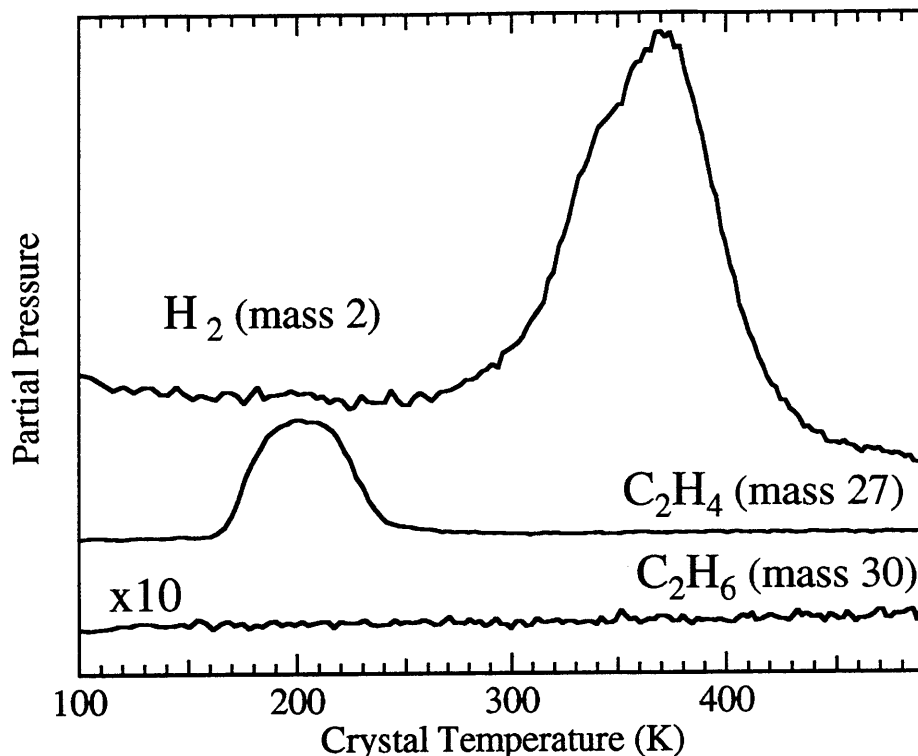
Figure 1 A thermal desorption spectrum of 0.10 ML C_2H_4 coadsorbed with 0.7 ML surface H at a crystal temperature of 80 K. Corrected for C^{13} and cracking patterns.

bulk H atoms begin to recombine and desorb from the surface. Different ratios of ethylene to ethane products are achieved with different ratios of bulk H to adsorbed ethylene. More detail on these reactions is available,[4,5] but it is clear that the reactive species in ethylene hydrogenation is not surface H, but bulk H.

The hydrogenation of ethylene on other nickel surfaces has been studied with results that are consistent with our observation on Ni(111). Ethylene hydrogenation on Ni(100) has been studied by Zaera.[6] The (100) face of nickel is similar to the (111) face in that it is considered flat, but the hollow sites on the surface are four-fold sites instead of three-fold sites. The individual nickel atoms are not as closely packed, and these four-fold sites are larger than
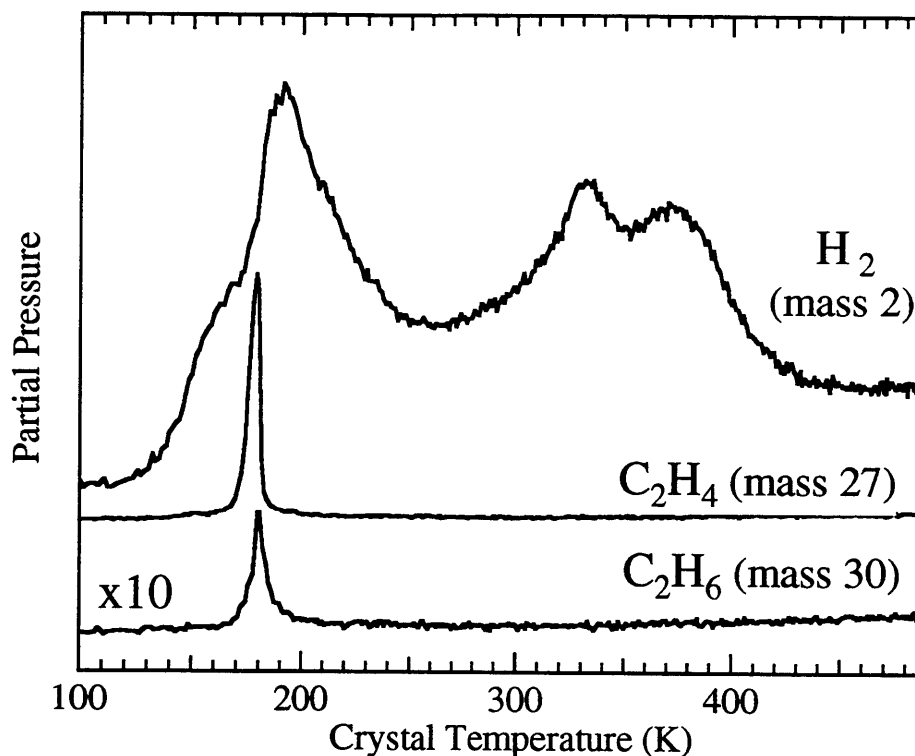
Figure 2 A thermal desorption spectrum of 2 ML hydrogen in the bulk and 0.25 ML of C_2H_4 adsorbed in the center of the crystal at 80 K. Corrected for C^{13} and cracking patterns.

the three-fold ones. In this study, the ethylene and H surface are coadsorbed using two different procedures: hydrogen is adsorbed on the surface followed by exposure to ethylene, or ethylene is adsorbed on the surface followed by exposure to H_2. In both cases the proportions of surface H and ethylene were the same. No ethane is observed in thermal desorption scans when hydrogen adsorption follows ethylene adsorption, consistent with the picture that surface H does not react with ethylene from a side-on approach. However, when the ethylene is adsorbed on top of surface H a very small ethane signal is observed. An argument is made that preadsorbed hydrogen weakens the ethylene surface bonds, thereby making the C_2H_4 more reactive. The evidence of this weakening is a slight lowering in the

temperature of ethylene desorption, as well as a tenuous assignment of small shifts in C_2H_4 loss

features in an HREEL spectra. The extremely small ethane production can almost all be

explained by contamination of the ethane signal by the natural abundance of $^{13}C_2H_4$ and the

possibility of H/D exchange. If any ethane is actually produced in this experiment, then given

the modified geometry of ethylene adsorbed on top of surface H, the H may add to ethylene

from below the ethylene molecule.

Ethylene hydrogenation has also been studied on the Ni(110) surface.[7] This surface

differs from the two flat surfaces in that it is corrugated with peaks and troughs, and its

saturation coverage of surface hydrogen is 1.5 ML. When its surface H coverage exceeds 1

ML, a new H_2 desorption feature is observed at 230 K which is reminiscent of bulk hydrogen

recombination and desorption.[8] On this surface, no ethane is observed in thermal desorption

measurements of coadsorbed C_2H_4 and surface H for H coverages less than 1 ML. However,

when the H coverage is above 1 ML, ethane is observed to desorb at 230 K, the precise

temperature of the new hydrogen feature. This leads to our conclusion that this new bulk-like

H is responsible for ethane formation. These Ni(110) results are then consistent with our

findings that surface H is not an active species in ethylene hydrogenation, but hydrogen

approaching from below does hydrogenate ethylene. Neither of these experiments had a

method for detecting bulk H atoms.

2.1 *What is Known About the Mechanism of Hydrogen Addition to Unsaturated*

Hydrocarbons?

Previous work of ethylene hydrogenation on Ni(111) demonstrates that surface H will

not add to adsorbed ethylene, which lies with its molecular plane parallel to the surface, and

forms two σ bonds to the Ni(111) surface as the carbon orbitals rehydridizes.[10] But H

emerging from the bulk will react with adsorbed C_2H_4 to form gas phase C_2H_6. This stark

contrast in reactivity should provide clues as to why hydrogen atoms successfully add to

hydrocarbons in some instances, but are totally unreactive in others. In the previous chapter, a

number of differences between surface and bulk H atoms were discussed. These differences lie

chiefly in the geometry of approach of the two hydrogen species to the hydrocarbons and their

relative energies.

The geometry differences that create different directions of approach for the bulk and

surface H atoms to the hydrocarbons are not insignificant, and lead to different reaction

barriers. Since the plane of an ethylene molecule is approximately parallel to the plane of the

surface,[9,10] a surface H atom has almost a coplanar approach to the ethylene molecule, thereby

encountering steric hindrance from the C-H bond as it tries to reach the carbon atom. The

bulk H atom does not encounter this steric hindrance when it emerges out of a three fold

hollow site beneath the ethylene molecule. Rather, the bulk H atom has direct access to the

rehybridized π orbital which provides an electron rich reaction pathway. The different

approaches result in different energy barriers for addition of the H atom to the hydrocarbon.

Differences in the energy barrier for H addition to ethylene with direction of approach

are known for the complementary gas phase reaction. The experimentally measured barrier is

2.1 kcal/mol.[11] Theoretical calculations conclude that the optimum geometry for the addition

of a gas phase H atom to an ethylene molecule is along the direction of the π orbital

perpendicular to the plane of the ethylene molecule,[12,13,14] and reproduce the experimental

barrier to within a factor of two.[12,15,16] The barrier for hydrogen addition along the side-on

approach is calculated to be on the order of 15 kcal/mol.[14,17] The dependence of the barrier for

addition on the direction of approach of the H atoms to the hydrocarbon captures the essence

of the difference between bulk H and surface H addition to adsorbed ethylene. These two

directions of approach are depicted in Figure 3. The schematic of a gas phase ethylene

molecule represents a simplification of the orbitals of adsorbed ethylene, but nevertheless, the

steric factors that lead to the significant difference in the barriers are still present for adsorbed

ethylene, as well as the favorable access to the electron rich π orbitals, with which a new bond

is formed.
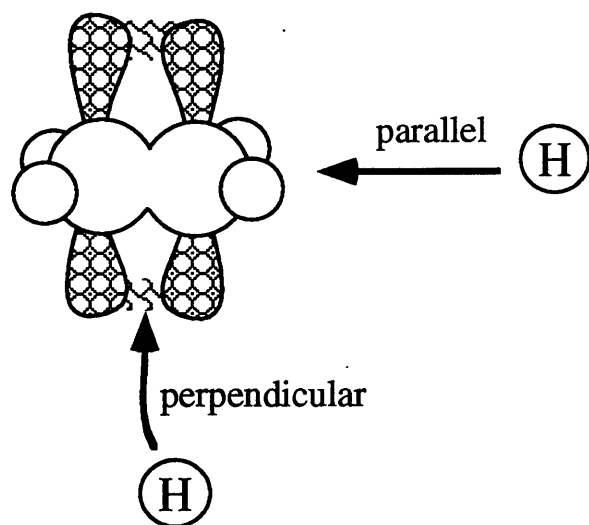
Figure 3 A pictorial representation of two possible approaches of H atoms to an ethylene molecule.

Besides the difference in the energy barrier for the addition of surface and bulk H to ethylene, there is also a stark difference in the relative energies of the two species of H atoms that further explains their distinct reactivity, the energetics are described in more detail in Chapter 2. At 220 K, the temperature at which ethylene starts to decompose and desorb, the surface H atoms have an average energy of below 1 kcal/mol. However, the bulk H atoms emerge with as much as 24 kcal/mol of potential energy. So there are two major differences between bulk and surface adsorbed H. The geometry of approach most likely creates a higher energy barrier for surface H addition to ethylene, and bulk H atoms have much more energy available to overcome the barrier to reaction than surface H atoms.

2.2 *Motivation to Study Acetylene + Surface H Reaction*

Considering the framework that has been constructed to explain the different reactivities of surface and bulk H with ethylene, the most important difference between ethylene and acetylene is that acetylene has two mutually perpendicular π orbitals. From a very simple view of hydrocarbon adsorption, depicted in Figure 4, the fact that acetylene has two π orbitals means that one π orbital is in the plane of the surface. The calculations and experiments for the addition of H to ethylene demonstrate that hydrogen adds most effectively along the direction of the π orbital. The significant π character of adsorbed acetylene in the surface plane leads to the proposal that surface H will react with adsorbed acetylene.

Certainly, this view of acetylene bonding to the Ni(111) surface is simplistic and possibly naive. While experiments have been done in an attempt to probe the bonding of acetylene to the surface, a thorough and consistent picture of the structure, hybridization, and
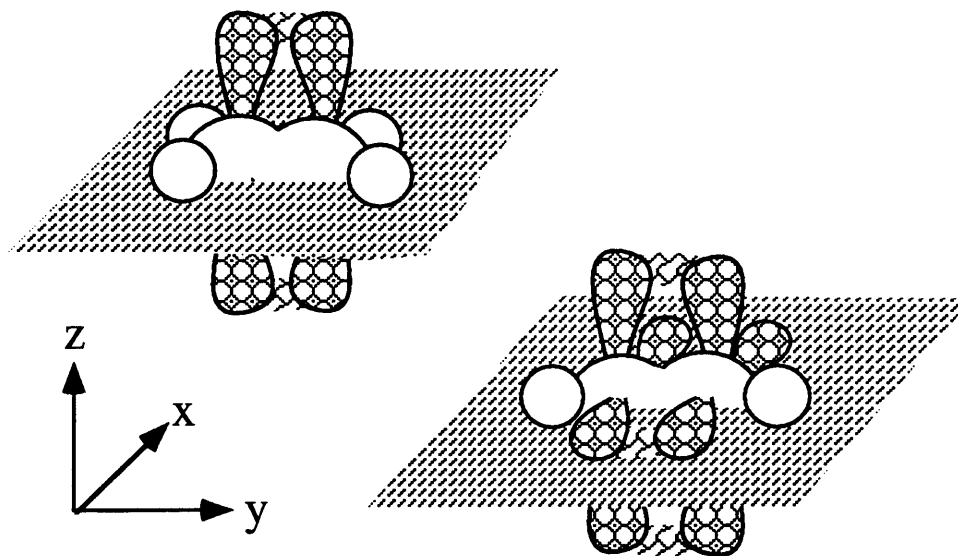
Figure 4 A pictorial representation of an adsorbed ethylene and acetylene molecule to show the orientation of the π orbitals.

the occupation of molecular orbitals of bound acetylene is not yet available. A brief overview of proposals for acetylene bonding follows, with measurements that support π orbital character in the surface plane highlighted.

Numerous techniques have been applied to determine the structure (bond lengths and bond angles), hybridization and occupation of molecular orbitals of adsorbed acetylene. However, for our prediction of acetylene reactivity with surface H, the molecular orbital picture provided by UV photoelectron spectroscopy (PES) is the most vital. The first of these studies was done by Demuth in 1974.[18,19] The model for bonding between acetylene and the Ni(111) surface that emerged was a π-d type interaction. This model is well known in inorganic chemistry as the Dewar-Chatt-Duncansen (DCD) bonding model[20,21] in which the electron density from the π bond of the hydrocarbon is transferred to vacant d orbitals of the metal, and then the filled metal d orbitals donate intensity to the π^* orbital of the hydrocarbon.

The acetylene is bound primarily though the π orbitals and there is no significant rehybridization of the carbon atoms that would be expected for the other possible bonding model, di-σ bonding. In this study, the two different π orbitals of acetylene are not separately identified.

Demuth revisited the issue of acetylene bonding to Ni after HREELS suggested that acetylene was strongly hydridized and di-σ bonded to the surface.[22,23] In this later UV photoelectron spectroscopy work, done with a new high-intensity light source, he identified a C(2s) state that is strongly shifted upon adsorption. A π orbital shift of similar magnitude to the C(2s) shift is observed as before, but this shifted π orbital is now considered to have the main contributions from the $2p_z$ carbon atomic orbital, with the $2p_x$ and $2p_y$ atomic orbitals being described as mainly contributing to the σ_{CC} and σ_{CH} molecular orbitals. All orbital directions are defined in Figure 4, with a p_x, p_y, or p_z orbital having lobes parallel to the x, y, or z axis, respectively. The σ_{CC} and σ_{CH} orbitals are not observed to shift strongly upon adsorption. This observation of a weakly bonding π orbital in the plane of the molecule supports the prediction that surface H will react with adsorbed acetylene. There are two possible explanations given by Demuth for the strong shift in the C(2s) and $\pi(p_z)$ states. The first possibility is an orbital-dependent initial-state potential shifts, due to an adsorption surface barrier which is expected to lead to shifts in orbitals perpendicular to the molecular plane, specifically the $C(2p_z)$ and C(2s) derived orbitals. The second possible explanation of these shifts is a rehydridization of the C(2s) and $C(2p_z)$ orbitals during surface bonding. Comparison of the measured relative molecular orbital shifts with those calculated for a range of different

adsorbed structures of acetylene, from a π bonded undistorted molecule to a rehybridized and

highly distorted molecule, are found to agree best with calculations of acetylene bound to a

single Be atom. The precise geometry of acetylene in the Be complex is not known.

However, it is described as strongly distorted, with CCH bond angles of ~125°, a C-C bond

distance of 1.38-1.43 Å and C hydridization of roughly $sp^{2.5}$. This hydridization agrees with

the vibrational spectroscopy of C_2H_2 adsorbed on Ni(111).[24]

Interpreting photoelectron spectroscopy is a challenge. In these studies, molecular

orbital assignments which lead to molecular orbital shifts are based on comparison with gas

phase molecules. When acetylene adsorbs on the surface, *all* of its molecular orbital energies

shift from their values in the gas phase. Rather, it is relative shifts of the molecular orbitals that

determine which molecular orbitals are involved in bonding. In order to predict accurately a

particular bonding geometry, molecular orbital calculations are made in order to predict

accurately the relative energy spacings for distinct geometries that result from a particular

hybridization. Other models and calculations have been put forth to explain the PES data and

the bonding of acetylene. Felter and Weinberg[25] present an approach for determining the

adsorption geometry that integrates both PES and EELS data. They conclude that acetylene is

sp^3 rehybridized, with CCH bond angles of ~109° and a C-C bond distance of 1.5 to 1.6 Å.

Presumably acetylene uses the extra sp^3 orbital to form σ bonds to the Ni(111) surface. A

theoretical study by Ohno and von Niessen[26] points out an incorrect approximation made by

Demuth in all his work,[18,19,22,23,24] and come to a conclusion that the π orbital is the most

strongly perturbed orbital and that acetylene is π bonded to the surface. This conclusion is

based on comparison of their calculation with angularly resolved PES of acetylene on

Ni(110),[27] not with Demuth's data. They also note that to fully understand bonding on

Ni(111), an angle-dependent PES study must be done.

This type of angle dependent study has been completed for acetylene adsorption on

Ni(110) [27] by Weinelt and coworkers. They conclude that acetylene is most likely bound in a

trough geometry, with strong interactions to the Ni atoms on either side of the trough. Even

though the structure of this Ni surface is different from that of Ni(111), some of their

observations are relevant to this study. One of these observations stems from the advantage of

angle-resolved PES. In angle-resolved PES, it is possible to distinguish the different π orbitals

because of their different orientations in space. The two π_u orbitals are separated by 1.5 eV

and are derived from the p_x orbital parallel to the surface and the p_z orbital which is

perpendicular to the surface. The p_z derived orbital is the most strongly shifted with its energy

level below the substrate d-band, indicating a strong bond. The p_x orbital also aids in bonding,

but it is not as strongly shifted as the p_z orbital.

A synthesis of the idea of charge transfer consistent with the DCD model and

rehybridization to yield σ bonding is made in a theoretical study using density functional theory

by Fahmi and van Santen.[28] They identify what they call a μ-bridge configuration for acetylene

adsorption on Ni(111), with a CCH bond angles of ~120°, a C-C bond distance of 1.2 Å, in

which the carbon atoms are directly above three fold sites, with each carbon atom interacting

with three Ni atoms. This configuration is consistent with the geometry determined for

adsorbed acetylene on Ni(111) using photoelectron diffraction.[29] In characterizing the bond,

the authors calculate charge transfer from the π orbitals of C_2H_2 to the metal, as well as from

the metal into the π^* orbitals. This charge transfer is the essence of the DCD model.

However, they further argue that charge transfer always occurs, in either a di-σ (with each

carbon atom interacting with a single Ni atom) or μ-bridge adsorbate geometry, leading to the

rehybridization of carbon towards sp^3 in either bonding geometry. In the initial work by

Demuth,[18,19] charge transfer between the hydrocarbon π orbitals and d metal orbitals as

described in the DCD model is considered mutually exclusive from carbon rehybridization.

This study may hint at the true nature of the acetylene-Ni bond, which involves net charge

transfer as well as carbon hybridization changes.

It is clear that the bonding of acetylene to the surface is not fully understood. The PES

studies do suggest that the acetylene π orbital derived from the p_z atomic orbitals participates

fully in bonding while the π orbital derived from the atomic p_x orbitals participate much less.

Since the π orbital derived from the atomic p_x orbitals lies in the surface plane, the residual π

character not used in acetylene bonding is available for surface H atom addition. This residual

π character is expected to lead to a much lower energy barrier for C-H bond formation than

exists in the reaction of ethylene with surface H.

3 Experimental Probes of Surface H and Acetylene Reactions

3.1 *Acetylene + H(s) Gas Phase Products*

The reactivity of surface H with adsorbed acetylene is probed initially by observing the

gas phase products as the crystal is heated. The experimental procedure is as follows. Using

the molecular beam, 0.13 ML of acetylene is adsorbed on the surface held at 80 K. The
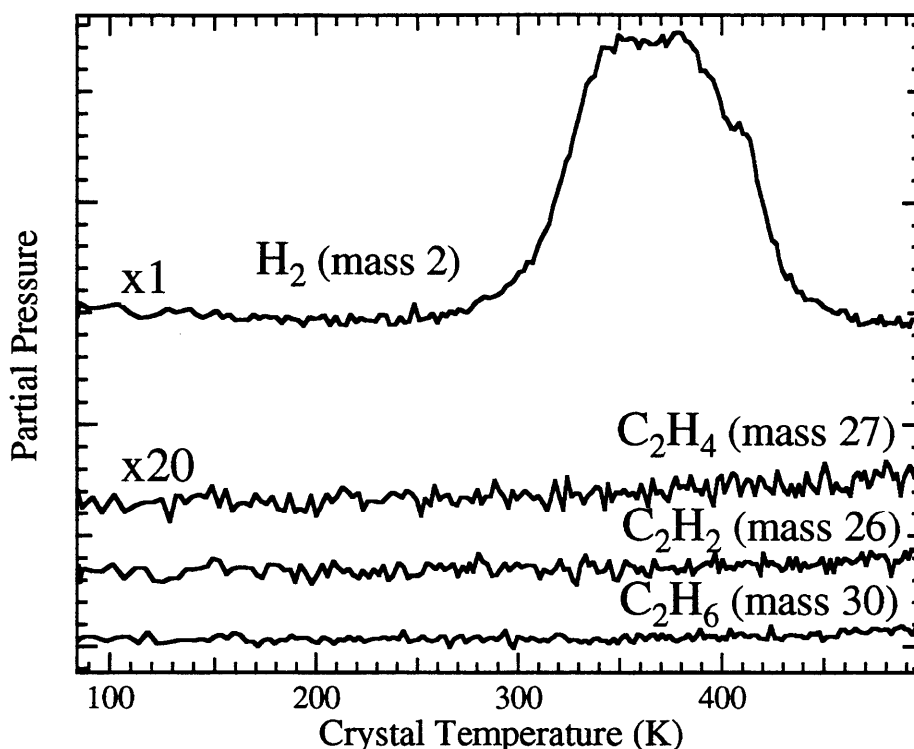
Figure 5 A thermal desorption spectrum of 0.13 ML C_2H_2 coadsorbed with 0.7 ML surface H at a crystal temperature of 80 K. Crystal heated at 2 K/s. Partial pressure of different molecules versus crystal temperature is shown. With H_2 monitored as m/e=2 signal, C_2H_4 as m/e=27 signal, C_2H_2 as m/e=26 signal, and C_2H_6 as m/e=30 signal.

remaining sites are then saturated with surface bound H by exposure of the crystal at 80 K to

3×10^{-5} Torr H_2 for 5 min, yielding a maximum coadsorbed surface H coverage of 0.66 ML.

The partial pressures at m/e=2, 26, 27 and 30 are then monitored as the crystal temperature is

raised at 2 K/s. The traces of partial pressure versus crystal temperature are shown in Figure

5. As is apparent, no gas phase hydrogenation products are observed. If the ratio of acetylene

coverage to surface bound hydrogen coverage is changed, with acetylene coverages from 0.03

ML to 0.21 ML and with surface H coverages of 0.95 to 0.46, there are still no gas phase

hydrogenation products observed. This lack of gas phase products is in contrast to the

arguments presented above as to why surface bound H atoms should react with adsorbed

acetylene. Are all of these arguments disproved with this one experiment? The answer is no.

The next step is to observe what species exist on the surface after the crystal has been heated.

3.2 Acetylene + H(s) Surface Products

HREEL spectroscopy is a powerful tool to identify chemically the surface species

present during the reaction of acetylene with surface bound H. Most of the experiments were

carried out using the deuterated species, C_2D_2 and D_2 as reactants. The reason for this arises

from spectral overlaps. In a fully hydrogenated system, the most intense CCH_3 feature is the

C-C stretching mode at 1129 cm^{-1}, which is too close to the symmetric H mode at 1150 cm^{-1},

to be clearly resolved. A fully deuterated system allows these features to be well separated in

frequency.

A surface with 0.17 ML of C_2D_2 coadsorbed with 0.5 ML of surface bound D is

prepared. In this experiment, the C_2D_2 has been made from the decomposition of C_2D_4 by

heating 0.25 ML C_2D_4 to 270 K at a rate of 2 K/s. After exposure to D_2, the crystal is heated

at a rate of 2 K/s to a given crystal temperature, and cooled at ~2 K/s to 80 K at which

temperature an HREEL spectrum is measured. As will be explained later, cooling to 80 K

does not change the relative coverages of reactants. The reaction is frozen as the crystal is

cooled. Therefore, spectra measured at the reaction temperature and those measured at 80 K

do not differ. Figure 6 shows a progression of EEL spectra after each subsequent heating and

cooling. The bottom trace shows the vibrational spectrum of the coadsorbed layer of D and

C_2D_2 before heating. All of the loss features can be assigned to known frequencies of
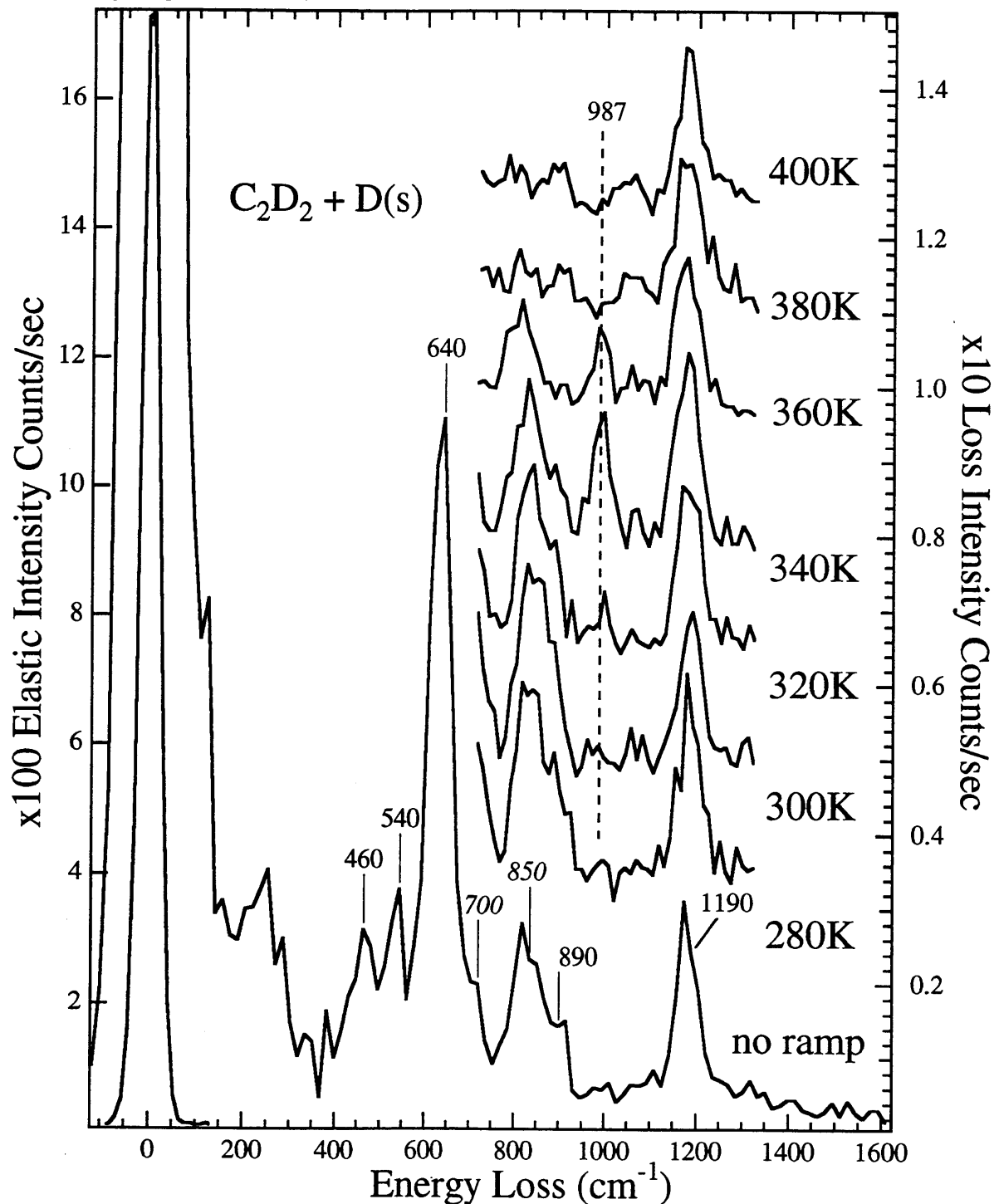
Figure 6 HREEL spectra of 0.17 ML C_2D_2 (from the decomposition of C_2D_4) and 0.5 ML surface D heated at 2 K/s to temperatures indicated. Surface D features labeled in *italics*. All spectra taken at 80 K, at 6° off specular with 6.5 eV electrons, average ΔE_{fwhm} 45 cm^{-1}.

adsorbed C_2D_2[30] and adsorbed D.[31,32] The features at 460 cm^{-1}, 540 cm^{-1}, 640 cm^{-1}, and 890

cm^{-1}, and 1190 cm^{-1} are assigned to the symmetric C-Ni stretching, symmetric and

antisymmetric C-D out-of-plane bending, antisymmetric C-D in-plane bending, and C-C

stretching mode of C_2D_2.[33] The two features at 700 cm^{-1} and 850 cm^{-1} are assigned to the

antisymmetric and symmetric stretch of surface bound D, respectively. The coadsorption of

these two species does not lead to changes in the bonding of either, as evident by the absence

of any shift in their vibrational frequencies upon coadsorption. However, the relative

intensities of individual C_2D_2 loss features do change when coadsorbed with D. With

increasing temperature up to 340 K, a new feature at 987 cm^{-1} grows in intensity, then

decreases in intensity as the crystal temperature increases beyond 340 K, and finally disappears

at 400 K. The absolute intensities of each spectrum does not vary, as seen by the constant

intensity of C_2D_2 features. While these experiments clearly show that a new species has been

formed, the spectrum remains dominated by the vibrational features of acetylene, making

assignment of the new feature impossible.

In order to allow the reaction to proceed further towards this new product so that the

spectrum will be dominated by its vibrational modes, the experiment is repeated for the same

initial conditions as the experiment in Figure 6, but the crystal temperature is held at an

elevated value instead of only experiencing a higher temperature momentarily. The crystal

temperature is raised to 280 K, held at 280 K for 30 minutes and then the spectrum is

measured at 280 K. The temperature is raised and maintained at 280 K by controlling the

amount of liquid nitrogen in the cryostat. Figure 7 shows this vibrational spectrum. The
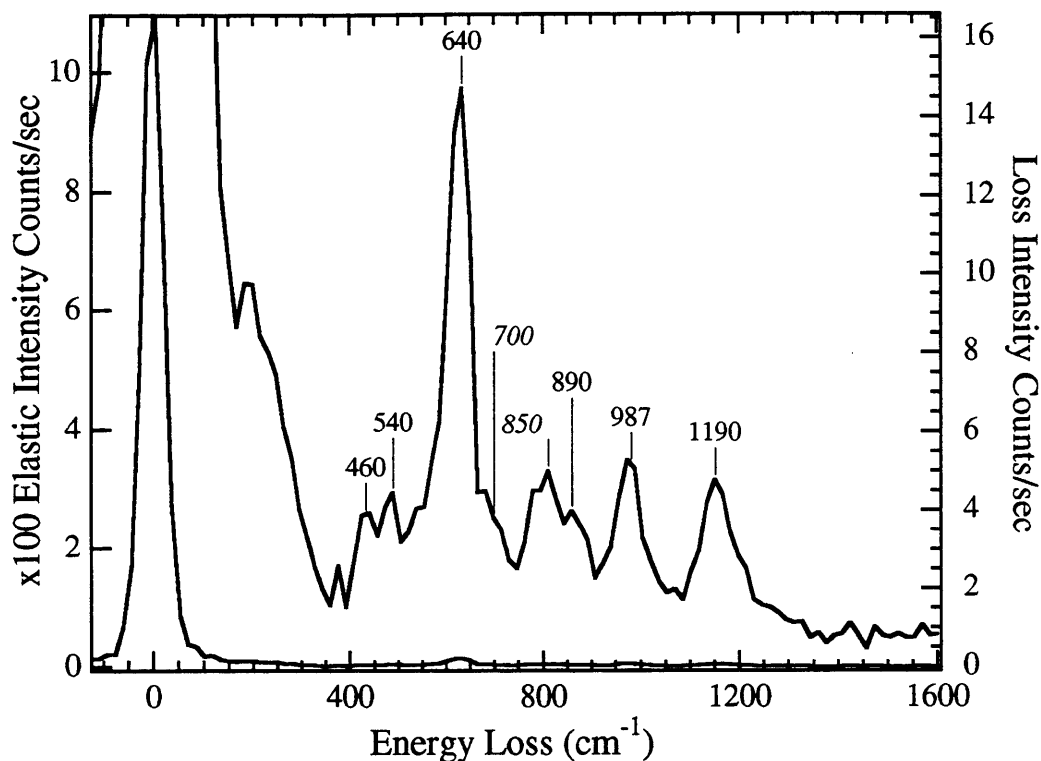
Figure 7 HREEL spectra of 0.17 ML C_2D_2 (from the decomposition of C_2D_4) coadsorbed with 0.5 ML surface D at a surface temperature of 80 K and then warmed to 280K and annealed for 30 min. Surface D features labeled in *italics*. Spectra taken at 280 K, at 10° off specular with 6.5 eV electrons, ΔE_{fwhm} 49 cm^{-1}.

crystal is not held at a higher temperature because the deuterium slowly recombines and desorbs at temperatures above 280 K. The desorption of surface bound D would eliminate one of the reactants and therefore change the composition of the surface. The feature at 987 cm^{-1} representing the new species is indeed larger in this experiment than in the previous experiment. Unfortunately, the spectrum is still dominated by the loss features from C_2D_2 and D as labeled and assigned in Figure 6.

The next experiment was designed to overcome the possibility that the adsorbed deuterium was acting like a limiting reagent. That is, since D is consumed in this reaction,
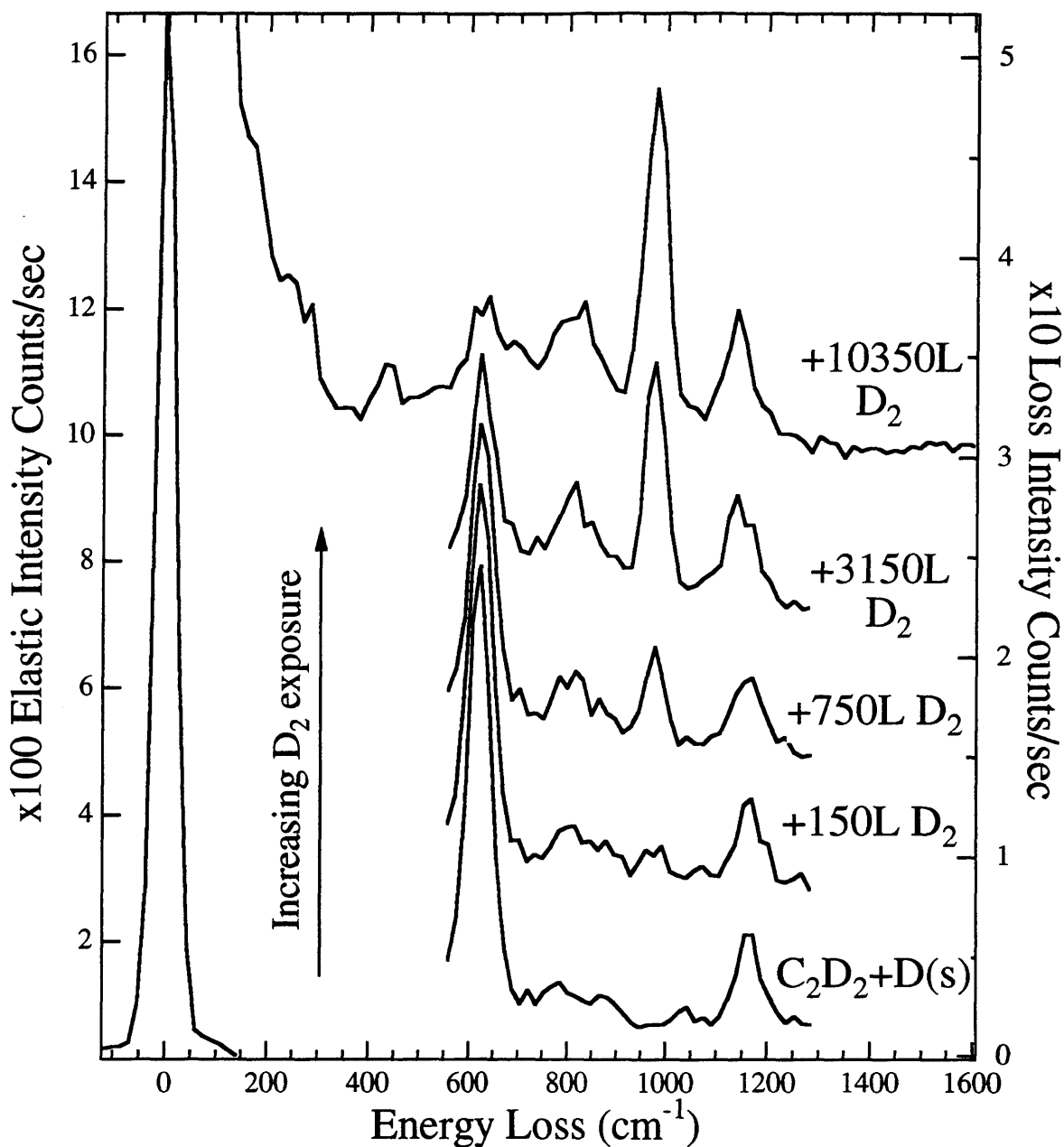
Figure 8 HREEL spectra of 0.17 ML C_2D_2 (from the decomposition of C_2D_4) coadsorbed with 0.5 ML surface D, and with addition of D_2 at 280 K and 30 min anneal for each additional spectrum. Total D_2 exposures are given. Spectra taken at 280 K, at 10° off specular with 6.5 eV electrons, ΔE_{fwhm} average 45 cm^{-1}. See text for procedure.

additional D maybe needed to push the equilibrium towards products. A coadsorbed layer of

0.17 ML of C_2D_2 and 0.5 ML of adsorbed D at 80 K is prepared. The crystal is then heated to

280 K and held at this temperature for 30 minutes. A HREEL spectrum is then measured

while the crystal temperature is still held at 280 K. The surface is then exposed to D_2 at 280 K

for the purpose of increasing the surface bound D coverage. After exposure to D_2, the crystal

is again annealed at 280 K for 30 min and a HREEL spectrum is measured at a crystal

temperature of 280 K. This sequence of steps is repeated several times, and the corresponding

spectra are shown in Figure 8. The new feature at 987 cm^{-1} continues to grow with increasing

D_2 exposure while the acetylene features almost vanish. Figure 9 shows the spectrum from

Figure 8 resulting from a total D_2 exposure of 10350 L with the frequencies of the features

labeled. The product can now be easily identified as ethylidyne, -CCD_3, by the features at 436

cm^{-1}, 836 cm^{-1}, 987 cm^{-1}, 1152 cm^{-1}, 2079 cm^{-1}, and 2201 cm^{-1} which correspond to the

assigned modes of the asymmetric C-Ni stretch, the CD_3 bend, the symmetric CD_3

deformation, the C-C stretch, and the C-H symmetric and antisymmetric stretch, respectively,

as previously identified for ethylidyne on the Ni(111) surface.[34] No other hydrocarbon can be

consistently assigned to these loss features. Two other modes at 640 cm^{-1} and 700 cm^{-1} are

marked in italics, since they are not assigned to the adsorbed ethylidyne species. The feature at

640 cm^{-1} is the antisymmetric C-D out-of-plane bend mode of C_2D_2,[30] and the feature at 700

cm^{-1} is the antisymmetric stretch mode of coadsorbed deuterium.[31] The spectrum of

deuterated ethylidyne coadsorbed with D synthesized from the reaction of C_2D_4 with gas phase

D atoms is shown at the top of Figure 9 for comparison.[34] The similarity of these two spectra
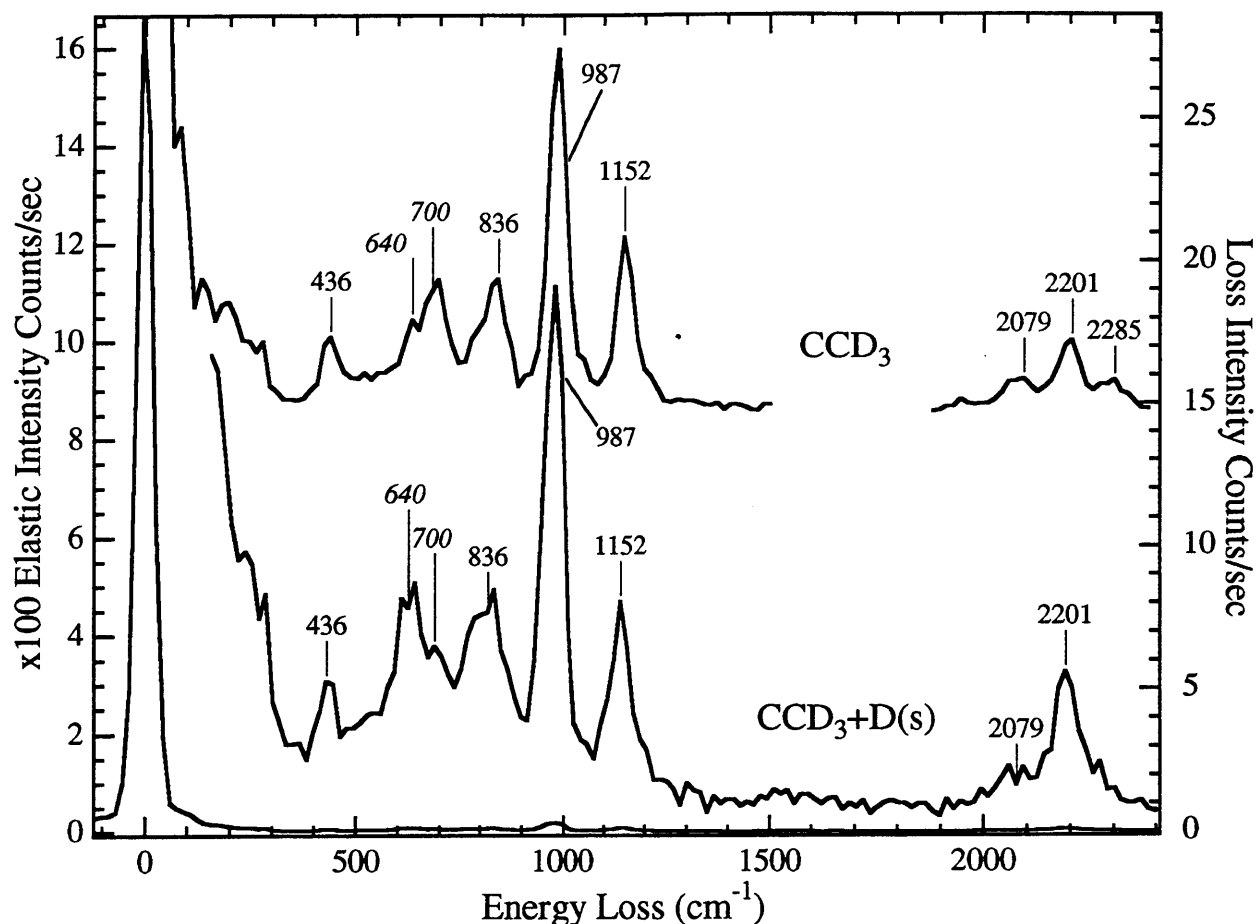
Figure 9 HREEL spectrum of 0.17 ML C_2D_2 (from the decomposition of C_2D_4) and 10350 L total D_2 exposure from Figure 8. Spectrum taken at 280 K, at 10° off specular with 6.5 eV electrons, ΔE_{fwhm} 45 cm^{-1}. Surface D features labeled in *italics*. Spectrum of CCD$_3$ coadsorbed with D shown for comparison, synthesized from 0.25 ML C_2D_4 + D atoms from 5x10^{-6} torr D_2 for 120 sec with front filament on, see reference 34. Spectrum taken at 80 K, 6° off specular, ΔE_{fwhm} 45 cm^{-1}.

provides clear evidence that ethylidyne is the product of the reaction of adsorbed acetylene and surface bound D. This shows that surface deuterium adds to and hydrogenates acetylene in a new way. In this case, surface bound D has hydrogenated C_2D_2 not to the gas phase products C_2D_4 and C_2D_6 but to an adsorbed product.

Ethylidyne is a species that has been studied extensively in surface chemistry. Its C-C axis is perpendicular to the surface, and its the carbon atom is triply bonded to the surface in a three-fold hollow site. There is a single bond between the two carbon atoms and then three hydrogen atoms are bonded to the top carbon. The first observation of ethylidyne was on platinum where it was formed as the decomposition product of ethylene or acetylene.[35] From the time of the initial discovery of ethylidyne, it was proposed to be an intermediate in ethylene hydrogenation since it is formed so easily from ethylene. However, the most recent evidence identifies ethylidyne as a spectator during the hydrogenation of ethylene on platinum under high pressure conditions.[36] The chemistry of ethylidyne on nickel surfaces is much different than on platinum. Ethylidyne is not a decomposition product of either ethylene or acetylene. Ethylidyne has only been spectroscopically identified in two studies, one on a supported nickel catalyst under high pressure conditions,[37] and another on Ni(111) using gas phase H atoms to synthesize ethylidyne.[34] Ethylidyne has a very different chemistry on Ni than on Pt. It is stable to 500 K on the Pt surface, whereas on Ni, ethylidyne decomposes to acetylene at 350 K.

3.3 Evidence for Equilibrium

A series of observations lead to the conclusion that the reaction of surface D and adsorbed C_2D_2 to make CCD_3 is an equilibrium reaction, described by the chemical equation,

$$C_2D_2 + D \leftrightarrow CCD_3 .$$

First, a given coverage of surface bound D and adsorbed acetylene will only produce a specific amount of ethylidyne, as represented by the HREEL spectrum in Figure 7. This figure shows a coadsorbed layer of 0.5 ML surface D and 0.17 ML C_2D_2 that was annealed at 280 K for 30

minutes. The HREEL spectrum does not change with further annealing at 280 K. All of the

loss features in this spectrum have been assigned to C_2D_2 coadsorbed with D except the feature

at 987 cm^{-1} which is the symmetric CD_3 deformation mode of CCD_3. If the reaction follows

the stoichiometry of the chemical reaction written above, the surface bound D will not act as a

limiting reactant in this experiment, since there is more than twice the coverage of surface D as

the coverage of C_2D_2.

The vibrational spectra shown in Figure 8 are the results of an experiment in which

C_2D_2 is exposed to repeated D_2 exposures to increase the surface D coverage, and annealing at

280 K to allow the reaction to CCD_3 to occur. In the reaction of surface bound D and C_2D_2,

one surface D atom is consumed with synthesis of each CCD_3 molecule. Therefore, as the

reaction progresses, sites open on the surface. The successive D_2 exposures increase the

surface bound D coverage by filling these open sites. This increase in surface D coverage

should shift the equilibrium towards product. Indeed, as the total D_2 exposure is increased, the

dominant feature in the spectra shifts from the C-D out-of-plane antisymmetric bend mode of

C_2D_2 at 640 cm^{-1} to the CD_3 deformation mode of CCD_3 at 987 cm^{-1}. More and more CCD_3 is

produced consistent with an equilibrium reaction.

The coverages of C_2D_2 and CCD_3 can be quantified after repeated exposure to D_2. In

this experiment, 0.17 ML C_2D_2 is adsorbed on the surface at 80 K, the crystal is then warmed

to 280 K, and held at this temperature for repeated cycles of 10 minute exposure to D_2 at

$2x10^{-5}$ Torr followed by an anneal at 280 K for 60 minutes. After 1 to 4 cycles, yielding a total
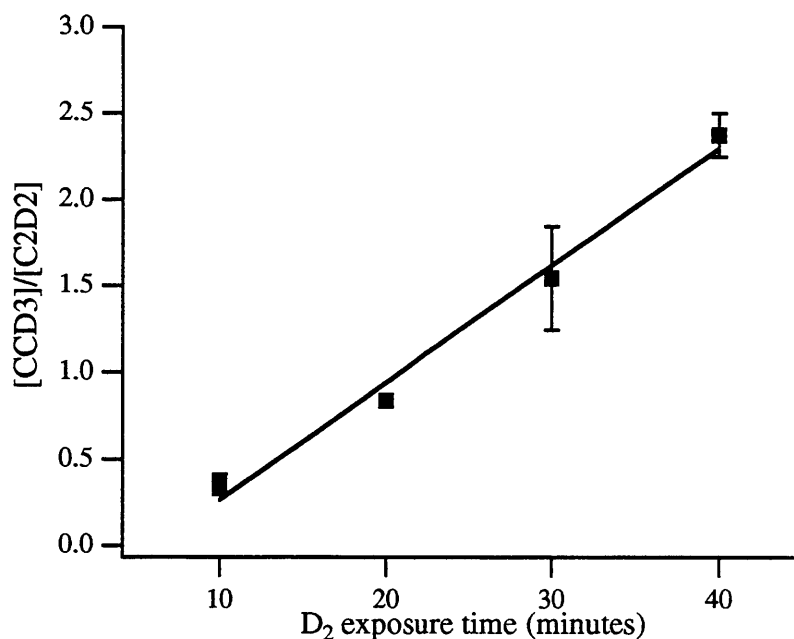
Figure 10 CCD_3/C_2D_2 ratio from measured HREELS intensities versus D_2 dose time with D_2 pressure of 2×10^{-5} torr at 280 K with linear fit. Procedure explained in the text. Error bars are 90% confidence interval from 2-4 repeated measurements, 20 sec point has no error bar.

D_2 exposure of between 10 and 40 minutes, the crystal is cooled to 80 K and a HREEL

spectrum is measured. It is known that a 5400 L exposure of D_2 at a crystal temperature of

180 K will saturate the surface,[4] so each 12000 L D_2 exposure at 280 K fully saturates the

surface with surface bound D. The above procedure is repeated to obtain a number of spectra

for D_2 exposure times of 10, 20 ,30 and 40 minutes. In each of these spectra, the intensity of

the largest acetylene loss feature at 640 cm^{-1} and the intensity of the largest ethylidyne loss

feature at 987 cm^{-1} are measured. These intensities are proportional to the coverage of each

species, as will be explained later in detail. From the intensities, a ratio of the CCD_3 coverage

to the C_2D_2 coverage, $[CCD_3]/[C_2D_2]$, is calculated. Figure 10 shows the ratio of

$[CCD_3]/[C_2D_2]$ versus D_2 exposure time. The ratio of $[CCD_3]/[C_2D_2]$ increases linearly with

increasing D_2 exposure, as expected for equilibrium behavior. The error bars on the plot are the 90% confidence interval of repeated measurements, except for the 20 minute point which was measured only once and has no error bar.

Figure 10 also shows that the ratio of $[CCD_3]/[C_2D_2]$ can be reproduced with the same pattern of D_2 exposures and annealing at 280 K. This reproducibility demonstrates that the only factors that effect the $[CCD_3]/[C_2D_2]$ ratio are the D_2 exposure and annealing. The role of the 280 K anneal is to allow the reaction to proceed to completion, thereby creating open sites (the CCD_3 product is bound to fewer Ni atoms than the C_2D_2 and surface bound D reactants so as CCD_3 is formed, surface Ni atoms sites are opened) on which D_2 molecules from a subsequent exposure dissociatively adsorb as surface bound D atoms. Surface bound D is additionally being consumed during the exposure, because the D_2 exposure is done at the same temperature as the reaction. It is the uniform coverage of surface bound D added in each cycle, that leads to the linear dependence of $[CCD_3]/[C_2D_2]$ on D_2 exposure.

Another element of an equilibrium is that, under equilibrium conditions, both reactants and products are present. The value of the equilibrium constant determines the coverages of the reactants and products. The existence of a small coverage of acetylene coadsorbed with ethylidyne is not proof of an equilibrium reaction when acetylene is one of the reactants because it can be argued that the reaction did not go to completion. However, a small coverage of acetylene is always present with the ethylidyne that is synthesized from ethylene and gas phase H atoms (this reaction is described in Chapter 5). Figure 11 show the
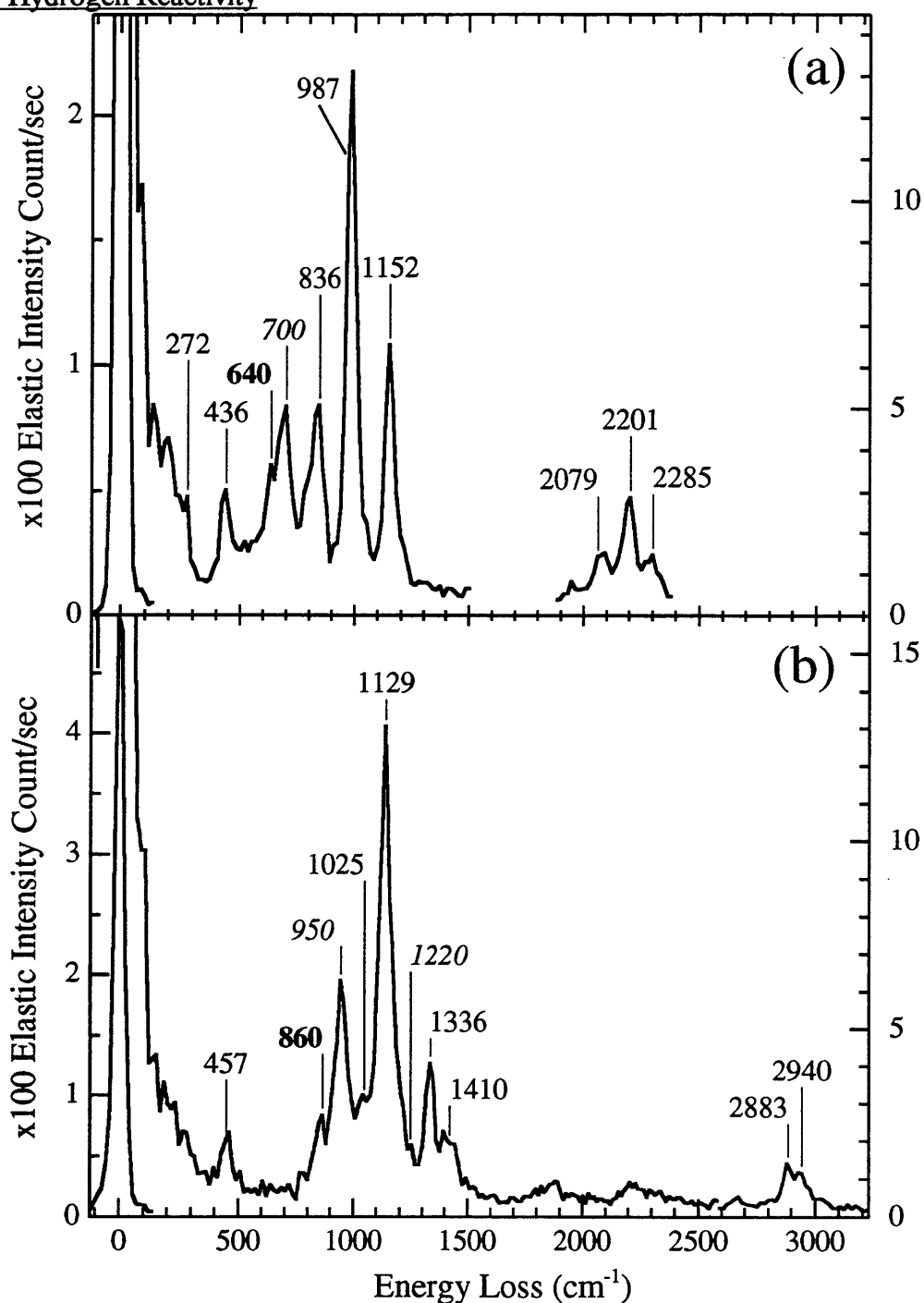
Figure 11 HREEL spectra of CCD_3 in (a) and CCH_3 in (b). Synthesis for both consists of 0.25 ML C_2D_4 (C_2H_4) + D(H) atoms from $5x10^{-6}$ torr $D_2(H_2)$ for 120 sec with front filament on. All spectra taken at 80 K. Both spectra taken 10° off specular with 6.5 eV electrons, ΔE_{fwhm} of 44 cm^{-1} for (a) and 45 cm^{-1} for (b). See reference 34.

vibrational spectra resulting from the synthesis of CCH_3 and CCD_3 from adsorbed ethylene

after exposure to gas phase H(D) atoms. In both spectra, the most intense acetylene feature,

the antisymmetric C-H(D) bend,[30] is visible at 860(640) cm^{-1}. This acetylene feature is present

in the spectra regardless of the specific method of synthesis including, the total exposure time

to gas phase H(D) atoms, the temperature of the crystal, and the initial hydrocarbon (either

acetylene or ethylene). It is impossible to eliminate the acetylene features from the spectra.

The presence of acetylene could be explained by the decomposition of ethylene, but C_2H_4

decomposition to C_2H_2 does not begin until a surface temperature of 220 K. Under typical

conditions for ethylidyne synthesis the crystal temperature does not rise above 120 K. It

appears that during the reaction to form ethylidyne, there is an equilibrium established between

acetylene, ethylidyne, surface H atoms and gas phase H atoms.

The decomposition of ethylidyne also supports the idea of an equilibrium. Figure 12

shows the spectra of ethylidyne, synthesized from ethylene and gas phase H atoms, measured

at 80 K after the crystal temperature was raised at the rate of 2 K/sec to the given temperature.

There is a dramatic change in the surface species above 350 K. The three spectra at 300, 340

and 350 K are all dominated by the CD_3 deformation mode of CCD_3 at 987 cm^{-1}. At 370 K,

the intensity of this CCD_3 feature has decreased enormously. At the same time, there is a

dramatic increase in intensity of the C-D out-of-plane antisymmetric bend of C_2D_2 at 640 cm^{-1}.

In the 380 K spectrum, it appears that there is no CCD_3 remaining on the surface from the

absence of any loss intensity at 987 cm^{-1}. A spectrum of acetylene coadsorbed with deuterium

from the decomposition of C_2D_4 is shown in the top trace in Figure 12. From the excellent
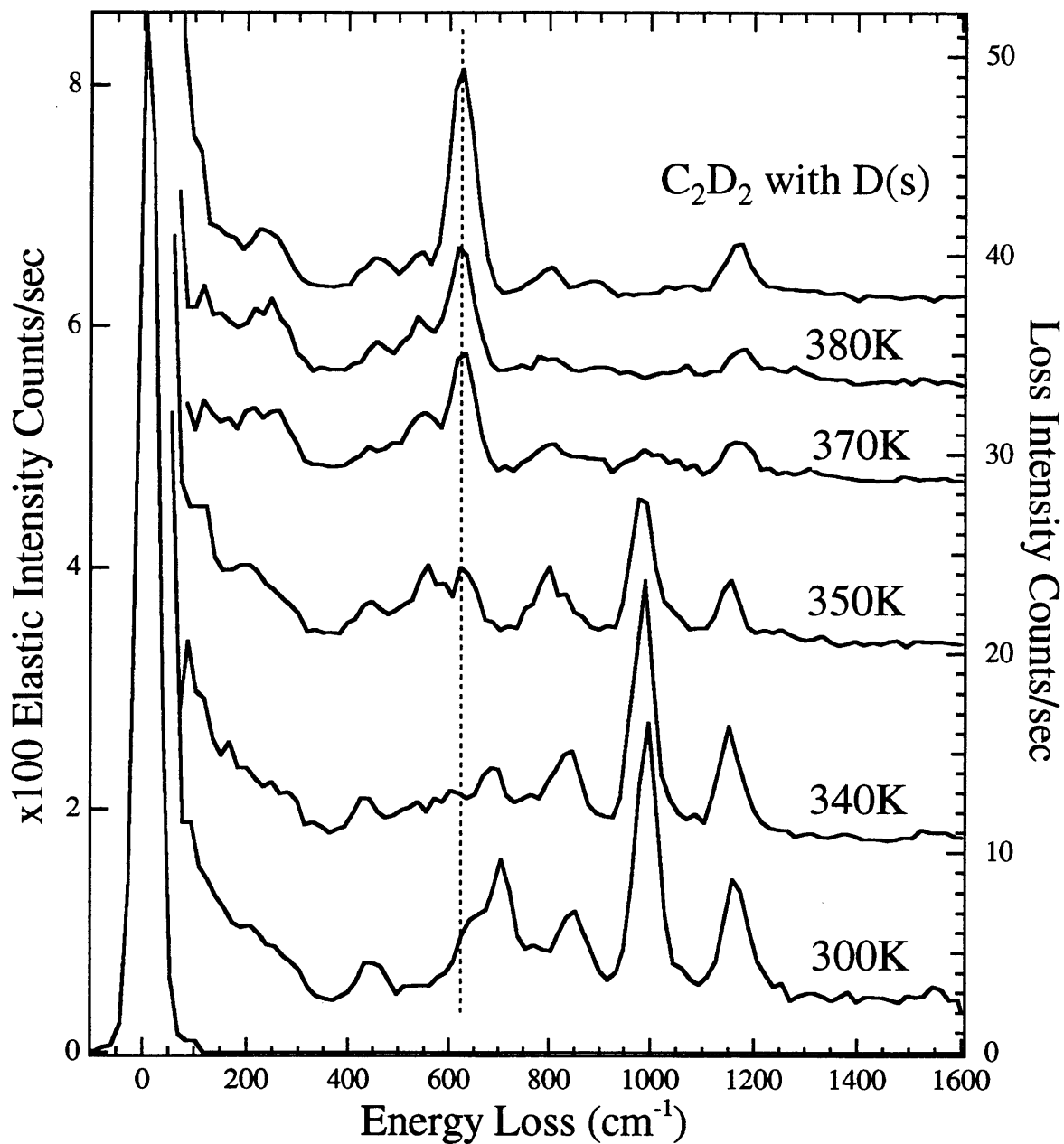
Figure 12 HREEL spectra showing decomposition of CCD$_3$, spectra measured at 80 K after heating to indicated temperature. C$_2$D$_2$ + D(s) trace from decomposition of 0.25 ML C$_2$D$_4$. All spectra taken at 80 K, decomposition spectra taken at 10° off specular and C$_2$D$_2$ + D(s) spectra taken at 6° off specular, ΔE_{fwhm} average 45 cm^{-1}.

agreement between this spectrum and the spectrum of ethylidyne heated to 380 K, it is clear

that ethylidyne decomposes to acetylene. How does this decomposition support the idea of

equilibrium? There is another process that occurs at 350 K, the recombination and desorption

of surface D. While the observation of ethylidyne decomposition at the same temperature as

the recombination and desorption of D_2 does not definitively demonstrate casuality of these

two processes, the behavior can be well described by the idea of equilibrium. As the D begins

to desorb at 340 K, the reaction shifts back towards acetylene, and with the significant loss of

deuterium above 350 K, the reaction shifts almost entirely back to the reactant, acetylene. The

alternate explanation for this coincident behavior is that the ethylidyne simply happens to

decompose at the same temperature as the surface bound D recombines and desorbs. If the

recombination and desorption of D_2 and decomposition of CCD_3 are only a coincidence, the

observation that ethylidyne decomposes to acetylene demonstrates a reverse reaction between

the two species.

During the ethylidyne decomposition in the previous experiment, surface bound D

atoms recombine and desorb. The surface bound D coverage changes by the second while the

crystal is heated, with no attempt to bring the system to equilibrium. Ethylidyne

decomposition to acetylene above 340 K is shown, but the reverse equilibrium reaction is not

demonstrated. The following experiment more strongly suggests that the reverse reaction of

$CCD_3 \rightarrow C_2D_2 + D$ is an equilibrium process. Figure 13a shows the spectrum of a surface of

0.17 ML C_2D_2 after three cycles of exposure to 2×10^{-5} Torr D_2 for 10 min at 280 K followed

by a 30 minute anneal at 280 K. This repeated D_2 exposure pushes the equilibrium towards
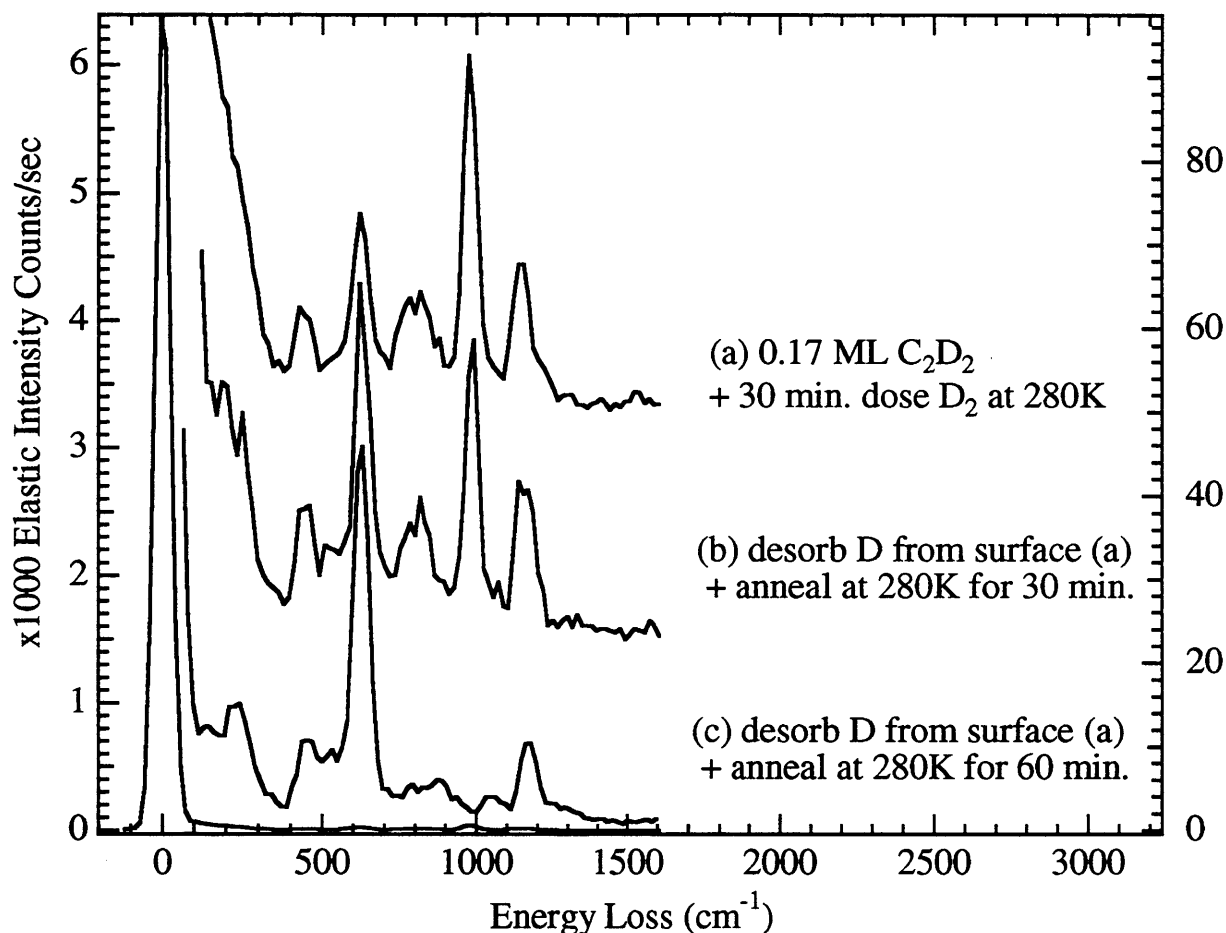
Figure 13 HREEL spectra showing the reverse equilibrium of CCD_3 to C_2D_2.
(a) shows spectrum of mostly CCD_3 from 0.17 ML C_2D_2 with addition of D_2
and 30 min anneal at 280 K repeated three times, (b) shows surface (a) after
desorption of some D and anneal at 280 K for 30 min, (c) shows surface (b)
after further annealing at 280 K for 30 min. Spectra taken at 80 K, at 10° off
specular with 6.5 eV electrons, ΔE_{fwhm} average 52 cm^{-1}.

product, resulting in CCD_3 as the major surface species, which is easily observed from the

dominance of the 987 cm^{-1} feature of CCD_3, over the 640 cm^{-1} feature of C_2D_2. The crystal is

then heated at 2 K/s to 330 K in order to desorb a small amount of deuterium, between 0.03

and 0.08 ML, as measured from the amount of D_2 desorbed during heating to 330 K and the

amount of D_2 desorbing from the surface at the end of the experiment. Figure 13b shows a

vibrational spectrum of the crystal at 80 K after further annealing at 280 K for 30 min, the

temperature at which the forward reaction takes place. It is clear that the 640 cm^{-1} feature of

C_2D_2 is more intense than the 987 cm^{-1} feature of CCD_3. The spectrum measured after

annealing of the crystal for another 30 min at 280 K is shown in Figure 13c. The dominance of

the 640 cm^{-1} feature of C_2D_2 clearly indicates that the reaction has reverted back to reactants.

The slow shift in coverage of the surface species over the period of one hour strongly suggests

an equilibrium process in this single experiment. If the coverage of surface bound D atoms

before and after the 330 K ramp could be measured, the equilibrium constant,

$[CCD_3]/[C_2D_2][D]$, could be calculated. Calculating the same equilibrium constant before and

after desorption of D and the shift in equilibrium would prove an equilibrium process.

Unfortunately, it is difficult to measure the surface bound D coverage well enough to

make this comparison. The reason for this stems from a number of factors. The only method

available to measure the surface bound D coverage is to record the partial pressure of D_2

(m/e=4) while the crystal is heated at a rate of 2 K/s. The integral of this signal is a measure of

the surface bound D. This measurement is more difficult for a layer of C_2D_2 and CCD_3

coadsorbed with D. Both C_2D_2 and CCD_3 decompose to surface D and C in the same

temperature range as the surface bound D desorbs. This means that the partial pressure signal

at m/e=4 for D_2 has contributions from all three species that are not separable. It is possible to

subtract the contributions of the hydrocarbon species from the raw partial pressure signal at

m/e=4 if the coverage of each species is known, and it is assumed that all D atoms from the

hydrocarbon recombine and desorb from the surface during the decomposition. However,

regardless of these adjustments there are still enormous errors in these measurements. The

measurement of individual C_2D_2 and CCD_3 coverages do introduce a small amount of error,

but the cause of most of this error is unknown. Surface D measurements taken of the same

surface on different days vary by up to 50%, even though the signal of the saturated surface is

measured on each day to calibrate the magnitude of the partial pressure signal. Significant

improvements in this random error can be made by measuring all surface D coverages on the

same day.

It is appropriate, at this point, to revisit the previous assertion that no shift in the

surface equilibrium occurs when the crystal is cooled. The crystal is typically cooled to 80 K

after a reaction has occurred at a particular elevated temperature in order to take an EEL

spectrum. The potential for a backward reaction while cooling the crystal would depend on

the cooling rate, the total time the crystal spent at intermediate temperatures, the temperature

dependence of the equilibrium constant, and the reverse rate constants. First, the cooling rate

of the crystal is ~ 2 K/s. Control experiments have been done that show no reaction occurs at

220 K. The crystal only spends a total of 30 seconds at temperatures between 280 K to 220 K.

The second factor necessary to experience a reverse in the reaction is an equilibrium constant

that is much lower at crystal temperatures under 280 K and a rapid reverse rate constant to

establish this new equilibrium. All attempts to measure a change in C_2D_2 and CCD_3 coverage

with temperature show little temperature dependence. This suggests that either the equilibrium

constant does not change with temperature or that the reverse reaction rate is so slow that the

new equilibrium is not established. Absolutely no shift is seen in the equilibrium C_2D_2 and

CCD_3 coverages from 280 K to 270 K over a 2 hour equilibration time. Only a very small shift

is seen in the equilibrium coverages from 290 K to 260 K over a 45 minute equilibration time.

Between the rapid cooling rate of the crystal, and the non-existent to minimal shift in the

surface coverages with temperature decreases on time scale of many minutes, it is concluded

that there is no shift in the equilibrium when rapidly cooling the crystal to 80 K for the purpose

of measuring the EEL spectrum.

4 Measurement of an Equilibrium Constant

If the reaction of surface D with adsorbed C_2D_2 is in equilibrium, then it should be

possible to measure an equilibrium constant (K_{eq}). The measurement of C_2D_2, CCD_3 and D

coverages allow a calculation of K_{eq} based on the simplest equation for the reaction,

$$C_2D_2 + D \leftrightarrow CCD_3. \tag{1}$$
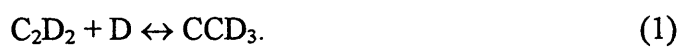
There are more complex mechanisms with which this reaction could proceed and two of these

mechanisms are explored below. The equilibrium constant for the 'simplest' equation written

$$K_{eq} = \frac{[CCD_3]}{[C_2D_2][D]} \tag{2}$$

When writing an equilibrium constant it is assumed that the system is ideal. This means there

is a random mixing of all adsorbates and there are no interactions between the adsorbates. The

goal of the work presented here is to investigate whether this equation for K_{eq} is an accurate

representation of the chemical equation shown in Equation 1.

Experimentally, the ethylidyne [CCD_3] coverage, the acetylene [C_2D_2] coverage, and

the surface bound deuterium [D] coverage are measured at equilibrium for different initial

C_2D_2 and D coverages. The initial [D]/[C_2D_2] ratio is varied from 2.6 to 48. The initial D

coverage is measured by integrating the thermal desorption signals and the coverage of the two

hydrocarbons is measured using the EELS intensities of the most intense features of each

species. Descriptions of the method used for each measurement are given below.

4.1 *D coverage - Thermal Desorption Measurement*

It is not possible to measure the surface bound D coverage from integrating a thermal

desorption spectrum of D_2 taken *after* establishing equilibrium, as discussed above, because the

uncertainty in the measurement from day to day is too high. A new method to measure the

equilibrium D coverage is constructed to minimize this uncertainty. In this method, the

coverage of surface bound D is measured *before* establishing equilibrium. This measurement is

done for all surfaces at one time which significantly reduces the error in the data set.

Measurement of the initial surface D coverage is carried out as follows. A known

coverage of acetylene, between 0.02 and 0.23 ML, is adsorbed on the entire crystal face at 80

K using the molecular beam. The crystal is then exposed to $2x10^{-5}$ Torr of D_2 for 15 min at a

crystal temperature of 220 K, which fills all possible adsorption sites. Previous work has

shown that the maximum hydrogen coverage occurs with a 5,400 L exposure of H_2 to a

Ni(111) surface at 180 K.[4] The exposure used in this measurement is 18,000 L with a crystal

temperature of 220 K. With three times the D_2 exposure and a higher crystal temperature as

compared to the previously reported saturation exposure,[4] the surface should be well

saturated. The crystal is cooled back to 80 K. A thermal desorption experiment is then carried

out and the partial pressure of D_2 is recorded and integrated. Because D_2 from the
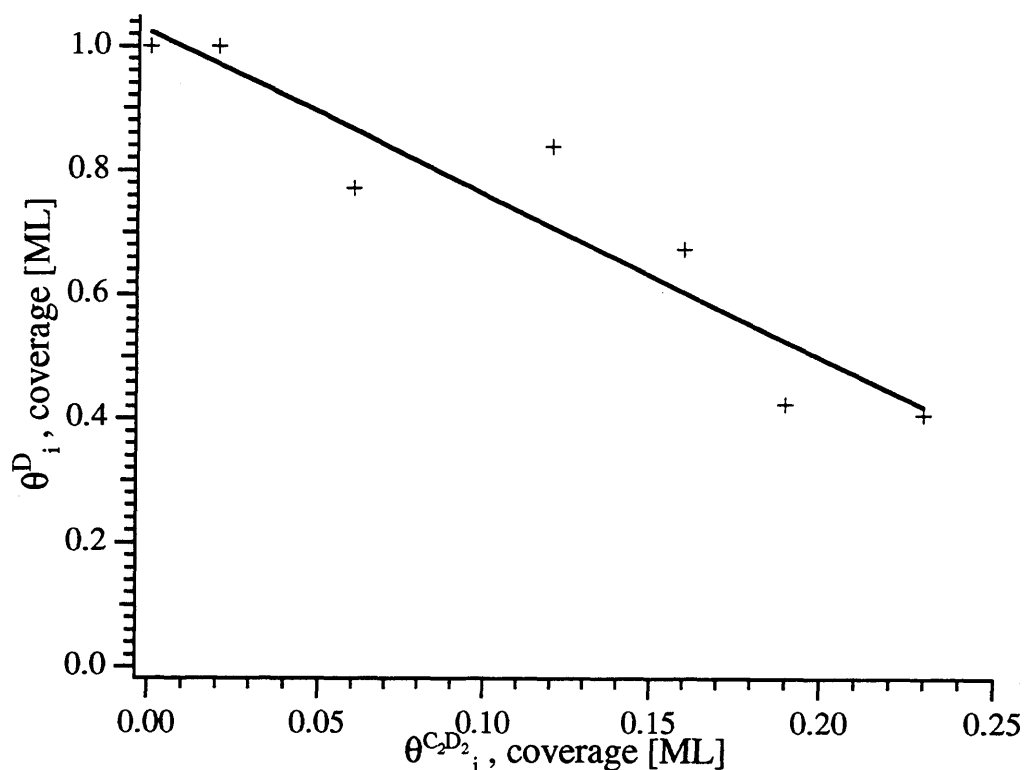
Figure 14 The initial coverage of deuterium coadsorbed with different initial acetylene coverages at 220 K. See text for procedure.

decomposition of acetylene also contributes to the partial pressure of D_2 and overlaps the signal arising from the surface bound D around 400 K, a reference thermal desorption spectrum of D_2 arising from a neat layer of acetylene is measured. The TD signal of D_2 arising from the C_2D_2 decomposition is integrated and this integrated value is subtracted from the integral of the D_2 signal of C_2D_2 coadsorbed with surface D to obtain an integrated D_2 signal corresponding to only that of coadsorbed surface bound D. This value of the integrated D_2 signal from surface bound D is then compared to the integrated D_2 TD signal from a saturated D surface, which is known to be 1 ML, in order to express the surface bound D coverage as a fraction of a ML. The surface saturated with D is prepared by exposure of the crystal to 2×10^{-5} Torr of D_2 for 15 min at a crystal temperature of 220 K. The results of the measurement of

surface bound D coverage versus C_2D_2 coverage are shown in Figure 14. The equation of the

line that is fit to these data is

$$\Theta_i^D = 1.02 \pm 0.06 - 2.6 \pm 0.4 \Theta_i^{C_2D_2} \qquad (3)$$

where the initial D coverage is Θ_i^D and the initial C_2D_2 coverage is $\Theta_i^{C_2D_2}$. This function is then

used to obtain the initial coverage of D coadsorbed with a given coverage of C_2D_2. The error

bars in this equation are the standard deviation of each parameter generated from a linear

regression fit. Note that the 2.6 coefficient of the acetylene coverage has physical meaning.

Each C_2D_2 molecule occupies 2.6 times as many surface sites as a D atom.

While this function for the coverage of D coadsorbed with an initial coverage of C_2D_2

provides a reliable way to measure the *initial* D coverage, the quantity needed for the

determination of K_{eq} is the surface D coverage *at equilibrium*. However, it is possible to

determine the surface D coverage *at* equilibrium from the initial coverage of coadsorbed D and

the coverage of coadsorbed acetylene and ethylidyne at equilibrium using the following

procedure. Measurement of K_{eq} is carried out by first creating a layer of coadsorbed C_2D_2 and

D in the same way as just described above for the measurements of the initial coverage of D

coadsorbed with C_2D_2. The surface is then annealed at 280 K, where the reaction occurs at its

highest rate, for 60 minutes. A HREEL spectrum is taken at 80 K to measure the coverages of

each hydrocarbon. Since one D atom is consumed for each ethylidyne molecule produced, and

no D desorbs from the surface during the experiment, the equilibrium D coverage is the initial

D coverage minus the coverage of ethylidyne.

4.2 *EELS Measurement Methodology- Acetylene and Ethylidyne Ratios*

Electron energy loss spectroscopy is most commonly used to identify species on the surface and not to measure their coverages quantitatively. This is why a detailed description follows on how the coverage of both acetylene and ethylidyne on the surface using HREEL spectroscopy is measured. The procedure to extract the coverages of acetylene and ethylidyne is to measure the ratio of intensities of the most intense acetylene feature, the antisymmetric C-D bend at 640 cm^{-1}, to that of the ethylidyne feature, the symmetric CD_3 deformation at 987 cm^{-1}. All EEL spectra are measured at a scattering angle of 10° off specular, the impact scattering regime. The intensity of each feature is determined by measuring its height above the background signal that is extrapolated to the frequency of the loss feature from a higher frequency where there are no loss features. The intensities are then transformed into absolute coverages using the known absolute acetylene coverage. This technique rests on a number of assumptions which are further explored in the next few paragraphs.

Use of the intensities in EEL spectra to measure coverage assumes a linear relationship between hydrocarbon coverage and the intensity of a vibrational feature, specifically the antisymmetric C-D bend of C_2D_2 and the symmetric CD_3 deformation of CCD_3. Because the absolute intensity of EEL features is very sensitive to crystal position, the tuning of the instrument, and the history of the crystal, the precision of these intensity measurements was investigated. Six measurements of the intensity of the 640 cm^{-1} feature from a single exposure of C_2H_2 were made after removing the crystal from the spectrometer in between measurements. The 90% confidence interval of the value for these intensity measurements is

C_2D_2 in ML
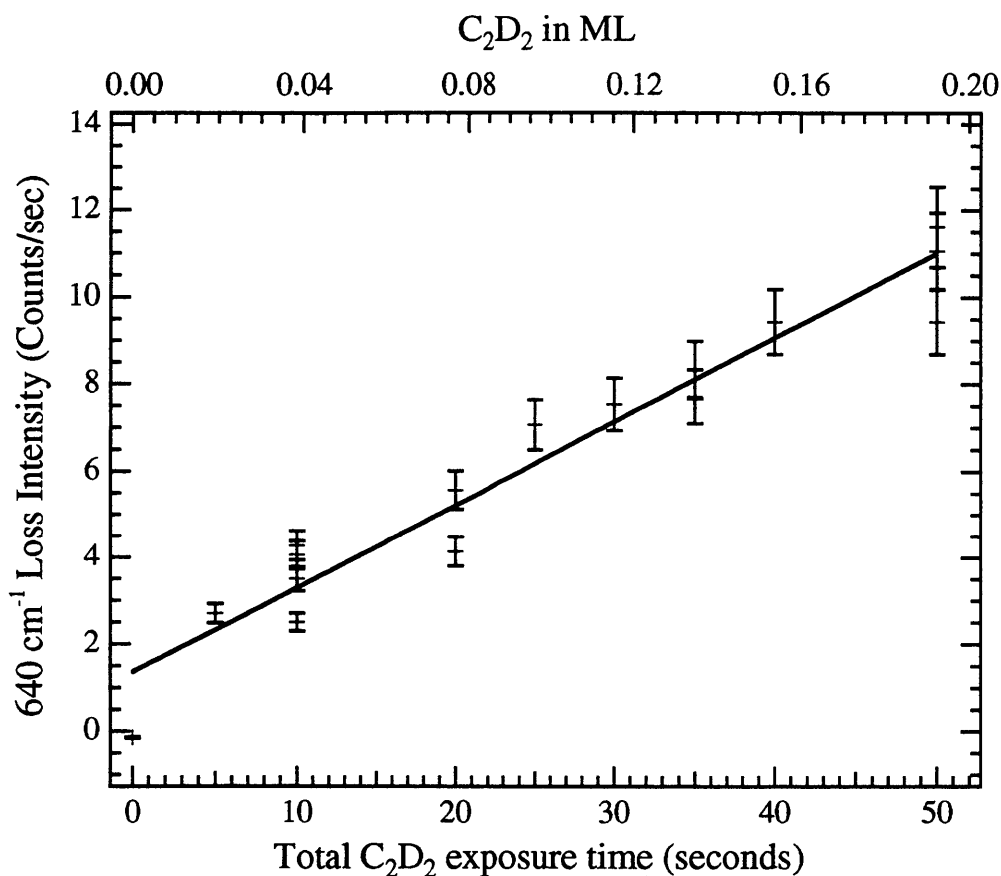
Figure 15 Intensity of 640 cm^{-1} feature for acetylene from HREELS versus acetylene exposure time. 7% error bars on data are from 90% confidence interval for a single EELS intensity measurement repeated 6 times.

±7%. Because of this large measured error, only very minimal retuning of the instrument is done between the intensity measurements shown in Figure 15. In this figure, the measurement of the intensities of the acetylene antisymmetric C-D bend at 640 cm^{-1} versus acetylene exposure time is shown. These intensity measurements are taken in several sequences of increasing coverage. That is, an intensity measurement is made at a given exposure and then the coverage of acetylene is increased by reexposure of the surface to C_2D_2. In this way, the acetylene coverage is built up in a succession of acetylene exposures with an EELS spectrum
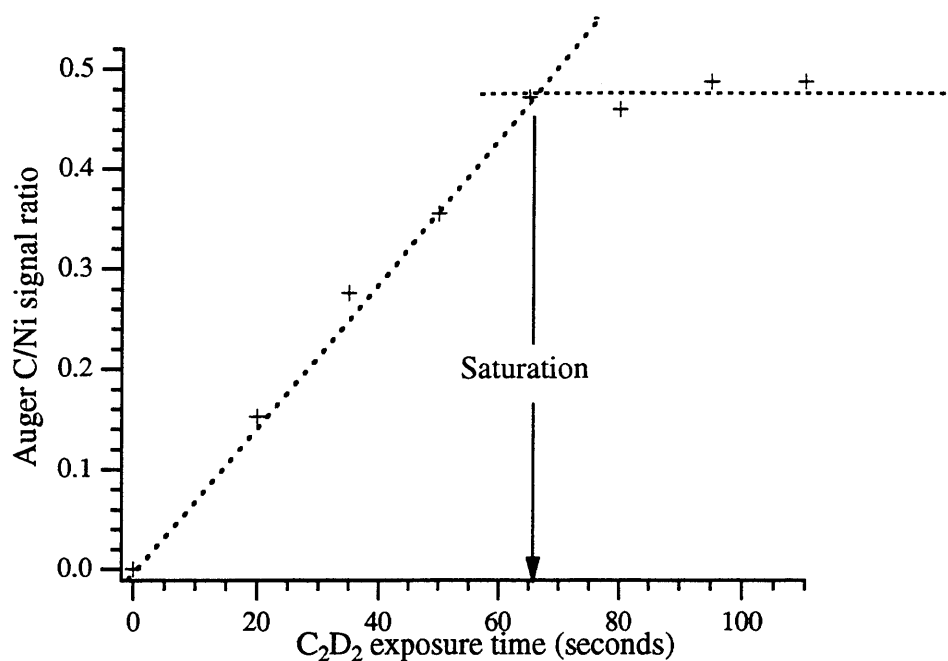
Figure 16 Auger carbon to nickel signal versus time of acetylene exposure.

measured after each additional exposure. Acetylene is added to the surface incrementally

because heating the crystal to remove acetylene prior to a new experiment affects the intensity

of EELS features, presumably from small charging effects due to the high energy electrons

used to heat the crystal. After controlling many of the variables which affect the loss intensity,

a linear relationship between the loss intensity of the acetylene feature at 640 cm^{-1} versus C_2D_2

coverage is measured. The ±7% error bars in Figure 15 are from the repeated measurement of

a single C_2D_2 exposure. The acetylene coverage in monolayers is determined from a plot of

the C/Ni ratio measured with Auger spectroscopy vs acetylene exposure time, as explained in

Chapter 2, and shown in Figure 16. The error in the acetylene exposure is derived from the

standard deviation of the slope from a linear regression fit of the line in Figure 16. This
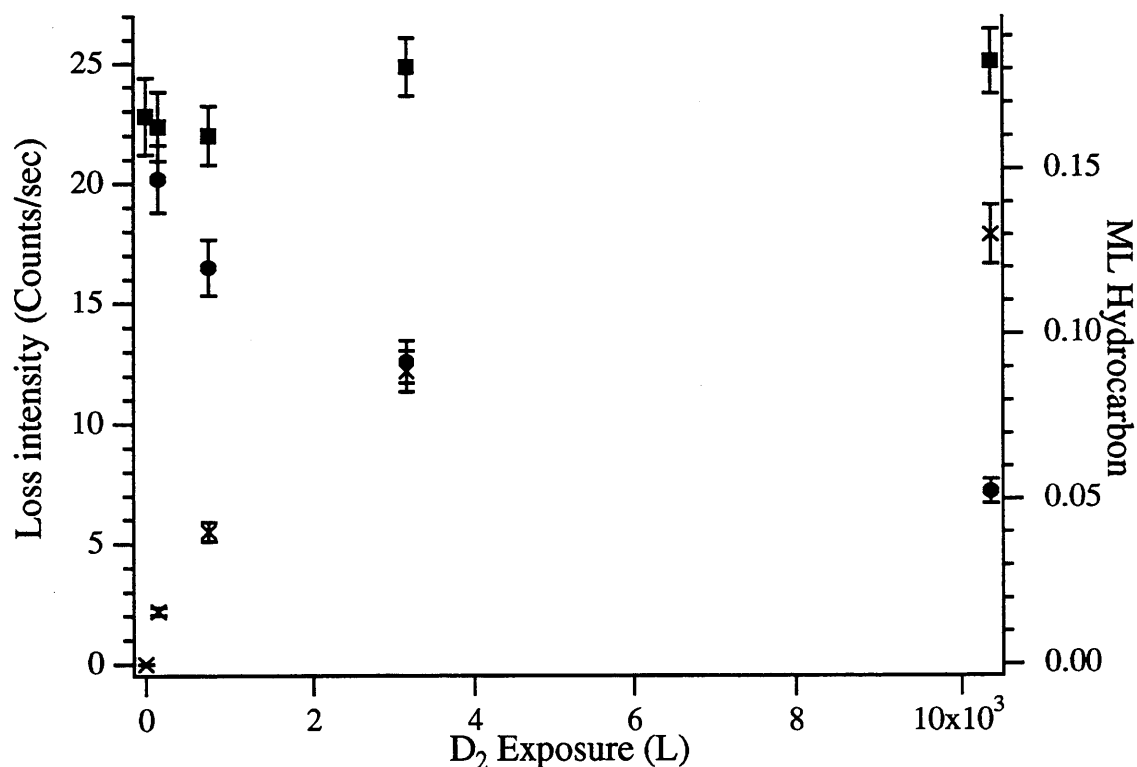
Figure 17 HREELS intensities of C_2D_2 (●), CCD_3 (x), and sum (■) of these two signals with progression of reaction. Intensities from data in Figure 8. 7% error bars on data are from 90% confidence interval for a single EELS intensity measurement repeated 6 times.

analysis yields an error of ±2.5%. The top axis in Figure 15 displays the monolayer coverage of C_2D_2 for the exposure time given on the bottom axis.

It is also important to show that the intensity of the ethylidyne feature, the symmetric CD_3 deformation at 987 cm^{-1}, is also linear with coverage of CCD_3. The piece of evidence used to justify the linearity of the CCD_3 intensity is that the sum of the measured acetylene and ethylidyne features is basically constant as the reaction proceeds from acetylene to ethylidyne. This is shown in Figure 17, where the intensity of the antisymmetric C-D bend of C_2D_2 at 640 cm^{-1}, and intensity of the symmetric CD_3 deformation of CCD_3 at 987 cm^{-1} are plotted vs the total D_2 exposure. These intensities are measured from the set of HREEL spectra in Figure 8.

There was little to no tuning of the EEL spectrometer between these measurements. The error

bars are the $\pm 7\%$ determined from repeated measurement of a single C_2D_2 exposure. As the

intensity of the C_2D_2 feature decreases, the intensity of the CCD_3 feature increases by the same

amount. The sum of the two intensities is about constant. Since a linear relationship between

the C_2D_2 intensity and the C_2D_2 coverage has been established, and a constant value for the

sum of C_2D_2 and CCD_3 intensities is observed, this suggests that the ethylidyne intensity is also

linear with coverage. The only other possibility is that the intensity versus coverage

relationship is anticorrelated for acetylene and ethylidyne under these conditions. This

conclusion seems unlikely given that a linear relationship for the intensity of C_2D_2 and the

coverage of C_2D_2 has been found.

One other important fact is that the carbon coverage on the surface does not change

over the course of an experiment. The constancy of the carbon coverage was tested by

warming the crystal with 0.17 ML C_2H_2 to 270 K, doing a sequence of four H_2 exposures and

anneals to produce a surface of mostly CCD_3, and then using Auger spectroscopy to

measurement the carbon coverage. The surface carbon coverage of an initial 0.17 ML of C_2H_2

after this sequence of H_2 exposures and anneals is identical to that of 0.17 ML of C_2H_2 as

shown in Figure 18. Therefore, the sum of the acetylene and ethylidyne coverage at any point

in the equilibrium are equal to the initial acetylene coverage.

It is now possible to calculate the coverages of each hydrocarbon. The linearity of the

EELS intensity with acetylene and ethylidyne coverage and the constant sum of the two

intensities means that the intensity of each species is proportional to the surface coverage. The
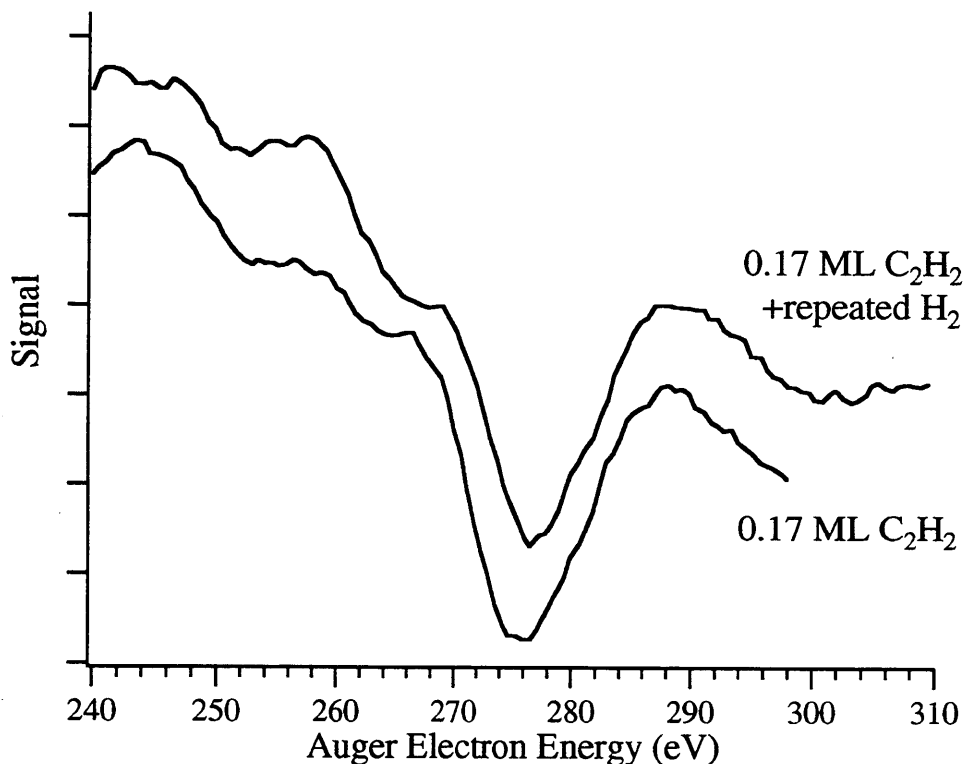
Figure 18 First derivative Auger carbon signal at 275 eV for 0.17 ML C_2H_2 with and without repeated H_2 exposures and anneals, taken at 80 K.

EELS intensities of both species are a measurement of the relative coverages of adsorbed

acetylene and ethylidyne. The initial amount of carbon on the crystal, in the form of C_2D_2, is

well known and does not change. Combining the relative EELS measurement with the

absolute carbon coverage results in the absolute coverage of each species. Defining $I(C_2D_2)$

and $I(CCD_3)$ as the measured EELS intensities of each species, and $\Theta_i^{C_2D_2}$ as the initial C_2D_2

coverage in monolayers, the coverages of C_2D_2 and CCD_3 in monolayers labeled as $[C_2D_2]$ and

$[CCD_3]$, are given by the formulas

$$[C_2D_2] = \Theta_i^{C_2D_2}\left(\frac{I(C_2D_2)}{I(C_2D_2)+I(CCD_3)}\right) \text{ and} \qquad (4a)$$

$$[CCD_3] = \Theta_i^{C_2D_2}\left(\frac{I(CCD_3)}{I(C_2D_2)+I(CCD_3)}\right). \qquad (4b)$$

4.3 *Results of Equilibrium Constant Measurements*

Equilibrium coverages are measured for different initial coverages of C_2D_2 and surface

bound D. The surface bound D is produced by exposing the C_2D_2 covered surface to 2×10^{-5}

Torr of D_2 for 15 minutes (18,000L) while the crystal temperature is 220 K. This D_2 exposure

saturates the surface with D for all initial C_2D_2 coverages. A control experiment has been done

to insure that no ethylidyne is formed during exposure of the crystal at 220 K to D_2. The

spectrum of the surface for this experiment is shown in Chapter 6. The initial C_2D_2 coverages

range from 0.03 to 0.19 ML, while the corresponding initial D coverages are varied from 0.94

to 0.52 ML, so that the ratio of $[C_2D_2]/[D]$ ranges from 0.03 to 0.37. The saturation coverage

of C_2D_2 is 0.25 ML, compared to the 1.0 ML for D, which is why the above C_2D_2 and D

coverage values do not add to one. The range of $[C_2D_2]$ and $[D]$ values are expected to

produce a range in the CCD_3 coverage. After preparation of this coadsorbed layer, the crystal

is heated to 280 K, where the reaction rate is highest without the risk of desorbing deuterium,

and held for 60 minutes to attain equilibrium. There is no change in the ratio of products and

reactants if the crystal is held at 280 K for a longer time, confirming that equilibrium is

reached. No carbon or deuterium is removed from the surface during this anneal. The crystal

is then cooled to 80 K at which temperature an EEL spectrum is measured.
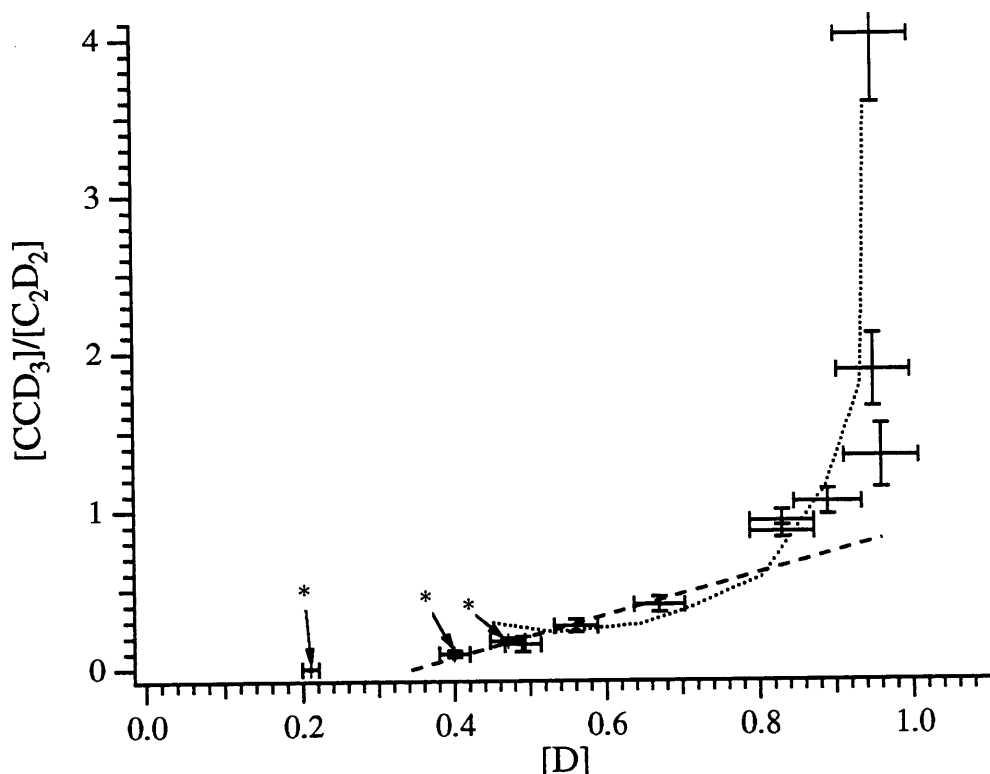
Figure 19 Ratio of coverages, [CCD$_3$]/[C$_2$D$_2$] versus coverage of [D] at equilibrium for [ES]=0.05. Points with stars (*) have [ES]>0.38. Error bars are explained in text and in Table 1.

The results of the equilibrium coverage measurements are plotted as [CCD$_3$]/[C$_2$D$_2$] vs [D], where all coverages are in monolayers, as shown in Figure 19. The error bars for the values plotted in Figure 19 are determined by propagating the error estimated for each raw datum measurement through the calculations. A summary of the errors used for each raw measurement and the equations used to calculate [CCD$_3$]/[C$_2$D$_2$] and [D] are presented in Table 1. The errors used for the EELS intensity measurements are derived from the error in determining the level of the background signal. If this equilibrium reaction obeys the equilibrium constant expressed in Equation 2 above, the data should lie on a line including the origin, the slope of which will be the value of K$_{eq}$. It is clear that this system does not obey

Raw measurement/ calculated value	description	error
$I(C_2D_2)$	intensity of C_2D_2 EEL spectral feature	0.5 cts
$I(CCD_3)$	intensity of CCD_3 EEL spectral feature	0.5 cts
$\Theta_i^{C_2D_2}$	initial coverage of C_2D_2 in monolayers	2.5%
From these data		
$[C_2D_2]$	equilibrium coverage of C_2D_2 in monolayers	
$[CCD_3]$	equilibrium coverage of CCD_3 in monolayers	
are calculated: using the equations	$[C_2D_2] = \Theta_i^{C_2D_2}\left(\dfrac{I(C_2D_2)}{I(C_2D_2)+I(CCD_3)}\right)$	error varies
	$[CCD_3] = \Theta_i^{C_2D_2}\left(\dfrac{I(CCD_3)}{I(C_2D_2)+I(CCD_3)}\right).$	error varies
Θ^D_i	initial surface D coverage	
is calculated from:	$\Theta_i^D = 1.02 \pm 0.06 - 2.6 \pm 0.40\Theta_i^{C_2D_2}$	
	average propagated error for Θ^D_i used is	5%
$[D]$	equilibrium coverage of D in monolayers	
is calculated from	$[D] = \Theta_i^D - [CCD_3]$	error varies
Equilibrium Constant calculated as	$K_{eq} = \dfrac{[CCD_3]}{[C_2D_2][D]}$	error varies

Table 1 Estimated or measured precision of measurements and definition of calculated quantities and their propagated error used in calculating equilibrium constant values.

well this expression for the equilibrium constant. As discussed below, the data can be

described by a line or a curve, but neither fit includes the origin.
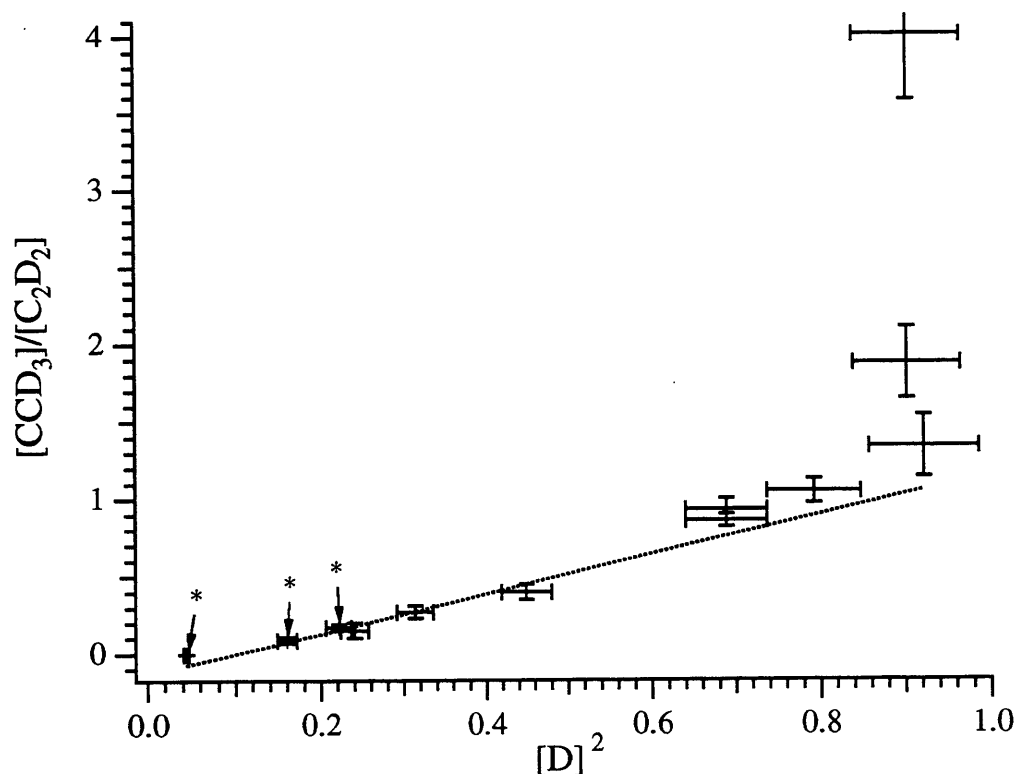
Figure 20 Ratio of coverages, $[CCD_3]/[C_2D_2]$ versus coverage of $[D]^2$ at equilibrium for $[ES]=0.05$. Points with stars (*) have $[ES]>0.38$. Error bars are explained in text and in Table 1.

4.4 *Discussion of Equilibrium Constant Data*

Two possible fits, a straight line and a curve, to the equilibrium data are shown in

Figure 19. A third potential fit for these data is shown in Figure 20 where the ratio

$[CCD_3]/[C_2D_2]$ is plotted vs $[D]^2$. Each of these fits makes different assumptions about how

this reaction is more complex than it is written in Equation 1. The straight line fit in Figure 19

shows that if the [D] coverage is expressed as $[D]_{measured}-0.34$ ML, then the data fit a line

through the origin and the value of K_{eq} is the slope. Physically, this fit suggests that the

reaction is nonideal and that the first 0.34 ML of D adsorbed on the surface do not participate

in the reaction. The surface interactions between D and the adsorbed hydrocarbons could be

responsible for this behavior, with the repulsive forces between coadsorbates separating them

until the coverage is high enough that they must interact. This fit will be referred to as the

offset [D] fit.

The model fit shown in Figure 20 also suggests interactions between adsorbates. The

origin of this fit is a picture in which a second D atom is consumed in this reaction. One way

this could occur is if the final CCD_3 species is actually stabilized by nearby D atoms, forming

some kind of weak CCD_3-D complex. The chemical equation would be written as

$$C_2D_2 + 2D \leftrightarrow CCD_3\text{-D}, \tag{5}$$

where the equilibrium constant for this reaction is

$$K_{eq} = \frac{[CCD_3]}{[C_2D_2][D]^2} . \tag{6}$$

The fit of a straight line to the plot of $[CCD_3]/[C_2D_2]$ vs $[D]^2$ describes the trend for data in

Figure 20, particularly at high D coverage which the fit in Figure 19 did not accomplish well.

This linear fit also includes the origin without any adjustments. Unfortunately, there are

additional equilibrium data that will be introduced in Section 4.6 that are incompatible with this

model.

The curved fit in Figure 19 represents another idea about how the reaction could be

written. This fit is derived from the equation of the equilibrium constant for the chemical

reaction written in Equation 7. This fit assumes that it is important to include empty sites (ES)

in the equilibrium.

$$C_2D_2 + D \leftrightarrow CCD_3 + 2ES \tag{7}$$

Empty sites are expected to be formed during this reaction because the reactants occupy a total

of 3.6 sites, 2.6 sites for C_2D_2 and one for D, while the CCD_3 product only occupies 1.5 sites. The origin of this value of 1.5 will be discussed later. In this way, empty sites are created for each CCD_3 molecule made. The idea that empty sites are important in the reaction of ethylidyne has been documented before[43,44] and will be discussed later. The surface is distinct from a gas phase or liquid reaction since there are a limited number of sites to be occupied by reactants or products. In order to increase the D coverage in the system, it must be repeatedly added to the surface to fill sites as they become available. At the beginning of the reaction, the surface is fully saturated with D, but as the reaction proceeds, one D atom is consumed, and 2 surface sites are opened up as adsorbed acetylene is transformed into ethylidyne. This curve fit displayed on Figure 19 is more successful than the straight line fit at higher D coverage, but less successful at lower D coverage.

4.5 *Elimination of the Empty Site Mechanism*

To probe the possibility of an empty site as a reactant species as expressed in Equation 7, the number of empty sites on the surface is varied. Under the experimental conditions used for the measurement shown in Figure 19, the ES coverages at equilibrium are calculated to be a constant of 0.05 ML. This value of the empty site coverage is calculated by subtracting the number of sites blocked by the C_2D_2, CCD_3, and D coverage at equilibrium from 1 ML. The number of sites blocked by C_2D_2 or CCD_3 is not equal to their specific coverages, where the coverage is given as a fraction of the top layer of Ni atoms, or a monolayer. Each hydrocarbon species has a footprint on the surface, occupying a particular number of sites or number of Ni atoms per molecule. The measured number of sites for the C_2D_2 molecule is 2.6 sites, obtained

from the slope of the line fit to the plot of Θ_i^D versus $\Theta_i^{C_2D_2}$, in Figure 14 and Equation 3. The

value used for the number of sites that CCD_3 occupies is 1.5. This number is calculated from

actual equilibrium surface D measurements of saturated surfaces with the same total carbon

coverage, but different relative CCD_3 and C_2D_2 coverages. If CCD_3 and C_2D_2 each occupy the

same number of surface sites there would be no change in coadsorbed D coverage as the

surface is converted from all C_2D_2 to CCD_3. However, the amount of coadsorbed D does

change as C_2D_2 is converted to CCD_3. The measurement of the coadsorbed D coverage for

surfaces with different relative CCD_3 and C_2D_2 coverages is a measure of how many sites not

blocked by both hydrocarbons. Each coadsorbed D coverage depends on the footprint of

hydrocarbons and the coverage of each hydrocarbon. Since the footprint of C_2D_2 is known, it

is then possible to calculate the value of the footprint of CCD_3. The equation for the empty

site coverage is

$$[ES] = 1 - 2.6[C_2D_2] - 1.5[CCD_3] - [D]. \tag{8}$$

Three measurements of K_{eq} were carried out using an initial C_2D_2 coverage of 0.06 ML

and different coverages of D between 0.21 and 0.48 ML, compared to the saturated D

coverage of 0.86 ML used in the previous experiments when the initial C_2D_2 coverage was

0.06 ML. The lower coverages of D compared to the saturation D coverage were formed by

exposure of the surface to D_2 for shorter times and at lower D_2 pressure. Other than the

different D coverage, the experimental procedure was exactly the same as in the previous

equilibrium measurements. If empty sites act as a reactant species, the increase in empty site

concentration from 0.05 ML to at least 0.36 ML is expected to shift the equilibrium

substantially resulting in a hydrocarbon coverages dominated by C_2D_2. These three

measurements are marked with astericks in Figures 19 and 20. These three points agree with

the two straight line fits very well. There is no strong shift in the equilibrium back towards the

C_2D_2 reactant for these points with a large coverage of empty sites. The coverage of empty

sites does not change the equilibrium. This experiment eliminates the empty site mechanism

for this reaction. This leaves two possible fits, the offset [D] fit and the $[D]^2$ fit, which are

both driven by the idea that this reaction is nonideal, because the equilibrium is controlled by

interactions between the coadsorbates. Each of these fits represents a different way to

conceive of the nonideal nature of the equilibrium. It is not possible to choose one fit over the

other, because there is no experimental evidence to support the decision. This means that the

actual chemical equation and the form and value of K_{eq} cannot be determined.

4.6 *Equilibrium Points Measured with Repeated D_2 Exposures*

In addition to making equilibrium measurements after a single exposure to D_2 and a

single anneal at 280 K, measurements were also made after several exposures to D_2 and

subsequent 280 K anneals. In these experiments, measurement of the equilibrium coverage of

surface bound D is much more difficult, as discussed earlier. Integrated D_2 values from TD

measurements provided unsatisfactory results. Instead, the surface D coverage at equilibrium

is calculated, assuming that the surface is fully saturated with D from the repeated D_2

exposures, by subtracting the number of sites blocked by the experimental values of the C_2D_2

and CCD_3 coverages.

$$[D] = 1 - 2.6[C_2D_2] - 1.5[CCD_3] \qquad (9)$$

This calculation systematically overestimates the surface D coverage, because it does not

account for empty sites. The value of the empty site coverage is calculated to be a maximum

of 0.05 ML, so the surface D coverage is off by 0.05 ML at most.

The procedure for these multiple D_2 exposure points is as follows. A surface is

prepared with between 0.12 ML and 0.19 ML of C_2D_2 at 80 K. The crystal is then warmed to

220 K and a 10 min exposure to $2x10^{-5}$ Torr D_2 occurs. The crystal is then warmed to 280 K

where the reaction to make CCD_3 occurs, and is held at this temperature for 30 min. The

crystal is then cooled to 220 K for a second D_2 exposure, the same as the first. Another 280 K

anneal follows, and the cycle of D_2 exposures and anneals are repeated for up to 13 times. The

last 280 K anneal is always 60 minutes to insure equilibrium is established. After the final

anneal, the crystal is cooled to 80 K and the EEL spectrum is measured. From the intensities

of the features of C_2D_2 and CCD_3 and the initial C_2D_2 coverage, the absolute coverage of each

hydrocarbon and surface bound D are calculated from Equations 4a, 4b, and 9 above. Figure

21 shows the addition of these multiple D_2 exposure equilibrium points to the graph of

$[CCD_3]/[C_2D_2]$ vs [D] with the single D_2 exposure points (shown as filled in circles). The

results of the equilibrium measurements for three initial C_2D_2 coverages after multiple

exposures to D_2 and annealing to 280 K are shown by hollow symbols. There is a dramatic

increase in the $[CCD_3]/[C_2D_2]$ ratio with repeated D_2 exposures. With repeated exposure to

D_2, most of the C_2D_2 can be converted to CCD_3. It is clear that there is a different equilibrium

behavior between the single D_2 exposure and the multiple D_2 exposure data. The increase in

CCD_3 coverage with repeated D_2 exposure completely separates these points from the single
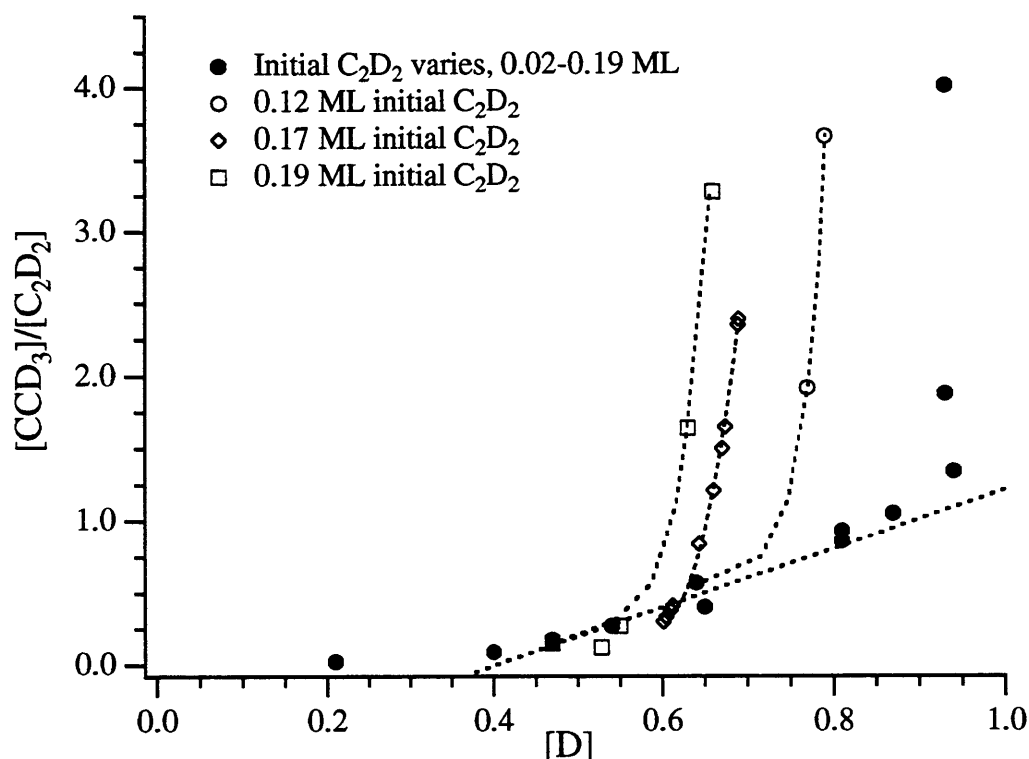
Figure 21 Ratio of coverages, $[CCD_3]/[C_2D_2]$ versus coverage of [D] at equilibrium for [ES]=0.05. Solid symbols are for single D_2 exposure points, while open symbols are for multiple D_2 exposures.

D_2 exposure points. It is impossible to consistently explain all the data in terms of a single equilibrium constant.

4.7 Islanding, Ordering, Site Blocking and Ensemble Effects

The indisputable observation that there is no single value of K_{eq} that can be fit to both the single and multiple D_2 exposure data demonstrates that the equilibrium in this surface reaction is much more complex that the simple chemical reaction written in Equation 1. Neither of the alternate descriptions of the reaction involving the offset [D] coverage or the CCD_3-D complex can explain the trend in the equilibrium data. One possible explanation for

$$E_a^f$$

$$E_a^r$$

$$C_2D_2 + D$$

$$\Delta H$$

$$CCD_3$$
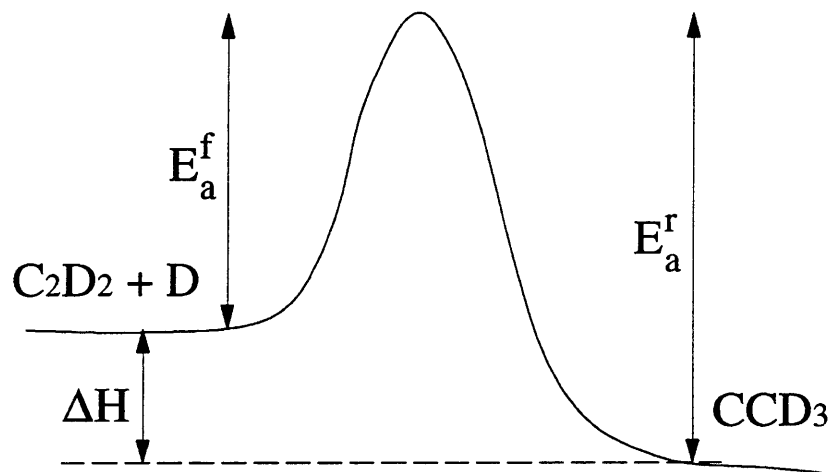
Figure 22 One dimensional schematic representation of the energy barrier between acetylene and ethylidyne formation.

the complexity is that the system is non-ideal due to interactions between coadsorbates. The question of coadsorbate interactions will be discussed in the next section.

The changes in the K_{eq} value also suggest changes in the potential energy surface. Figure 22 shows a one-dimensional slice of the potential energy for this surface. It is possible that the changes in K_{eq} that are observed in this system result from enthalpy or entropy changes. The equation,

$$\Delta H = T\Delta S - RT\ln K_{eq}, \qquad\qquad (10)$$

describes the relationship between K_{eq} and the ΔH and ΔS values. Enthalpy has not been measured in this study. Later in this chapter, forward activation energy measurements which provide some information about the entropy are presented.

The possibility of rearrangement and ordering of surface species could lead to large enthalpy and entropy changes. The ordering could occur with changes in surface bound D and

C_2D_2 coverages. This ordering could lead to the separation of the two adsorbates into islands. Island formation in the similar reaction of C_2H_4 decomposition to CCH_3 on Pt(111) has been experimentally observed by scanning tunneling microscopy.[38] Images recorded during the conversion of C_2H_4 to CCH_3 show inhomogenous surface structure, which the authors interpret as evidence that the reaction takes place at edges of CCH_3 islands. Erley and coworkers[44] studied the kinetics of this same reaction and found evidence for the necessity of an ensemble of empty surface sites for a C_2H_4 molecule to decompose to CCH_3. The result of a Monte Carlo calculation well describes the kinetic data and also predicts a patchy, non-uniform, surface structure. In the C_2D_2 and surface bound D system, an order-disorder phase transition may occur at a particular ratio of D/C_2D_2 coverages, with a well mixed layer in one regime and island formation in the other regime. This phase transition is a cooperative motion of D and C_2D_2 which most likely results in a change in the local potential energy surface of both adsorbates. Such island formation and changes in local potential energy have been observed for C_2H_2 adsorbed on Pd(111) using scanning tunneling microscopy.[39] On the edges of these islands, C_2H_2 molecules trimerize to benzene.[39] A separate study has measured coverage dependent activation energy values for this trimerization reaction.[58] Changes in the activation energy with coverage imply changes in the potential energy surface with coverage.

Another explanation for the dramatic increase in CCD_3 coverage with repeated addition of surface bound D is that the backward rate is suppressed because the backward reaction requires an ensemble, or specific number of adjacent empty sites, to occur. The continued addition of D atoms could block the empty sites necessary for the backward reaction. The
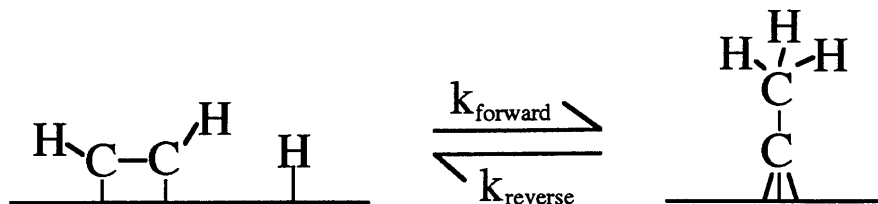
Figure 23 Schematic of adsorbed acetylene and deuterium reacting to form ethylidyne. Notice that the reactants occupy three surface sites while the product occupies one site.

existence of ordering and islanding would exacerbate this effect, since a more extreme range of individual molecular environments would exist. The need for an ensemble of empty sites in the backward reaction is a consequence of the C_2D_2 and D products occupying more sites than the CCD_3 reactant. When adsorbed CCD_3, which is bound to a single three fold hollow site, tries to decompose to adsorbed C_2D_2 and surface bound D, with the acetylene bound to two, three fold sites and the D to a third, at least two empty surface sites are needed to accommodate the products. This bonding picture is shown in Figure 23. If there is an insufficient number of empty sites on the surface in the vicinity of a CCD_3 molecule, because of layer rearrangements, it will not be able to decompose. It will be trapped. When CCD_3 molecules are trapped they do not participate in the equilibrium, and the reverse rate constant, $k_{reverse}$, is suppressed. A lower value of $k_{reverse}$ leads to an increase in the value of K_{eq} since

$$K_{eq} = \frac{k_{forward}}{k_{reverse}}.$$
(11)

This trapping of CCD_3 is most likely to occur in the repeated D_2 exposure equilibrium experiments because the repeated D_2 exposures and annealing promote layer rearrangements that trap CCD_3 by creating a wide range of environments. Figure 24 shows a plot of K_{eq} versus total ML of surface sites blocked. The total number of surface sites blocked are
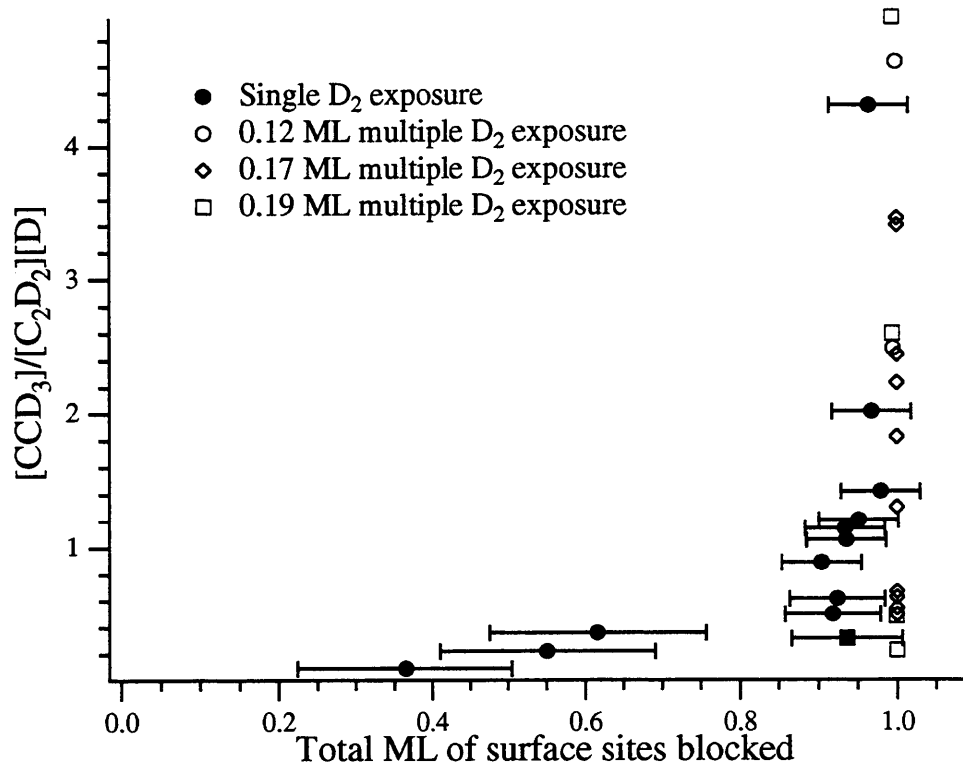
Figure 24 $K_{eq} = [CCD_3]/[C_2D_2][D]$ versus total ML of surface sites blocked, Solid symbols are for single D_2 exposure points, while open symbols are for multiple D_2 exposures.

calculated from summing the coverage of each adsorbed species times the number of surface sites it blocks, as described in Section 4.5. The error bars are propagated as described in Table 1. Error bars are not shown for multiple D_2 exposure points for clarity, although they are of a similar magnitude to those shown. Notice that all values of K_{eq} are observed with the same total coverage, or empty site coverage, within the limits of the error bars. The lack of correlation between the empty site coverage and the K_{eq} value suggests that the apparent trapping of the CCD_3 product is not due to simple crowding of the surface with D. Instead, it leads to the speculation that rearrangement of the homogeneous layer to create a wide range of environments is responsible for the trapping observed.

There is a precedence for the need for an ensemble of surface sites in a surface

reaction. An ensemble size for adsorption and decomposition has been measured using

bismuth as an inert site blocker for several molecules on platinum. An adsorption site for C_2H_4

is determined to be four Pt atoms with an ensemble of six Pt atoms needed for decomposition

of C_2H_4 to CCH_3.[40] The number of additional surface sites for dehydrogenation of

cyclopentane, cyclohexane, benzene, cyclopentene and cyclohexene have been measured to be

up to twice the number of sites occupied by the chemisorbed molecule.[41]

Much study has been done to understand CCH_3 formation from the decomposition of

C_2H_4 on Pt. Some of this work establishes the need for an ensemble of surface sites in C_2H_4

decomposition. An ensemble of empty sites is needed in the decomposition of C_2H_4 because

the transition state requires a new H-Ni bond while the existing C-Ni bonds of C_2H_4 are intact.

In an experiment on a supported palladium catalyst, the CCH_3 coverage is shown to rise and

plateau with time at given C_2H_4 pressure.[42] When the C_2H_4 pressure is subsequently reduced,

more CCH_3 is observed. The interpretation is that at high pressure, the combination of high

flux and finite residence time of C_2H_4 molecules block sites needed for decomposition. A

similar effect is seen in another experiment that measured the decomposition temperature of

CCH_3 on Ru(001) using FTIR.[43] An increase in the decomposition temperature of CCH_3 was

observed in an elevated partial pressure of H_2 compared to CCH_3 decomposition in vacuum.

Again, the argument is made that the increased flux of H_2 molecules on the surface creates a

larger steady state population that blocks empty sites. As the crystal temperature is increased,

the residence time of the H_2 decreases, resulting in an increase in the empty site coverage and

an increase in the decomposition of CCH_3. Erley and coworkers[44] have observed changes in the rate of decomposition of the C_2H_4 reactant during CCH_3 formation as a function of C_2H_4 coverage on Pt(111). The rate data are successfully fit with a Monte Carlo simulation assuming an ensemble size of four Pt atoms.

Considering the additional adsorption sites needed for ethylidyne decomposition to acetylene and surface bound D, empty sites are necessary for the reaction to occur. In the multiple D_2 exposure equilibrium data, the repeated D_2 exposures and annealing promote layer rearrangements, ordering and islanding of the originally homogeneous surface, thus creating a wide range of environments. The single D_2 exposure data points at high D coverages also exhibit this ordering and diversity of environments. In some of these environments, the small coverage of empty sites likely results in the inability of ethylidyne to decompose back to acetylene. This ordering and islanding may independently lead to changes in ΔH and/or entropy, both of which would shift the K_{eq} value.

5 Measurement of Rates and Activation Energy

This reaction is slow enough that it is possible to measure the initial rate of ethylidyne formation from C_2D_2 and surface D. Initial rates of ethylidyne formation are measured at different crystal temperatures. From a set of rate measurements at different temperatures, the activation energy (E_a) is extracted from an Arrhenius plot.

The procedure for the rate measurement is as follows. A known coverage of C_2D_2 is adsorbed on the crystal at 80 K. The remaining surface sites are saturated with surface bound D by exposure of the crystal at 220 K to 2×10^{-5} Torr of D_2 for 15 minutes. Control

280K   270K   260K

Loss Intensity

Energy Loss (cm^{-1})
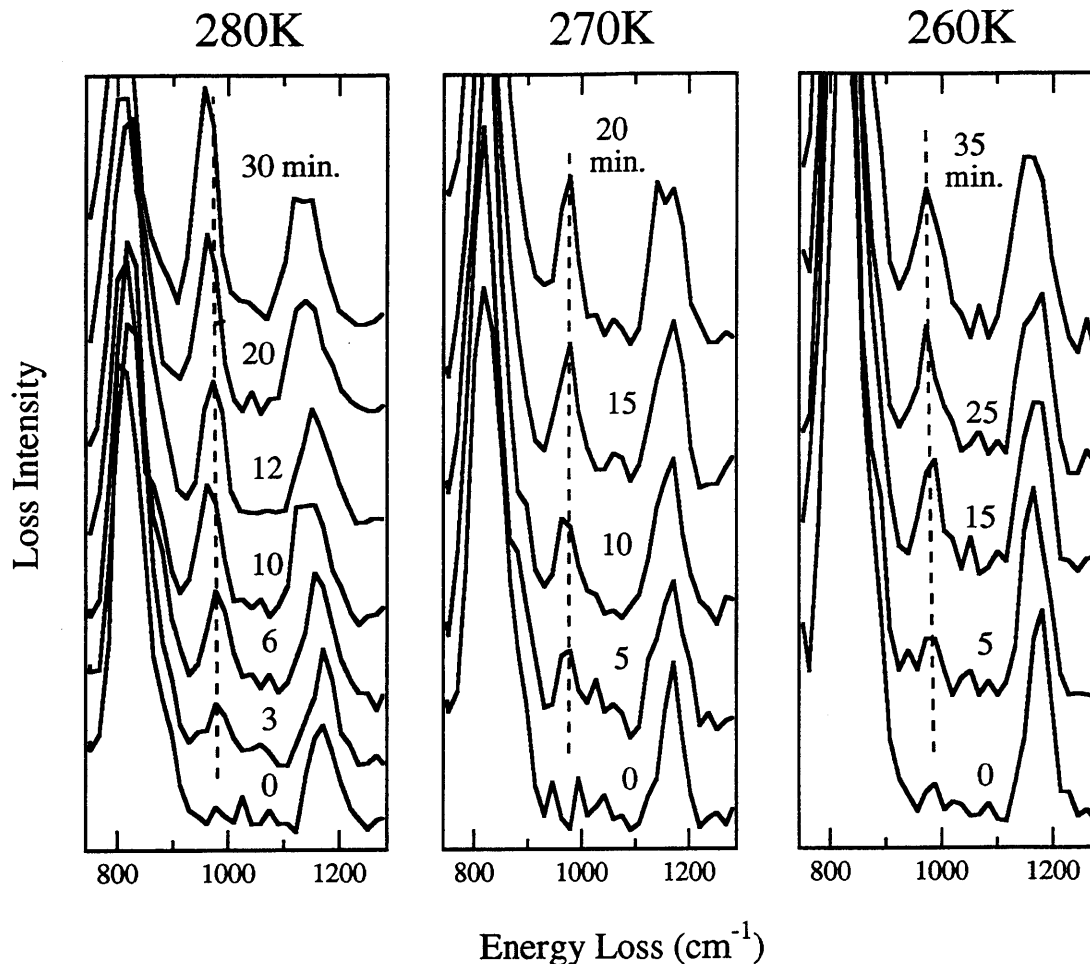
Figure 25 HREEL spectra measured as a function of time of the reaction C$_2$D$_2$ + surface bound D at three temperatures, 280 K, 270 K and 260 K. Initial coverage 0.06 ML C$_2$D$_2$ and 0.86 ML D. Dotted line marks frequency of the mode of CCD$_3$ product. Spectra taken at 80 K, at 10° off specular with 6.5 eV electrons, ΔE$_{fwhm}$ average 43 cm^{-1}.

experiments show that no ethylidyne is formed and no acetylene is desorbed during

exposure to D$_2$. These experiments are described in detail earlier in this chapter and in Chapter

6. The surface is then heated at ~1 K/s to the reaction temperature, between 250 K and 280 K,

for a specific time, and cooled at ~2 K/s to 80 K. There is no backward movement in the

equilibrium during this cooling, as discussed earlier. At 80 K, the reaction is frozen and does

280K   270K   260K

Loss Intensity

Energy Loss (cm^{-1})
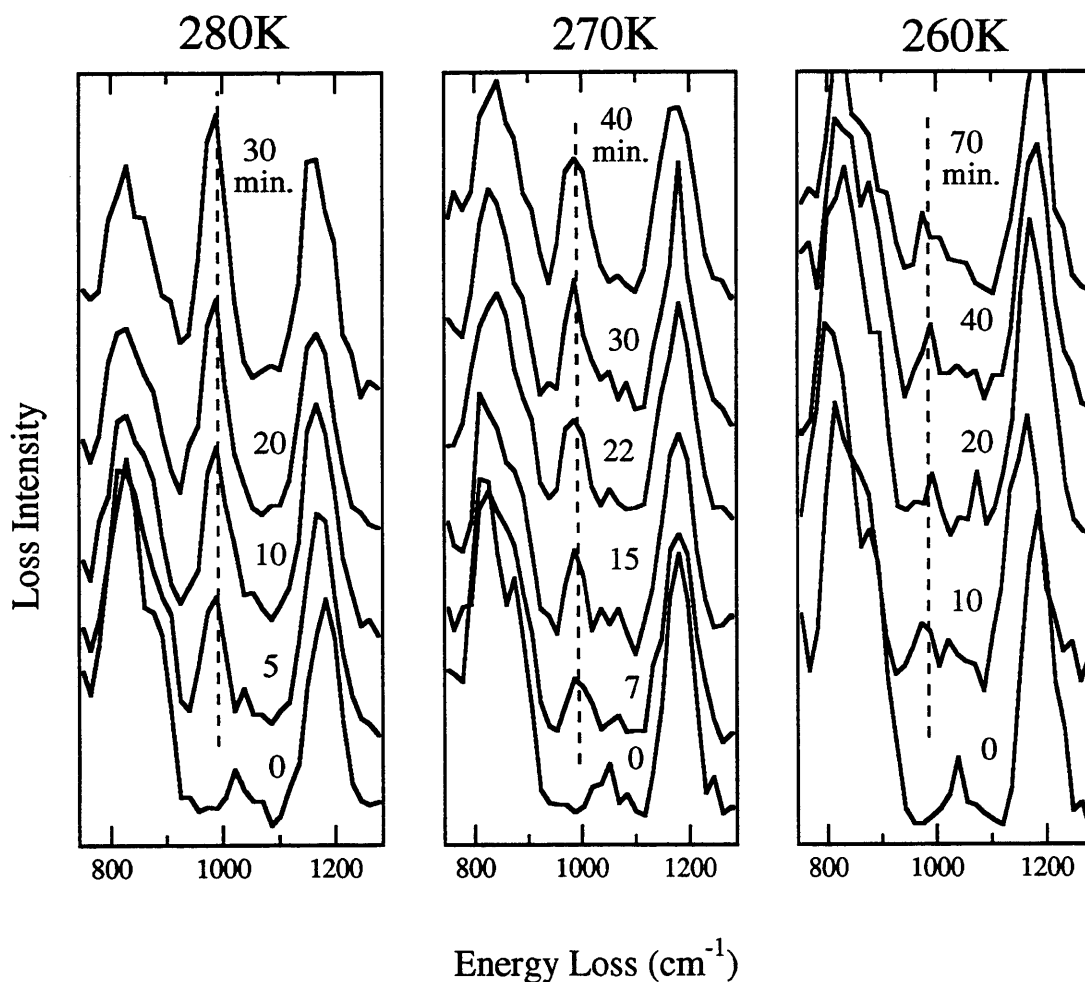
Figure 26 HREEL spectra measured as a function of time of the reaction C_2D_2 + surface bound D at three temperatures, 280 K, 270 K and 260 K. Initial coverage 0.12 ML C_2D_2 and 0.70 ML D. Dotted line marks frequency of the mode of CCD_3 product. Spectra taken at 80 K, at 10° off specular with 6.5 eV electrons, ΔE_{fwhm} average 45 cm^{-1}.

not proceed. A vibrational spectrum is measured to obtain the absolute coverages of adsorbed

acetylene and ethylidyne on the surface. The crystal is then heated to the reaction temperature

for another time increment, cooled to 80 K, and another vibrational spectrum is measured to

monitor the progress of the reaction. In this way, a series of spectra corresponding to different

reaction times are measured. Figure 25 shows slices of a series of EEL spectra as a function of
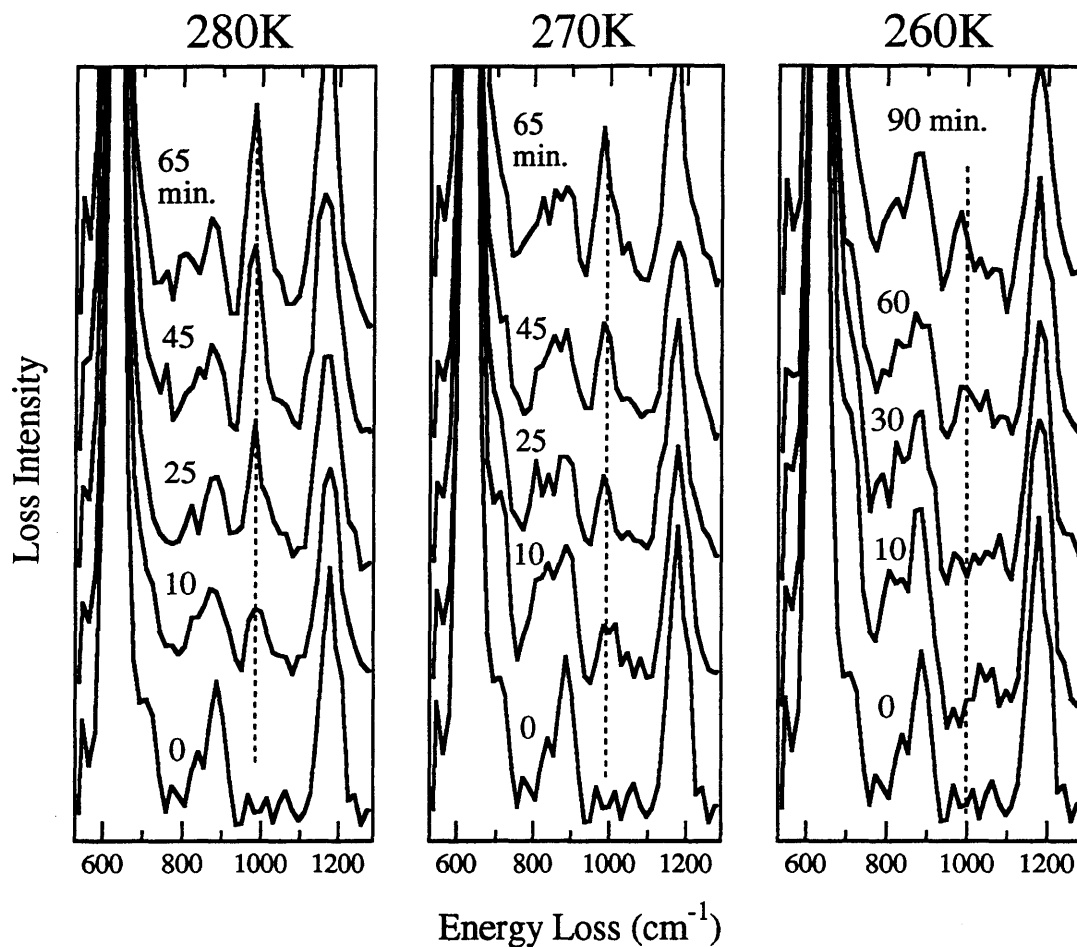
Figure 27 HREEL spectra measured as a function of time of the reaction C_2D_2 + surface bound D at three temperatures, 280 K, 270 K and 260 K. Initial coverage 0.17 ML C_2D_2 and 0.57 ML D. Dotted line marks frequency of the mode of CCD_3 product. Spectra taken at 80 K, at 10° off specular with 6.5 eV electrons, ΔE_{fwhm} average 54 cm^{-1}.

reaction time measured for three temperatures for an initial C_2D_2 coverage of 0.06 ML.

Figures 26 and 27 show the same series of spectra for initial C_2D_2 coverages of 0.12 ML and

0.17 ML. This technique of measuring surface kinetics with EELS has been used by

others.[45,46,47]

To obtain the initial rate of ethylidyne formation, the ethylidyne coverage is plotted

versus the reaction time as shown in Figures 28a, 29a, 30a, 31a, and 32a. Initial rates of

ethylidyne formation have been measured at several crystal temperatures for five initial C_2D_2

coverages of 0.06, 0.09, 0.105, 0.12, and 0.17 ML with a saturation exposure of D_2. Five

initial C_2D_2 coverages are measured to probe possible coverage dependent changes in the

activation energy. The initial rate of ethylidyne formation as a function of crystal temperature

has also been measured in a single experiment where the surface is not saturated with surface

bound D after C_2D_2 adsorption. In this way, empty sites are present initially and the activation

energy for a coadsorbate system with the presence of empty sites is determined. These rate

measurements are shown in Figure 33a for the initial coverage of 0.06 ML C_2D_2, 0.57 ML D,

and 0.29 ML empty sites.

The CCD_3 coverage increases rapidly at short times, and then levels off at longer times.

These data are fit to the time dependence of product formation for an approximate solution of

the second order reaction, A + B → AB, where the rate is first order in each reactant. The

slope of the fitted curve at zero time is the initial rate of CCD_3 formation. The functional form

is:

$$[CCD_3] = A\left(1 - e^{-\frac{st}{A}}\right) \quad (12) \qquad \text{with} \qquad \frac{d[CCD_3]}{dt} = -s \cdot e^{-\frac{st}{A}} \quad (13)$$

where A and s are arbitrary constants. It is clear from Equation 12 that the constant s is the

value of the slope at t=0 and is the initial rate. The fits of Equation 11 to these rates are also

shown in Figures 28a, 29a, 30a, 31a, 32a, and 33a. The initial rates for each initial C_2D_2
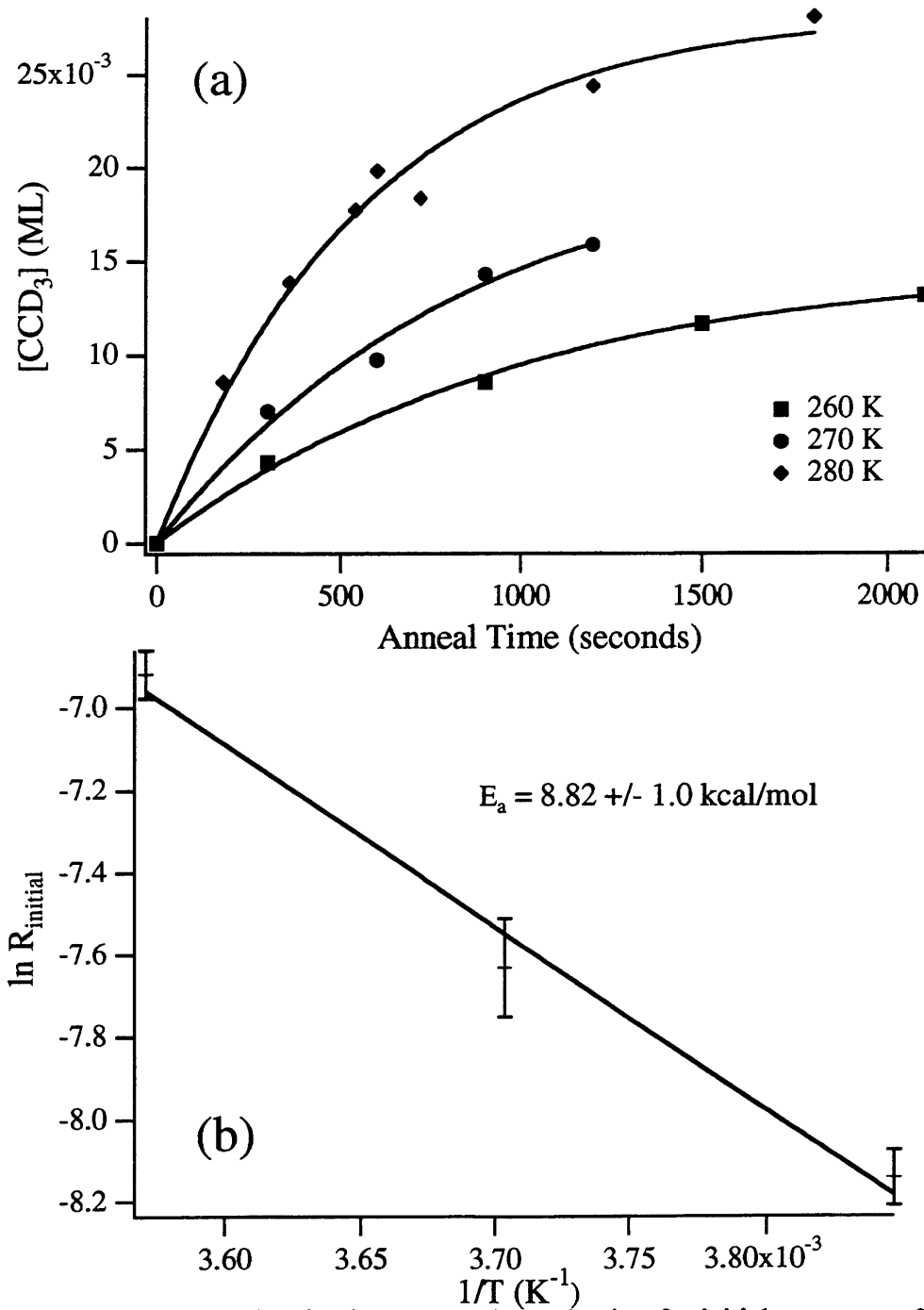
Figure 28 Rates and activation energy determination for initial coverage of 0.06 ML C_2D_2 and 0.86 ML D. (a) Coverage of CCD_3 versus time used to determine initial rate of D addition at different temperatures. (b) Arrhenius plot of $Lnk_{initial}$ versus $1/T$. Error bars are explained in the text.
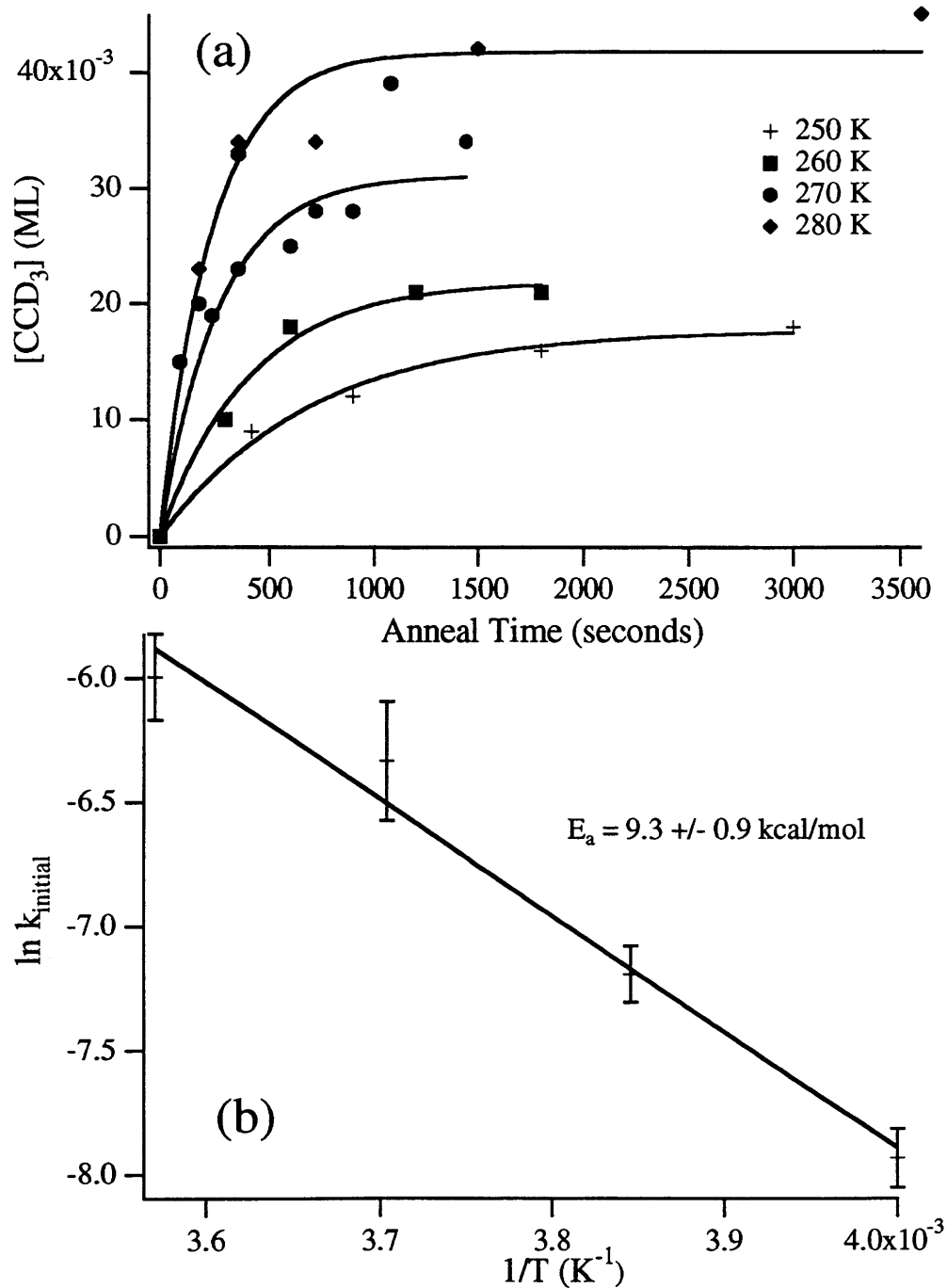
Figure 29 Rates and activation energy determination for initial coverage of 0.09 ML C_2D_2 and 0.78 ML D. (a) Coverage of CCD_3 versus time used to determine initial rate of D addition at different temperatures. (b) Arrhenius plot of $Lnk_{initial}$ versus 1/T. Error bars are explained in the text.
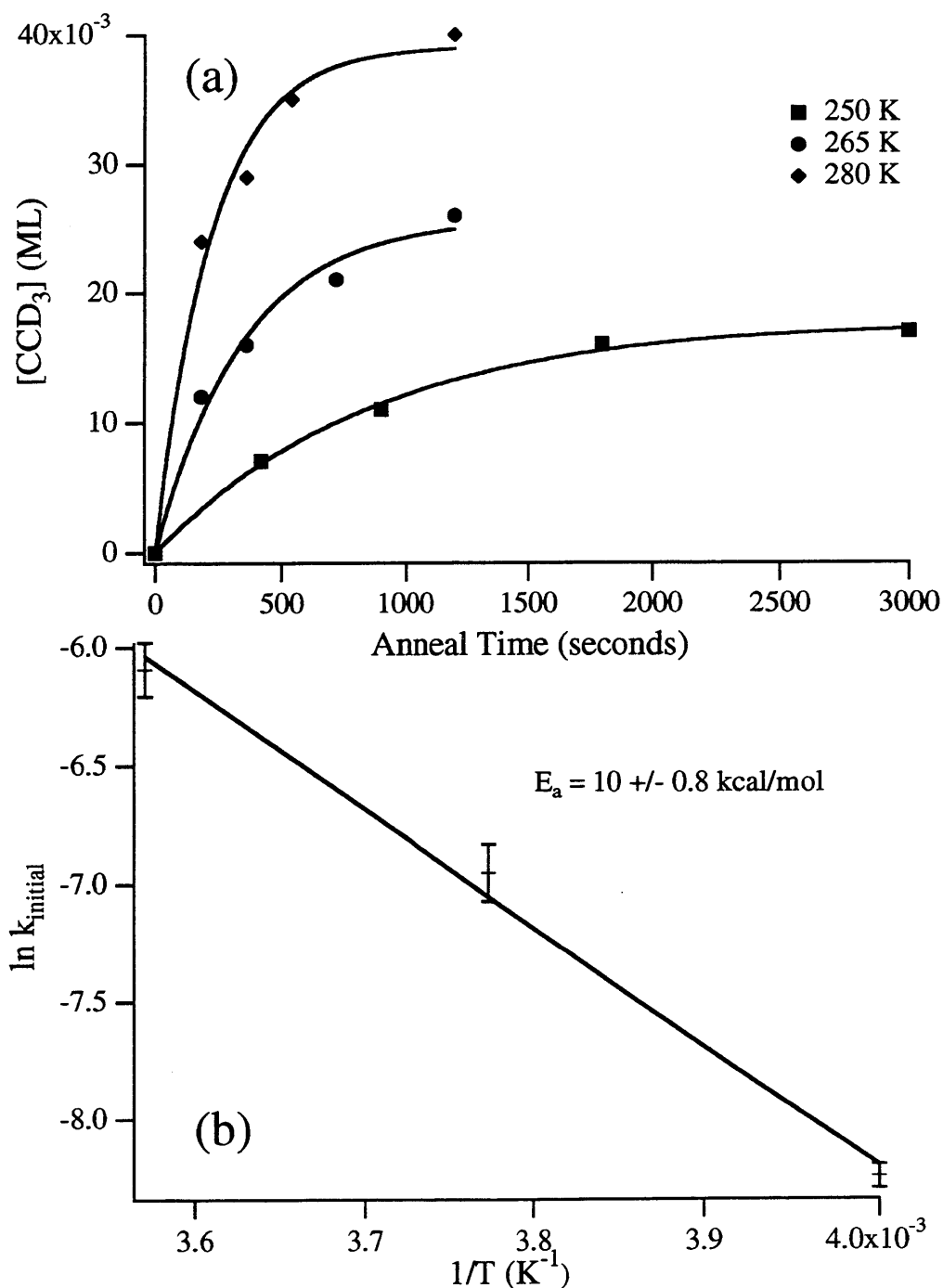
Figure 30 Rates and activation energy determination for initial coverage of 0.105 ML C_2D_2 and 0.74 ML D. (a) Coverage of CCD_3 versus time used to determine initial rate of D addition at different temperatures. (b) Arrhenius plot of $Lnk_{initial}$ versus 1/T. Error bars are explained in the text.
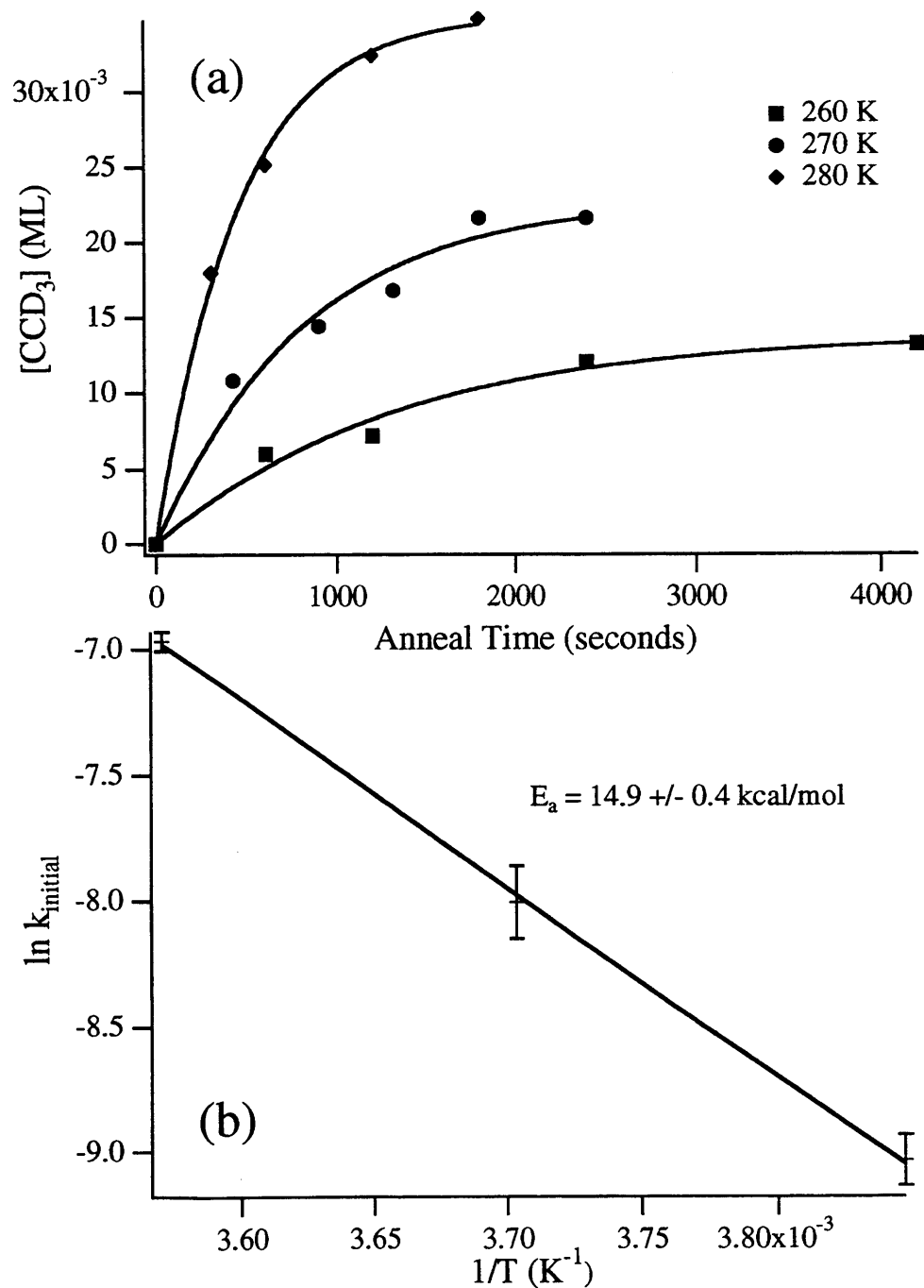
Figure 31 Rates and activation energy determination for initial coverage of 0.12 ML C_2D_2 and 0.70 ML D. (a) Coverage of CCD_3 versus time used to determine initial rate of D addition at different temperatures. (b) Arrhenius plot of $Lnk_{initial}$ versus $1/T$. Error bars are explained in the text.
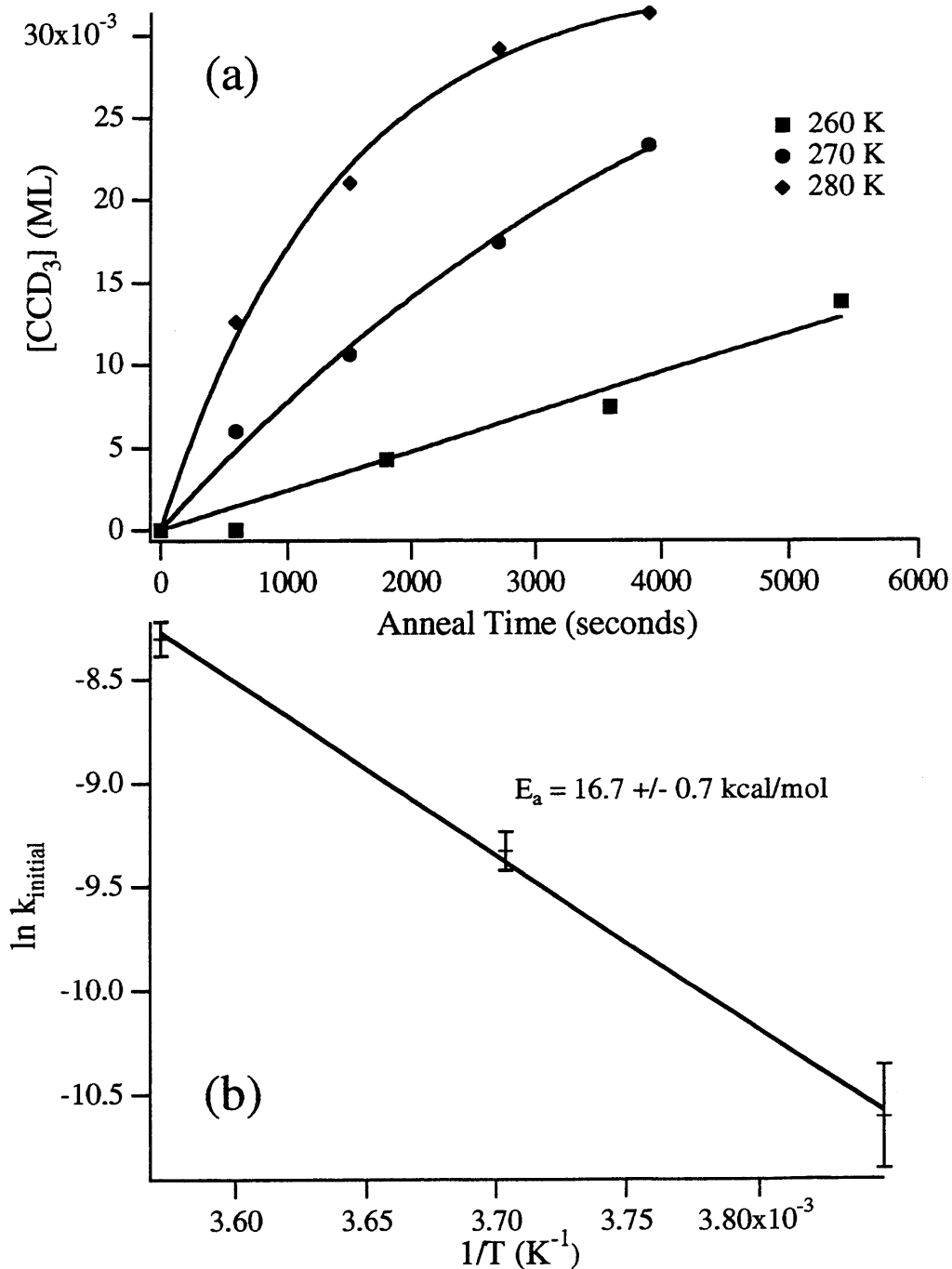
Figure 32 Rates and activation energy determination for initial coverage of 0.17 ML C_2D_2 and 0.57 ML D. (a) Coverage of CCD_3 versus time used to determine initial rate of D addition at different temperatures. (b) Arrhenius plot of $Lnk_{initial}$ versus 1/T. Error bars are explained in the text.
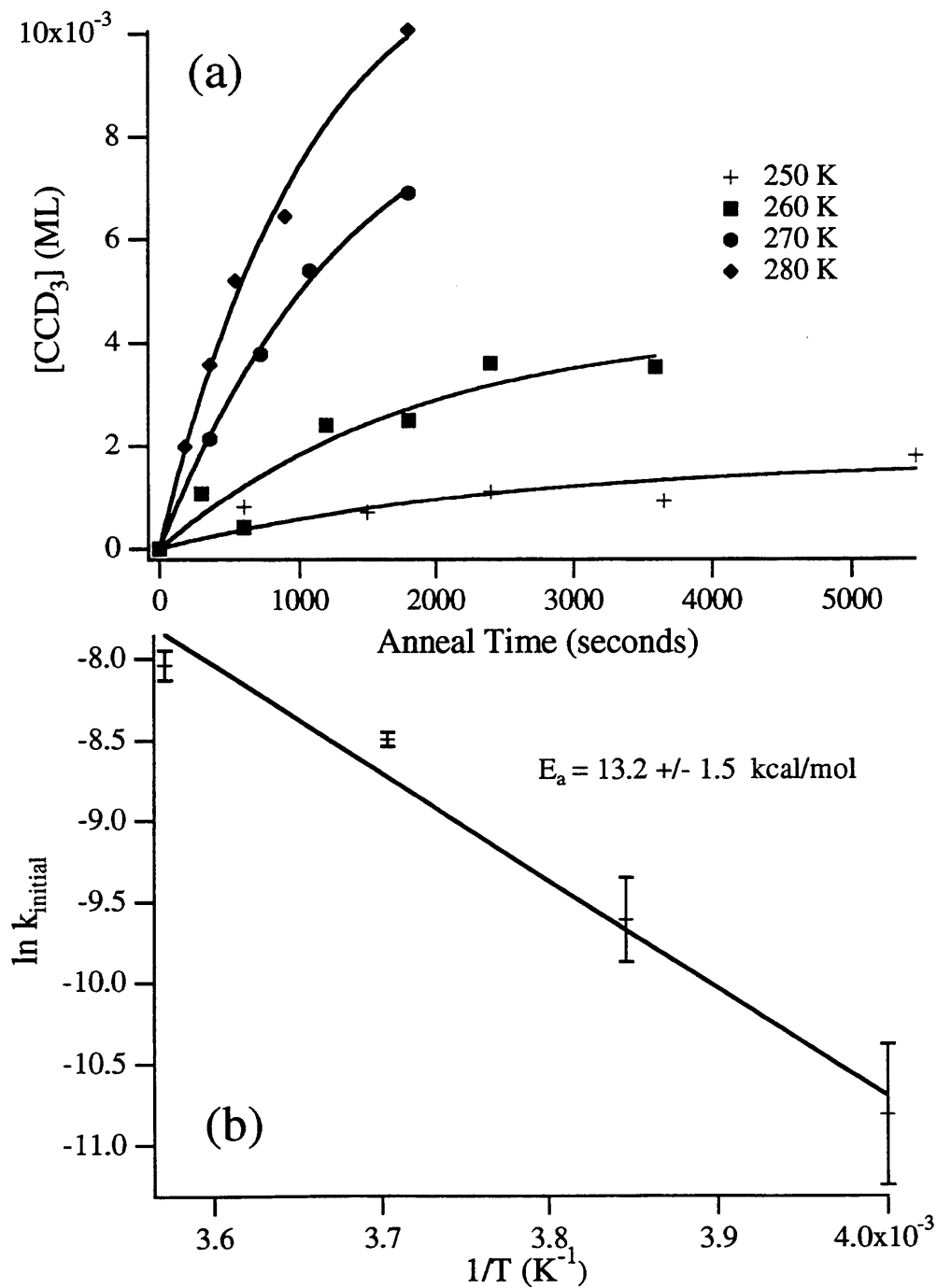
Figure 33 Rates and activation energy determination for initial coverage of 0.06 ML C_2D_2, 0.57 ML D, and 0.29 ML empty sites. (a) Coverage of CCD_3 versus time used to determine initial rate of D addition at different temperatures. (b) Arrhenius plot of $Lnk_{initial}$ versus 1/T. Error bars are explained in the text.

| Initial Surface Coverage	Temperature (K)	initial rate(s) (ML/s)	rate constant $(ML*s)^{-1}$
0.06 ML C_2D_2+0.86 ML D	260	$1.5\pm0.1\times10^{-5}$	$2.9\pm0.2\times10^{-4}$
	270	$2.5\pm0.3\times10^{-5}$	$4.9\pm0.6\times10^{-4}$
	280	$5.1\pm0.3\times10^{-5}$	$9.9\pm0.6\times10^{-4}$
0.09 ML C_2D_2+0.78 ML D	250	$2.5\pm0.3\times10^{-5}$	$3.6\pm0.4\times10^{-4}$
	260	$5.3\pm0.6\times10^{-5}$	$7.5\pm0.9\times10^{-4}$
	270	$1.3\pm0.3\times10^{-4}$	$1.9\pm0.4\times10^{-3}$
	280	$1.8\pm0.3\times10^{-4}$	$2.6\pm0.4\times10^{-3}$
0.105 ML C_2D_2+0.74 ML D	250	$2.0\pm0.1\times10^{-5}$	$2.6\pm0.1\times10^{-4}$
	265	$7.4\pm0.9\times10^{-5}$	$9.5\pm0.1\times10^{-4}$
	280	$1.8\pm0.2\times10^{-4}$	$2.3\pm0.3\times10^{-3}$
0.12 ML C_2D_2+0.70 ML D	260	$1.0\pm0.1\times10^{-5}$	$1.2\pm0.1\times10^{-4}$
	270	$2.8\pm0.4\times10^{-5}$	$3.3\pm0.4\times10^{-4}$
	280	$7.9\pm0.3\times10^{-5}$	$9.4\pm0.4\times10^{-4}$
0.17 ML C_2D_2+0.57 ML D	260	$2.4\pm0.6\times10^{-6}$	$2.5\pm0.6\times10^{-5}$
	270	$8.6\pm0.8\times10^{-6}$	$8.9\pm0.8\times10^{-5}$
	280	$2.4\pm0.2\times10^{-5}$	$2.5\pm0.2\times10^{-5}$
0.06 ML C_2D_2+0.57 ML D	250	$6.9\pm3\times10^{-7}$	$2.0\pm0.9\times10^{-5}$
	260	$2.3\pm0.6\times10^{-6}$	$6.7\pm0.2\times10^{-5}$
	270	$7.0\pm0.3\times10^{-6}$	$2.0\pm0.1\times10^{-4}$
	280	$1.1\pm0.1\times10^{-5}$	$3.2\pm0.3\times10^{-4}$

Table 2 Initial rate and rate constant (k) values at different temperatures for the six different initial acetylene and deuterium coverages.

coverage and reaction temperature are listed in Table 2. The error bars on these values in Table 2 come from the standard deviation generated from the covariant matrix during the nonlinear χ^2 Levenberg-Marquardt fitting algorithm used by the Igor program.[48] More details on this fitting algorithm can be found in *Numerical Recipes*.[49]

After the initial rates of the reaction of $C_2D_2 + D \rightarrow CCD_3$ are determined, the rate

constant, k, is calculated from each initial rate using the equation:

$$k = \frac{s}{[C_2D_2]_{initial}[D]_{initial}} \qquad (14)$$

Since the initial rate for CCD_3 formation is measured, the initial C_2D_2 and D coverage are used

in this calculation. The rate constant values are listed in Table 2.

The activation energy for the reaction is calculated from the rate constants measured at

different crystal temperatures using an Arrhenius form:

$$k(T) = Ae^{-\frac{E_a}{kT}} \quad \text{which can also be expressed as} \quad \ln(k) = \ln A - \frac{E_a}{kT}. \qquad (15)$$

A plot of ln(k) versus 1/T is made and E_a is extracted from the slope of the plot. These

Arrhenius plots are shown in Figures 28b, 29b, 30b, 31b, 32b, and 33b. The values of the

activation energy, E_a, and the pre-exponential factor, A, are listed in Table 3 for the different

$[C_2D_2]_i$ ML	0.06	0.09	0.105	0.12	0.17	0.06
$[D(s)]_i$ ML	0.86	0.78	0.74	0.70	0.57	0.57
$[ES]_i$ ML	0	0	0	0	0	0.29
E_a(kcal/mol)	8.8±1.0	9.3±0.9	10±0.8	14.9±0.4	16.7±0.7	13.2±1.5
pre-exponent $(ML^*sec)^{-1}$	$7 \times 10^{3\pm1}$	$5.2 \times 10^{4\pm1}$	$1.5 \times 10^{5\pm1}$	$4.3 \times 10^{8\pm0.3}$	$2.6 \times 10^{9\pm0.5}$	$7.4 \times 10^{6\pm2}$
$[D]_i/[C_2D_2]_i$ ratio	14	8.7	7.0	5.8	3.4	9.5

Table 3 Activation energy and pre-exponential factors for the reaction of C_2D_2
with surface D for different initial coverages of C_2D_2 and D(s). Values taken
from data in Figures 28-33. Also listed is ratio of the initial coverages of
D/C_2D_2.

initial C_2D_2 and surface bound D coverages. The error bar on the E_a value comes from the

standard deviation of the slope of the line that fits the three or four points of the Arrhenius

plot.

The E_a measurements do show variation with initial C_2D_2 and surface D coverages.

These variations have been plotted in Figure 34, which shows the activation energy versus

initial surface D coverage in (a), and versus initial C_2D_2 coverage in (b). The error bars for the

initial D coverage come from the error bars for the coadsorbed D coverage from Equation 3.

The error bars for the initial C_2D_2 coverage are ±2.5%, as determined in Figure 16. For the

five E_a measurements with different initial C_2D_2 coverages and a D_2 exposure that saturates all

remaining surface sites, there are two clear regimes with clearly distinct E_a values. The values

of E_a are similar and within experimental error for the initial C_2D_2 coverages of 0.06, 0.09, and

0.105 ML, being between 8.8 and 10 kcal/mol. The values of E_a are similar and within

experimental error for the initial C_2D_2 coverages at 0.12 and 0.17 ML, being between 14.9 and

16.7 kcal/mol. The activation energy measurement in the case where there is a significant

number of empty sites is unique. The E_a value for an initial C_2D_2 coverage of 0.06 ML, an

initial D coverage of 0.57 ML, and 0.29 ML empty sites is 13.2±1.5 kcal/mol. This activation

energy value does not fall into the range of E_a values for an initial C_2D_2 coverage of 0.06 to

0.105 ML, but instead is more consistent with the E_a values for the higher initial C_2D_2

coverage of 0.12 and 0.17 ML. This E_a value with 0.29 ML empty sites may suggest the

activation energy is partially determined by the number of D atoms surrounding an adsorbed
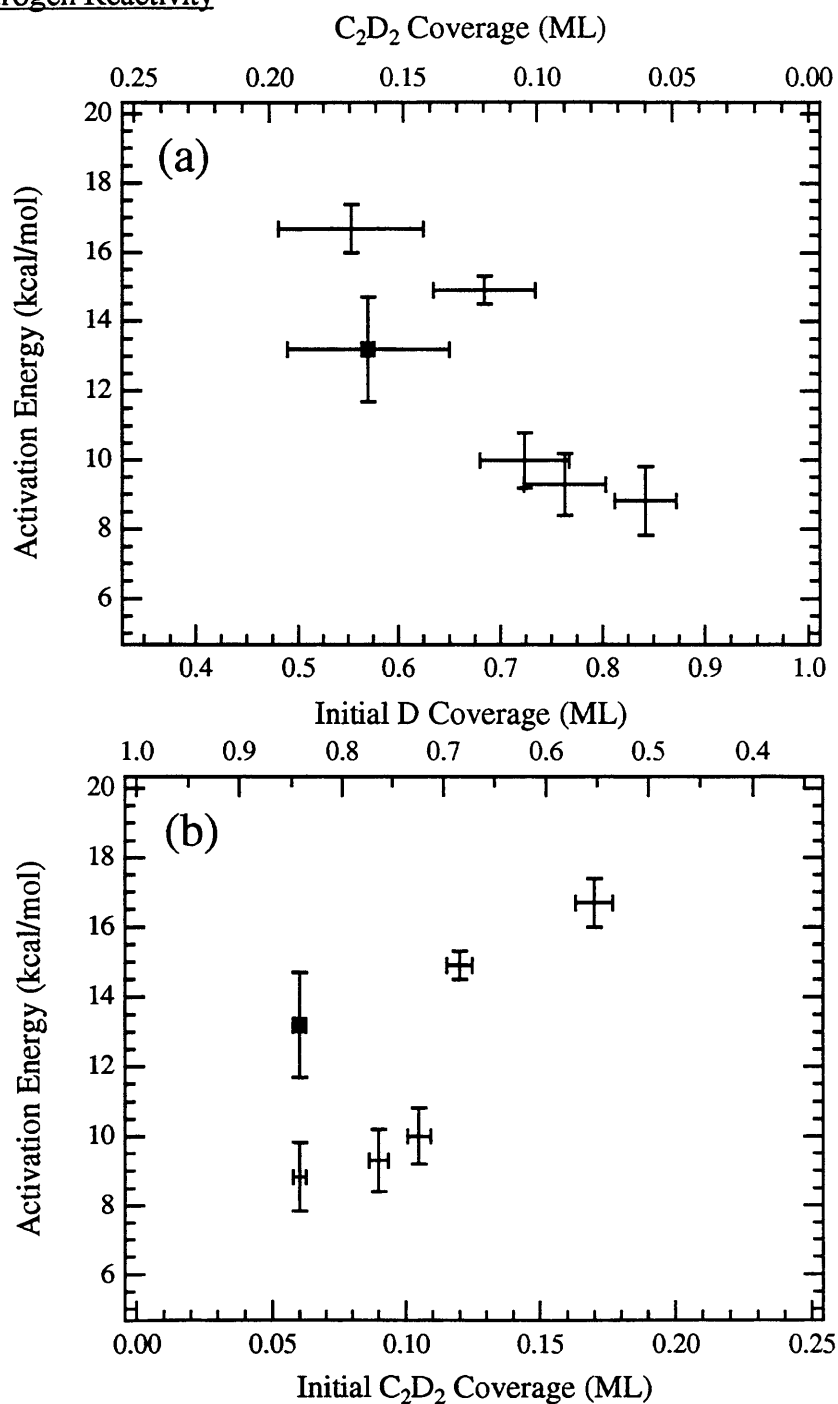
Figure 34 Trends in measured E_a values versus initial D coverage in (a) and versus initial C_2D_2 coverage in (b). Single point marked with (■) is for measurement with initial coverage of 0.29 ML empty sites. Error bars are explained in the text.

C_2D_2 molecule. To further explore this effect, the ratio of the D/C_2D_2 coverage is given for all

the conditions measured in Table 3, and will be further discussed.

5.1 *Discussion of Kinetics Measurements and Activation Energies*

   Coadsorbate Effects in an Interacting System

   EEL vibrational spectroscopy, as well as other detection methods, have been previously

used to measure rates and then activation energies. In this reaction of $C_2D_2 + D \leftrightarrow CCD_3$, the

first step is likely C-D bond formation to form $CDCD_2$. Chapter 6 describes the proposed

mechanism for this reaction, in which the formation of vinyl, $CDCD_2$, is the first step in the

reaction. The absence of a spectroscopic observation of an intermediate suggests the first step

in this reaction is the rate limiting step, which is further supported by kinetic data presented in

Chapter 5. Assuming vinyl is the first intermediate in CCD_3 formation, and the first step in the

reaction to form vinyl is the rate limiting step, then the initial rate and therefore the activation

energy measured is that of this first C-D bond formation. There are no studies that similarly

measure this C-D bond formation, so there are no data for direct comparison.

   The activation energy values for this C-D bond formation reaction depend on the initial

C_2D_2 coverage. To understand this reaction, an explanation of this dependence is desired.

Many activation energy studies of CCH_3 formation from C_2H_4 decomposition on metal

surfaces other than Ni have been done. The coverage dependence in several of these

measurements is relevant to explain the coverage dependence observed here. The rate of

ethylidyne formation on Pt(111) measured by IR spectroscopy results in E_a values of 18 ± 1,

14 ± 1, and 13 ± 2 kcal/mol for C_2H_4 coverages of 0.18, 0.11 and ~0.04 ML respectively.[50]

Hemminger and coworkers[44] use the technique of laser-induced thermal desorption with

fourier transform mass spectrometry to follow the decomposition of C_2H_4 on Pt(111). They

measure the E_a for the appearance of CCH_3 as 17.9 ± 0.8 and 16.0 ± 0.4 kcal/mol for initial

coverages of 0.25 ML and 0.17 ML, respectively. In different experiments, kinetic

measurements of the rate of C_2H_4 conversion to CCH_3 on Rh(111) can only be fit with E_a

values that are a function of the product coverage as well as the initial C_2H_4 coverage.[51] The

activation energy values vary from an initial value of 8.9 kcal/mol in the limit of no product for

all coverages to 12.4 kcal/mol for full conversion of 0.33 ML C_2H_4. In a different study of

C_2H_2 conversion to CCH_2 on Rh(111), King and coworkers see similar trends.[52] Activation

energy values vary from 9.3 kcal/mol at all initial coverages in the limit of no product to 14.3

kcal/mol for full conversion of an initial 0.25 ML coverage of C_2H_2. While this study is more

similar to our experiment in that it shows coverage effects of adsorbed acetylene, none of these

studies are as complex as our system with two adsorbed reactants. They are all modeled as

first order reactions of a single adsorbate.

The explanations given for these previously observed coverage dependent activation

energies distills to either interactions between coadsorbates, and/or a transition state that needs

an ensemble of surface sites for the reaction to occur. Ensemble effects and ordering could

explain our equilibrium data, but coadsorbate effects could also be responsible for the trend of

E_a values with changes in the C_2D_2 and surface bound D coverages. This trend is in the same

direction as all other coverage dependent shifts previously studied, namely higher E_a values are

measured for higher C_2D_2 coverages. There are several experimental methods that could

demonstrate coadsorbate effects. One is direct observation of a change in the bonding of a

species as observed by a frequency shift in the vibrational modes when the species is

coadsorbed with an interacting species. While frequency shifts in the vibrational spectra of

C_2D_2 coadsorbed with surface bound D are not observed in the EEL spectra, studies of the

highly interacting system of CCH_3 and CO measure only 4-6 cm^{-1} shifts at low CO coverages

using IR reflection adsorption spectroscopy.[43] The ΔE_{fwhm} for the HREEL spectrometer is 40

cm^{-1}, compared to 4 cm^{-1} for IR spectroscopy, which does not make it possible to detect such

small shifts.

Coadsorbate effects on surfaces have been studied, and some theoretical frameworks

have been constructed to understand these effects. Coadsorbate interactions are generally

defined as the forces exerted on an adsorbate by the other adsorbates, either of the same

species or a different species. These interactions span from the subtle forces that extend past

neighbor interactions, to strong forces between atoms or molecules that poison or promote a

reaction. Most coadsorbate interactions can be explained and understood by considering the

short range electrostatic and long range electronic interactions.[53] Molecules with electron

withdrawing or donating effects such as CO, O, K, and S have been frequently examined.

Much less study has been done on interactions in systems with hydrocarbons and hydrogen.

The present system, C_2D_2 and surface bound D, has more subtle interaction effects than a

system with a strong electron withdrawing or donating atoms or molecules. Still, there is some

evidence to support coadsorbate interactions in systems with surface hydrogen and

hydrocarbons.

Coadsorbate interactions are seen in layers of H and CO on Ni surfaces. Not only do the electrostatic interactions from the electron withdrawing O atom create changes in the H adsorption, but surface H atoms also create changes in the adsorption of CO. Both adsorbates affect each other. If the adsorption of both species are changed the entire potential energy surface of the reaction is changed. If H atoms can change the energy landscape of CO molecules they may very well change the energy landscape of acetylene. In thermal desorption spectra of mixed layers of CO and H, on Ni (111), the H desorption temperature rises compared to adsorption of H alone on the (111) surface.[54,55] Further studies on Ni(100)[56] describe a new low temperature CO desorption feature at 220 K. The feature is described as arising from a weakened CO-Ni bond due to H covered Ni surface. Thermal desorption, ultraviolet and inverse photoemission have been used to study CO and H on Ni(110). With these methods, Rangelov and coworkers conclude that a H-CO complex is formed on the surface with bonding and antibonding orbital overlap[57].

In moving from hydrogen to hydrocarbon interactions, there is evidence that C_2D_2 adsorption changes with coverage. In a study of benzene formation from acetylene on Pd(111), strong coverage dependence is observed in the E_a values.[58] Between a half and full saturation coverage of acetylene, the E_a value for formation of benzene varies from 5.8 to 10.4 kcal/mol. The justification for this trend is that the work function ($\Delta\phi$) of the system decreases with increasing acetylene coverage. This $\Delta\phi$ decrease is a consequence of the electron transfer from acetylene molecules to the Pd surface which increases the local value of the Fermi energy. The increase in the Fermi energy results in further transfer of electron density to the anti-

bonding orbitals of acetylene, resulting in increased adsorbate-substrate interactions. The

work function of acetylene adsorbed on Ni(111) is observed to decrease with increasing

acetylene coverage,[59] reaching a similar $\Delta\phi$ value for an acetylene-saturated Ni surface as for

an acetylene-saturated Pd surface. This reasoning is analogous to applying the inorganic,

metal-hydrocarbon bonding model, known as the Dewar-Chatt-Duncansen (DCD)[20,21] model,

to a metal surface. This explanation for a change in E_a values with coverage for the Pd surface

is plausible. The higher acetylene coverage leads to stronger C-Ni bonds and higher activation

energies to form benzene. The large difference in E_a values for benzene formation on Pd is

close to the difference in E_a values observed in our study. While these arguments could

account for the trend in activation energy values for the five data points with varied C_2D_2

coverages and D saturated surfaces, the one E_a value for a surface with 0.29 ML empty sites

cannot be explained by acetylene coverage dependence . This argument would predict the

same E_a value for points with the same acetylene coverages. It is necessary to consider the

coadsorbate effects between C_2D_2 and surface D to understand our observed behavior.

The activation energy and the pre-exponential factor have been measured for six

different initial coverages of C_2D_2 and surface D. Both quantities describe different aspects of

the reaction and exhibit coverage dependence that can be explained by coadsorbate effects. A

discussion of the pre-exponential factor for the six data points listed in Table 3 follows. The

pre-exponential factor is a measure of the frequency of a reaction. From collision theory an

upper limit of the pre-exponential factor, assuming every collision results in a reaction, is

calculated from the product of the average velocity and the cross-sectional area of reacting

molecules. For a bimolecular elementary surface reaction step, the order of magnitude of the pre-exponential factor is 10^{13} $(ML*s)^{-1}$.[60] The values observed here are well below this upper limit. Transition state theory provides a framework for understanding trends in the pre-exponential factor (A), by deriving the equation

$$A \propto Te^{\frac{\Delta S_{act}}{R}} \tag{16}$$

which predicts a linear temperature dependence and an exponential dependent on ΔS_{act}, the entropy change from the initial state to the transition state, for pre-exponential factors.[61]

There are two different explanations for the trend in the measured pre-exponential factors. In our data, the trend is to lower pre-exponential values with lower C_2D_2 coverages and higher D coverages. Lateral interactions can significantly suppress the pre-exponential factor, and therefore the rate of a reaction. The pre-exponential factor is expected to decrease with increasing coverage due to the decreased mobility and lower entropy of the transition state.[61] In this study, the decrease in the pre-exponential factor correlates with the increase in the surface bound D coverage. Therefore, lateral interactions from the increasing D coverage are consistent with the pre-exponential factor trend. Another explanation that is consistent with the trend originates from the increases in the C_2D_2 coverage with increasing pre-exponential factor values. If the strength of the C_2D_2-surface bond increases with increasing C_2D_2 coverage, as described above, the entropy of the reactant will decrease. If the entropy of the transition state is unchanged, then the ΔS_{act} will increase leading to an increased pre-exponential factors with increasing C_2D_2 coverages as the C_2D_2 reactant is more tightly bound.[62] Therefore, there are two consistent explanations for the trend in the pre-exponential

factor, a trend of decreasing pre-exponential values for increasing surface bound D coverage

and a trend to increasing pre-exponential values for decreasing C_2D_2 coverages.

The pre-exponential value for the surface with 0.29 ML empty sites is higher than the

value for the surface that is initially saturated with surface bound D and has the same C_2D_2

coverage. There are a number of explanations that are consistent with this higher pre-

exponential value. The larger number of empty sites can lead to fewer restrictions on the

transition state, leading to a larger ΔS_{act} and a larger pre-exponential value, as observed. On

the surface with 0.29 ML of empty sites the coverage of D has been lowered. If lateral

interactions based on D coverage are a factor, then this lower D coverage is also expected to

yield a higher pre-exponential factor, as explained above. There is a second comparison to be

made between the two experiments with the same D coverage, the first with 0.06 ML C_2D_2,

0.57 ML surface D, and 0.29 ML ES initial coverages and the second with the 0.57 ML D and

0.17 ML C_2D_2 initial coverages. The pre-exponential value is higher for the saturated surface

with 0.17 ML C_2D_2. The higher value of the pre-exponential factor for the surface with 0.17

ML C_2D_2 as compared to 0.06 ML C_2D_2 is consistent with an increase in the pre-exponential

factor with increasing C_2D_2 coverage, as explained above. In this comparison, the number of

empty sites does not affect the pre-exponential value strongly. The argument above that the

pre-exponential value should increase with increasing empty sites is not observed.

While the trend in pre-exponential values can be explained through transition state

theory, the shifting of the E_a value for this experiment cannot be explained as easily. Unlike

the pre-exponential values that are a measure of the entropy of the reaction, the E_a value is a

probe of the potential energy surface, and is not expected to change in an ideal system. There are a number of different E_a value comparisons that can be made for this set of measurements. For the two experiments with identical initial coverages of 0.57 ML D, the E_a values are 13.2 ± 1.5 and 16.7 ± 0.7 kcal/mol for the initial C_2D_2 coverages of 0.06 to 0.17 ML, respectively. This suggests that the activation energy is higher for higher C_2D_2 coverages. A second comparison of E_a values can be made between the two experiments with the same initial C_2D_2 coverage of 0.06 ML. The E_a value increases dramatically from 8.8 ± 1.0 to 13.2 ± 1.5 kcal/mol when the surface bound D coverage is decreased from 0.86 ML D to 0.57 ML D, respectively. This suggests that the C_2D_2 coverage is not the sole factor in changing the E_a value. It is possible that the activation energy is higher for lower D coverages. However, there is a third consideration, which is that in each of these comparisons the two experiments do not have the same empty site coverage. The common experiment in these two comparisons has an initial coverage of 0.57 ML D and 0.06 ML C_2D_2, and also has an initial coverage of 0.29 ML of empty sites.

The consequence of exploring a surface reaction is that it is not possible to vary all surface coverages independently. Instead of trying to include empty sites as a third reactant, which is shown to be an inappropriate description of this reaction in Section 4.5, the ratio of the D to C_2D_2 coverage captures the effect of increasing empty sites on the two reactants. The D/C_2D_2 ratio also has a physical meaning, the number of D atoms surrounding each C_2D_2 molecule. D/C_2D_2 ratio values are listed in Table 3. How do the D/C_2D_2 ratio values correlate

with E_a values? There is a direct correlation in the decrease in E_a values with an increase in

D/C_2D_2 values, not including the one experiment with empty sites.

The D/C_2D_2 ratio and the E_a value for the surface with an initial coverage of 0.29 ML

of empty sites do not fit into the trend of E_a values with D/C_2D_2 ratio for the surfaces with no

initial empty sites coverage. The measured activation energy value is higher than expected for

the value of the D/C_2D_2 ratio. However, even though the E_a value from the 0.29 ML empty

site experiment does not directly fit into the pattern of other E_a values with D/C_2D_2 ratios, it

does follow the general trend of a higher E_a value with decreasing D/C_2D_2 value. This

comparison is made between the experiment with 0.06 ML C_2D_2 and 0.86 ML D and the

experiment with 0.06 ML C_2D_2, 0.57 ML D and 0.29 ML empty sites. In these two

experiments the D/C_2D_2 ratio decreases, from 14 to 9.5, and the E_a value increases from

8.8±1.0 to 13.2±1.5 kcal/mol, respectively. The D/C_2D_2 ratio decreases to 9.5 for the

experiment with 0.29 ML empty sites, but to match the E_a value increase predicted by the

saturation experiments, it would have to fall to a value between 6 and 7. It is possible that

with a significant coverage of empty sites, the effective D/C_2D_2 ratio is lower than the

calculated one, because the large empty site coverage reduces the interactions between D and

C_2D_2 more strongly than the ratio suggests. In this picture, the E_a value for the first C-D bond

formation to make $CDCD_2$ is lowered when a C_2D_2 molecule is surrounded by a large number

of D atoms. With an increase in the empty site coverage the D atoms are less likely to

surround a C_2D_2 molecule and the E_a value is further increased. Previous experiments in the

literature report an increase in the E_a value with increasing acetylene coverage in reactions

where acetylene is the sole reactant. The present study supports this trend, but also suggests there could be an opposite trend in E_a values for increasing coverages of coadsorbed D. By comparing E_a values for experiments with both the same D coverage and the same C_2D_2 coverage, contributions to the activation energy changes from both adsorbates are clearly observed.

5.2 The Bigger Picture

Surface bound D, which is the lowest energy D species with under 1 kcal/mol at 300 K, will react with adsorbed C_2D_2. The D addition does not result in gas phase products. The only observed product is adsorbed CCD_3. Both acetylene[63] and ethylene[64] adsorb parallel to the surface with C-D bonds generally in the surface plane. For acetylene, the barrier for reaction with surface D atoms is lower due to the existence of a second π orbital in the surface plane, which ethylene lacks. This residual π character in the plane provides an electron rich lower energy pathway for D addition. The intermediate in the formation of ethylidyne is expected to be a vinyl species, $CDCD_2$, which is formed after the addition of a single D atom. The vinyl species then transforms to ethylidyne. This work shows that surface D is not the active species in acetylene or ethylene hydrogenation to the gas phase product ethane.

Further study of the equilibrium and the activation energy of the reaction of surface bound deuterium with acetylene to make ethylidyne reveals a system that is not ideal. The individual equilibrium coverages of surface species are measured, and K_{eq} values are calculated in three different forms to reflect three different possible ways the reaction could occur. None of the models produce a consistent value of K_{eq} for different reactant conditions. The best

explanation of this inability to determine a K_{eq} value is that the system is not an ideal

homogeneous layer for all reaction conditions. Trapping of the CCD_3 product is observed,

particularly for repeated D_2 exposures, but is not correlated with the total number of empty

sites on the surface as would be expected for ensemble effects on a homogeneous surface.

Therefore it appears that repeated D_2 exposure and anneals lead to an inhomogeneous surface

with ordering and islanding that provides a diversity of molecular environments, some of which

promote product trapping. Similarly, activation energy measurements are not constant with

different initial reactant coverages. The observation of coverage dependent trends can be

explained in several different ways. The most general explanation is that each coadsorbate

changes the potential energy surface of the reaction. It is further possible to imagine these

energy changes arising from fundamental reorganization and ordering of the surface. In order

to fully understand the range of non-ideal behavior more information is needed. A study of this

system with a higher resolution spectroscopy could allow changes in bonding of both surface D

and C_2D_2 to be discerned. The conformation of ordering or islanding in this system requires an

imaging technique. Study of this system with scanning tunneling microscopy could provide

such an image. The technique of near field optical microscopy that combine spectroscopic

identification with spatial information could also address the question of ordering and

islanding. It is possible to imagine many different causes of non-ideal behavior. With further

experimental evidence to confirm or disprove a particular cause it could be possible to

determine the major source of non-ideality in this reaction.

[1] I. Horiuti and M. Polanyi, Trans. Far. Soc. **30**, 1164 (1934)

[2] A. Farkas, L. Farkas and E.Rideal, Proc. Roy. Soc. **146**, 630 (1934) Rideal and coworker also suggested that surface hydrogen added to ethylene, however they did not suggest a specific mechanism.

[3] A. Molnar and G.V. Smith, *Hydrogen Effects in Catalysis: Fundamentals and Applications*, Z. Paal and P.G. Menon, eds,. Marcel Dekker (1988)

[4] S.P. Daley, Ph.D. Thesis, Massachusetts Institute of Technology (1994)

[5] S.P. Daley, A.L. Utz, T.R. Trautman and S.T. Ceyer, J. Am. Chem. Soc. **116**, 6001 (1994)

[6] F. Zaera, J. Catalysis **121**, 318 (1990)

[7] A.M. Glines and A.B. Anton, Surf. Sci. **286**, 122 (1993)

[8] K. Christmann, F. Chehab, V. Penka, and G. Ertl, Surf. Sci. **152/153**, 356 (1985)

[9] S. Lehwald and H. Ibach, Surf. Sci. **89**, 425 (1979)

[10] L. Hammer, T. Hertlein and K Müller, Surf. Sci. **178**, 693 (1986)

[11] P.D. Lightfoot and P.J. Pilling, J. Phys. Chem. **91**, 3373 (1987)

[12] O. Nomura and S. Iwata, Bull. Chem. Soc. Jpn. **53**, 61 (1980)

[13] H.B. Schiegel J. Phys. Chem. **86**, 4878 (1982)

[14] W.L. Hase, G. Mrowka and R.J. Brudzyski, J. Chem Phys. **69**, 3548 (1978)

[15] H.B. Schiegel, K.C. Bhalla and W.L. Hase, J. Phys. Chem. **86**, 4883 (1982)

[16] L.B. Harding, J. Am. Chem. Soc. **103**, 7469 (1981)

[17] W.L. Hase, D.M. Ludlow, R.J. Wolf and T. Schlick, J. Phys. Chem. **85**, 958 (1981)

[18] J.E. Demuth and D.E. Eastman, Phys. Rev. Lett. **32**, 1123 (1974)

[19] J.E. Demuth and D.E. Eastman, Phys. Rev. B **13**, 1523 (1976)

[20] M.J.S. Dewar, Bull. Soc. Chim. Fr. **18**, C79 (1951)

[21] J. Chatt and L.A. Duncansen, J. Chem. Soc. (London) 2939 (1953)

[22] J.E. Demuth, Phys. Rev. Lett. **40**, 409 (1978)

[23] J.E. Demuth, Surf. Sci. **84**, 315 (1979)

[24] J.E. Demuth and H. Ibach, Surf. Sci. **85**, 365 (1979)

[25] T.E. Felter and W.H. Weinberg, Surf. Sci. **103**, 265 (1981)

[26] M. Ohno and W. von Niessen, Surf. Sci **366**, 209 (1996)

[27] M. Weinelt, W. Huber, P.Zebisch, H.-P. Steinrück, P. Ulbricht, U. Birkenheuer, J.C. Boettger, and N. Rösch, J. Chem. Phys. **102**, 9709 (1995)

[28] A. Fahmi and R.A. van Santen, Surf. Sci. **371**, 53 (1997)

[29] S. Bao, Ph. Hofmann, K-M. Schindler, V. Fritzsche, A.M. Bradshaw, D.P. Woodruff, C. Casado, and M.C. Asensio, Surf. Sci. **307-309**, 722 (1994)

[30] H. Ibach and S. Lehwald, J. Vac. Sci. Technol. **18**, 625 (1981)

[31] Q.Y. Yang, Ph.D. Thesis, Massachusetts Institute of Technology (1989)

[32] A.D. Johnson, K.L. Maynard, S.P. Daley, Q.Y. Yang and S.T. Ceyer, Phys. Rev. Lett. **67**, 927 (1991)

[33] H. Ibach and D. Druchmann, Phys. Rev. Lett. **44**, 36 (1980)

[34] T. Bürgi, T.R. Trautman, K.L. Haug, A.L. Utz and S.T. Ceyer, J. Phys. Chem. B **102**, 4952 (1998)

[35] H. Ibach, H. Hopster and B. Sexton, Appl. Surf. Sci. **1**, 1 (1977)
Ethylidyne was incorrectly assigned to ethylidene this first study, the assignment was changed in the further literature.

[36] P.S. Cremer, X. Su, Y.R. Shen and G.A. Somorjai, J. Am. Chem. Soc. **118**, 2942 (1996)

[37] M.P. Lapinski and J.G. Ekerdt, J. Phys. Chem. **92**, 1708 (1988)

[38] T.A. Land, T. Michely, R.J. Behm, J.C. Hemminger and G. Comsa, J. Chem. Phys. **97**, 6774 (1992)

[39] T.V.W. Janssens, S. Völkening, T. Zambelli and J. Wintterlin, J. Phys. Chem. B **102**, 6521 (1998)

[40] R.G. Windham and B.E. Kohl, Langmuir **3**, 1113 (1988)

[41] C.T. Campbell, J.M. Campbell, P.J. Dalton, F.C. Henn, J.A. Rodriguez, and S.G. Seimanides, J. Phys. Chem. **93**, 806 (1989)

[42] M.R. Albert and J.T. Yates, Surf. Sci **192**, 225 (1987)

[43] C.A. Mimes, M.D. Weisel, F.M. Hoffmann, J. Sinfelt, and J.M. White, J. Phys. Chem. **97**, 12656 (1993)

[44] W. Erley, Y. Li, D.P. Land and J.C. Hemminger, Surf. Sci. **301**, 177 (1994)

[45] W. Ho, Surf. Sci. **211/212**, 289 (1989)

[46] L. Hammer, B. Dötsch, C. Harder and K. Müller, Vacuum **41**,121 (1990)

[47] A. Morgante, S. Modesti, M. Bertolo, P. Rudolf and R. Rosei, Surf. Sci **211/212**, 829 (1989)

[48] *Igor Pro version 3-Users Guide*, WaveMetric (1996)

[49] W.H. Press, *Numerical Recipes in Fortran*, Cambridge University Press (1992)

[50] S.B. Moshin, M. Trenary and H.J. Robota, Chem. Phys. Lett. **154**, 511 (1989)

[51] D.C. Papageorgopoulos, G. Ge and D.A. King, Surf. Sci. **397**, 13 (1998)

[52] D.C. Papageorgopoulos, G. Ge, S. Nimmo and D.A. King, J. Phys. Chem. B **101**, 1999 (1997)

[53] J.K. Nørskov in *The Chemical Physics or Solid Surfaces*-Volume 6 D.A. King and D.P. Woodruff, eds, Elsevier (1993)

[54] D.E. Peebles, J.R. Creighton, D.N. Belton and J.M. White, J. Catal. **80**, 482 (1983)

[55] H. Conrad, G. Ertl, J. Küppers, and E.E. Latta, *in Proceedings of the Sixth International Congress on Catalysis VI*, G.C. Bond, P.B. Wells, and F.C. Tompkins, eds, (1977)

[56] L. Westlund, L. Jönsson and S. Andersson, Surf. Sci. **199**, 109 (1988), and references therein

[57] G. Rangelov, U. Bischler, N. Memmel, E. Bertel, V. Dose, M. Pabst and N. Rösch, Surf. Sci. **273**, 61 (1992)

[58] I.M. Abdelrihim, T.E. Caldwell and D.P. Land, J. Phys. Chem. **100**, 10265 (1996)

[59] J-C. Bertolini, J. Massardier and G. Dalmai-Imelik, J. Chem Soc. Faraday Trans. I **74**, 1720 (1978)

[60] M. Boudart and G. Djéga-Mariadassou, *Kinetics of Heterogeneous Catalytic Reactions*, Princeton University Press (1984)

[61] R.A. van Santen and J.W. Niemantsverdriet, *Chemical Kinetics and Catalysis*, Plenum Press (1995)

[62] A.A. Deckert, M.V. Arena, J.L. Brand and S.M. George, Surf. Sci. **226**, 42 (1990)

[63] H. Ibach and S. Lehwald, J. Vac. Sci. and Tech. **18**, 625 (1981)

[64] S. Lehwald and H. Ibach, Surf. Sci. **89**, 425 (1979)

Chapter 4

Reactivity of Bulk Hydrogen Atoms

with Adsorbed C_2H_2

1 Introduction

Bulk hydrogen atoms are present below the Ni surface under high H_2 pressure

conditions typical of heterogeneous catalytic reactions. The bulk H atom reacts with a surface

species as it emerges from the bulk to the surface. Once it overcomes the barrier to migration

from the bulk to the surface, it is a very energetic species with as much as 24 kcal/mol more

energy than a surface bound H atom. If it does not react with an adsorbate, it will loose its

energy to the surface and ultimately equilibrate with it to become a surface bound H atom.

However, at any point during its equilibration, it can react with an adsorbate, so that the

energy of the reacting bulk H atom relative to a surface bound H may be lower than 24

kcal/mol. Nevertheless, the energy of the bulk H atom as it emerges from the bulk is still much

larger than the average energy of 0.6 kcal/mol of a surface H atom. The additional energy that

bulk H atoms possess could lead to a richer chemistry with hydrocarbons than the reactions of

surface bound H atoms with hydrocarbons, because the higher energy of bulk H atoms allows them to overcome higher chemical reaction barriers.

Bulk H atoms are important to study because they are present under typical catalytic conditions. It has been shown that bulk H is present in Raney Ni, one of the main industrial Ni catalysts, under hydrogenation conditions.[1,2,3] Unfortunately under catalytic conditions, there is also a large coverage of surface H atoms, so it is not possible to separate the reactivity of bulk H from that of surface bound H in these reactions. Bulk H atoms are not easy to study. As discussed in Chapter 2, bulk H atoms are not normally present under ultra-high vacuum (UHV) conditions. Techniques for synthesizing and detecting this high pressure H species under UHV conditions have been developed and are detailed in Chapter 2. These techniques allow us to probe bulk H reactions under single collision conditions where individual reaction steps can be discerned and other reactants commonly present, such as surface H, can be eliminated. Through these studies, the products of the reaction of bulk H with different adsorbed hydrocarbon species are determined. Comparison of the products from the reactions of surface bound H atoms to those of bulk H atoms lead to an understanding of the differences in the chemistry of these two species.

2 Experiments

2.1 Bulk H + Ethylene

In Chapter 3, the story of the bulk H and ethylene reaction was described in detail to motivate the study of the reaction of surface H with acetylene. A brief summary of this system follows. Bulk H atoms hydrogenate adsorbed C_2H_4 to C_2H_6 as they emerge from the bulk to

the surface. Ethylene also desorbs from the surface as bulk H atoms emerge onto the surface.

Vibrational spectra show that bulk H does not affect the bonding of C_2H_4 to the surface.[4] The

ratio of gas phase products is determined by the coverage of C_2H_4 and amount of bulk H. No

carbon is left on the surface after the desorption of bulk H.[4]

The reasons why bulk H hydrogenates C_2H_4 while surface H does not are related to

both the energetics and geometry of the reaction. Bulk H has much more energy than surface

bound H to overcome barriers to chemical reaction. In addition, its pathway for reaction with

C_2H_4 has a lower energy barrier for H addition than that of the surface H because of the bulk H

atom's angle of approach. The lower barrier for bulk H is due to the electron density from the

π orbital perpendicular to the surface plane. C_2H_2 has π orbitals both perpendicular and

parallel to the surface plane. The reactivity of C_2H_2 with surface H demonstrates that the H

atom approach along the plane of a π orbital does indeed lower the energy barrier of the

reaction path.

What reactivity is predicted for acetylene plus bulk H atoms? Bulk H atoms are

expected to add to C_2H_2 to form gas phase hydrogenation products, similarly to C_2H_4.

Although there is no direct measurement of the binding energy of C_2H_2, because C_2H_2 does not

desorb from the surface, C_2H_2 is more tightly bound to the Ni surface than C_2H_4. Indirect

evidence for its stronger bonding will be presented below. The stronger bonding of C_2H_2 to

the surface manifests itself by less molecular desorption of the reactant as H emerges from the

bulk than in the reaction with C_2H_4. In addition to gas phase hydrogenation products, another

hydrogenation channel is observed for bulk H and C_2H_2 reaction. It is the formation of an
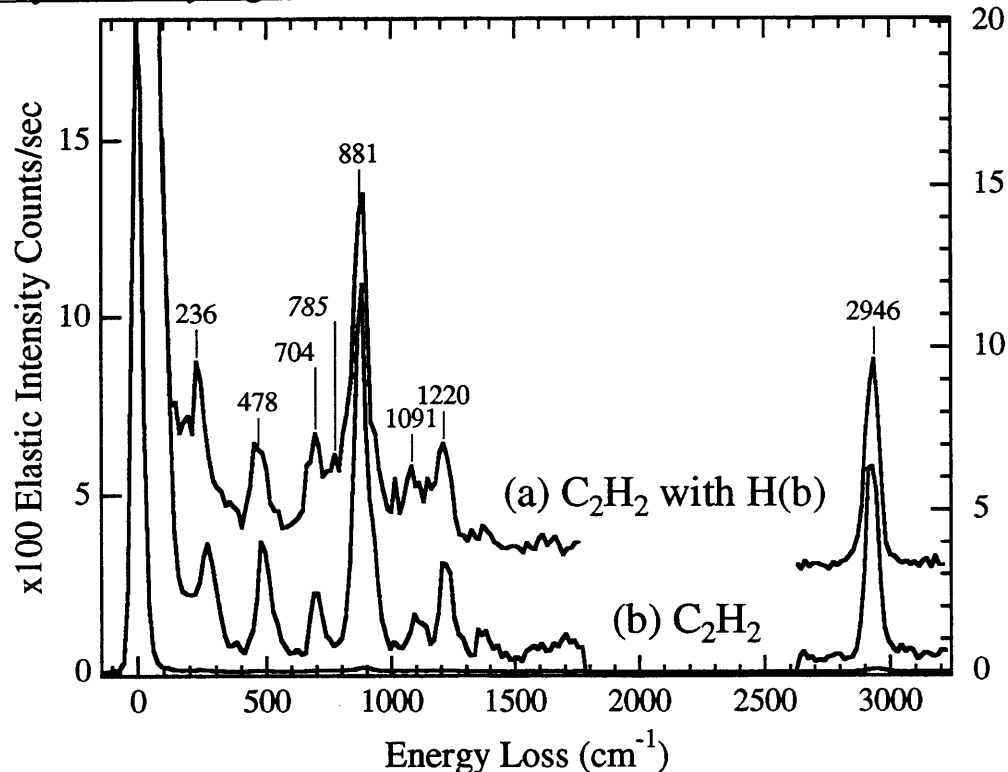
Figure 1 HREEL spectra of (a) an equivalent of 3.7 ML of bulk H and 0.25 ML C_2H_2, and (b) 0.25 ML C_2H_2 on a clean surface. Spectra taken at 80 K, with 6.5 eV electrons at 6° and 8° off specular, respectively, and with a ΔE_{fwhm} of 43 and 39 cm^{-1}. The bulk H vibration labeled in *italics* at 785 cm^{-1} is seen in spectrum (a).

adsorbed product, ethylidyne. Its formation was first observed as the product of the reaction of C_2H_2 and surface H, which is described in Chapter 3.

2.2 Bulk H + Acetylene- Gas Phase Products

First, bulk H does not change the adsorption and bonding of C_2H_2 on the surface. The vibrational spectrum of adsorbed C_2H_2 with H in the bulk is shown in Figure 1a with the spectrum of C_2H_2 adsorbed in the absence of bulk H shown in Figure 1b. The bulk H loss feature is visible in Figure 1a at 785 cm^{-1}. The agreement between the vibrational frequencies in these two spectra suggests that the presence of bulk H does not modify the bonding of C_2H_2
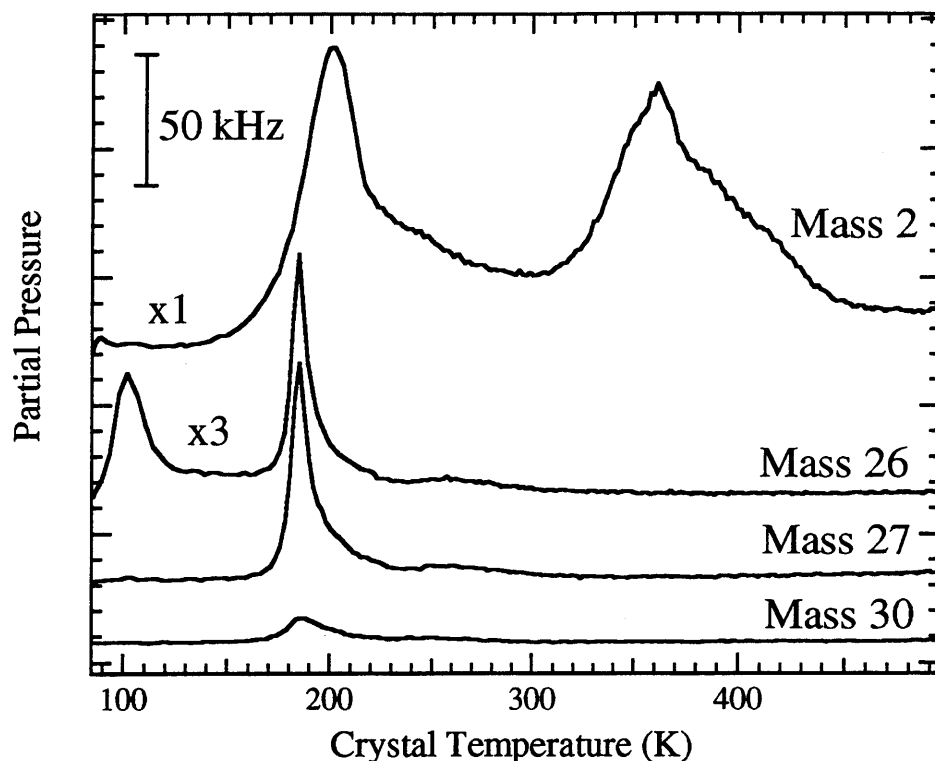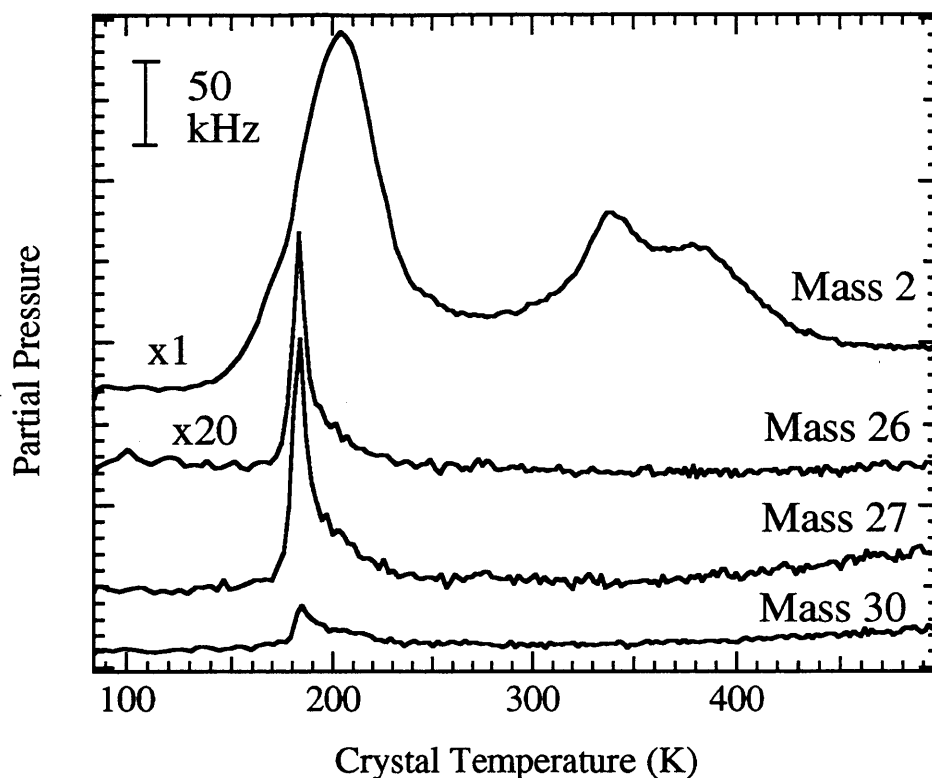
Figure 2 A thermal desorption spectrum resulting from the reaction of an equivalent of 1.8 ML of bulk H and 0.25 ML C_2H_2. Traces show m/e=2, 26, 27 and 30 signals. The low temperature feature in the signal C_2H_2 is due to desorption of C_2H_2 from the cryostat.

to the surface. This same conclusion has been drawn for the bonding of other hydrocarbons to the surface in the presence of bulk H.[5,6]

The reactivity of bulk H with adsorbed C_2H_2 to form gas phase products is probed in thermal desorption measurements. This experiment is done by preparing an equivalent of 1.8 ML of H in the bulk, as described in Chapter 2, and then adsorbing a saturated layer, 0.25 ML, of C_2H_2 on surface. The partial pressures at m/e= 2, 26, 27 and 30 are then measured as the crystal temperature is raised at a rate of 2 K/s. The results are shown in Figure 2. The low temperature feature in the m/e=26 signal is from C_2H_2 desorbing from surfaces surrounding the crystal, most likely the crystal support rods or rear heating filament. When C_2H_2 adsorption is

Figure 3 A thermal desorption spectrum resulting from the reaction of an equivalent of 2.4 ML of bulk H and 0.12 ML C_2H_2 limited to the center of the crystal. Traces show m/e=2, 26, 27 and 30 signals.

limited to the center of the crystal, by restricting the molecular beam aperture, this low temperature feature is absent, as shown in Figure 3.

To obtain an accurate measure of one hydrocarbon at a particular m/e, contributions from other hydrocarbons must be subtracted from the measured signal. The signature cracking patterns for C_2H_2, C_2H_4, and C_2H_6 are shown in Table 1 of Chapter 2. The m/e=30 signal (named 30*signal* below) only has contributions from C_2H_6. The m/e signals at 26 and 27 (named 26*signal* and 27*signal* below) have contributions from C_2H_2, C_2H_4, and C_2H_6. Since the m/e=30 signal represents only C_2H_6, it can be used to subtract the contributions of C_2H_6 from the m/e=26 and 27 signals after being weighted by the appropriate ratio of cracking

fractions. For example, the m/e=26 signal with contributions from only C_2H_2 and C_2H_4,

26signal(C_2H_2+C_2H_4), is calculated as shown, where crackingC$_2$H$_6$(X), represents the

cracking ratio of C_2H_6 at mass X,

$$26signal\left(C_2H_2 + C_2H_4\right) = 26signal - 30signal\left(\frac{crackingC_2H_6(26)}{crackingC_2H_6(30)}\right). \quad (1)$$

The m/e=27 signal with contributions from C_2H_2 and C_2H_4 only, 27signal(C_2H_2+C_2H_4), is

calculated similarly.

$$27signal\left(C_2H_2 + C_2H_4\right) = 27signal - 30signal\left(\frac{crackingC_2H_6(27)}{crackingC_2H_6(30)}\right) \quad (2)$$

The results of the operations in Equation 1 and 2 are signals at m/e=26 and 27 that have

contributions from C_2H_2 and C_2H_4 only.

To obtain the contribution of C_2H_2, 26signal(C_2H_2), to the 26signal(C_2H_2+C_2H_4) and

the contribution of C_2H_4, 27signal(C_2H_4), to the 27signal(C_2H_2+C_2H_4) the two equation

shown below are solved simultaneously.

$$27signal\left(C_2H_2 + C_2H_4\right) = 27signal\left(C_2H_2\right) + 27signal\left(C_2H_4\right) \quad (3)$$

$$26signal\left(C_2H_2 + C_2H_4\right) = 26signal\left(C_2H_2\right) + 26signal\left(C_2H_4\right) \quad (4)$$

after eliminating the unknown C_2H_2 and C_2H_4 contributions to m/e=26, named 26signal(C_2H_2)

and 26signal(C_2H_4), from Equation 4 by expressing it as:

$$26signal\left(C_2H_2 + C_2H_4\right) = 27signal\left(C_2H_2\right)\left(\frac{crackingC_2H_2(26)}{crackingC_2H_2(27)}\right) + 27signal\left(C_2H_4\right)\left(\frac{crackingC_2H_4(26)}{crackingC_2H_4(27)}\right). \quad (5)$$

The labels crackingC$_2$H$_x$(Y) refer to the cracking pattern of hydrocarbon C_2H_x at mass Y. All

values in Equation 3 and in Equation 5 are known except for the two values 27signal(C_2H_2)

and 27signal(C_2H_4). These equations are solved for the value of 27signal(C_2H_2). Then the

m/e=27 signal with contributions from C_2H_4 only is calculated from:

$$27signal\left(C_2H_4\right) = 27signal\left(C_2H_2 + C_2H_4\right) - 27signal\left(C_2H_2\right) \tag{6}$$

and the m/e=26 signal with contributions from C_2H_2 only is calculated from:

$$26signal\left(C_2H_2\right) = 26signal\left(C_2H_2 + C_2H_4\right) - 27signal\left(C_2H_4\right)\left(\frac{crackingC_2H_4(26)}{crackingC_2H_4(27)}\right). \tag{7}$$

After the mass signals have been reduced to a contribution from only one molecule,

they are scaled by the ratio of the total of the cracking fractions for the molecule being

detected over the cracking at the particular observed mass. The total cracking signal (named

totalsignalC_2H_x) is the sum of the cracking fractions at all masses, the value of which is listed

in Table 1 of Chapter 2. This scaling eliminates intensity differences from detecting a

particular molecule at a particular mass. In the final scaling step, the signals are also corrected

for the total ionization cross section (σ_{total}), which adjusts for differences in the ionization cross

section of the three hydrocarbon species. The value of σ_{total} is given in Chapter 2 and is an

average of measured values from the literature. The result of these two scaling steps is a

quantity, named signal(C_2H_x), which is proportional to the number density or partial pressure

of each hydrocarbon. An example calculation is:

$$signal\left(C_2H_4\right) = 27signal\left(C_2H_4\right)\left(\frac{totalsignalC_2H_4}{crackingC_2H_4(27)}\right)\left(\frac{1}{\sigma_{total}}\right). \tag{8}$$

The partial pressures of C_2H_2, C_2H_4, and C_2H_6 as a function of crystal temperature are
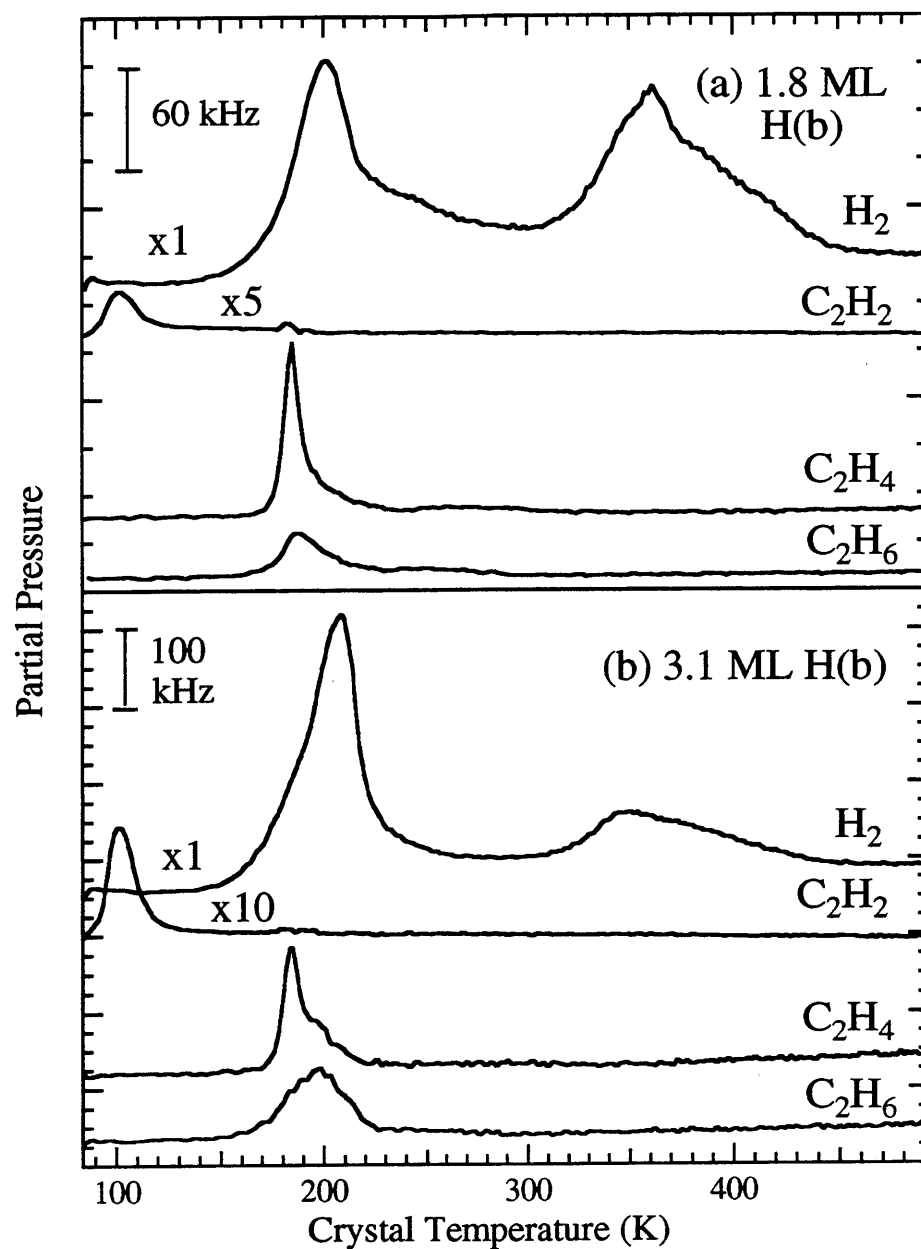
Figure 4 A thermal desorption spectrum resulting from the reaction of (a) an
equivalent of 1.8 ML of bulk H with 0.25 ML C_2H_2, and (b) an equivalent of
3.1 ML of bulk H with 0.25 ML C_2H_2. C_2H_2, C_2H_4, C_2H_6 traces shown
originate from m/e=26, 27 and 30 signals, respectively, and have been corrected
for cracking patterns and ionization probabilities as explained in the text. The
low temperature feature in the signal C_2H_2 is due to desorption of C_2H_2 from
the cryostat.

displayed in Figure 4a. The major product of the reaction of an equivalent of 1.8 ML of H in the bulk and 0.25 ML C_2H_2 is C_2H_4, with a significant amount of C_2H_6 and a small amount of desorbing C_2H_2. Figure 4b shows a similar experiment done by preparing an equivalent of 3.1 ML of H in the bulk, and then adsorbing 0.25 ML of C_2H_2 on surface. With more H adsorbed in the bulk, a larger amount of C_2H_6 is produced.

The distribution of gas phase products for an equivalent of 1.8 ML of bulk H and 0.25 ML C_2H_2 on the surface is much different than that for the very similar experiment with an equivalent of 1.7 ML of bulk H and 0.25 ML C_2H_4 on the surface. Figure 5 shows the partial pressures of gas phase hydrocarbons produced from the reaction of bulk H with each adsorbed species. For the C_2H_4 reaction, the major reaction channel is unreactive desorption, whereas for the C_2H_2 reaction, only a very small amount of the acetylene reactant is unreactively desorbed. Gas phase C_2H_2 hydrogenation products include both C_2H_4 and the double hydrogenation product, C_2H_6. The ratio of C_2H_6/C_2H_4 is different for the two reactions, with a value of 0.08 for the C_2H_4 reaction and 0.59 for the C_2H_2 reaction, which is curious. After C_2H_2 is hydrogenated to C_2H_4, a naïve expectation is that C_2H_4 would be preferably displaced by the emerging H and therefore yield the same value for the C_2H_6/C_2H_4 product ratio as observed for C_2H_4 hydrogenation.

However, notice that the gas phase products of C_2H_2 hydrogenation by bulk H desorb over a broader temperature range, representing a slower rate of formation of both hydrogenation products,while the sharp features observed for the reaction of bulk H and C_2H_4 suggest that the reaction happens very quickly. It is possible that the bulk H atoms increase
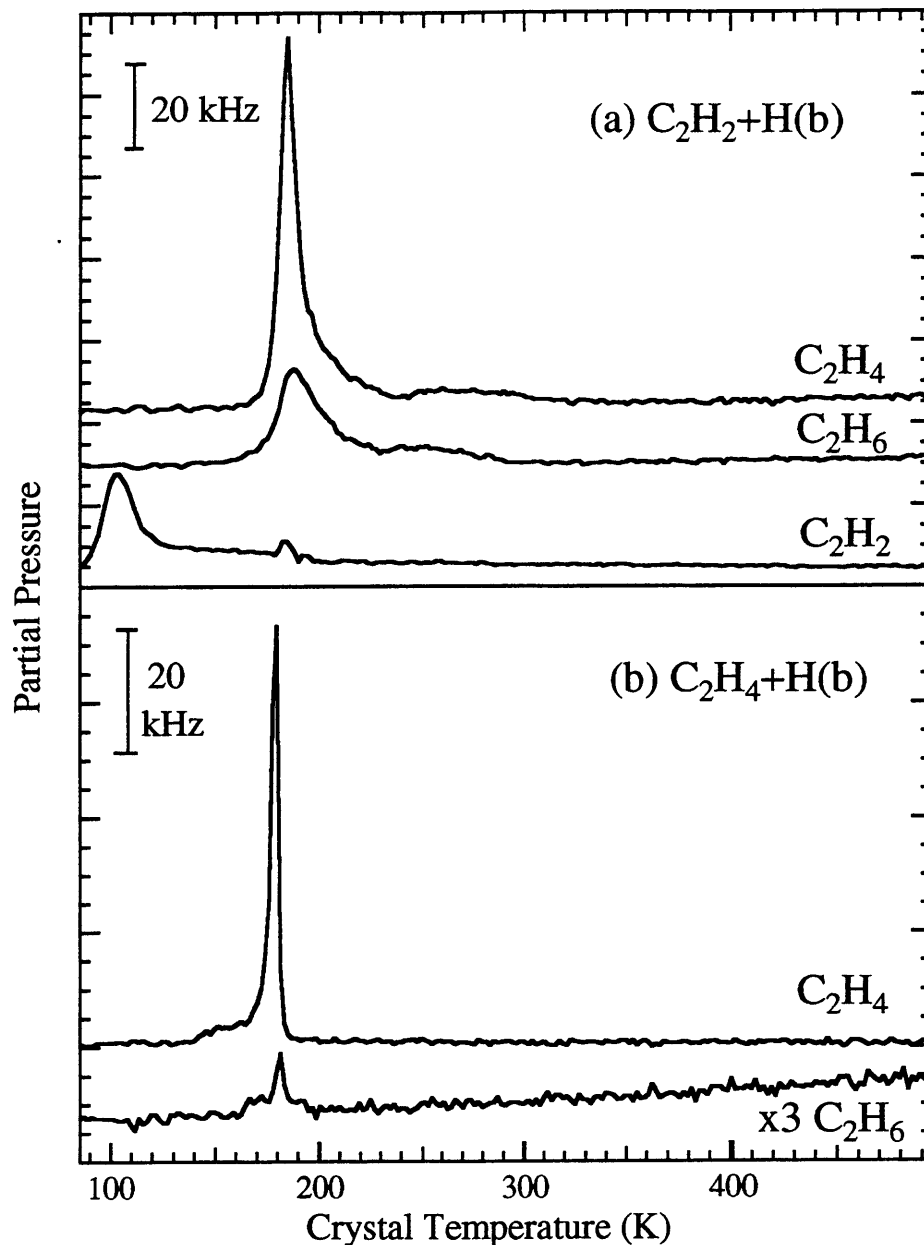
Figure 5 A thermal desorption spectrum resulting from the reaction of (a) an equivalent of 1.8 ML of bulk H and 0.25 ML C_2H_2, and (b) an equivalent of 1.7 ML of bulk H and 0.25 ML C_2H_4. Crystal heating rates are identical. C_2H_2, C_2H_4, C_2H_6 traces shown originate from $m/e=26$, 27 and 30 signals, respectively, and have been corrected for cracking patterns and ionization probabilities as explained in the text. The low temperature feature in the signal C_2H_2 is due to desorption of C_2H_2 from the cryostat.

the local surface temperature and lead to enhanced C_2H_4 desorption. Since C_2H_4 has a low

binding energy, molecularly desorbing at 220 K, in contrast to C_2H_2 which is stable to 400 K,

any temperature increase would affect C_2H_4 not C_2H_2. As the bulk H atoms emerge with 24

kcal/mol and equilibrate on the surface, particularly the ones that form the first saturated

monolayer of H on the surface, these energetic surface bound H atoms could locally transfer

their energy to the first few layers of the Ni. This energy transfer increases the surface

temperature in the vicinity of the C_2H_4 molecules from the measured temperature of 180 K to

the 220 K which preferentially desorbs C_2H_4 but not C_2H_2. After the surface is saturated with

H atoms, the remaining bulk H atoms that emerge have multiple reaction pathways and

possible methods to dissipate their energy. For example, if a bulk H atom recombines with a

surface H atom and desorbs, which is how a bulk H atom is measured in thermal desorption,

the excess energy of the bulk H atom is transferred into excess energy in the newly formed H_2

molecule, and is not dissipated into the surface and translated into heat. So surface heating

due to bulk H atoms is reduced after a saturated monolayer of H is formed. The result of this

greater surface heating due to the initial bulk H atoms is that a much higher fraction of C_2H_4

molecules desorb in the C_2H_4 reaction than in the C_2H_2 reaction. The C_2H_2 product ratio

represents production of C_2H_4 and C_2H_6 under conditions where there is less heating of the

surface. Essentially, for the C_2H_2 reaction, the residence time of the C_2H_4 molecules on the

surface is longer and each C_2H_4 is therefore exposed to an increased number of bulk H atom

that leads to further hydrogenation.
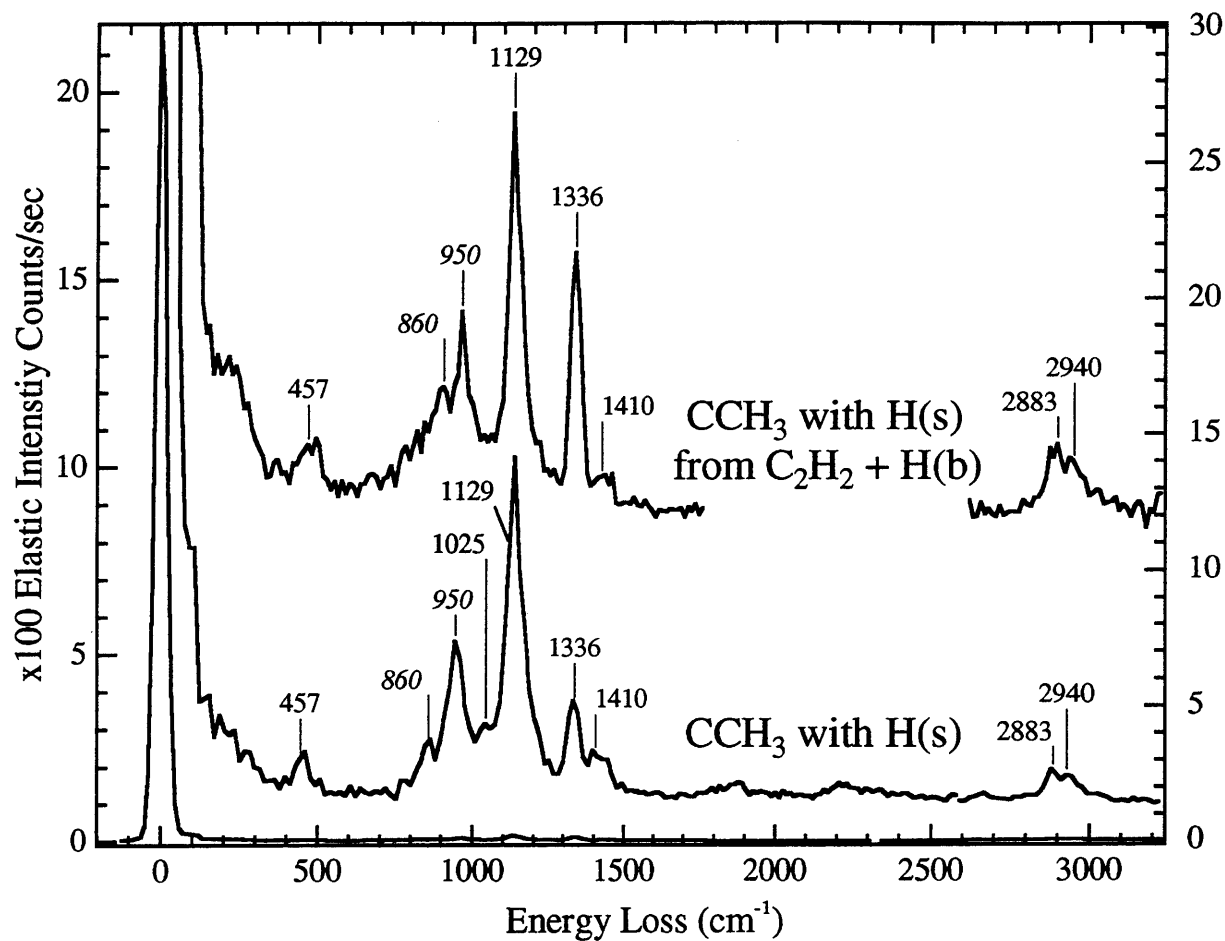
Figure 6 HREEL spectrum from the reaction of an equivalent of 3.7 ML of bulk H and 0.22 ML C_2H_2 along with a spectrum of CCH_3 with coadsorbed H(s) from the reaction of C_2H_4 and gas phase H atoms. Features labeled in *italics* are from H and C_2H_2. Spectra taken at 80 K, with 6.5 eV electrons at 5° and 10° off specular, respectively, and with a ΔE_{fwhm} of 40 and 45 cm^{-1}.

2.3 *Bulk H + Acetylene- Surface Products*

Unlike the reaction of C_2H_4 with bulk H, carbon remains on the surface after the reaction of

bulk H with C_2H_2. Figure 6 shows the EEL spectrum of the residual species after reaction of

an equivalent of 3.7 ML bulk H with 0.22 ML C_2H_2 initiated by heating the crystal to 220 K at

a rate of 2 K/s. In this reaction, 70% of the carbon remains on the surface as measured by

Auger electron spectroscopy. The main residual species is assigned to ethylidyne. For

comparison, an ethylidyne spectrum made from C_2H_4 and gas phase H atoms is shown. This

specific bulk H and C_2H_2 coverage maximizes the surface coverage of CCH_3 relative to the

surface coverage of C_2H_2. The feature at 860 cm^{-1}, which is the C-H out-of-plane

antisymmetric bend[7] of C_2H_2, indicates there is still C_2H_2 on the surface. The ratio of CCH_3

product to the C_2H_2 reactant on this surface is estimated to be 3 from the ratio of the EELS

intensity of the 1129 cm^{-1} feature which is the C-C stretch of CCH_3 to that of the 860 cm^{-1}

feature which is the C-H out of plane antisymmetric bend of C_2H_2. Different initial coverages

of C_2H_2 result in different product to reactant ratios. For example, with an equivalent of 3.7

ML bulk H and initial C_2H_2 coverages of 0.25, 0.16, and 0.07 ML, the ratios of the CCH_3

product to the C_2H_2 reactant are estimated to be 1.5, 3, and 5.5, respectively. Increases in bulk

H above 3.7 ML are not observed to increase the product to reactant ratio significantly.

Again, the C_2H_2 chemistry is very different from the C_2H_4 chemistry. No carbon is left

on the surface after the reaction of C_2H_4 with bulk H if there is more than 1.1 equivalent ML of

bulk H.[4] However, 70% of the carbon is left on the surface after the C_2H_2 reaction with 3.7

equivalent ML of bulk H, and the surface species is CCH_3. The large difference in the

desorption of these two species can be partially understood from their adsorption energies.

The heat of adsorption is larger for C_2H_2 than for C_2H_4. There are several observations that

support this statement. First, C_2H_2 does not to desorb molecularly from the surface. Instead, it

begins to decompose at 400 K.[8] In contrast, a fraction of a saturated monolayer of C_2H_4

molecularly desorbs at 220 K.[4] These values for the desorption and dissociation temperatures

lead to an adsorption energy of C_2H_2 on Ni of at least 20-28 kcal/mol and an adsorption energy

of C_2H_4 on Ni of between 10-18 kcal/mol.[9] Another experimental measure of the adsorption

energy of the two species is that when adsorbed C_2H_4 is warmed to 210 K and annealed for 30

minutes in a partial pressure of $2x10^{-5}$ Torr H_2, no carbon remains on the surface. If C_2H_2 is

exposed to a partial pressure of $2x10^{-5}$ Torr H_2 at 220 K for 30 minutes, there is no change in

the carbon coverage, as measured by Auger electron spectroscopy. The adsorption energy of a

H_2 molecule to form two surface bound H atoms is 23 kcal/mol. Since adsorbed C_2H_4 is

displaced by H_2, this suggests that it is bound to the surface by less than 23 kcal/mol, while the

adsorbed C_2H_2 which is not displaced should be bound by more than 23 kcal/mol. These

experimental observations are consistent with theoretical calculations for the adsorption energy

of 15 kcal/mol for C_2H_4 and 18 kcal/mol for C_2H_2 on Ni(111)[10] and a separate calculation of

17 kcal/mol for C_2H_4 and 37 kcal/mol for C_2H_2 on Pt(111).[11] Adsorbed acetylene is simply

more tightly bound to the surface than ethylene. The experimental observation that most of the

C_2H_4 molecularly desorbs from the surface during reaction with bulk H atoms while little to

none of the C_2H_2 molecularly desorbs from the surface during reaction with bulk H is

consistent with the binding energy of each molecule. The higher binding energy of C_2H_2 also

means a larger number of C_2H_2 molecules are present on the surface at higher surface

temperatures where they are exposed to a continued flux of bulk H atoms, resulting in broader

desorption features for C_2H_2 gas phase hydrogenation products as compared to C_2H_4.

However, the precise mix of gas phase and surface products depends on the rates of the

different reaction channels and the stability of the intermediates in the pathways to particular

gas phase and surface products. The production of ethylidyne is emerging as a trend in C_2H_2

chemistry and suggests a similarity between the surface hydrogen and bulk hydrogen reactions.

2.4 Mechanism and Product Ratios of Bulk H Reactions

The proposed intermediates in the reactions of C_2H_4 and C_2H_2 with bulk H provide a

basis for understanding the observed product distributions. The distribution of products are

shown in Figure 7a. Reaction A shows the branching between gas phase C_2H_4 and C_2H_6

products for the reaction of an equivalent of 3.3 ML bulk H and 0.25 ML C_2H_4. Ethylene is

the most abundant gas phase product. Reaction B shows the branching between adsorbed and

gas phase products for the reaction of an equivalent of 3.7 ML bulk H and 0.22 ML C_2H_2. In

this reaction, 70% of the initial carbon remains on the surface, with the majority of the carbon

incorporated into the CCH_3 product. The remaining 30% of the initial C_2H_2 desorbs as

hydrogenation products, with twice as much C_2H_6 formed as C_2H_4.

Figure 7b shows the proposed mechanism for each reaction. For C_2H_4, the addition of

one H atom produces an adsorbed ethyl species, C_2H_5, with a second H atom needed to fully

hydrogenate to C_2H_6. Ethyl is a very unstable species at these temperatures.[12] The 7% ethane

product distribution may underestimate the success of bulk H addition to ethylene because the
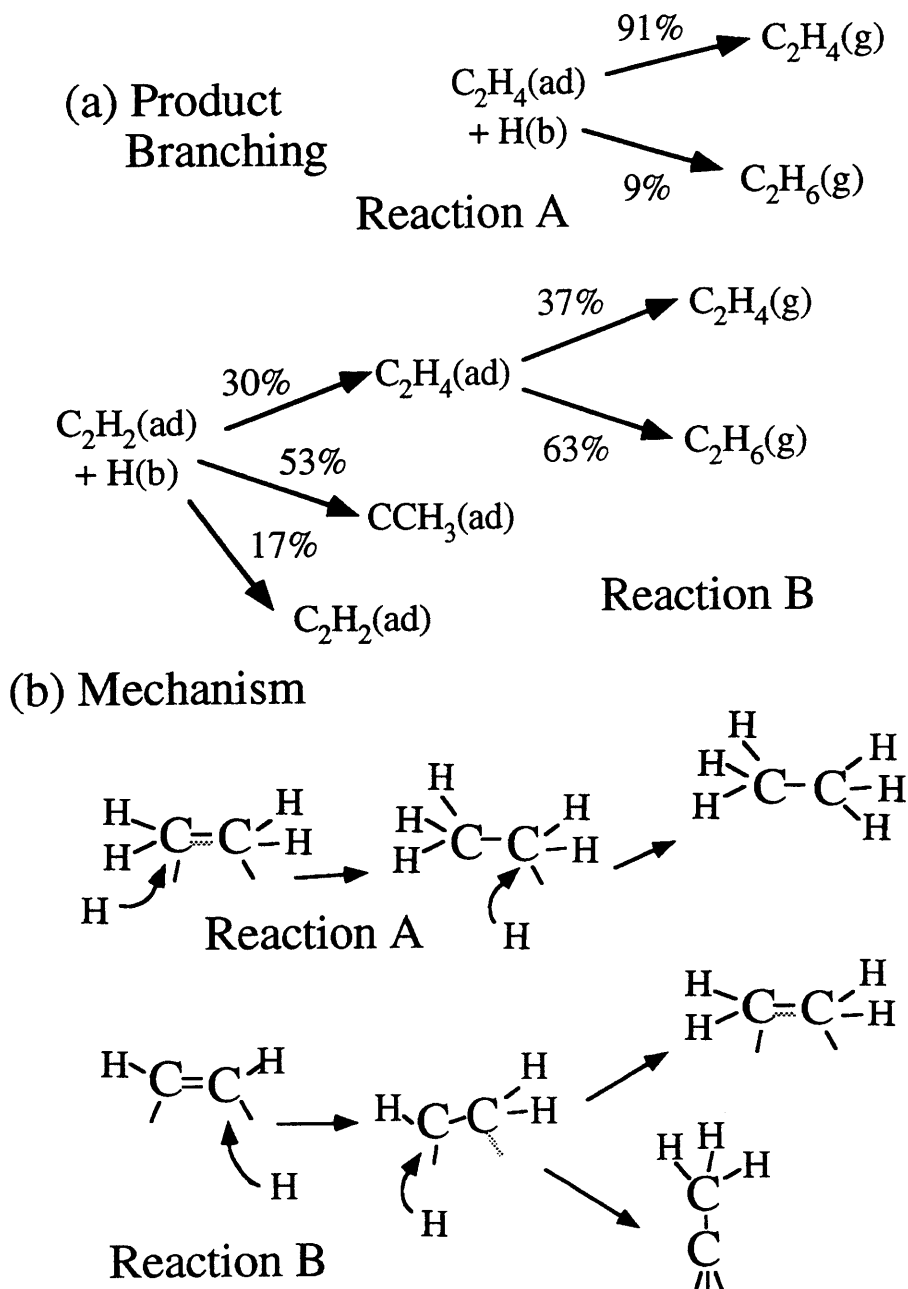
Figure 7 (a) Product branching showing the reactions of bulk H with C_2H_4 and bulk H with C_2H_2. Product distributions for the reaction of 0.25 ML C_2H_4 and an equivalent of 3.3 ML of bulk H, and the reaction of 0.22 ML C_2H_2 and an equivalent of 3.7 ML of bulk H. (b) Proposed mechanisms for each reaction.

short lived ethyl may decompose back to ethylene before a second H atom, either a bulk H or a surface bound H, can add.

The proposed mechanism shown in Figure 7b for reaction of bulk H with C_2H_2 is more complex. Acetylene is hydrogenated to adsorbed C_2H_4, which then either desorbs or is further hydrogenated to C_2H_6. A competing reaction is the formation of the surface product CCH_3. In the reaction of one bulk H atom with a C_2H_2 molecule, the common intermediate in both C_2H_4 and CCH_3 formation is believed to be vinyl, $CHCH_2$. This is the same intermediate believed to be formed when surface H adds to C_2H_2 to form CCH_3. Chapter 6 discusses the evidence to support vinyl as the intermediate in these reactions. The vinyl intermediate is then converted to either C_2H_4 by addition of a second H atom, either a bulk H or a surface bound H, or to CCH_3. After C_2H_4 is formed it can either molecularly desorb, or be converted to C_2H_6 via the mechanism for Reaction A. The ratio of CCH_3 to C_2H_4, 53/30, is due to the different rates of the two competing steps of $CHCH_2$ conversion to CCH_3 and H addition to $CHCH_2$ to make C_2H_4. The rates for these two reactions are most likely determined by the energy barrier for each reaction. In the reaction of surface H with C_2H_2, the only product formed, through the vinyl intermediate, is ethylidyne. Since the sole product in the reaction of surface bound H with the vinyl intermediate is CCH_3 not C_2H_4, and since surface bound H atoms are lower energy species than bulk H atoms, it seems reasonable to conclude that the energy needed to form CCH_3 is lower than that needed to form C_2H_4. If the barrier determines the rate to form a particular intermediate, then the lower barrier to CCH_3 formation explains the higher amount of CCH_3 product. However, the energy barriers for H addition to $CHCH_2$ to form C_2H_4 and

conversion of $CHCH_2$ to CCH_3 may themselves be different for the two different H atom

species. Because the ratio of CCH_3 to C_2H_4 products for this bulk H reaction with $CHCH_2$

demonstrates a majority of CCH_3 product, this suggests that the energy barriers and rates for

the two reaction channels of CCH_3 and C_2H_4 formation are similar to those for surface

bound H.

There is an absence of CCH_3 production in the reactions of C_2H_4 with bulk H. The

reason is that the route to vinyl formation in the reaction of bulk H with C_2H_4 involves the

abstraction of a H atom from C_2H_4 by bulk H to form the $HCCH_2$ intermediate. However, the

H abstraction from a C-H bond by a bulk H is an endothermic reaction, and therefore cannot

occur under these conditions. Since no vinyl intermediate can be formed, no CCH_3 is

produced.

Up to this point, bulk H has been depicted as reacting with a hydrocarbon as it emerges

from the bulk. However, it is also possible that this energetic H atom does not encounter a

hydrocarbon immediately as it emerges. Instead, some of the excess energy of the H atom is

converted into translational motion. In this case, this translationally 'hot' surface hydrogen

atom may be responsible for the increased reactivity seen in bulk H reactions. If a majority of

the bulk H atoms react with hydrocarbons as translationally hot surface species then the

distinguishing difference between surface and bulk H atoms is the energy they possess rather

than the direction of approach. Unfortunately, there is no method to distinguish experimentally

between the reaction of a bulk H atom as it emerges from the bulk from the reaction of a

translationally hot surface H atom with the energy of a bulk H atom.

A clear comparison of the reactivity of surface H atoms and bulk H atoms with C_2H_2 is now possible. In the reaction of surface H with C_2H_2, the π orbital in the surface plane makes it possible for a slow reaction to occur at 280 K leading to CCH_3 formation, a surface bound product. No hydrocarbon species are desorbed during this reaction. On the other hand, bulk H atoms add to C_2H_2 to produce both the surface bound CCH_3, as well as the gas phase hydrogenation products, C_2H_4 and C_2H_6. The higher energy of the bulk H atoms and their favorable approach along the direction of the π orbital of the adsorbed molecules as they emerge from the bulk are both responsible for the gas phase hydrogenation products observed. As explained previously, in contrast to the C_2H_2 chemistry, C_2H_4 will not react with surface bound H atoms, presumably due to the lack of a π orbital in the surface plane. Bulk H addition to C_2H_4 similarly produces gas phase hydrogenation products because the bulk H atoms have the same favorable approach along the direction of the single C_2H_4 π orbital perpendicular to the surface. These observations demonstrate that bulk H atoms are the active species in acetylene and ethylene hydrogenation to gas phase products. This study confirms that it is critical to study bulk H reactions to fully understand and mimic high pressure catalytic activity.

[1] J.I. Macnab and R.B. Anderson, J. Catal. **29**, 338 (1973)

[2] I. Nicolau and R.B. Anderson, J. Catal. **68**, 339 (1981)

[3] P. Fouilloux, Appl. Catal. **8**, 1 (1983)

[4] S.P. Daley, Ph.D. Thesis, Massachusetts Institute of Technology (1994)

[5] S.P. Daley, A.L. Utz, T.R. Trautman and S.T. Ceyer, J. Am. Chem. Soc. **116**, 6001 (1994)

[6] A.D. Johnson, S.P. Daley, A.L. Utz and S.T. Ceyer, Science **257**, 223 (1992)

[7] H. Ibach and S. Lehwald, J. Vac. Sci. Technol. **18**, 625 (1981)

[8] S. Lehwald and H. Ibach, Surf. Sci. **89**, 425 (1979)

[9] R. Masel, *Principles of Adsorption and Reaction on Solid Surfaces*, John Wiley and Sons (1996)

[10] A.T. Bell and E. Shustorovich, Surf. Sci. **235**, 343 (1990)

[11] E.A. Carter and B.E. Koel, Surf. Sci. **226**, 339 (1990)

[12] T.T. Trautman, Ph.D. Thesis, Massachusetts Institute of Technology (1996)

Chapter 5

# Gas Phase H Atom Reactivity

with Adsorbed C_2H_2, C_2H_4, and C_2H_6

1 Introduction

Gas phase H atoms are high energy species which are facile at breaking and forming C-H bonds. Gas phase H atoms are exotic species. They are not typical reactants in catalysis due to the high temperatures that are required to thermally activate the dissociation of the strong H_2 bond. For this reason, gas phase H atom reactions are not likely to play key roles in catalysis. However, studies of the reactions of gas phase H atoms with adsorbed hydrocarbons are valuable for extending our understanding of the hydrogen reactions with small hydrocarbons. Gas phase H atoms as reactants provide a higher potential energy and wider range of approach angles to the hydrocarbon than either surface H or bulk H, thereby allowing the hydrogenation reactions of adsorbed acetylene, ethylene, and ethane to be investigated over a larger region of the potential energy surface for these reactions.

What makes these studies possible is the easy synthesis of H atoms by dissociation of

H_2 over a hot tungsten filament, as described in detail in Chapter 2. The filament is placed in

front of the crystal and provides the localized heat needed to form the gas phase H atoms.

There is a small increase in surface temperature during H atom exposures due to radiative

heating from the filament. This synthesis method is only possible under vacuum conditions

where H_2 molecules are the only gas phase species present. Under the high pressure conditions

of heterogeneous catalysis, in which gas phase hydrocarbons as well as H_2 molecules are

present, a hot filament would initiate gas phase reactions which would ultimately affect the

surface chemistry.

From the perspective of gas phase H atoms as reactants that provide a high potential

energy and a broad angular approach, what predictions can be made for their reactivity? Gas

phase H atoms, similar to bulk H, have enough energy to add to and to form new C-H bonds

with both adsorbed C_2H_2 and C_2H_4. The gas phase hydrogenation products, C_2H_4 and C_2H_6, are

expected from both C_2H_2 and C_2H_4 reactants. The gas phase H atoms could also displace intact

reactant molecules, most likely C_2H_4, and cause their desorption. However, once a H atom adds

to C_2H_2, the vinyl intermediate is created and the possibility of forming CCH_3 is introduced.

Unlike bulk H, gas phase H atoms can abstract H from adsorbed C_2H_4 to synthesize vinyl.

Indeed, if vinyl is the intermediate to CCH_3 formation, CCH_3 should be observed as the product

of the reaction of gas phase H with C_2H_4. The reaction of gas phase H with C_2H_6 is also

explored. Similar to C_2H_4 chemistry, gas phase H atoms can abstract H from C_2H_6. With a

succession of H abstractions from C_2H_6, C_2H_4 and ultimately CCH_3 could be formed.
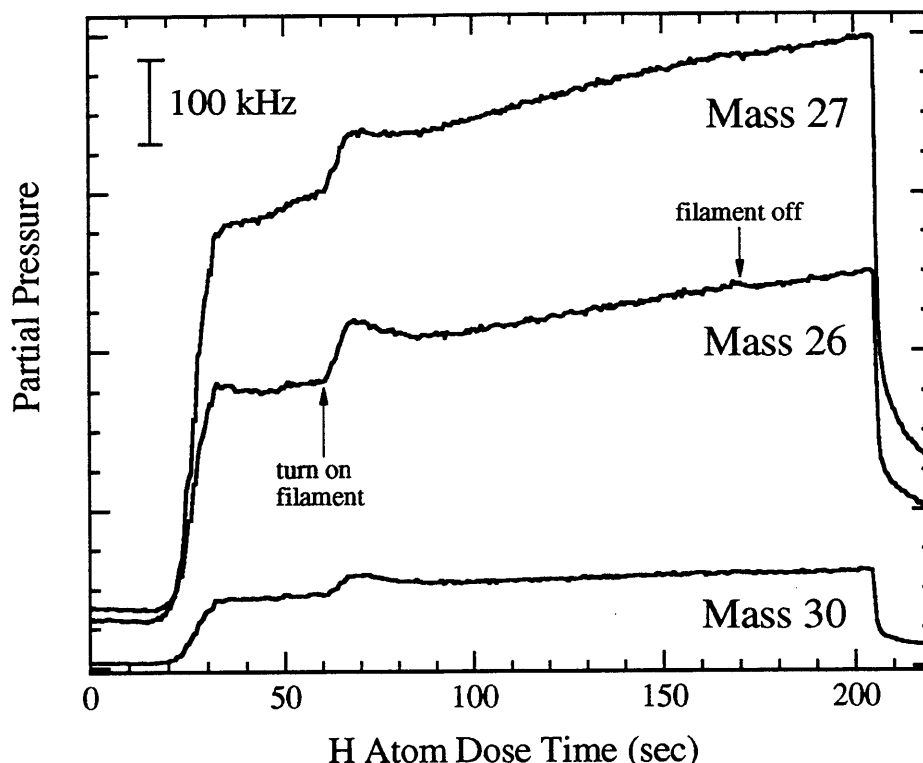
Figure 1 Partial pressure at m/e=26, 27 and 30 for 0.25 ML C_2H_4 plus gas phase H atoms at a temperature is 120 K. Initial rise in signal at 20 sec from increase in H_2 pressure to 5×10^{-6} Torr.

2 Experiments

2.1 Gas Phase Products

Measurements of the gas phase products of H atom addition to adsorbed C_2H_2 and C_2H_4 have been made. Unlike the thermal desorption measurements that probe the gas phase products of surface H and bulk H, the crystal temperature is held constant in this experiment. The surface at 80 K is saturated with one of the hydrocarbons. The front filament is heated in an increased partial pressure of H_2 to produce H atoms while the partial pressure of different gas phase species are monitored. During the exposure to H atoms, the crystal temperature increases to 120 K.

The partial pressures at m/e=26, 27, and 30 are plotted upon exposure of adsorbed
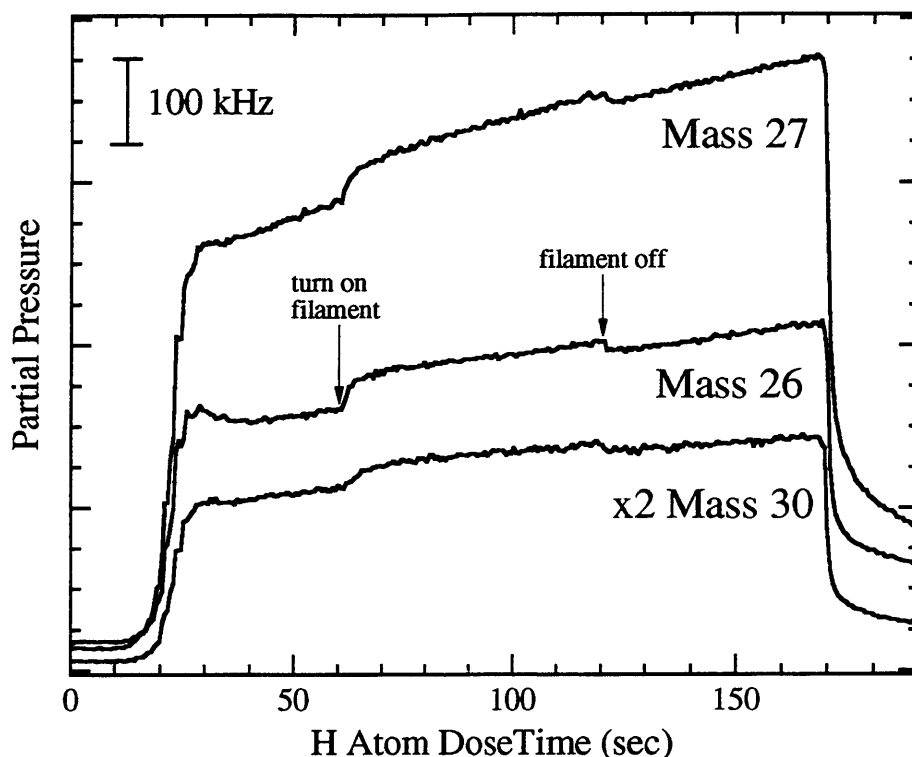
Figure 2 Partial pressure at m/e=26, 27 and 30 for 0.25 ML C_2H_2 plus gas phase H atoms at a temperature is 120 K. Initial rise in signal at 20 sec from increase in H_2 pressure to 5×10^{-6} Torr.

C_2H_4 to gas phase H atoms in Figure 1 and upon exposure of adsorbed C_2H_2 to gas phase H atoms in Figure 2. The baseline at very short times is the background signal at each m/e value. These measurements are challenging because the synthesis of H atoms requires the presence of a high partial pressure of H_2 molecules. This increased pressure leads to a steep increase in the baseline signal at about 20 seconds as a result of introducing 5×10^{-6} Torr of H_2 into the main chamber. While the origin of this signal increase was not specifically investigated, introduction of a gas into a vacuum chamber causes both collision induced desorption and displacement of molecules adsorbed on the chamber walls. The arrows note when the front filament is turned on and off, signaling when the H atom exposure begins and ends. For adsorbed C_2H_4 plus gas

phase H atoms, Figure 1, increases in the m/e= 26, 27 and 30 signal occur at the start of the H

atom exposure. This signal increase is approximately 30 seconds long, after which it drops to

almost a baseline value. The results for C_2H_2, Figure 2, have a much different appearance. As

in the C_2H_4 reaction, there is an increase in the signal at m/e= 26, 27, and 30 at the start of the

H atom exposure. However, for C_2H_2, this signal increase is not limited to the first 30

seconds. It occurs over the entire 60 seconds of exposure to gas phase H atoms.

In addition to noting the time dependence of the production of gas phase products, an

analysis of the composition of the desorbing products is possible. This analysis is similar to

that explained in Chapter 4. First, the partial pressures at each m/e value are integrated over

time after subtracting the baseline signal that is established from the signal before and after the

gas phase H atom exposure. The large range of baseline signals that can be subtracted from

the signal lead to significant error bars on these integrated values. The integrated value for

m/e=30 only has contributions from C_2H_6 and is named $\int_{ethane} 30$ below, but the m/e=27 integrated

value has contributions from both C_2H_4 and C_2H_6 and is named $\int_{total} 27$ below. All of the m/e=26

signal, which is the signature mass for acetylene, is accounted for by the cracking of C_2H_4,

therefore acetylene is not considered as a product. An integrated value that has contributions

from ethylene only, $\int_{ethylene} 27$, is calculated by subtracting the C_2H_6 contributions from the m/e=27

integrated value after being weighted by the appropriate ratio of cracking fractions, as shown

below. The cracking fractions are named $crackingC_2H_x(Y)$, for the hydrocarbon C_2H_x at mass

Y, and are listed in Table 1 in Chapter 2.

$$\int_{ethylene} 27 = \int_{total} 27 - \int_{ethane} 30 \left(\frac{crackingC_2H_6(27)}{crackingC_2H_6(30)} \right) \tag{1}$$

The two integrated values, $\int_{ethane} 30$ and $\int_{ethylene} 27$ now represent contributions from only C_2H_6

(m/e=30) or only C_2H_4 (m/e=27). Each integrated value, at a particular mass, is then scaled by

the ratio of the total of the cracking fractions over the cracking at the particular observed mass

for the molecule being detected. This total cracking value is listed in Table 1 in Chapter 2, and

named as *totalsignalC$_2$H$_x$* for the hydrocarbon C_2H_x. This scaling eliminates differences in

intensity from detecting a particular molecule at a particular mass. In this final scaling, a

second correction is also made to adjust for differences in the ionization cross section of the

two hydrocarbon species. This last adjustment is done by dividing by the total ionization cross

section (σ_{total}) for the particular molecule. The value of σ_{total} used is given in Chapter 2 and is

an average of measured values from the literature. The result of these two scaling steps is a

quantity, named *signal(C$_2$H$_x$)*, which is proportional to the number density or partial pressure

of each hydrocarbon. As an example, the calculation for ethylene is as follows.

$$signal(C_2H_4) = \int_{ethylene} 27 \left(\frac{totalsignalC_2H_4}{crackingC_2H_4(27)} \right) \left(\frac{1}{\sigma_{total}} \right) \tag{2}$$

The conditions of this experiment may introduce error into this analysis. The

background pressure of 5×10^{-6} Torr of H_2 may lead to gas phase reactions in the ionizer

between H atoms and hydrocarbon fragments that result in the increase of particular

hydrocarbon fragments leading to systematic error in analyzing the data. This possibility was

not checked or taken into account. For the reaction of 0.25 ML C_2H_4 with gas phase H atoms,

$57 \pm 10\%$ of the gas phase product is C_2H_4 and $43 \pm 10\%$ of the gas phase product is C_2H_6. For

the reaction of 0.25 ML C_2H_2 with gas phase H atoms, 18±17% of the gas phase product is

C_2H_4 and 83± 17% of the gas phase product is C_2H_6. Error bars come from the variation in

the baseline signal of a single data set for each hydrocarbon.

2.2 Interpretation of Gas Phase Results

In the reaction of gas phase H atoms with C_2H_4, the H atoms displace C_2H_4 causing

molecular desorption. This molecular desorption is not observed in the reaction of C_2H_2 and

gas phase H due to the stronger C_2H_2 surface bond as compared to C_2H_4. The difference

between the time profile of the partial pressure signals from C_2H_2 and C_2H_4 suggest that the

reaction of gas phase H atoms with C_2H_2 is slower than the reaction of gas phase H atoms with

C_2H_4. The desorption and hydrogenation steps for C_2H_4 occur at a faster relative rate, shown

by the larger increase in the QMS signals at short times. Similarly, the C_2H_2 reaction channels

of hydrogenation occur at a slower relative rate, shown by the steady product signal over a

longer time. These relative desorption rates are summarized in Table 1 which lists average

count rate at the three m/e values in the first 30 seconds of the reaction. These are the raw

signal count rates. These signals are measured under precisely the same conditions with

identical initial coverages of 0.25 ML for C_2H_2 and C_2H_4 and with the same H atom flux from

$5x10^{-6}$ Torr H_2 and 3V across the front filament 0.25" from the crystal. The initial count rate

at all m/e values is twice as large for the reaction of gas phase H with C_2H_4 as that for the

reaction of gas phase H with C_2H_2. The average count rate at m/e=26 and 27 for reaction

times past the first 30 seconds of the reaction are the same for C_2H_4 and C_2H_2, while the

average count rate for m/e=30 is twice as large for C_2H_2 compared to C_2H_4. It is difficult to

m/e signal	Average count rate C_2H_4 (10^3 counts/s)	Average count rate C_2H_2 (10^3 counts/s)
26	1.3	0.5
27	1.5	0.7
30	0.5	0.2

Table 1 Average count rate at m/e for gas phase products desorbed in the first 30 seconds of the reaction of adsorbed C_2H_4 and C_2H_2 with gas phase H atoms, from a single measurement.

know what leads to these trends. There are two main issues that control the product branching in this reaction: the rates to form a particular intermediate from the reactants and the stability of that intermediate. The trends suggest that the rates to form intermediates and products are faster for the ethylene reactions.

In comparison to the gas phase products for the reaction of bulk H atoms with adsorbed C_2H_2 and C_2H_4, the gas phase products in the gas phase H atoms reaction are shifted to more fully hydrogenated species. What may shift the ratio of gas phase products is that the gas phase H flux is ten times higher that the bulk H atom flux. This will increase the rate of H atom induced reactions by a factor of 10.

2.3 Surface Products

The surface product from the reaction of gas phase H atoms with C_2H_2, C_2H_4, and C_2H_6, as observed by EEL spectroscopy, is shown in Figure 3. The separate reactions of 0.25 ML adsorbed C_2H_2 and 0.25 ML adsorbed C_2H_4 with a standard gas phase H atom exposure of 120 seconds with 3V across the front filament placed 0.25" from the crystal and with a H_2

background pressure of 5×10^{-6} Torr are shown in Figure 3a and 3b. During these H atom

exposures, the temperature of the crystal rises from 80 K to 120 K. The reaction of a

saturated surface of 0.20 ML C_2H_6 with gas phase H atoms generated from 3V across the front

filament 0.25" in front of the crystal with a background pressure of 3×10^{-5} Torr H_2 for a 10

minutes exposure is shown in Figure 3c. The higher pressure of H_2 provides a higher flux of H

atoms in this reaction with C_2H_6. During this reaction, the crystal is warmed from 70 K to 78

K. These three spectra are similar and can each be identified as ethylidyne, $-CCH_3$. This

assignment is made from the features at 457 cm^{-1}, 1025 cm^{-1}, 1129 cm^{-1}, 1336 and 1410 cm^{-1},

and 2883 and 2940 cm^{-1}, which correspond to the assigned CCH_3 modes of the C-Ni stretch,

the CH_3 bend, the C-C stretch, the symmetric and antisymmetric CH_3 deformation, and the

symmetric and antisymmetric C-H stretch.[1] Features in italics at 860 cm^{-1} and 950 cm^{-1} are

assigned to modes of C_2H_2 and surface H, respectively. No other hydrocarbon can be

consistently assigned to these loss features. The C_2H_6 spectrum shows a large signal for

surface H at 950 cm^{-1} due to displacement of C_2H_6 and from desorption of C_2H_6 at the elevated

crystal temperature of 78 K. This crystal temperature is high enough that partial desorption

occurs due to the weak C_2H_6 physisorbed bond characterized by the desorption of C_2H_6 at

100 K.[2]

2.4 *Implications of Surface Products in Understanding Mechanisms*

What does it mean for there to be a common CCH_3 surface product, resulting from the

reaction of gas phase H atoms with C_2H_2, C_2H_4, and C_2H_6? It suggests that gas phase H atoms

are able to make a common intermediate in CCH_3 formation from each hydrocarbon species.
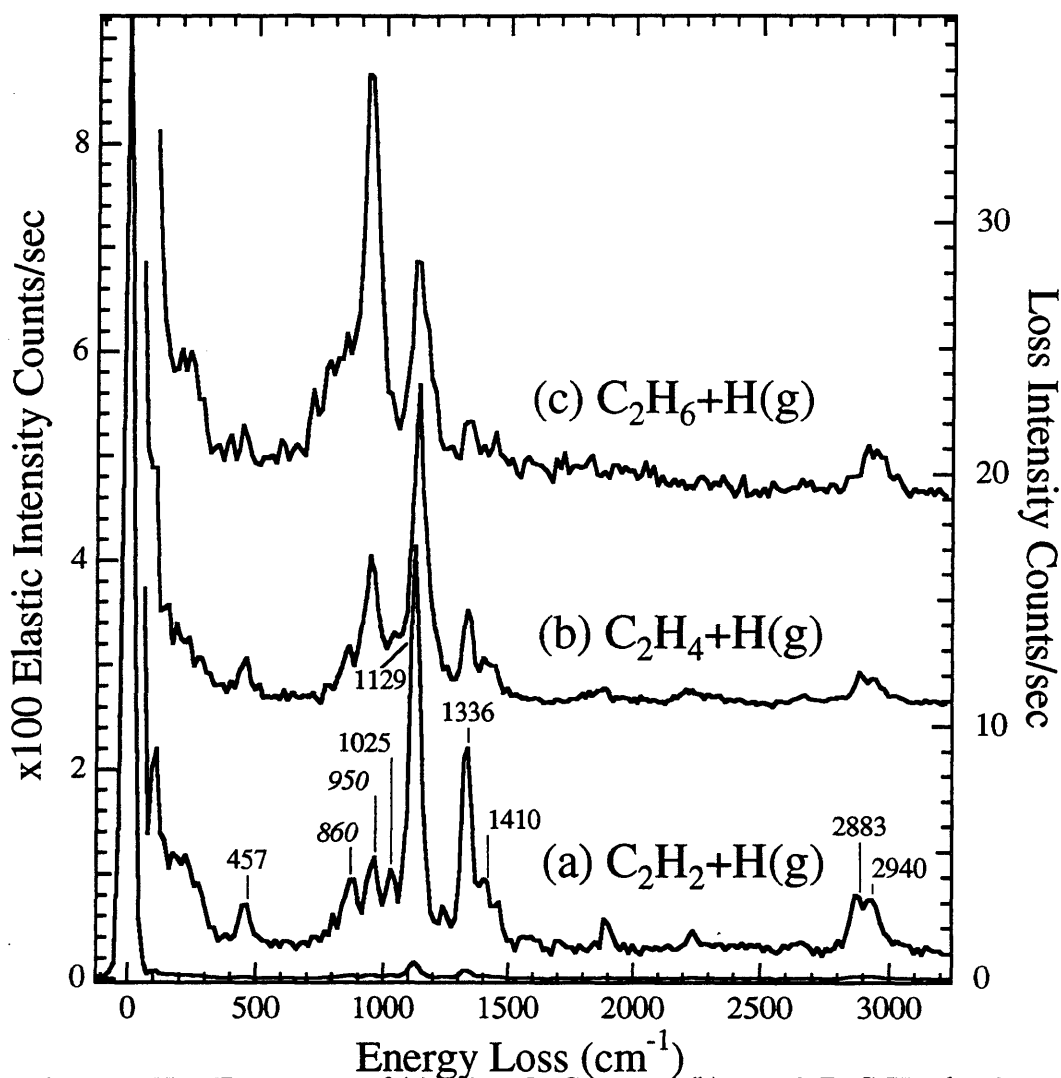
Figure 3 HREEL spectra of (a) 0.25 ML C_2H_2 and (b) 0.25 ML C_2H_4 plus 2 min gas phase H atoms at a H_2 pressure to $5x10^{-6}$ Torr, 120 K during H exposure, 6.5 eV electrons, 10° off specular and ΔE_{fwhm} of 44 and 43 cm^{-1}, respectively. And (c) 0.20 ML C_2H_6 plus 10 min gas phase H atoms at a H_2 pressure to $3x10^{-5}$ Torr, 78 K during H exposure, 6.5 eV electrons, 10° off specular and ΔE_{fwhm} of 48 cm^{-1}.

This is the first time C_2H_4 and C_2H_6 are observed to form CCH_3, but C_2H_2 can readily

make CCH_3 from reaction with surface bound H and bulk H, as well as gas phase H. What are

the ideas about CCH_3 formation from C_2H_2 that can explain the reactivity observed with the

other two hydrocarbons? The C_2H_2 reactions with surface bound H, bulk H, and gas phase H

are consistent with the picture of a single H atom adding to an adsorbed C_2H_2 molecule to

form a vinyl intermediate, $CHCH_2$, that further rearranges to CCH_3. The first elementary step

to CCH_3 formation from C_2H_2 is a H addition. On the other hand, for $CHCH_2$ to be formed

from C_2H_4 and C_2H_6, the first elementary reaction that must occur is a C-H bond cleavage.

Ethylidyne has not been observed as a product in reactions of surface or bulk H with C_2H_4.

One reason is the inability of surface H and bulk H to abstract a H atom, breaking a C-H bond,

to form the vinyl intermediate required for CCH_3 synthesis. Neither surface H nor bulk H have

enough energy to abstract a H atom. These reactions are endothermic. From this perspective,

it is clear why gas phase H atoms do create CCH_3. They have enough energy to abstract a H

atom and form the vinyl intermediate! The synthesis of CCH_3 from gas phase H atoms and

C_2H_6 is a further demonstration of the ability of the gas phase H atoms to break C-H bonds.

Presumably, gas phase H atoms remove three H atoms from C_2H_6 to make CCH_3. The

common CCH_3 product indicates that it is a very stable species on Ni. In the high energy

environment of gas phase H atoms, there is sufficient energy to overcome all barriers. This

allows the system to access the most stable C_2 hydrocarbon, CCH_3.

3 Auger Experiment- Exploring Three Reactions in the Time Domain.

The relative rate information extracted from the partial pressure curves at m/e=26, 27,

and 30 discussed above is a crude attempt to understand the rate of the reaction of gas phase H

atoms with adsorbed hydrocarbon species. This apparatus is not designed to observe direct

desorption of gas phase products. In this detection of gas phase products, the partial pressure

observed is the background pressure, the product molecules bounce around the chamber

before detection. Differences in pumping speed and adsorption on the walls between different

molecules may affect detection. Better measurements would both clarify the differences

between the rate of reaction of different adsorbed hydrocarbons and could be of high enough

quality to provide further mechanistic information. Another way to measure the amount of

desorption of gas phase products is to measure the carbon remaining on the surface after a gas

phase H atom exposure. Unlike the desorption signal, it is possible to make a high quality

measurement of the carbon remaining on the surface. The dependence of the Auger carbon

signal versus time of H atom exposure is the consequence of the rates of all the processes

taking place during the exposure of the hydrocarbon to gas phase H atoms: displacement of the

reactant, hydrogenation and desorption of the product, and surface reaction. Following an

explanation of the measurement and description of these Auger data, the results from modeling
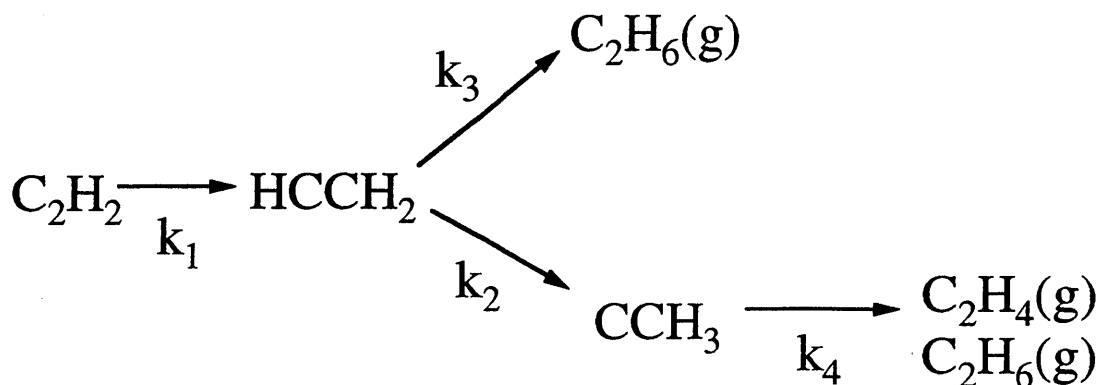
this system with simple kinetics are presented.

3.1 *Auger Measurements*

By exposing adsorbed hydrocarbons to gas phase H atoms for different times the extent

of the reaction is varied. A measurement of the remaining surface carbon, which is a sum of

the carbon from the initial reactant and that from the CCH_3 product, can then be done. The

procedures used to measure the carbon coverage after exposure to gas phase H atoms for all

three hydrocarbons follows. First, the surface is saturated with the hydrocarbon of interest at

80 K, 0.25 ML of C_2H_2 or C_2H_4 or 0.20 ML of C_2H_6. All H atom exposures are then carried

out with liquid He in the crystal cryostat. Lower temperatures than 80 K are necessary to keep

the C_2H_6 from desorbing as a result of the temperature rise of the crystal from radiative heating
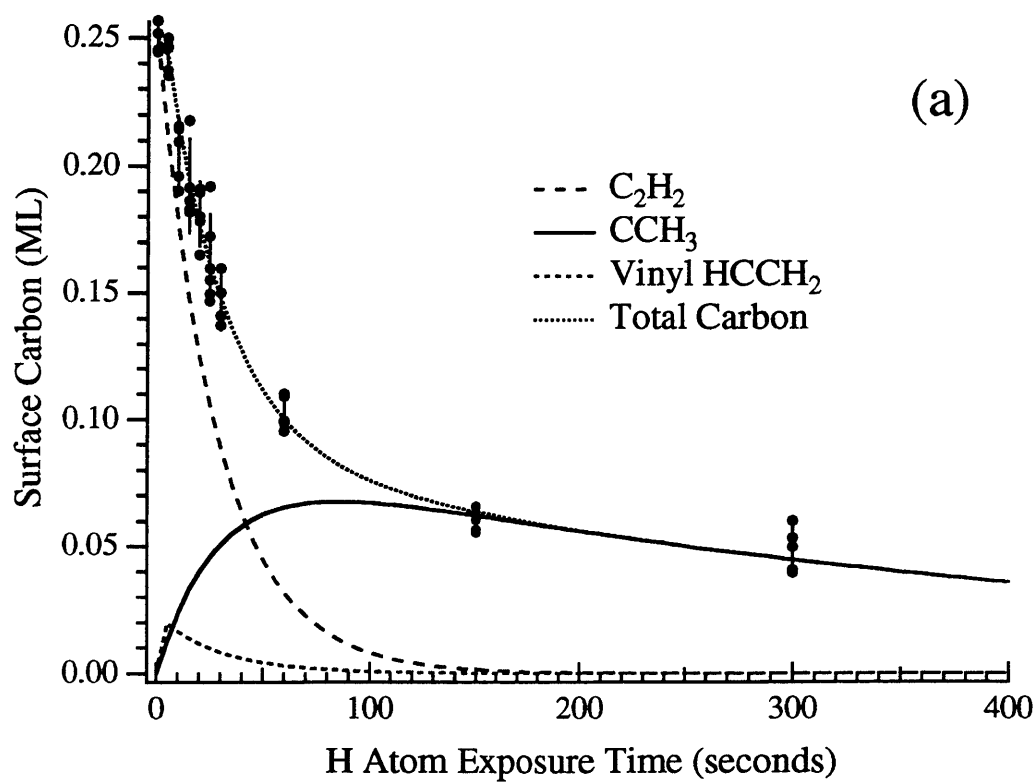
by the H atom filament. With liquid He in the cryostat, the crystal temperature increases to 60

K during the H atom exposure, which is well below the 100 K desorption temperature of

C_2H_6.[2] All hydrocarbon measurements are done with liquid He cooling for consistency. This

surface is then exposed to gas phase H atoms for a specific time, after which a carbon Auger

measurement is done. Specific H atom exposure times were chosen, and the experiment was

repeated five times for each exposure time. The repetition allowed calculation of an average

carbon coverage with a 95% confidence interval error bar.

Figure 4a and 5a show the carbon coverage versus H atom exposure time for C_2H_2 and

C_2H_4. The shapes of these curves are similar for the two hydrocarbons. There is a steep decline

in the amount of carbon remaining on the surface at short times. At longer times, the carbon

coverage decays much more slowly, apparently because the hydrocarbon species formed after

the initial exposure to H atoms is much less reactive with the incoming gas phase H atoms.
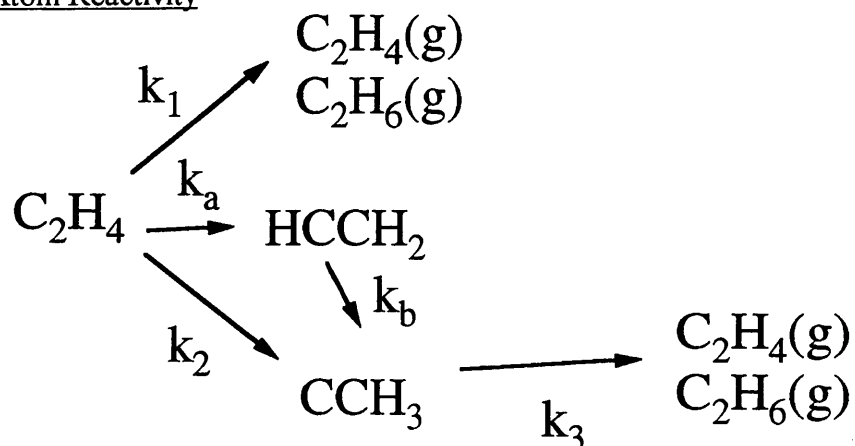
In the case of C_2H_6, it is possible to measure the unreacted C_2H_6 remaining on the

surface after H atom exposure separately and the adsorbed product CCH_3. Since C_2H_6 is

physisorbed and is not strongly bound to the nickel surface, the C_2H_6 will desorb by heating the

crystal at 2 K/s to 120 K, at which temperature the CCH_3 product and the possible C_2H_4

intermediate are stable. The partial pressure of C_2H_6 at m/e=30 is measured during this crystal

temperature increase and the resulting signal is integrated and then compared to the integral of

the m/e=30 signal of a saturated C_2H_6 surface, determined by Auger electron spectroscopy, to

determine the C_2H_6 coverage in monolayers. Five repetitions of the remaining C_2H_6 coverage

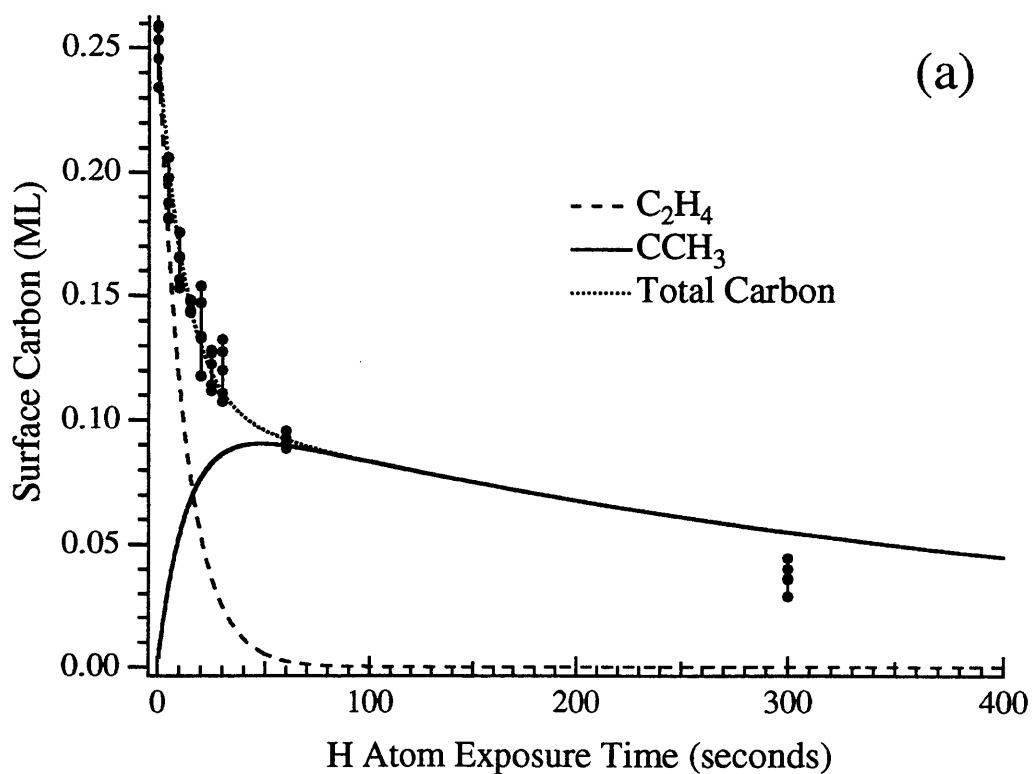are done for each H atom exposure time. After desorption of the unreacted C_2H_6, the coverage

$$C_2H_2 \xrightarrow{k_1} HCCH_2 \xrightarrow[k_2]{k_3} \begin{array}{c} C_2H_6(g) \\ \\ CCH_3 \xrightarrow{k_4} \begin{array}{c} C_2H_4(g) \\ C_2H_6(g) \end{array} \end{array}$$
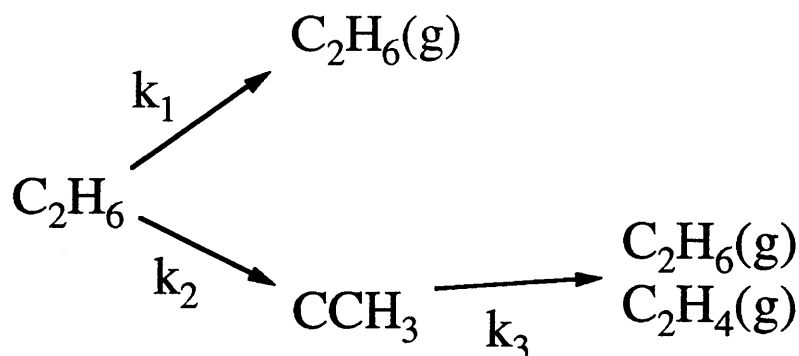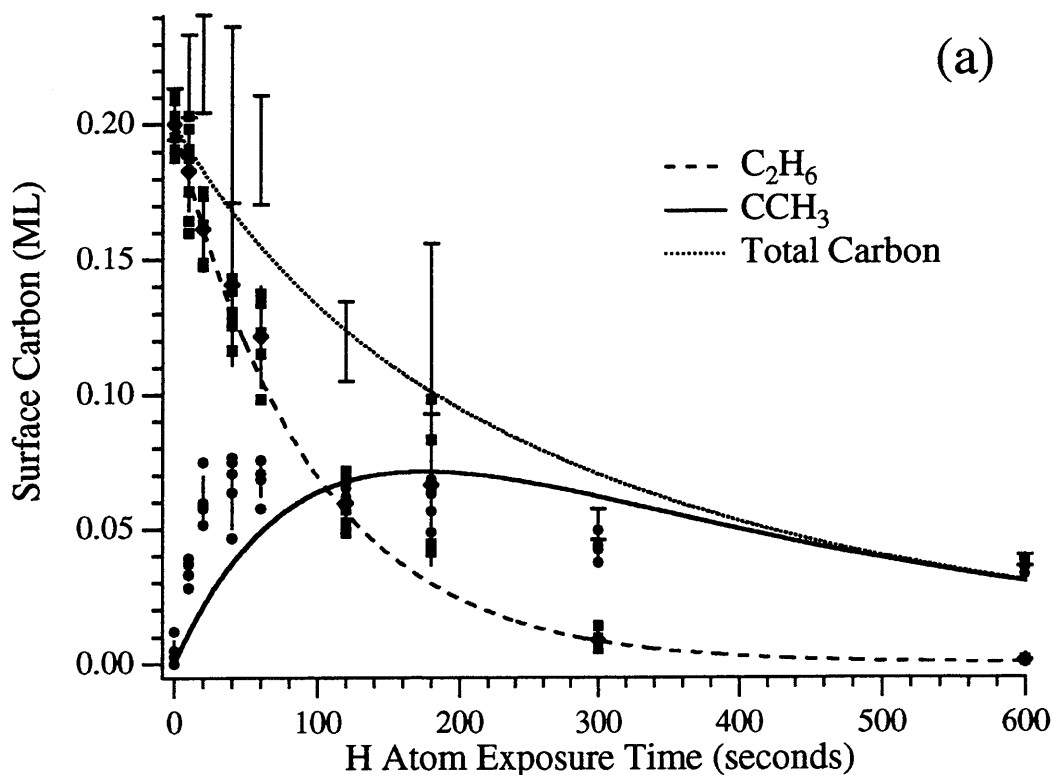
(b) Model Reaction Mechanism

Figure 4 (a) Carbon Auger signal (•) expressed in monolayers versus gas phase H atom exposure time. Error bars represent 95% confidence limit for five measurements. Solid and dashed lines are calculated coverages of individual molecules. (b) Representation of reaction mechanism used in kinetic model for 0.25 ML C_2H_2 plus gas phase H atoms.

$$C_2H_4(g)$$
$$C_2H_6(g)$$

$$C_2H_4 \xrightarrow{k_a} HCCH_2$$

$$CCH_3$$

$$C_2H_4(g)$$
$$C_2H_6(g)$$

(b) Model Reaction Mechanism

(a)

--- C$_2$H$_4$
—CCH$_3$
·········Total Carbon

Figure 5 (a) Carbon Auger signal (•) expressed in monolayers versus gas phase H atom exposure time. Error bars represent 95% confidence limit for five measurements. Solid and dashed lines are calculated coverages of individual molecules. (b) Representation of reaction mechanism used in kinetic model for 0.25 ML C$_2$H$_4$ plus gas phase H atoms.

Figure 6 (a) Carbon Auger signal (•) and remaining C_2H_6 surface coverage from desorption (■) expressed in monolayers versus gas phase H atom exposure time, the sum of these two values is shown as vertical bars. Error bars represent 95% confidence limit for five measurements. Solid and dashed lines are calculated coverages of individual molecules. (b) Representation of reaction mechanism used in kinetic model for 0.25 ML C_2H_6 plus gas phase H atoms.

of the adsorbed CCH_3 product with a small contribution from the possible C_2H_4 intermediate are measured by the Auger electron spectroscopy.

The CCH_3 coverage as measured by Auger electron spectroscopy and the coverage of unreacted C_2H_6 are plotted versus gas phase H atom exposure time in Figure 6a. All data points have error bars that represent the 95% confidence intervals from five repeated measurements. The separate measure of the unreacted surface bound C_2H_6 reactant and the surface CCH_3 shows a predicted decrease in the C_2H_6 coverage and a corresponding increase in surface CCH_3 coverage with H atom exposure time. However, in comparison with the other two hydrocarbons these changes occur more slowly. Figure 6a also shows a trace for the sum of the CCH_3 and the unreacted surface bound C_2H_6 coverages. This trace is the measure of the carbon remaining on the surface after the gas phase H atom exposure. It can be directly compared to trace of the Auger carbon signal versus gas phase H atom exposure time for C_2H_2 and C_2H_4 as shown in Figure 4a and 5a, respectively. The decrease in the carbon coverage for C_2H_6 is slow, with the curve reaching a more stable value at 300-400 seconds, as compared with 100-200 seconds for the C_2H_2 and C_2H_4 plots.

3.2 Modeling with Simple Kinetics

In an attempt to understand the time dependence of the carbon remaining on the surface after the reaction of C_2H_2, C_2H_4, and C_2H_6 with gas phase H atoms and that of the integrated thermal desorption measurement of the coverage of unreacted C_2H_6 remaining on the surface after gas phase H atom exposure, these data are fit to simple kinetic models devised to capture the essence of the reaction without introducing so many parameters that none of

them have any meaning. The reaction mechanism used for each set of data is shown in Figures

4b, 5b, and 6b. For all three hydrocarbon species, the rate equations are solved numerically.

In the rate equations below, the coverage of reactants and products are represented by $[C_xH_y]$

for the C_xH_y species. Coverages of each reactant and product are calculated from initial

coverages and initial guesses for the rate constants. For the C_2H_2 and C_2H_4 data sets, the sum

of the calculated remaining initial hydrocarbon coverage and calculated CCH_3 coverage are

compared to the measured carbon coverage. For the C_2H_6 data sets, the calculated remaining

C_2H_6 coverage is compared to the measured thermal desorption C_2H_6 coverage and the

calculated CCH_3 coverage is compared to the measured carbon coverage simultaneously. All

measured data are fit using a least-squares procedure, which is a nonlinear χ^2 fitting routine

based on Levenberg-Marquardt methods.[3] Initial guesses for rate constants are varied to

assure a global minimum for the fit of the experimentally observed quantities, carbon coverage

for C_2H_2 and C_2H_4 fits and CCH_3 and C_2H_6 coverage for the C_2H_6 fit. The models are

consistent with the data. The goodness of fit value Q is the probability that a value of χ^2 as

good as the value calculated cannot occur by chance. The Q value for the three fits are

between 0.003 and 0.007, which indicates acceptable agreement between the data and the

model.[3] Each reaction is considered a pseudo-first order reaction, since there is a large and

continual supply of gas phase H atoms measured to be 0.2 ML/sec as detailed in Chapter 2.

The calculated coverage of the reactant and the products of each model are plotted with the

raw data in Figure 4a, 5a, and 6a. The values of the rate constants obtained from the fit are

shown in Table 2. The product and reactant curves from the fit add more meaning to the raw

data. Therefore a general comparison of the fitted results for the three reactions will be made here before the mechanism is discussed in detail. The C_2H_2 reactant and CCH_3 product curves plotted in Figure 4a show that the C_2H_2 does decrease rapidly, reaching zero coverage at about 100 seconds. The CCH_3 product coverage rises steadily from zero time and levels off at about 80 seconds. As discussed below, the C_2H_2 reaction is modeled with the vinyl intermediate which increases at very short times, peaking under 10 seconds, and then decreasing to zero coverage. In comparing the C_2H_2 reaction to the C_2H_4 reaction in Figure 5a, there are differences in the time scale of the two reactions that are more apparent with the product and reactant fits than they were with the measured data. The C_2H_4 coverage also decreases rapidly, but reaches zero at close to 50 seconds. Consistent with this faster decrease in reactant, the CCH_3 product reaches a plateau at ~40 seconds. The C_2H_6 product and reactant fits in Figure 6a yield fewer surprises then the other two data sets, because the measured data already separated the remaining C_2H_6 reactant from the CCH_3 product. The calculated curves follow the data, showing that the C_2H_6 coverage does not decrease to zero until 300 seconds, and that the CCH_3 coverage does not plateau until over 100 seconds. The comparison of the three hydrocarbons certainly shows that the C_2H_6 reaction is the slowest of the three hydrocarbons.

The reaction mechanism of C_2H_2 and gas phase H atoms used in the kinetic model is shown in Figure 4b. This reaction mechanism includes the vinyl intermediate, $CHCH_2$, as the first step in the reaction. It is necessary to include $CHCH_2$ in the model because it is the only possible product of a single H atom addition to C_2H_2, which is the first step in either

	Rate Constant (s^{-1})	Mechanism
Acetylene		
k_1	0.034 ± 0.005	$C_2H_2 \rightarrow CHCH_2$ H addition
k_2	0.049 ± 0.017	$CHCH_2 \rightarrow CCH_3$ migration/H addition
k_3	0.32 ± 0.11	$CHCH_2 \rightarrow C_2H_6(g)$ hydrogenation/desorption
k_4	0.0009 ± 0.0005	$CCH_3 \rightarrow C_2H_4/C_2H_6(g)$ hydrogenation/desorption
Ethylene		
k_1	0.046 ± 0.002	$C_2H_4 \rightarrow C_2H_4/C_2H_6(g)$ desorption
k_2	0.031 ± 0.003	$C_2H_4 \rightarrow CCH_3$ H abstraction
k_3	0.0021 ± 0.0002	$CCH_3 \rightarrow C_2H_4/C_2H_6(g)$ hydrogenation/desorption
Ethane		
k_1	0.0046 ± 0.0007	$C_2H_6 \rightarrow C_2H_6(g)$ desorption
k_2	0.0060 ± 0.0004	$C_2H_6 \rightarrow CCH_3$ H abstraction
k_3	0.0027 ± 0.003	$CCH_3 \rightarrow C_2H_4/C_2H_6(g)$ hydrogenation/desorption

Table 2 Rate constants obtained from fit of kinetic model shown in Figures 4a, 5a, and 6a, to measurements of carbon coverage versus time of H atom exposure.

hydrogenation to gas phase products or hydrogenation to CCH_3. The rate constant for H

addition to C_2H_2 to produce vinyl is k_1. The rate constant for further hydrogenation of vinyl to

gas phase products is k_3, and the rate constant for formation of CCH_3 from vinyl is k_2. The

rate equations solved for C_2H_2 are:

$$\frac{d[C_2H_2]}{dt} = -k_1[C_2H_2]$$

$$\frac{d[CHCH_2]}{dt} = k_1[C_2H_2] - k_2[CHCH_2] - k_3[CHCH_2]$$

$$\frac{d[CCH_3]}{dt} = k_2[CHCH_2] - k_4[CCH_3],$$

where the total carbon measured by Auger spectroscopy is fit to the sum of the coverage of the

three surface bound hydrocarbons calculated during the fitting process from the model, as

shown,

$$SurfaceCarbon = [C_2H_2] + [CHCH_2] + [CCH_3].$$

Figure 4a shows the calculated coverages of each surface species versus H atom

exposure time, including the sum of the three calculated coverages. The calculated coverages

agree well with the experimentally measured carbon coverage values. The k values fit to the

Auger data are listed in Table 2 and are consistent with our idea of how this reaction proceeds.

The k_1 value is lower than either k_2 or k_3. Vinyl formation is the rate limiting step to both

hydrogenation to gas phase products and further reaction to make CCH_3. The consequence of

the rate of vinyl formation being lower than the two rates for the reactions that consume vinyl,

is that the vinyl intermediate is short lived, with a transient surface coverage. The coverage of

$CHCH_2$ as calculated in the fit is shown in Figure 4a. The vinyl coverage is very low overall,

peaking at very short gas phase H atom exposure times. The largest rate of vinyl consumption

is for gas phase hydrogenation products, not CCH_3 formation, which results in rapid depletion

of $CHCH_2$ and as a result rapid loss of carbon from the surface. This depletion is expected,

given the rapid drop in carbon coverage on the surface at short times. The rate constant for

further hydrogenation of CCH_3 to gas phase products, k_4, is very small, indicating that CCH_3 is

not hydrogenated effectively by gas phase H atoms.

The C_2H_4 reaction is modeled differently from the C_2H_2 reaction. The mechanism used

is shown in Figure 5b. In this model, the hydrogenation/desorption channel, k_1, and the CCH_3

synthesis channel, k_2, originate directly from C_2H_4. These two channels originate from C_2H_4

because each one has a different initial elementary reaction step. The addition of a H atom is

required for hydrogenation while abstraction of a H is needed for CCH_3 synthesis. This initial

step is indicated by k_a, with the reaction from $CHCH_2$ to CCH_3 indicated by k_b. The rate

constant for further CCH_3 hydrogenation and desorption is k_3. The rate equations solved for

C_2H_4 are:

$$\frac{d[C_2H_4]}{dt} = -k_1[C_2H_4] - k_2[C_2H_4]$$

$$\frac{d[CCH_3]}{dt} = k_2[C_2H_4] - k_3[CCH_3],$$

where the total carbon coverage measured by Auger spectroscopy is fit to the calculated sum

of the coverages of the two surface bound hydrocarbons in the model,

$$SurfaceCarbon = [C_2H_4] + [CCH_3].$$

Figure 5a shows the calculated coverages of each surface species versus H atom

exposure time, including the sum of the two calculated coverages. The calculated coverages

agree well with the experimentally measured carbon coverage values. The k values fit to the

Auger data are listed in Table 2. The rate constant for CCH_3 synthesis, k_2, is 0.031 s^{-1}, which

is very similar to the value of the rate constant for $CHCH_2$ formation from C_2H_2, 0.034 s^{-1}.

Since CCH_3 synthesis is limited by the rate of $CHCH_2$ formation, the rate limiting elementary

step is the first H abstraction from C_2H_4 (k_a). Vinyl, $CHCH_2$, formation is the rate limiting step

because the intermediate in CCH_3 synthesis cannot be identified, as discussed in Chapter 6.

The agreement between the rates of CCH_3 formation from both C_2H_2 and C_2H_4 suggests that H

addition to C_2H_2 and H abstraction from C_2H_4 occur at a similar frequency.

However, the decrease in the C_2H_4 surface coverage in Figure 5a shows that the

depletion of C_2H_4 from the surface progresses faster than the C_2H_2 depletion from the surface

shown in Figure 4a. The rate constants for formation of gas phase products from the model

have values of 0.034 s^{-1} for C_2H_2 and 0.046 s^{-1} for C_2H_4. As observed in Figures 4a and 5a, the

C_2H_4 coverage reaches zero at 50 seconds, compared to the C_2H_2 coverage which reaches zero

at 100 seconds. This difference in the initial decrease of the reactant hydrocarbon is the same

type of measurement made when the average count rate of the gas phase products are

measured in the first 30 seconds of the reaction. Table 1 shows that the count rate of gas

phase products produced in the C_2H_4 reaction is double that in the C_2H_2 reaction. The Auger

data does not agree well with the gas phase product data. For the reaction of C_2H_2 with gas

phase H atoms, there is 0.12 ML carbon left on the surface after 30 seconds, and for the

reaction of C_2H_4 with gas phase H atoms there is 0.13 ML carbon left on the surface. Since

both hydrocarbons have an initial coverage of 0.25 ML this means that the desorption between

the two is basically the same. There is a large discrepancy between the desorption after a 30

second exposure to gas phase H atoms from the carbon coverage data, which are basically

constant for the two hydrocarbons, and the gas phase average count rate data from the

desorption of gas phase products in the first 30 seconds of the reaction, which are different by

a factor of two between C_2H_2 and C_2H_4. The apparent disagreement in the relative magnitude

of C_2H_2 hydrogenation between the carbon coverage data and the direct measure of gas phase

products could occur for a number of reasons. As explained earlier, this apparatus is not

designed to observe direct desorption of gas phase products. Differences in pumping speed

and adsorption on the walls between molecules may affect product detection. The final rate

constant, k_3, measures the hydrogenation of CCH_3 and the subsequent desorption of C_2H_4 and

C_2H_6. This value is again very small.

The reaction mechanism of C_2H_6 is shown in Figure 6b. It is the same mechanism used

for C_2H_4, although there are more steps involved in the conversion of C_2H_6 to CCH_3. To

synthesize CCH_3, the gas phase H atoms must abstract at least two H atoms from C_2H_6. One

gas phase H abstraction will form an ethyl species, C_2H_5, which will thermally decompose to

C_2H_4. A second gas phase H is then needed to break another C-H bond to form vinyl, $CHCH_2$,

which further react to CCH_3. The rate constant for this combined reaction to form CCH_3 is k_2.

The rate constant for C_2H_6 desorption is k_1 and the rate constant for further CCH_3

hydrogenation and desorption is k_3. The rate equations solved for C_2H_6 are:

$$\frac{d[C_2H_6]}{dt} = -k_1[C_2H_6] - k_2[C_2H_6]$$

$$\frac{d[CCH_3]}{dt} = k_2[C_2H_6] - k_3[CCH_3],$$

where the total carbon measured by Auger spectroscopy is fit to the CCH$_3$ coverage calculated

from the model,

$$SurfaceCarbon = \left[CCH_3\right].$$

The surface C$_2$H$_6$ coverage measured from the integrated C$_2$H$_6$ desorption signal after the gas

phase H atom exposure is fit to the C$_2$H$_6$ coverage calculated from the model as

$$EthaneDesorption = \left[C_2H_6\right].$$

Figure 6a shows the calculated coverages of each surface species versus H atom

exposure time, including the calculated C$_2$H$_6$ coverage which agrees well with the

experimentally measured C$_2$H$_6$ coverage using thermal desorption, and the calculated CCH$_3$

coverages that agrees less well with the experimentally measured carbon coverage values. The

k values fit to the Auger data are listed in Table 2. The rate constant k_2 of the combined CCH$_3$

formation step is five times lower than the similar rate constant for CCH$_3$ formation from

C$_2$H$_4$. This indicates that the first C-H bond cleavage of C$_2$H$_6$ is much slower than the second

C-H bond cleavage of C$_2$H$_4$ in this reaction, and is the rate limiting step. This result is not

surprising. Ethane is physisorbed, not chemisorbed to the surface. In a chemisorbed molecule,

internal bonds are weakened in order to create bonds to the surface, which may lead to a lower

activation energy, and higher rate, for internal bond cleavage. An alternate explanation of the

trend in the H abstraction rates is that the reaction occurs with a gas phase H atom after it

adsorbs on the surface. The physisorbed C$_2$H$_6$ molecules have weak bonds to the surface, and

are likely farther from the surface than the chemisorbed C$_2$H$_4$ molecules. The energetically

'hot' surface bound H atoms may interact at a higher frequency with the surface bound C$_2$H$_4$

molecules than with the weakly bound C_2H_6 molecules. The effect of ethane being physisorbed

also changes its desorption behavior. The rate constant for the desorption of C_2H_6 upon

exposure to gas phase H atoms, k_1, is ten times lower than the analogous rate constant for

C_2H_4, although the binding energy of C_2H_6 is lower than that of C_2H_4. From the difference in

binding energy it is strange that the C_2H_6 desorbs from the surface so slowly. It is possible that

gas phase H atoms can adsorb on the surface *under* the weakly bound C_2H_6, in contrast to their

reaction with C_2H_4, where H atoms must physically displace molecules to form surface bonds.

The value of the CCH_3 hydrogenation and desorption channel rate constant, k_3, is again very

small and similar to the C_2H_4 value.

The value of the rate constant for the CCH_3 hydrogenation and desorption channel, k_3

for ethylene and ethane, and k_4 for acetylene, is expected to be the same for all three reactions,

since the hydrogenation and desorption of CCH_3 should not depend on the molecule used to

form CCH_3. The values assigned from each fit are very small, with the ethylene and ethane

values almost overlapping. The value of this rate constant from the C_2H_2 reaction does not

overlap the other two values. However, since this rate constant value is derived from fitting

the long H atom exposure times where CCH_3 hydrogenation occurs, the variation in the C_2H_2

rate constant value can be viewed as arising from the variation in the small number of

measurements of the carbon coverage at long H exposure times. A larger number of carbon

coverage points at long H exposure times would improve the agreement between the C_2H_2 rate

constant and the C_2H_4 and C_2H_6 rate constant values for this process.

The C_2H_6 fit is unique because the remaining C_2H_6 surface coverage and the CCH_3

coverage are measured independently. In this reaction, the calculated profile for the C_2H_6

coverage versus time matches the measured one well but the calculated coverage for CCH_3

does not match the measured coverage extremely well, as seen in Figure 6a. The measured

CCH_3 coverage rises much more quickly at short times than the fit does. The cause of this

discrepancy is most likely due to the intermediate in the reaction, C_2H_4, which is on the surface

at these short times. The rate constant for C_2H_4 conversion to CCH_3, k_2, is much larger than

the rate constant for the formation of CCH_3 from C_2H_6, k_2. Because the initial C-H bond

breaking in C_2H_6 to form C_2H_4 is the rate limiting reaction in CCH_3 formation, the coverage of

C_2H_4 should never be large. However, similar to the vinyl intermediate in the C_2H_2 reaction, a

small coverage of the C_2H_4 intermediate will build up at small H atom exposure times. This

carbon will contribute to the surface carbon coverage at these small H atom exposure times.

4 Conclusions

The form of each kinetic model has been chosen to represent the mechanism believed

to occur in each reaction. The agreement between the model and the data suggests that each

mechanism is a reasonable physical picture of each reaction. The kinetic models for the

reactions of C_2H_2, C_2H_4, and C_2H_6 with gas phase H atoms provide several insights into the

formation of CCH_3 and H atom processes in general.

The rate of H addition to adsorbed C_2H_2 and of H abstraction from adsorbed C_2H_4 and

physisorbed C_2H_6 are measured. Very similar rates for H addition to adsorbed C_2H_2 and for H

abstraction from adsorbed C_2H_4 are observed. Hydrogen atom addition and H abstraction rate

have been measured for the analogous gas phase reactions. A collection of the rate constants

for such reactions are shown in Table 3. Rate constants are given for a range of temperatures,

because the rate constants of different reactions are measured in different temperature ranges.

Rate constant values in italics have been extrapolated past the temperature range in which they

were measured. In general, abstraction reactions do not occur at lower temperature.

	Measured Rates Constants $(cm^3$ molecules$^{-1}s^{-1})$			
Gas Phase Chemical Reaction	300 K	700 K	1700 K	*Ref*
$H + C_2H_2 \rightarrow C_2H + H_2$	*5.4x10^{-31}*	*2.1x10^{-19}*	2.7x10^{-14}	4
$H + C_2H_2 + M \rightarrow CHCH_2 + M$	1.8x10^{-13}	*2.2x10^{-12}*	*6.5x10^{-12}*	4
$H + C_2H_4 \rightarrow CHCH_2 + H_2$	*1.2x10^{-20}*	2.0x10^{-14}	1.1x10^{-11}	4
$H + C_2H_4 + M \rightarrow CH_2CH_3 + M$	1.3x10^{-12}	1.3x10^{-11}	*7.4x10^{-11}*	5
$H + C_2H_6 \rightarrow CH_2CH_3 + H_2$	4.93x10^{-17}	2.1x10^{-13}	1.8x10^{-11}	4

Table 3 Gas phase kinetic rate constants for H plus hydrocarbon reactions.
Rate constants given for three temperatures. Values in *italics* have been
extrapolated from the range in which measurements were made. M represents a
noble gas, rate constants for reactions written with M are given for k_∞ which is
independent of [M].

On the other hand, addition reactions are predominantly measured at low temperature. In

general, abstraction reactions have smaller rate constants than the addition reactions. The only

place where this is not the case is at 1700 K. There is a trend that the larger the number of C-

H bonds, the larger the rate constant for abstraction. For H addition reactions, rate constants

also increase with an increase in the number of C-H bonds in the hydrocarbon. For example, C_2H_4 has a larger rate constant for H addition than C_2H_2.

How do these surface rate constants compare with rate constants for the analogous reactions of the gas phase species? While hydrogen addition to adsorbed C_2H_2 and H abstraction from adsorbed C_2H_4 yield similar rate constants, the gas phase rate constants are larger for H addition compared to H abstraction except at 1700 K where the value for the H addition rate constant has been extrapolated well out of the temperature range for which the reaction was studied. The difference between the H addition and H abstraction rate constants is rooted in the difference in activation energy and entropy change values for the two reactions. In considering the activation energy values, H abstraction tends to have a higher barrier because breaking the C-H bond is less exothermic than formation of a C-H bond. Table 4 lists the ΔH values for the relevant gas phase reactions which shows that the abstraction reactions tend to be endothermic, while the addition reactions are clearly exothermic. The reaction enthalpy is not the same as the activation energy, but if there is a high positive reaction enthalpy then there must also be a large activation energy. When C_2H_2 and C_2H_4 are adsorbed on the surface, not only are the internal bonds weakened, but the surface can stabilize products. In contrast to the gas phase reactions, calculations of the enthalpy for reactions of gas phase H atoms with adsorbed hydrocarbons on a Ni surface are all exothermic as shown in Table 4. The enthalpy change for gas phase H addition to gas phase C_2H_2 is -37.2 kcal/mol as compared to gas phase H addition to adsorbed C_2H_2, which is -74 kcal/mol. The enthalpy change for H abstraction from gas phase C_2H_4 is 4.5 kcal/mol and from adsorbed C_2H_4 is -36 kcal/mol. The change in

Chemical Reaction-Gas Phase[6]	Calculated ΔH values (kcal/mol)		
$H(g) + C_2H_2(g) \rightarrow C_2H(g) + H_2(g)$	15.8		
$H(g) + C_2H_2(g) \rightarrow CHCH_2(g)$	-37.2		
$H(g) + C_2H_4(g) \rightarrow CHCH_2(g) + H_2(g)$	4.5		
$H(g) + C_2H_4(g) \rightarrow CH_2CH_3(g)$	-38		
$H(g) + C_2H_6(g) \rightarrow CH_2CH_3(g) + H_2(g)$	-5.3		
Chemical Reaction-Surface	$Ni(111)^{7}$	$Pt(111)^{7}$	$Pt(111)^{8}$
$H(g) + C_2H_2(ad) \rightarrow C_2H(ad) + H_2(g)$	-50.2	-39	-24
$H(g) + C_2H_2(ad) \rightarrow CHCH_2(ad)$	-74.2	-67	-66
$H(g) + C_2H_4(ad) \rightarrow CHCH_2(ad) + H_2(g)$	-35.5	-27.5	-45
$H(g) + C_2H_4(ad) \rightarrow CH_2CH_3(ad)$	-72	-65	-73
$H(g) + C_2H_6(ad) \rightarrow CH_2CH_3(ad) + H_2(g)$	-49.3	-39.3	—

Table 4 Enthalpy changes for gas phase and surface H abstraction and addition reactions. Surface calculations shown for three different calculations to give an impression of error.

the reaction enthalpy of $CHCH_2$ formation from C_2H_4 from endothermic to exothermic upon

adsorption of C_2H_4 could partially explain why the kinetic rate constant for the H abstraction

from adsorbed C_2H_4 is close to the value of the rate constant for H addition to adsorbed C_2H_2.

The other comparison to be made between our rate constant values and the gas phase

values is for the abstraction of H from C_2H_4 and C_2H_6. For gas phase reactions, the abstraction

of H from C_2H_6 is always faster than the abstraction of H from C_2H_4. The relationship is the

opposite for H abstraction from chemisorbed C_2H_4 and physisorbed C_2H_6. If the reaction

enthalpy values are used as an indicator of the activation energy values, H abstraction from

both hydrocarbons should have a dramatically lower barrier upon adsorption. In the

comparison of H abstraction from C_2H_4 and C_2H_6, the reaction enthalpy values are not a good

predictor of the activation energy values and the reaction rates.

[1] T. Bürgi, T.R. Trautman, K.L. Haug, A.L. Utz and S.T. Ceyer, J. Phys. Chem. B **102**,4952 (1998)

[2] T.R. Trautman, Ph.D. Thesis, Massachusetts Institute of Technology (1996)

[3] W.H. Press, *Numerical Recipes in Fortran*, Cambridge University Press (1992)

[4] D.L. Baulch, C.J. Cobos, R.A. Cox, C. Esser, P. Frank, Th. Just, J.A. Kerr, M.J. Pilling, J.Troe, R.W. Walker, and J. Warnatz, J. Phys. Chem. Ref. Data **21**, 411 (1992)

[5] W. Tsang and R.F. Hampson, J. Phys. Chem. Ref. Data **15**, 1087 (1986)

[6] S.W. Benson, *Thermochemical Kinetics*, J.Wiley and Sons (1976)

[7] A.T. Bell and E. Shustorovich, Surf. Sci. **235**, 343 (1990)

[8] E.A. Carter and B.E. Koel, Surf. Sci. **226**, 339 (1990)

Chapter 6

Further Arguments for a Vinyl Intermediate

1 Introduction

In the reactions of surface H, bulk H, and gas phase H atoms with C_2H_2, C_2H_4, and C_2H_6 to produce CCH_3, mechanisms with vinyl as a common intermediate have been proposed. This study of the reactions of the three different H atom species with hydrocarbons provide a wealth of results to test our mechanistic hypothesis. Certain intermediates are excluded in some mechanisms because their formation by H addition or H abstraction steps are endothermic. The proposed pathway through vinyl to ethylidyne is consistent with the products detected from all hydrocarbon and H atom reactions, whether these products are CCH_3 or not.

What is the value of knowing the reaction mechanism? Mechanistic information coupled with rate or barrier information can have significant meaning. If a molecule is observed to proceed through a particular reaction intermediate, this pathway may be universal, and any knowledge gained from this one step can be applied to understanding a similar step in another reaction. Evidence of a particular intermediate for an elementary reaction step along

with its measured rate or activation energy barrier is particularly valuable. Because there are

few reaction barriers and rates known for elementary surface reactions, it is difficult to predict

the path of surface reactions. If these quantities were known for a large number of elementary

reaction pathways, rates could be accurately predicted for multiple paths of multi-step

reactions. Comparing rates for competing mechanisms would provide the ability to predict a

specific mechanism and product for a reaction.

Chapters 5 and 3 describe the measurements of several rates for the reaction of gas

phase H with C_2H_2, C_2H_4, and C_2H_6 and the measurement of an activation barrier for the

reaction of surface bound H and C_2H_2, respectively. All reactions produce CCH_3. Proof of a

vinyl intermediate, $CHCH_2$, in CCH_3 reactions provides indisputable support that a particular

elementary reaction step is part of the larger reaction mechanism. What follows here are two

experimental pieces of evidence that further support the existence of a vinyl intermediate in

CCH_3 synthesis. Then the energy arguments that support the pattern of CCH_3 formation from

the different hydrocarbons and H atom species are presented. With this additional

experimental evidence and energy arguments, a compelling argument for why vinyl ($CHCH_2$)

and ethylidene ($CHCH_3$) are the two intermediates in CCH_3 synthesis is presented. Ethylidyne

mechanistic arguments have been made by others, particularly for the reaction of C_2H_2 and

C_2H_4 to make CCH_3 on Pt surfaces. A review of these mechanistic ideas on Pt is presented.

The observations on Pt are consistent with the mechanism presented for CCH_3 formation on

Ni.

2 Experimental Evidence for the Vinyl Intermediate

There are two preliminary experiments that provide evidence for a vinyl intermediate

on Ni(111). The first is an attempt to trap CHCH$_2$ at low temperature, by exposing 0.25 ML

of C$_2$H$_2$ to an extremely low flux of H atoms at 22 K. A crystal temperature of 22 K is

achieved by cooling the crystal cryostat with liquid helium, as described in Chapter 2, and

minimizing the radiative heating from the front filament. Experimentally, the extremely low H

atom flux is created by placing the H atom filament 3 inches from the crystal, compared to the

usual 0.25 inches. The larger distance of the filament from the crystal generates a H atom flux

approximately 100 times lower than the usual flux and minimizes radiative crystal heating. The

results of this exposure for both C$_2$H$_2$ and C$_2$D$_2$ are shown in Figure 1. Spectra are shown

both on-specular and off-specular to illuminate the dipole activity of the feature labeled in bold.

After the reaction of both isotopomers of acetylene with gas phase H or D, loss features

corresponding to both acetylene and ethylidyne are present. For the reaction of C$_2$H$_2$ with gas

phase H atoms, the signature features for C$_2$H$_2$ in Figure 1a are 460 cm^{-1}, 660 cm^{-1}, 860 cm^{-1},

and 1200 cm^{-1}, which correspond to the antisymmetric C-Ni stretch, the symmetric and

antisymmetric C-H bending, and the C-C stretch modes, respectively.[1] Features assigned to

CCH$_3$ are observed at 457 cm^{-1}, 1127 cm^{-1}, 1336 cm^{-1}, and 1450 cm^{-1}, which correspond to the

C-Ni stretch, the C-C stretch, and the symmetric and antisymmetric CH$_3$ deformation modes,

respectively.[2] All features can be accounted for by these two species. However, the 1450 cm^{-1}

feature is almost as intense as the 1336 cm^{-1} feature in the on-specular spectrum, while its

intensity is less than that of the 1336 cm^{-1} feature in the off-specular direction. A decrease in
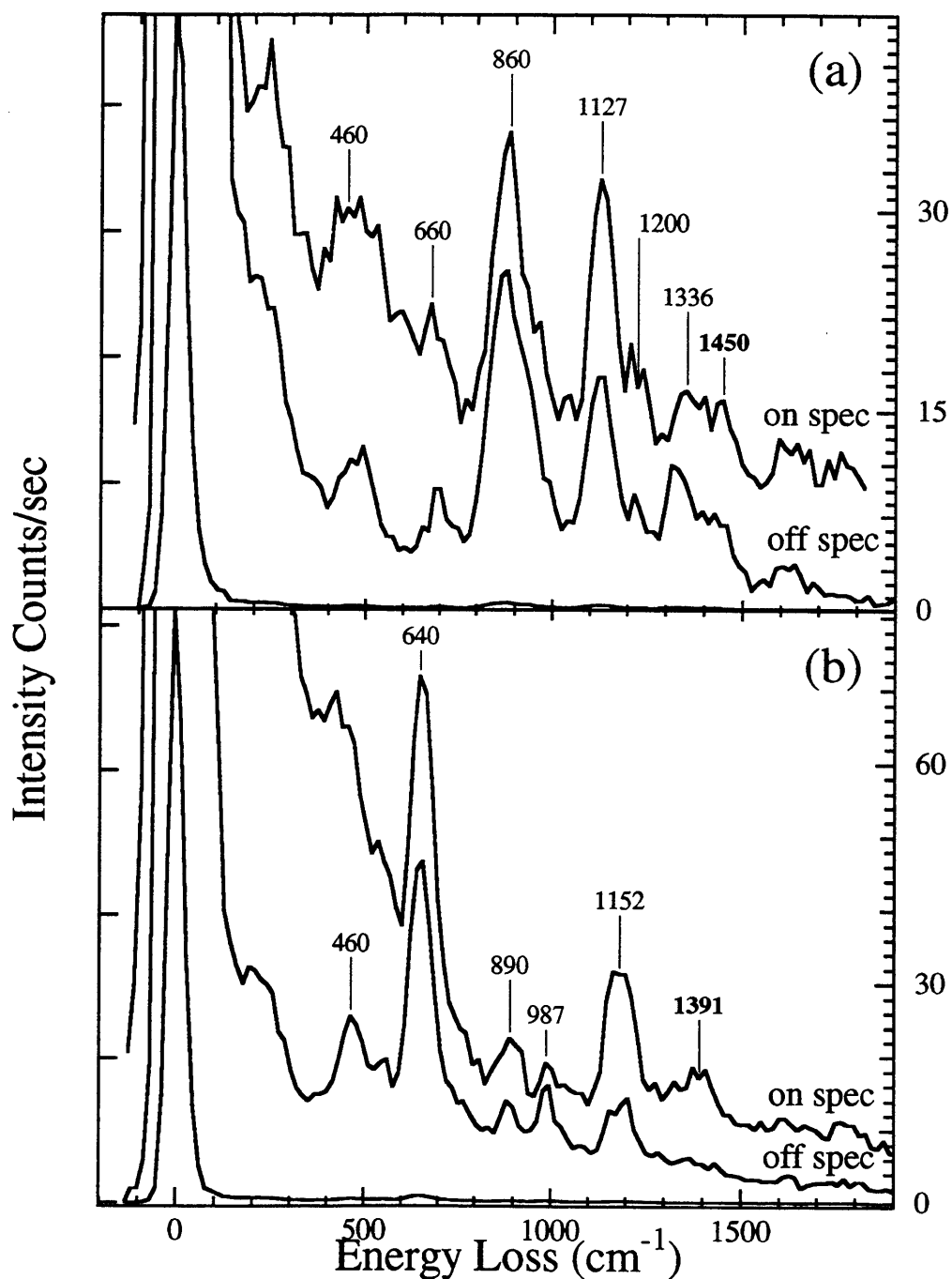
Figure 1 HREEL spectra showing C_2H_2 (a) and C_2D_2 (b) after addition of a low flux of gas phase H(D). Spectra of both species shown on specular and 10° off specular with an electron energy of 6.5 eV. Spectra of C_2H_2 (a) warmed to 22 K during H atom exposure, ΔE_{fwhm} of 52 cm^{-1} and 49 cm^{-1} for on and off specular scans. Spectra of C_2D_2 (b) warmed to 24 K during D atom exposure, ΔE_{fwhm} of 43 cm^{-1} and 48 cm^{-1} for on and off specular scans.

intensity as the scattering angle is moved away from the specular angle indicates a dipole active

feature. The symmetric and antisymmetric CH_3 deformation modes of CCH_3 assigned to 1336

cm^{-1} and 1450 cm^{-1} are not dipole active modes and do not exhibit any intensity variation with

scattering angle.[2] Vibrational modes that exhibit dipole active behavior must be totally

symmetric and have a dynamic dipole perpendicular to the crystal face. The dipole activity and

increased intensity of the 1450 cm^{-1} mode suggests it is from a new species. The spectra in

Figure 1b from the reaction of C_2D_2 with D atoms show a very similar loss feature. While the

features at 460 cm^{-1}, 640 cm^{-1}, and 890 cm^{-1} can be assigned to the symmetric C-Ni stretch,

antisymmetric C-D out-of-plane bending, and symmetric C-D in-plane bending modes of

C_2D_2,[1] respectively, and the features at 987 cm^{-1} and 1152 cm^{-1} can be assigned to the

symmetric CD_3 deformation and the C-C stretch modes of CCD_3,[2] respectively, the feature at

1391 cm^{-1} is unique. This suggests that the dipole active feature at 1391 cm^{-1} is from a new

species. The small frequency shift from 1450 cm^{-1} for the hydrogenated species to 1391 cm^{-1}

for the deuterated species suggests that this mode is primarily a carbon motion.

This dipole active 1450(1391) cm^{-1} feature could be assigned to be a number of

possible species. Possible intermediates include acetylide (CCH), vinylidene (CCH_2), vinyl

($CHCH_2$), or ethylidene ($CHCH_3$). The C-C stretch vibrational mode in CCH on Ni(110) has

been assigned to the frequency of 1290 cm^{-1},[3] which is significantly lower than the frequency of

the newly observed feature. While CCH_2 has not been observed on a nickel surface,

assignments of CCH_2 on Pt(111)[4] and in Os and Ru inorganic clusters[5] have been made. The

C-C stretching mode is observed at a frequency of 1306 cm^{-1} on Pt(111), 1331 cm^{-1} in the Os

cluster, and 1582 cm^{-1} in the Ru cluster. None of these values agree with the frequency of the new feature.

Is this new feature consistent with a $CHCH_3$ intermediate? The best comparison is with IR data from $(CHCH_3)Os_2(CO)_2$ in which there are no features above 1123 cm^{-1} for the deuterated species.[6] This eliminates the assignment of this new feature at 1450(1391) cm^{-1} to $CHCH_3$.

Another possible identification of this intermediate species is vinyl, $CHCH_2$. The feature assigned to the C-C stretching mode of $CHCH_2$ on Pt(111) from decomposition of 1,1,2-trichloroethane[7] is observed at 1450(1440) cm^{-1}, which is consistent with this new feature observed at 1450(1391) cm^{-1}. Further assignment of the lower frequency features in our spectra to vinyl is impossible due to congestion from the number of modes in the lower frequency range due to the mixture of CCH_3 and C_2H_2. The frequency of the new feature observed during the formation of CCH_3 at 22 K is consistent with the frequency of the C-C stretch mode of a $CHCH_2$ intermediate on Pt(111). The existence of a vinyl intermediate in CCH_3 synthesis will be further argued below, where a reaction pathway that includes $CHCH_2$ as the first intermediate and $CHCH_3$ as the second intermediate to CCH_3 formation is shown to be the most consistent with all of the experimental observations.

This observation of the $CHCH_2$ intermediate demonstrates a difference between the Ni and the Pt surfaces. Cremer has identified an intermediate observed during CCH_3 formation on Pt(111) as $CHCH_3$, based on the observation and assignment of a single feature in the C-H stretch region.[8] If the assignment of the intermediate in CCH_3 formation on Pt by Cremer and
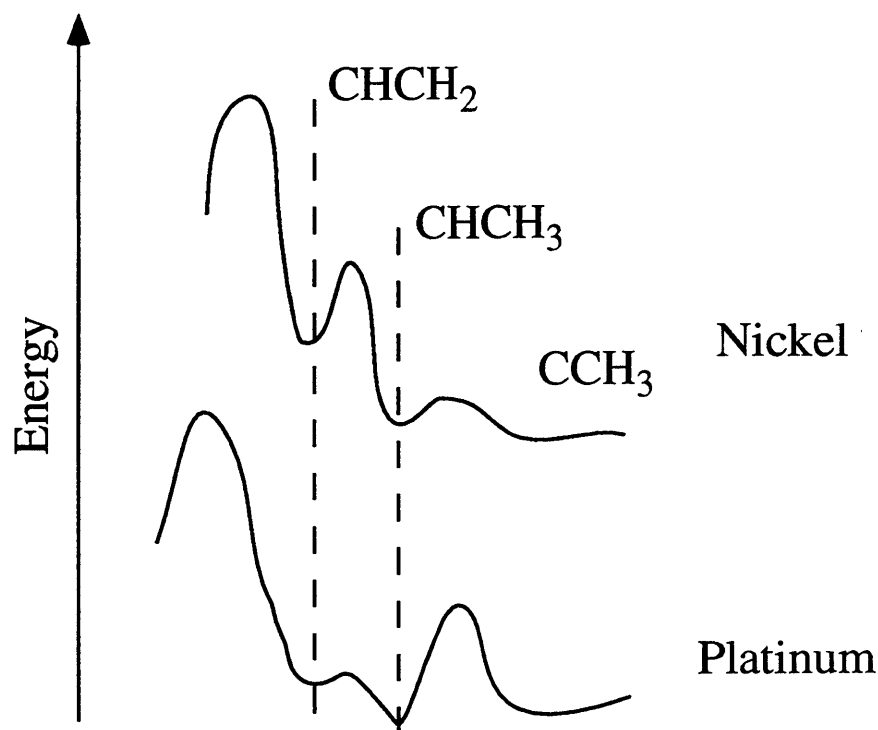
Figure 2 Schematic of possible potential energy surfaces for CCH_3 formation through a $CHCH_2$ and $CHCH_3$ intermediates on Ni and Pt.

the present intermediate assignment on Ni are correct, the reaction could follow the same pathway on the two metals, $CHCH_2 \rightarrow CHCH_3 \rightarrow CCH_3$. However, the activation energy barriers would necessarily be different on the two metals, as shown in Figure 2. On both metal surfaces, there is no buildup of an intermediate during the reaction, which means that the first step in the reaction to form vinyl is the rate limiting step. However, the relative heights of subsequent activation barriers from $CHCH_2 \rightarrow CHCH_3$ and from $CHCH_3 \rightarrow CCH_3$ determines which intermediate is observed when it can be trapped. It appears that on Ni, the barrier to $CHCH_3$ formation is higher than the barrier to CCH_3 formation, making it possible to trap $CHCH_2$, while on Pt the barrier to CCH_3 formation is higher than the barrier to $CHCH_3$ formation, making it possible to trap $CHCH_3$.

A second experiment provides additional evidence for a $CHCH_2$ intermediate. One reaction where $CHCH_2$ is expected to be an intermediate is in the thermal decomposition of C_2H_4 to C_2H_2, in which C-H bonds are sequentially broken. For a Ni(111) surface saturated with C_2H_4, previous work has demonstrated that complete conversion of C_2H_4 to C_2H_2 occurs only after heating the crystal at 2 K/s to 260 K.[9] In this present experiment, a saturated surface of 0.25 ML C_2D_4 is slowly warmed over 18 min from 80 to 210 K and then held at 210 to 220 K for 10 minutes. During this warming, the surface is continually exposed to D_2 from an elevated background pressure of 2×10^{-7} Torr D_2. The vibrational spectrum of this surface is shown in Figure 3. The spectrum is that of C_2D_2 with a small feature growing in at 987 cm^{-1}. Several additional C_2D_2 features are visible in this spectrum as compared to the C_2D_2 features observed in Figure 1. These additional features include the symmetric C-H out-of-plane bend and the antisymmetric C-H in-plane bend of C_2D_2 at 540 cm^{-1} and 1080 cm^{-1}, respectively. The feature at 250 cm^{-1} is assigned to the longitudinal S_2 phonon mode which is enhanced upon the presence of adsorbates on the Ni(111) surface.[10] The two features at 700 cm^{-1} and 850 cm^{-1} are assigned to the antisymmetric and symmetric modes of surface bound D, respectively.[2]

The new feature occurs at 987 cm^{-1}, the frequency of the symmetric CD_3 deformation in CCD_3. The assignment of this mode to CCD_3 is consistent with the picture of a vinyl species as an intermediate in this reaction. As the C_2D_4 molecules slowly decompose, short lived $CDCD_2$ species are formed. In the presence of surface bound D, a small number of these $CDCD_2$ molecules add a surface bound D atom to form $CDCD_3$, which then decomposes to CCD_3.
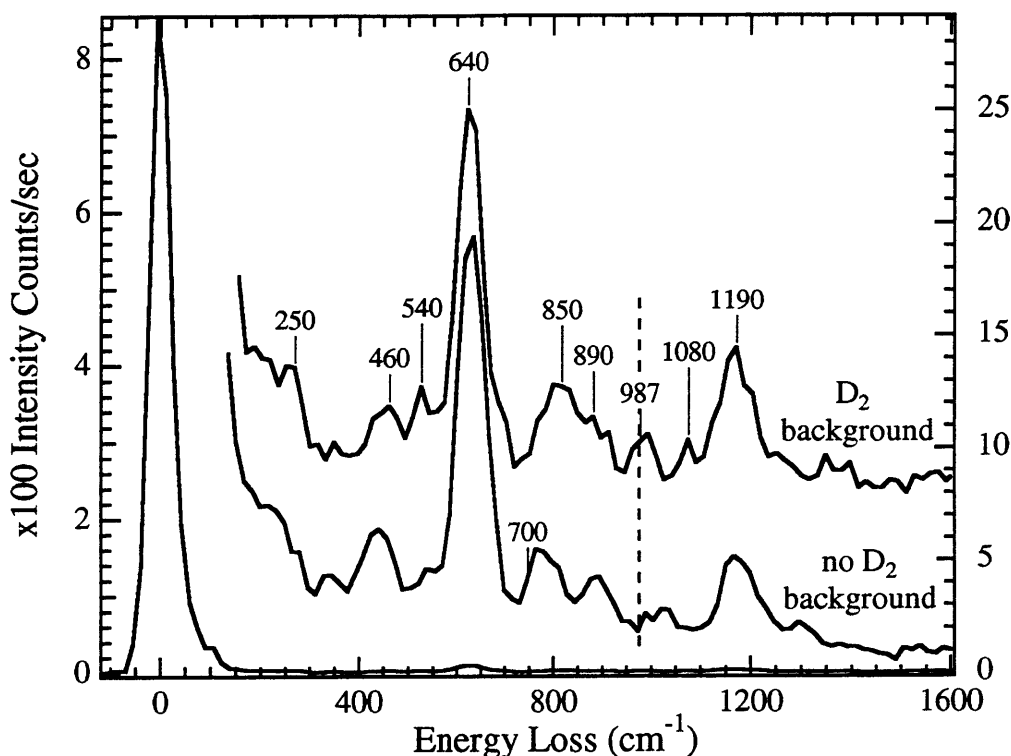
Figure 3 HREEL spectra showing 0.25 ML C_2D_4 after slowly warming and annealing at 210-220 K with or without a constant D_2 background. Both spectra are of predominantly C_2D_2. Spectrum with D_2 background was warmed from 80 to 210 K over 18 minutes and then held between 210 and 220 K for 10 minutes at a D_2 pressure of 2×10^{-7} Torr. Spectrum taken 6° off specular with an electron energy of 6.5 eV at a ΔE_{fwhm} of 48 cm^{-1}. Spectrum with no background was exposed to D_2 before warming to provide surface D. The surface was then slowly warmed and held at 200 K for 60 minutes. Spectrum taken 6° off specular with an electron energy of 6.5 eV at a ΔE_{fwhm} of 48 cm^{-1}.

The constant D_2 flux is a necessary component for the formation of a small amount of

CCD_3 during the decomposition of C_2D_4. Figure 3 also shows a spectrum of C_2D_4 coadsorbed

with D that is slowly warmed and held at 200 K for 60 minutes. This spectrum shows no new

feature at 987 cm^{-1}. The transient $CDCD_2$ is not converted to CCD_3 without a constant flux of

D_2. As a further control experiment, C_2D_2, the decomposition product of C_2D_4, is exposed to a

constant flux of 2×10^{-5} Torr D_2 at 220 K for a total of 30 minutes, in repeated 10 minute D_2

exposures followed by 30 minute anneals at 220 K. The spectrum of C_2D_2 after exposure to

D_2 in Figure 4 shows no intensity from the CD_3 symmetric deformation mode of CCD_3 at 987

cm^{-1}. Therefore the C_2D_2 product is not responsible for the appearance of CCD_3.

The coverage of the CCD_3 product in Figure 3 can be measured from the intensity of

the CCD_3 feature at 987 cm^{-1}, the most intense feature in the CCD_3 spectrum, as explained in

Chapter 4. From this measurement, 7% of the carbon on the surface is CCD_3. Attempts to

increase the coverage of CCD_3 were made by increasing the background D_2 pressure during

the C_2D_4 decomposition. However, as the background D_2 pressure is increased, for exposures

of the same total time, the Auger electron spectroscopy measurement of the carbon coverage

on the surface decreases. The D_2 molecules apparently displace C_2D_4 molecules from the

surface, and the higher the D_2 pressure the more C_2D_4 molecules are displacement. At higher

D_2 pressures, which should yield higher CCD_3 coverages, the remaining surface carbon

coverage is too small to obtain a high quality EEL spectrum.

The observation that the $CDCD_2$ intermediate will form CCD_3 under the proper

conditions at 220 K confirms that the measurement of the activation energy in the reaction of

C_2D_2 and surface bound D at 250-280 K, described in Chapter 3, is indeed a measurement of

the barrier for the C-D bond formation of surface bound D and C_2D_2. The C-D bond

formation step to synthesize $CDCD_2$ from C_2D_2 does not occur at 220 K, as shown by the non-

reactivity of C_2D_2 to D_2 in Figure 4. However, the subsequent reaction steps to make CCD_3

from $CDCD_2$ do occur, as shown in Figure 3, which proves that the initial C-D bond formation

step is the highest energy step in the reaction of D and C_2D_2 to form CCD_3.
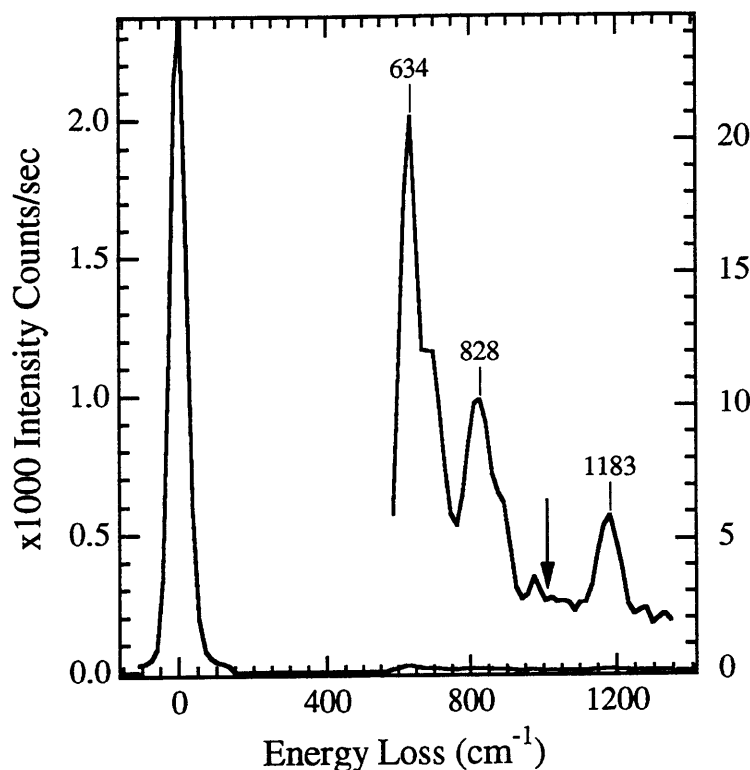
Figure 4 HREEL spectra showing 0.17 ML C_2D_2 (formed from decomposition of C_2D_4) after exposure to 2×10^{-5} Torr D_2 for 10 min at 220 K and an anneal at 220 K for 30 minutes, repeated three times. Spectrum taken at 80 K, taken 10° off specular with an electron energy of 6.5 eV at a ΔE_{fwhm} of 49 cm^{-1}.

3 Energetic Arguments for Vinyl

Some of the differences in the reactivities of the H atom species with hydrocarbons can be understood in terms of the energetics of producing the vinyl intermediate. Two methods can be used to calculate the reaction enthalpy, ΔH, which qualitatively agree. The first is an approximation of the reaction enthalpy calculated for H addition and H abstraction reactions by considering the strength of the C-H bond formed or broken, and the possible formation of H_2. This approach does not include any bond energy changes in the other bonds of the adsorbed hydrocarbon as the vinyl intermediate is formed. The first question in calculating the enthalpy

Molecule	Gas Phase Molecules		Adsorbed Molecules	
	hybrid-ization	bond strength[11]	hybrid-ization	bond strength
C_2H_2	sp	132	$sp^{2.5-3}$	106
C_2H_4	sp^2	106	sp^3	100
C_2H_6	sp^3	100		

Table 1 Gas phase hybridization and bond strength, in kcal/mol, as well as estimates for hybridization of adsorbed hydrocarbons along with bond strengths used for enthalpy calculations.

change is deciding what C-H bond energy to use, since these values are not known for adsorbed hydrocarbons. Both C_2H_2 and C_2H_4 molecules rehybridize upon adsorption on the Ni surface. The values for hybridization upon adsorption based on C-H stretch frequencies from HREELS studies are $sp^{2.5}$-sp^3 for C_2H_2[12] and sp^3-like for C_2H_4.[20] Table 1 shows the hybridization and C-H bond energy of gas phase C_2 hydrocarbons. For this calculation the C-H bond energy used for an adsorbed hydrocarbon is the C-H bond energy of the gas phase hydrocarbon with the closest hybridization to the adsorbed species. For adsorbed C_2H_2, sp^2 hybridization is used, since the discussion in Chapter 3 suggests that C_2H_2 is not fully σ bonded to the surface. Therefore, a bond energy of 106 kcal/mol is used for the C-H bond in C_2H_2 and a bond energy of 100 kcal/mol is used for the C-H bond in C_2H_4. The bond energy of a H-H bond is 104 kcal/mol.[11]

Using this approximate calculation the reaction of gas phase H atoms with adsorbed C_2H_2 to form $CHCH_2$ is exothermic by 106 kcal/mol. The H abstraction from C_2H_4 to form $CHCH_2$ and H_2 by a gas phase H atom is exothermic by 4 kcal/mol. Gas phase H atoms are

the most energetic H species and are experimentally observed to form CCH_3 from their

reactions with both C_2H_2 and C_2H_4, in agreement with these enthalpy values.

The reaction of bulk H with C_2H_2 and C_2H_4 yields different ΔH values. Bulk H is 48

kcal/mol less energetic than a gas phase H atom. The H addition reaction of $H(b) + C_2H_2 \rightarrow$

$CHCH_2$ is exothermic by 58 kcal/mol. But the H abstraction reaction of $H(b) + C_2H_4 \rightarrow$

$CHCH_2$ is endothermic by 44 kcal/mol. These reaction enthalpy values agree with

experimental observations. Bulk H atoms add to C_2H_2 to produce CCH_3. Experimentally, the

CCH_3 product from synthesis of the $CHCH_2$ intermediate is not observed for the reaction of

bulk H and C_2H_4. Bulk H atoms cannot abstract a H atom from a C-H bond. These reaction

enthalpies are based on our proposed mechanisms, and agree with the observed reactivity.

This calculation is a very approximate one. There are undoubtedly enthalpy changes in

the adsorbed species which cannot be easily predicted. These enthalpy changes arise from

changes in the strength of the C-C and C-Ni bonds, which are not taken into account in the

approximate calculation. For example, in the addition of H to C_2H_2, the vinyl product will

have one C atom with two C-H bonds instead of one. The C-C bond should weaken and most

likely the strength of both C-Ni bonds change as well. The second method for obtaining

enthalpy changes for these reactions is from a single theoretical study of the enthalpy changes

for these adsorbates on Ni(111).[13] This calculation does include the changes in the internal

molecular bonds and the bonds to the surface. For gas phase H addition to C_2H_2, the

calculated enthalpy change is -74.2 kcal/mol, and the enthalpy change for a gas phase H atom

abstracting a H atom from a C-H bond of C_2H_4 is -35.5 kcal/mol. For the reaction of bulk H

Chemical Reaction	ΔH Approximate	calculation[13]
$H(g) + C_2H_2(ad) \rightarrow HCCH_2(ad)$	-106	-74.2
$H(g) + C_2H_4(ad) \rightarrow HCCH_2(ad) + H_2(g)$	-4	-35.5
$H(b) + C_2H_2(ad) \rightarrow HCCH_2(ad)$	-58	-26.2
$H(b) + C_2H_4(ad) \rightarrow HCCH_2(ad) + H_2(g)$	44	12.5

**Table 2** Values of the enthalpy change for addition of gas phase H and bulk H atoms for both an approximate model explained in text and a theoretical calculation.

addition to C_2H_2 and for the reaction a bulk H atom abstracting a H atom from a C-H bond of C_2H_2 the enthalpy changes are -26.2 kcal/mol and 12.5 kcal/mol, respectively. These results as well as the results from the above approximate calculation qualitatively agree with each other and are shown in Table 2. The calculated enthalpy changes are less exothermic for the H addition reactions, and more exothermic for the H abstraction reactions, as compared to the approximate calculation. These theoretical results are physically reasonable and the trends between the two calculations can be explained. What are missing from the approximate calculation are the C-C and C-Ni bond energy changes. After a H addition reaction, a carbon atom has an additional C-H bond, which weakens both the C-C and the C-Ni bond for this carbon atom in the product, decreasing the reaction exothermicity. However, after a H abstraction event, a C-H bond is lost, strengthening the remaining C-C and C-Ni bonds in the product and thereby increasing the reaction exothermicity.

4 Discussion of the Mechanism of CCH₃ Formation on Ni

Ethylidyne synthesis is observed from gas phase H atom reactions with adsorbed C_2H_2,

C_2H_4, and physisorbed C_2H_6, as well as by the reactions of surface bound H and bulk H with

adsorbed C_2H_2 on the Ni(111) surface. From careful examination of experiments that lead to

CCH₃ formation as well as the experiments that do not lead to CCH₃ formation, an argument

for vinyl, CHCH₂, as the first intermediate and ethylidene, CHCH₃, as the second intermediate

to CCH₃ is made. It is assumed that all CCH₃ synthetic paths proceed through these two

intermediates. These arguments build on previous work.[14] For the reaction of each H atom

species with a hydrocarbon, there is a three way branching in the possible reaction pathways.

These three elementary reaction steps are addition of a H atom, loss of a H atom, or migration

of a H atom from one carbon to another.

The three reactants in CCH₃ formation are adsorbed C_2H_2, C_2H_4, and physisorbed

C_2H_6. Beginning with the first step in the reaction of an adsorbed C_2H_2 molecule, the three

possible reaction pathways are shown in Figure 5. The three possible intermediates are

acetylide (CCH), vinylidene (CCH₂), or vinyl (CHCH₂). It is possible to eliminate two of the

three reaction pathways. The loss mechanism to form CCH from C_2H_2 is eliminated in the

following way. One way CCH can be formed is by thermal activation of the C-H bond of

C_2H_2. However, C_2H_2 is stable on the surface up to 400 K,[20] a temperature well above any

used in CCH₃ synthesis. A second pathway that forms CCH is the abstraction of a H atom

from C_2H_2, which can be eliminated because neither surface bound H atoms nor bulk H atoms

are able to abstract a H atom from a C-H bond, as explained in the above section. It is possible

Acetylene
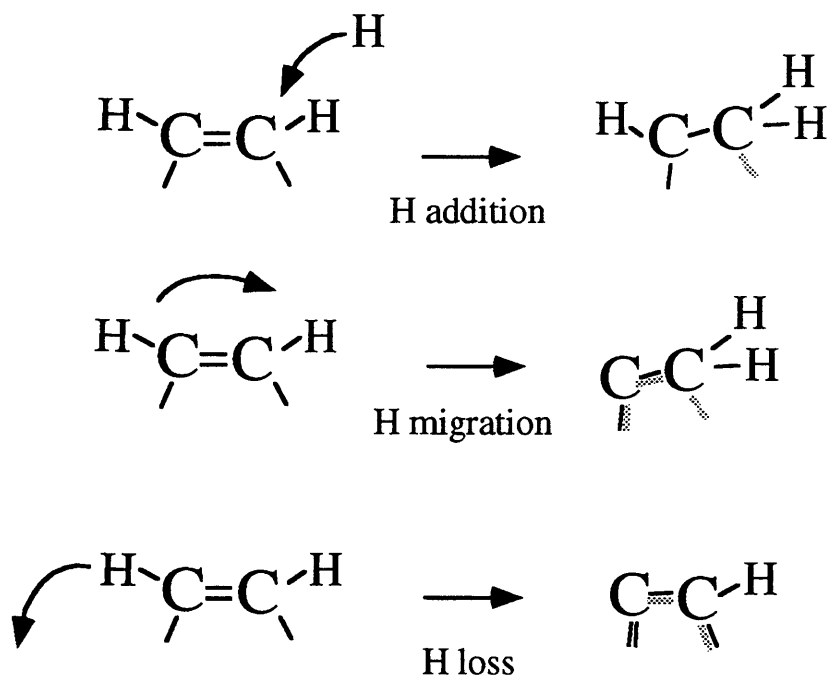
Figure 5 Schematic diagram showing the different possible initial reaction pathways from acetylene.

for a gas phase H atoms to abstract a H atom from C_2H_2 to form CCH. However, the experimental evidence of an intermediate presented in Section 2 is incompatible with a CCH. Since the evidence of an intermediate is observed after exposure of C_2H_2 to gas phase H atoms, it seems unlikely that CCH is the dominant intermediate in gas phase H atom reactions. This conclusion is consistent with measured rates for H abstraction versus H addition for related systems done by other groups. On a diamond film, abstraction is seen to occur 0.05 times as efficiently as H addition.[15] Separate studies on amorphous hydrocarbon films measure a similar ratio of 0.04 for the H abstraction rate over the H addition rate.[16,17] Between these low probabilities for gas phase H abstraction of a H from on an adsorbed hydrocarbon and the

elimination of CCH as the dominant intermediate in the C_2H_2 reaction with gas phase H atoms, it seems unlikely that this gas phase H atom channel is important.

A second path for the C_2H_2 reactant is thermal isomerization to CCH_2 through a H atom migration, followed by addition of a surface bound H atom to CCH_2 to form CCH_3. However, there is no direct evidence for the thermal isomerization of C_2H_2 to form CCH_2. Different experiments provide further evidence that CCH_2 is not the reactive intermediate. If this isomerization of C_2H_2 to CCH_2 is the process responsible for CCH_3 synthesis, then it must occur under all conditions where CCH_3 is formed. There are two experiments done at the same temperature that yield different results. The first experiment shows that adsorbed C_2D_2 will not form CCD_3 under repeated D_2 exposures at 220 K, as shown in Figure 4. However, in another experiment a small amount of CCD_3 is formed when C_2D_4 is warmed to 210 K and held at 210-220 K with a constant D_2 exposure, as shows in Figure 3. The contradiction between these two experiments at the same surface temperature eliminates CCH_2 as an intermediate. The third and final pathway of C_2H_2 is H addition to form $CHCH_2$. Since the two other mechanistic pathways have been eliminated, $CHCH_2$ remains as the only plausible first intermediate in CCH_3 synthesis from the C_2H_2 reactant.

Figure 6a shows the three initial reaction pathways from the second reactant, C_2H_4. It will again be possible to eliminate two of the potential intermediates, ethylidene ($CHCH_3$) and ethyl (CH_2CH_3), in CCH_3 synthesis leaving the H abstraction product, vinyl ($CHCH_2$), as the sole intermediate. The first possible pathway is thermal migration of a H atom from one carbon atom to the other to form $CHCH_3$. However, if C_2H_4 thermally rearranged to $CHCH_3$

(a) Ethylene

H addition

H migration

H loss

(b) Ethane

H loss
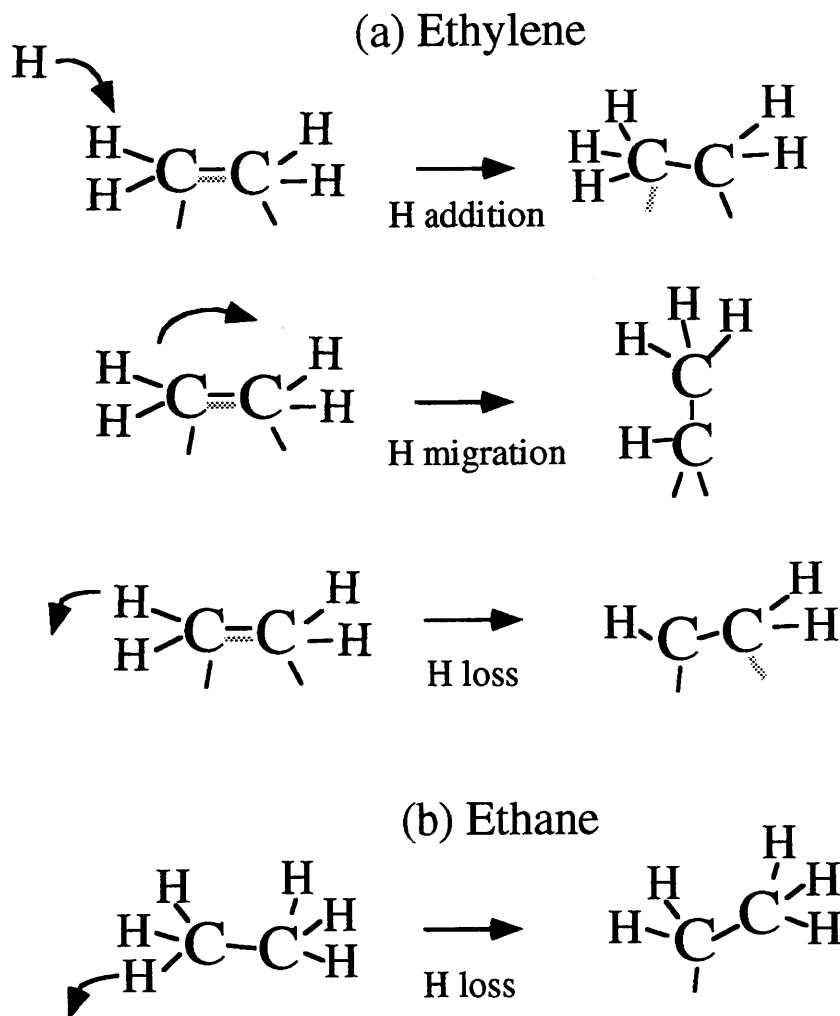
Figure 6 Schematic diagram showing the different possible initial reaction pathways from ethylene and ethane.

and then progressed to CCH_3, the CCH_3 product should be formed during heating of C_2H_4.

But no CCH_3 is observed to form when the surface temperature is raised with adsorbed C_2H_4.

Rather, C_2H_4 decomposes to C_2H_2.[21] One other observation to counter this H atom migration

reaction mechanism is the experiment in which a small coverage of CCD_3 is formed from C_2D_4

only in the presence of a low partial pressure of D_2, as described in Section 2 and in Figure 3.

If this mechanism involving thermal D atom migration to form CCD_3 were to take place, no additional D atoms would be required to form CCD_3. The second possible pathway is the H addition to C_2H_4 to make the CH_2CH_3 intermediate. The arguments against a CH_2CH_3 intermediate in CCH_3 formation apply not only to the initial step in which a H atom is added to C_2H_4, but also to the only initial pathway possible from the C_2H_6 reactant, H abstraction (shown in Figure 6b). The best evidence against CH_2CH_3 as an intermediate in CCH_3 formation is that CH_2CH_3 decomposes very efficiently to C_2H_4 on $Ni(111)$.[14] This is experimentally observed by the formation of C_2H_4 from C_2H_6 in a flux of 80 V electrons. The C-H bond of C_2H_6 presumably breaks to form CH_2CH_3, which then rapidly decomposes to the observed C_2H_4 product and adsorbed H at crystal temperatures of both 85 and 40 K. No CCH_3 is formed. In the reaction of C_2H_6 with gas phase H atoms to produce CCH_3, once C_2H_4 is formed, a second H is abstracted to form $CHCH_2$ and the rest of the path to CCH_3 progresses through the same intermediates as discussed for the C_2H_4 reactant.

From the above discussion of the initial step in CCH_3 formation from adsorbed C_2H_2, C_2H_4, and physisorbed C_2H_6, vinyl ($CHCH_2$) emerges as the only viable intermediate species after eliminating all other intermediates. The actual reaction mechanism to make $CHCH_2$ depends on the initial hydrocarbon and the H atom species, and is described for each hydrocarbon as follows. For reaction of surface bound H atoms with C_2H_2 to form CCH_3, as discussed in Chapter 3, the surface bound H atoms add to C_2H_2 at a surface temperature of 280 K to form $CHCH_2$, which then goes on to form CCH_3. In the reaction of bulk H with C_2H_2, the bulk H atoms add to adsorbed C_2H_2 as they emerge from the bulk beginning at 180

K to form $CHCH_2$ which goes on to form CCH_3. Gas phase H atoms are able to add and

abstract H atoms from all hydrocarbon species. Gas phase H atom addition to C_2H_2 forms

$CHCH_2$, gas phase H atoms abstract a H atom from C_2H_4 to forms $CHCH_2$, and gas phase H

atoms abstract a H atom from physisorbed C_2H_6 to form CH_2CH_3, which decomposes to C_2H_4,

and undergoes another abstraction of a H atom to form $CHCH_2$. From each of these gas phase

H reactions CCH_3 is observed as the final product at crystal temperatures from 60 K to 300 K.

Depending on the mechanism of $CHCH_2$ conversion to CCH_3, a second intermediate

could be involved. The three possible pathways to CCH_3 from the $CHCH_2$ intermediate are

shown in Figure 7. The reaction depicted in Figure 7a is H atom migration in $CHCH_2$ to

directly form CCH_3. Figure 7b depicts a H atom loss from $CHCH_2$ to make vinylidene (CCH_2)

followed by H addition to form CCH_3. Figure 7c depicts H atom addition to $CHCH_2$ to make

ethylidene ($HCCH_3$) followed by H loss to form CCH_3.

To begin with the possibility of a H atom migration reaction, there are experiments that

show that the rearrangement of $CHCH_2$ directly to CCH_3 does not occur. Electrons can be

used to break C-H bonds in C_2H_4 to form the stable C_2H_2 product, presumably through a

$CHCH_2$ intermediate. The stable C_2H_2 product of electron exposure is shown in the HREEL

spectrum in Figure 8a. It was made by exposure of 0.12 ML C_2H_4 to 40 V electrons for 5

minutes at a crystal temperature of 95 K. It is clear from the comparison of this spectrum with

the spectrum of C_2H_2, Figure 8b, that after the initial C-H bond is broken, the $CHCH_2$ species

does not undergo thermal H atom migration to form the product CCH_3. Instead, $CHCH_2$

looses a second H atom to form C_2H_2. Since rearrangement is a thermal process, is it possible

(a) Hydrogen migration

(b) Hydrogen loss

(c) Hydrogen addition
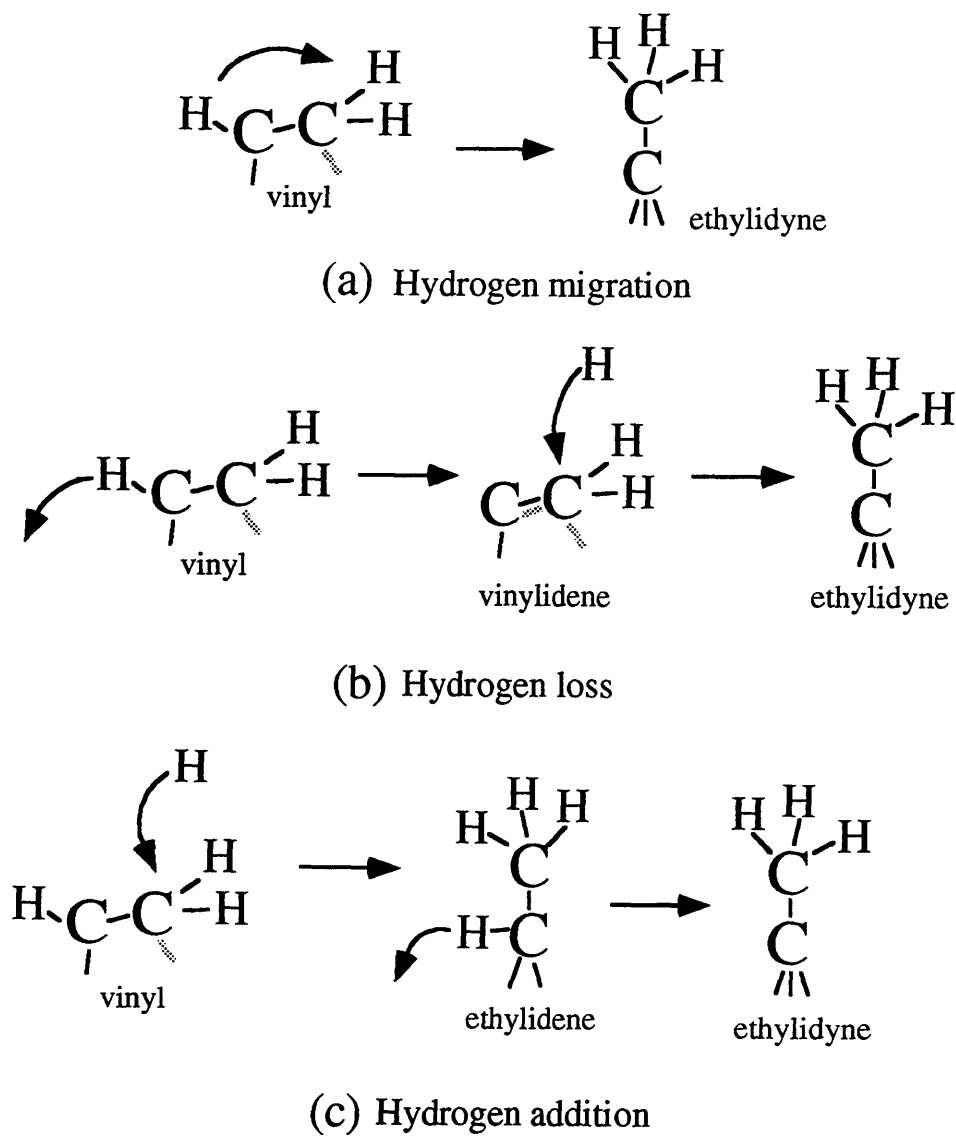
Figure 7 Schematic diagram of three possible mechanisms of ethylidyne formation from a vinyl intermediate.

that a higher crystal temperature is necessary? The answer is no, because C_2H_4 thermal decomposition to form C_2H_2 at 200-220 K, which must go through a $CHCH_2$ intermediate, shows no sign of CCH_3 formation.
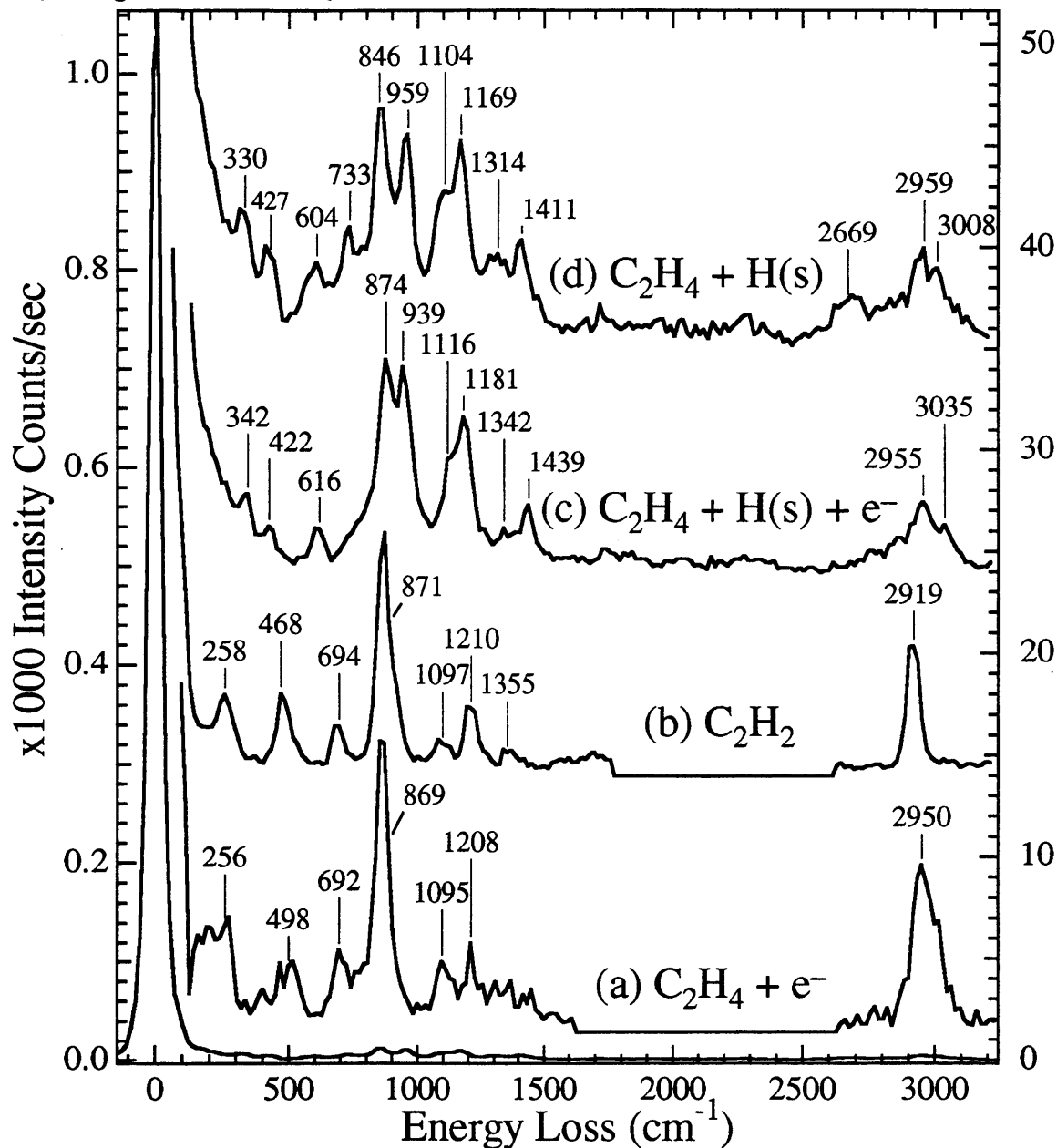
Figure 8 HREEL spectra showing (a) 0.12 ML C₂H₄ after an exposure to 40 V electron for 5 minutes at 95 K; spectrum taken at 80 K, at 10° off specular with a ΔE$_{fwhm}$ of 41 cm⁻¹, (b) 0.25 ML C₂H₂; spectrum taken at 80 K, at 8° off specular with a ΔE$_{fwhm}$ of 39 cm⁻¹, (c) 0.6 ML H with 0.19 ML C₂H₄ after exposure to 40 V electron for 5 minutes at 95 K; spectrum taken at 80 K, at 10° off specular with a ΔE$_{fwhm}$ of 48 cm⁻¹, (d) 0.12 ML C₂H₄ with saturation exposure to D₂ spectrum taken at 80 K; 10° off specular at a ΔE$_{fwhm}$ of 50 cm⁻¹. All spectra taken with 6.5 eV electrons.

An important issue in the electron induced chemistry is whether it is possible to

produce $CHCH_2$ in the presence of surface H to form CCH_3. This is not directly related to the

current argument on H atom migration, but the results of this experiment will be used shortly.

Additional electron induced chemistry experiments to produce CCH_3 have been attempted for

an initial surface of 0.6 ML H with a 0.19 ML exposure of C_2H_4. Figure 8c shows the HREEL

spectrum measured after exposure of this coadsorbed C_2H_4 + H(s) layer to 40 V electrons for

5 minutes at a crystal temperature of 95 K. From the agreement between this spectrum and the

one displayed in Figure 8d of a coadsorbed layer of 0.12 ML C_2H_4 and surface bound H, it is

apparent that no reaction has occurred after the electron exposure. Electrons clearly are able

to break C-H bonds, as seen from the formation of C_2H_2 after C_2H_4 is exposed to electrons. In

this experiment the saturation of the surface sites with H atoms seem to block the further

decomposition of $CHCH_2$ to C_2H_2, or the crystal temperature of 95 K limits further reactions.

Another possible mechanism to form CCH_3 from $CHCH_2$ is to loose a H atom and form

CCH_2, as shown in Figure 7b. This process could be thermally activated. However,

experimental evidence of C_2H_4 decomposition in which a $CHCH_2$ intermediate is expected to

occur shows no evidence of the CCH_3 product, which should be present if the thermal reaction

of $CHCH_2 \rightarrow CCH_2 \rightarrow CCH_3$ is a dominant mechanism. Even when C_2H_4 decomposition is

done slowly, as described and shown in Section 2 and Figure 3, no CCH_3 is observed. A

second possible mechanism to remove a H atom from $CHCH_2$ is by abstraction by another H

atom. While surface bound H and bulk H atoms do not have enough energy to abstract a H

atom from a hydrocarbon, gas phase H atoms do. There is no experimental evidence that can

rule out this channel in gas phase H atom reactions. However, since CCH_2 cannot be formed

by surface bound H atoms or bulk H it is not a possible common intermediate.

The only pathway to make CCH_3 from $CHCH_2$ that is consistent with all three H atom

species is the pathway through $CHCH_3$ depicted in Figure 7c. The first step in this mechanism

is the addition of a H atom to $CHCH_2$ to form $CHCH_3$. This H atom could be a surface bound

H atom, a bulk H atom, or a gas phase H atom. Each H atom species reacts with $CHCH_2$

under specific conditions. Surface bound D atoms reacts with $CDCD_2$ during the

decomposition of C_2D_4 at 220 K in the presence of D_2 background to form CCD_3. Surface

bound D atoms must be able to add to $CDCD_2$ to form $CDCD_3$ at 220 K. During the reaction

of bulk H atoms with C_2H_2, the CCH_3 product is formed at a temperature of 185 K as the H

atoms emerge from the bulk. In this reaction, both bulk H atoms and surface bound H atoms

are present. The first step to form $CHCH_2$ requires a bulk H atom. But the second H addition

to $CHCH_2$ to form $CHCH_3$ could be from either a bulk H atom or a surface H atom. Reactions

with gas phase H atoms and all three hydrocarbons occur at a surface temperature of 120 K.

Again, when gas phase H atoms are present so are surface bound H atoms. The gas phase H

atoms are necessary to form $CHCH_2$, but the second H addition to form $CHCH_3$ could occur

from either a gas phase H atom or a surface H atom. There is one experiment that suggest that

surface H atoms cannot add to $CHCH_2$ to form $CHCH_3$ at 95 K. Ethylidyne is not made from

coadsorbed C_2H_4 and H during exposure to 40 V electrons at 95 K, as shown in Figure 8c.

Vinyl is expected to be made under these conditions, and with ample surface H, CCH_3

formation would also be expected. It is possible that the surface H atoms at 95 K do not have

sufficient energy to add to $CHCH_2$.

The second part of the mechanism in Figure 7c is the loss of a H atom from $CHCH_3$ to

form CCH_3. This loss is expected to occur thermally for surface bound H and bulk H

reactions. The lowest temperature at which CCD_3 is formed is 220 K, from $CDCD_2$ (upon

C_2D_4 decomposition) in the presence of D_2. The loss of H from $CHCH_3$ to form CCH_3 in gas

phase H reactions could occur thermally, or from H abstraction by a gas phase H atom. Gas

phase H atom reactions to make CCH_3 occur over the temperature range of 60 K to 300 K

without noticeable changes in the rate of product formation. This suggests that either $CHCH_3$

thermally decomposes to CCH_3 in this entire temperature range, or abstraction of a H from gas

phase H atoms is independent of the crystal temperature. Evidence of the thermal stability of

other intermediates suggests that $CHCH_3$ could easily decompose to CCH_3 in this temperature

range. For example, neither ethyl, CH_2CH_3, or vinyl, $CHCH_2$, intermediate can be isolated at

surface temperatures between 20 and 40 K. Ethylidene, $CHCH_3$, could be similarly unstable

and decompose so quickly that the gas phase H atom abstraction channel does not participate

in the gas phase H atom reactions.

## 5 Literature on Ethylidyne Formation

Ethylidyne formation has been extensively studied on Pt surfaces. The studies of the

CCH_3 formation mechanism on Pt parallel the work presented here. However, there are

substantial differences between hydrocarbon reactions on Pt and Ni surfaces. It is critical to

acknowledge these differences before launching into mechanistic arguments presented for Pt

surfaces. The largest differences between the two surfaces is that CCH_3 decomposition occurs at lower temperatures on Ni. When CCH_3 is formed on Ni, it is stable only to 350 K, the same temperature that H desorbs, suggesting the necessity of coadsorbed H for its stability (see Chapter 3). Ethylidyne on Ni has rarely been observed.[18,2] On Pt, C_2H_4 decomposes to CCH_3 at 300 K, surface H recombines and desorbs at 350 K, and CCH_3 further decomposes to CCH and CH at 450 K.[19] On Ni, C_2H_4 decomposes to C_2H_2 at 220-260 K, which further decomposes to CCH at 400 K.[20,21] The barriers for hydrocarbon formation and decomposition are certainly different on these two metals. Certainly, intermediates on Pt maybe the same as those on Ni, but they need not be.

5.1 *Possible Intermediates*

In the following survey of mechanistic studies on Pt there is a consensus that formation of the first intermediate is the rate limiting step in CCH_3 formation and the coverage of the intermediate always remains low. In one study, direct observation of an intermediate is made during the reaction, which will be discussed. All other studies base mechanistic arguments on secondary observations or observation of intermediates on modified surfaces. Four different species which could form CCH_3 have been investigated as intermediates: vinylidene, CCH_2; ethyl, CH_2CH_3; vinyl, $CHCH_2$; and ethylidene, $CHCH_3$. With H addition, H abstraction, or H migration all four potential intermediates can be transformed to CCH_3 as shown in Figure 9.
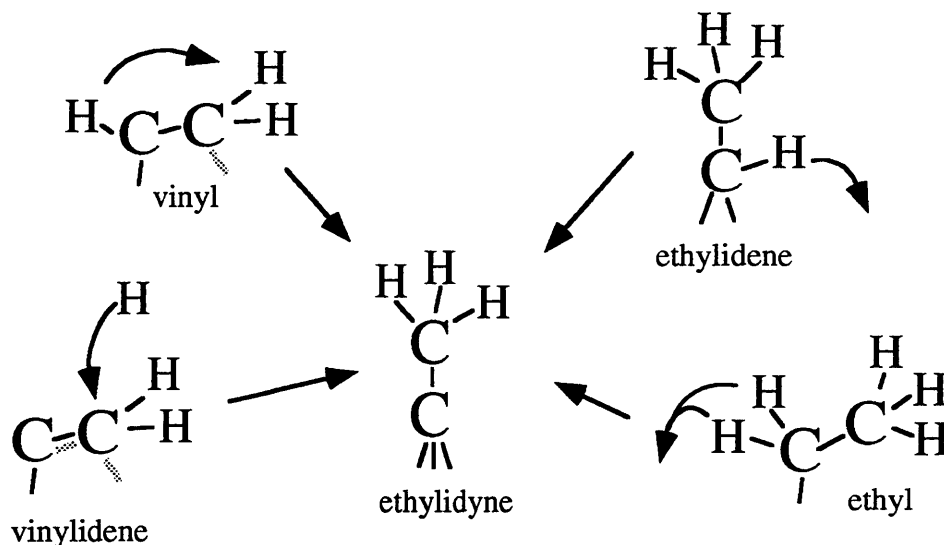
Figure 9 Schematic diagram showing the four different intermediates to ethylidyne formation and potential mechanisms for this reaction on Pt.

5.2 *Vinylidene*

On Pt surfaces, C_2H_2 is observed to form CCH_3 between 330 and 400 K. The reaction produces two species, CCH_3 and $CCH.^{22}$ When C_2H_2 and H are coadsorbed on the surface, only CCH_3 is formed at 350 K.[23] A mechanism in which the first step to CCH_3 formation is a H migration in C_2H_2 to CCH_2 with a subsequent H addition has been proposed.[23] However, separate experimental evidence discounts vinylidene as an intermediate to CCH_3.[22] HREEL spectra of C_2H_2 at different temperatures fail to show any evidence for CCH_2. The spectra of C_2H_2 on Pt at different surface temperatures are consistently assigned to a mixture of C_2H_2 and CCH_3.[22]

5.3 *Ethyl*

Ethyl as an intermediate to CCH_3 formation has been explored by several groups using ethyl halides as a source of adsorbed ethyl radicals. The concept is that the weak carbon-

halogen bond breaks thermally by warming the crystal or by photodissociation to form an

adsorbed ethyl and an adsorbed halogen atom. The drawback is that the chemistry observed is

on a surface with Br, I or Cl coadsorbates. It is not clear what the effect of these coadsorbates

are on the resulting chemistry, but they will certainly change the population of electrons at the

surface.[24] Decomposition of ethyl chloride by photodissociation has been observed using

HREEL spectroscopy by Lloyd and coworkers.[25] Molecularly adsorbed ethyl is observed at

100 K and is observed to decompose to C_2H_4 at 230 K. An absorption IR spectroscopy study

of the thermal activation of ethyl iodide by Hoffmann and coworkers also confirms that C_2H_4 is

formed at 240 K.[26] At a crystal temperature of 300 K, the temperature at which CCH_3

synthesis is observed, all of the CH_2CH_3 has decomposed to C_2H_4. This makes it very unlikely

that CH_2CH_3 is responsible for CCH_3 formation on Pt.

5.4 *Vinyl*

The real controversy in the discussion of CCH_3 intermediates on Pt is between vinyl,

$CHCH_2$, and ethylidene, $CHCH_3$. There are multiple arguments for a vinyl intermediate. Zaera

studied the C_2H_4 conversion to CCH_3 by TDS.[27] From observation of H recombination and

desorption, he concluded that C-H bond breaking is the first step to CCH_3 formation. A

temperature shift between the onset of desorption of H_2 and D_2 from C_2H_4 and C_2D_4 surfaces

further suggests that the rate limiting step in CCH_3 formation is breaking the initial C-H(D)

bond to form $CHCH_2$ and not a H(D) migration to form $CHCH_3$. If H migration to form

$CHCH_3$ is the rate limiting step, then the subsequent H(D) desorption steps would be fast, and

not exhibit an isotope shift. Similar conclusions were drawn by Zhou and coworkers in a study

of vinyl iodide using pre-adsorbed oxygen to titrate and measure the amount of surface H.[28]

From observations of H_2O desorption and previous static secondary ion mass spectroscopy

identification of CCH_3 products, they claim to measure a barrier to CCH_3 formation of 2.4

kcal/mol, but make no mention of the coadsorbate effects in this reaction due to I and O

atoms. Thankfully, there are two spectroscopic studies of vinyl iodide which provide more

direct evidence of a vinyl intermediate in CCH_3 formation, although caution from the unknown

effect of coadsorbed iodine in these studies is still warranted. Liu and coworkers observe

$CHCH_2$ species in EEL spectra at temperatures as low as 100 K, and CCH_3 at temperatures as

low as 120 K at certain coverages.[29] A more recent study using IR spectroscopy to probe the

reaction of vinyl iodide reaches different conclusions.[30] Upon heating $ICHCH_2$ to 150 K, a

mixture of CCH_2 and C_2H_2 is observed. The vinyl product from C-I bond cleavage is not

observed. However, the C_2H_2 frequencies are significantly shifted from those of C_2H_2 on clean

Pt. As the crystal is heated above 200 K, no IR features are evident. The absence of IR

features is attributed to the presence of C_2H_4, which has typically been difficult to observe by

IR spectroscopy. At 300 K, two features assigned to CCH_3 are observed. This study has been

used to discount vinyl as an intermediate, but the results are questionable. Vinyl is never

directly observed and neither is C_2H_4. The assignment of C_2H_2 is unsatisfactory, and the

explanation that acetylene is converted to ethylene with increasing surface temperature is not

supported by any prior evidence on clean Pt surfaces.[22]

Two kinetic studies support the presence of a vinyl intermediate in CCH_3 formation.

Erley and coworkers measure coverage dependent rates for C_2H_4 decomposition and CCH_3

formation.[31] In the logarithmic plots of the coverage of C_2H_4 versus time, measured by laser

induced thermal desorption, the slope of the data changes dramatically a some critical time,

yielding two regions that are fit separately to straight lines with different slopes. The result is a

faster decomposition rate of C_2H_4 at longer reaction times. The critical time changes for

different initial C_2H_4 coverages. For a saturated C_2H_4 surface, it occurs half of the way

through the reaction. For 27% saturation coverage, it occurs 20% into the reaction, and for

17% saturation, the decomposition rate never experiences a critical time and only exhibits the

faster rate. The logarithmic plot of the CCH_3 coverage does not exhibit a change in slope, with

the rates of CCH_3 formation matching the slower rates of C_2H_4 decomposition. The

explanation for this behavior is that ensemble effects change the rate of decomposition at

higher coverages because the transition state requires several surface sites. A convincing

Monte Carlo simulation is presented to model these ensemble effects. They argue that

ensemble effects are fully consistent with a vinyl intermediate, where sites are needed to adsorb

the H atoms after breaking the C-H bond. A second kinetic study of C_2H_4 conversion to CCH_3

on Rh(111) also argues for a vinyl intermediate.[32] Drastic changes in reaction rates are

observed with initial C_2H_4 coverage. As the coverage of surface H increases, it becomes more

difficult to find the necessary site to deposit a H atom from the dissociation of C_2H_4 to vinyl.

Again, these changes are consistent with C-H bond breaking as the rate limiting first step to

form $CHCH_2$ as compared to H atom migration to form $CHCH_3$ as the rate limiting first step.

5.5 *Ethylidene*

There are several studies that support ethylidene, $CHCH_3$, as the intermediate in CCH_3

formation. Ethylidene can be formed directly from the isomerization of C_2H_4 by migration of

a H atom. It is also possible that $CHCH_3$ is the second intermediate in CCH_3 formation. The

reaction could first form vinyl, and then add a H atom to produce $CHCH_3$ before the final

CCH_3 product is formed. The distinction between these two paths would be that the rate

limiting step for CCH_3 will be due to the formation of the first intermediate. In a study of H/D

exchange between C_2H_4 and D, Janssens and coworkers assert that $CHCH_3$ is the intermediate

for CCH_3 synthesis.[33] They rule out $CHCH_2$ because the rate constant for CCH_3 formation is

independent of coadsorbed surface H. The H migration reaction to form $CHCH_3$ does not

produce or consume a surface H atom. A dependence of the reaction on surface H coverage

would occur if H atoms were produced in the reaction. This argument does not address the

previous kinetics experiments described in the last paragraph that see changes in the rate of

CCH_3 formation with initial hydrocarbon coverage and during the course of the reaction,

where adsorbed H coverages must change.

There are three spectroscopic studies to support the $CHCH_3$ intermediate. In one, IR

spectroscopy is used to monitor CH_3CHI_2 decomposition with increasing surface temperature.

Ethylidyne is observed at 150 K as CH_3CHI_2 decomposes.[34] There is no identification of the

transient CH_3CH intermediate. The authors claim CCH_3 is formed via a direct α–H

elimination step, because D coadsorbed with CH_3CHI_2 does not result in deuterated ethylidyne

species. Along with other alkyl halide experiments, it is not clear what effect the adsorbed I

has in this reaction. While this study is significant, it is not fully convincing. Windham and

Koel spectroscopically identify CHCH₃ in the decomposition of C_2H_4 on Pt with 0.12 ML

coadsorbed potassium.[35] In the presence of K, the amount of C_2H_4 that decomposes decreases

and the activation energy for C-H bond cleavage increases. They argue that the presence of K

atoms blocks sites for decomposition and increases the activation energy for C-H bond

cleavage, thereby allowing observation of the metastable intermediate in CCH₃ formation,

CHCH₃.

Another study uses infrared-visible sum frequency generation to directly observe an

intermediate during the conversion of C_2H_4 to CCH₃ at a surface temperature of 255 K.[8] This

technique only monitors the C-H stretch region. A new feature is observed in the C-H stretch

region at 2957 cm⁻¹. This feature is close to the antisymmetric C-H stretch frequency of 2955

cm⁻¹ observed for CHCH₃ on Pt with coadsorbed K. Vinyl is eliminated as the origin of this

feature by comparison with frequencies of an inorganic Os complex and of adsorbed ICHCH₂.

A further experiment to eliminate vinyl as the source of this feature is by adsorbing ICHCH₂ at

130 K. At this temperature some of the ICHCH₂ is dissociated. The spectrum measures three

features at 2995 cm⁻¹, 3033 cm⁻¹, and 3068 cm⁻¹ which are assigned to intact vinyl iodide, vinyl

or vinylidene. All three frequencies are well above the value of the frequency for this new

intermediate feature at 2957 cm⁻¹. As the temperature of this surface is raised to 285 and 295

K, a new 2950 cm⁻¹ feature dominates the spectra. By 406 K the prominent spectral feature is

at 2878 cm⁻¹ and is assigned to the C-H symmetry stretch of CCH₃. Cremer and coworkers

suggest that while vinyl is not directly responsible for the 2957 cm⁻¹ feature, the decomposition

of vinyl goes through the same intermediate to form CCH_3 as is present during the synthesis of

CCH_3 from C_2H_4. This observation of a $CHCH_3$ intermediate in the reaction of $CHCH_2 \rightarrow$

$CHCH_3 \rightarrow CCH_3$ is fully compatible with our mechanism for CCH_3 formation on the Ni

surface. However, the assignment of $CHCH_3$ from a single C-H stretch is questionable. A

recent study of vinyl formation on Pt^{36} observes lower C-H stretch frequencies than those

observed for the Os cluster. These new frequency values are closer to the 2957 cm^{-1} observed

feature.

5.6 *Theoretical Studies*

Theorists have the advantage of being able to study enthalpies and activation energies

that are extremely difficult to experimentally observe. Several studies of this network of

carbon species have been done and predict the relative energy of reactants, intermediates,

products, and even reaction barriers in some cases. Kang and Anderson[37] make predictions for

the synthesis of CCH_3 from both C_2H_2 and C_2H_4. They predict a CCH_2 intermediate for both

C_2H_2 and C_2H_4 reactions, with C_2H_4 progressing through $CHCH_2 \rightarrow CCH_2 \rightarrow CCH_3$. They

examine the energetics of the $C_2H_4 \rightarrow CHCH_2 \rightarrow CHCH_3 \rightarrow CCH_3$ reaction mechanism, and

find a barrier that is 30% higher than for the CCH_2 path. One general result from the study is

that H migration has a significantly higher barrier than H addition and loss. Carter and Koel

favor the mechanism, $C_2H_4 \rightarrow CHCH_3 \rightarrow CCH_3$, with a H migration as the first step.[38]

Nevertheless, they do not eliminate the possibility of $CHCH_2$ as the first intermediate to CCH_3

formation. The study by Ditleven and coworkers proposes the mechanism $C_2H_4 \rightarrow CHCH_2 \rightarrow$

$CCH_2 \rightarrow CCH_3$.[39] They do not address the pathway of $C_2H_4 \rightarrow CHCH_2 \rightarrow CHCH_3 \rightarrow CCH_3$. This study predicts that H migration barriers will be twice as high as H addition or H loss barriers.

These studies of CCH_3 formation on Pt are consistent with the ideas presented here for the mechanism of CCH_3 synthesis on Ni. There is evidence to support both vinyl and ethylidene intermediates on Pt. Even though all of the above Pt studies do not advocate a mechanism that includes both intermediates, as presented for the mechanism on the Ni surface, $CHCH_2 \rightarrow CHCH_3 \rightarrow CCH_3$, all experimental evidence of vinyl as the first step in the reaction and ethylidene as an intermediate do agree with the Ni mechanism. The theory results include vinyl intermediates and favor H addition and H loss steps over H atom migration, similar to the mechanistic arguments in Section 4.

6 Conclusions

Identification of the intermediate in CCH_3 formation not only characterizes the behavior of the intermediate, but also allows our activation energy measurement to be associated with an elementary chemical reaction step, the C-H bond formation in the reaction of $C_2H_2 \rightarrow CHCH_2$. In Section 4 the argument that the synthesis of CCH_3 on nickel involves both vinyl and ethylidene intermediates is presented, the reaction is:

$$C_2H_2/C_2H_4 \rightarrow CHCH_2 \rightarrow CHCH_3 \rightarrow CCH_3$$
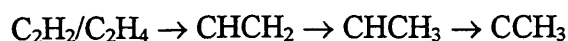
This mechanism is consistent with our two preliminary experimental observations that support a vinyl intermediate on Ni(111), with energetic arguments, with all experimental work on Ni(111) to date, and with studies of this reaction on the Pt(111) surface.

[1] H. Ibach and S. Lehwald, J. Vac. Sci. Technol. 18, 625 (1981)

[2] T. Bürgi, T.R. Trautman, K.L. Haug, A.L. Utz and S.T. Ceyer, J. Phys. Chem. B 102,4952 (1998)

[3] J.A. Stroscio, S.R. Bare and W. Ho, Surf. Sci 148, 499 (1984)

[4] F. Zaera and N. Bernstein, J. Am. Chem. Soc. 116, 4881 (1994)

[5] J. Evans and G.S. McNulty, J. Chem. Soc. Dalton Trans. 639 (1983)

[6] C.E. Anson, N. Sheppard, D.B. Powell, J.R. Norton, W. Fischer, R.L. Keiter, B.F.G. Johnson, J. Lewis, A.K. Bhattacharrya, S.A.R. Knox and M.L. Turner, J. Am. Chem. Soc. 116, 3058 (1994)

[7] G.S. Hsiao, W. Erley and H. Ibach, Surf. Sci. 396, 422 (1998)

[8] P. Cremer, C. Stanners, J.W. Niemantsverdriet, Y.R. Shen and G. Somorjai, Surf. Sci. 328, 111 (1995)

[9] S.P. Daley, Ph.D. Thesis, Massachusetts Institute of Technology (1994)

[10] H. Ibach and D. Druchmann, Phys. Rev. Lett. 44, 36 (1980)

[11] Handbook of Chemistry and Physics, R. West, editor, Chemical Rubber Co. (1977)

[12] J.E. Demuth and H. Ibach, Surf. Sci. 85, 365 (1979)

[13] A.T. Bell and E. Shustorovich, Surf. Sci. 235, 343 (1990)

[14] T.R. Trautman, Ph.D. Thesis, Massachusetts Institute of Technology (1996)

[15] B. D. Thoms, J.N. Russell, P.E. Pehrsson, and J.E. Butler, J. Chem. Phys. 100, 8425 (1994)

[16] A. Horn, J. Biener, A. Schenk, C. Lutterloh, and J. Küppers, Surf. Sci. 331-333, 178 (1995)

[17] C. Lutterloh, A. Horn, A. Schenk, J. Biener, B. Winter, and J. Küppers, Surf. Sci. 316, L1039 (1994)

[18] M.P. Lapinski and J.G. Eckardt, J. Phys. Chem. 94, 4599 (1990)

[19] N.R. Avery and N. Sheppard, Proc. R. Soc. London, Series A 405, 1 (1986)

[20] S. Lehwald and H. Ibach, Surf. Sci. 89, 425 (1979),

[21] L. Hammer, T. Hertlein and K Müller, Surf. Sci. 178, 693 (1986)

[22] N.R. Avery, Langmuir 4, 445 (1988)

[23] H. Ibach and S. Lehwald, J. Vac. Sci. Technol. 15, 407 (1978)

[24] J.K. Nørskov in The Chemical Physics or Solid Surfaces- Volume 6, D.A. King and D.P. Woodruff, eds, Elsevier (1993)

[25] K.G. Lloyd, B. Roop, A. Campion, and J.M. White, Surf. Sci. 214, 227 (1989)

[26] H. Hoffmann, P.R. Griffiths, and F. Zaera, Surf. Sci. 262, 141 (1992)

[27] F. Zaera, J. Am. Chem. Soc. 111, 4240 (1989)

[28] X-L Zhou, Z-M Liu and J.M. White, Chem. Phys. Letters 195, 618 (1992)

[29] Z-M Liu, X-L Zhou, D.A. Buchanan, J. Kiss and J.M. White, J. Am. Chem. Soc. 114, 2031 (1992)

[30] F. Zaera and N. Berstein, J. Am. Chem. Soc. 116, 4881 (1994)

[31] W. Erley, Y. Li, D.P. Land and J.C. Hemminger, Surf. Sci. 301, 177 (1994)

[32] D.C. Papageorgopoulos, G. Ge and D.A. King, Surf. Sci. 397, 13 (1998)

[33] T.V.W. Janssens, D. Stone, J.C. Hemminger, and F. Zaera, J. Catal. 177, 284 (1998)

[34] T.V.W. Janssens, and F. Zaera, J. Phys. Chem. 100, 14118 (1996)

[35] R.G. Windham and B.E. Koel, J. Phys. Chem. 94, 1489 (1990)

[36] G.S. Hsiao, W. Erley and H. Ibach, Surf. Sci. 396, 422 (1998)

[37] D.B. Kang and A.B. Anderson, Surf. Sci. 155, 629 (1985)

[38] E.A. Carter and B.E. Koel, Surf. Sci. 226, 339 (1990)

[39] P.D. Ditlevsen, M.A. Van Hove, and G.A. Somorjai, Surf. Sci. 292, 267 (1993)

Appendix-Data List

Chapter 2

Figure 4 & Figure 5 Oct2996.a02

Figure 6 carbon to nickel versus C_2H_2 Oct2896.a01

Figure 8 H(s) TDS Nov2095.002

Figure 9 H & D EELS H Apr2697.e02 and D Apr2897.e03

Figure 10 H(s) + H(b) TDS Apr1995.002

Figure 11 H(s) + H(b) HREEL Sep0993.e11

Figure 12 H addition and abstraction 0.8 ML D, room temp Nov 6, 1996

Figure 13 H addition and abstraction 0.5 ML and 0.8 ML D, LN_2 Nov 5 and Nov 4 1996

Chapter 3

Figure 1 C_2H_4 and H(s) TDS Feb2894.018

Figure 2 C_2H_4 and H(b) TDS Jan3094.008

Figure 5 C_2H_2 and H(s) TDS Mar2595.013

Figure 6 HREEL C_2D_2 and D heated Apr0497.e05 and Apr0597.e03-.e09

Figure 7 HREEL C_2D_2 and D and annealed at 280 K May1397.e11

Figure 8 HREEL C_2D_2 and repeated D_2 annealing May2297.e02-.e06

Figure 9 May2297.e06 and Feb2895.e06 standard

Figure 10 CCD_3/C_2D_2 ratio from HREELS intensities June 4- June 15, 1998

Figure 11 HREEL CCD_3 (Feb2895.e06) and CCH_3(Nov2295.e04 and Mar0795.e07)

Figure 12 HREEL of CCD_3 decomposition Feb2895.e03.e09.e11 and Mar0295.e08.e11 and standard Apr1097.e02

Figure 13 HREEL of reverse equilibrium of CCD_3 to C_2D_2 Jun1598.e02.e03.e04

Figure 14 D versus acetylene coverages Jun1998.001-.015

Figure 15 Intensity of 640 cm^{-1} acetylene feature versus C_2D_2 exposure Sep1597.e01-.e18

Figure 16 Auger carbon versus time of C_2D_2 exposure Sep1797.a01.a02

Figure 17 HREELS intensities of C_2D_2, CCD_3, and their sum May2297.e02-.e06

Figure 18 Auger carbon signal for C_2H_2 with and without repeated H_2 exposures and anneals Mar2698.a02

Figure 19 & Figure 20 [CCD$_3$]/[C$_2$D$_2$] versus coverage of [D] and [D]^2 at equilibrium. From June 18-19-24-26-30 and July 15 1998

Figure 21 [CCD$_3$]/[C$_2$D$_2$] versus coverage of [D] at equilibrium All data from previous points as well as July 17 1998 0.12 ML, June 19-25-27 1998 0.19 ML, June 4-5-6-12-15 1998 0.17 ML

Figure 24 [CCD$_3$]/[C$_2$D$_2$][D] versus total surface coverage at equilibrium. From all data in Fig 19-20-21.

Figure 25 HREEL spectra of 0.06 ML C$_2$D$_2$ and 0.86 ML D at three temperatures Jun1097.e02-e10 and Jun1197.e02-.e11

Figure 26 HREEL spectra of 0.12 ML C$_2$D$_2$ and 0.70 ML D at three temperatures Jun1798.e01-e11 and Jun1898.e01-.e05

Figure 27 HREEL spectra of 0.17 ML C$_2$D$_2$ and 0.57 ML D at three temperatures Jun0297.e07-.e10 and Jun0397.e02-.e11

Figure 28 Rates and activation energy determination for 0.06 ML C$_2$D$_2$ and 0.86 ML D. data from Figure 25

Figure 29 Rates and activation energy determination for 0.09 ML C$_2$D$_2$ and 0.78 ML D. Jul0198.e01-.e12 and Jul0298.e01-.e05 and Jul0398.e01-.e12

Figure 30 Rates and activation energy determination for 0.105 ML C$_2$D$_2$ and 0.74 ML D. Jul0798.e01-.e06 and Jul0898.e01-.e10

Figure 31 Rates and activation energy determination for 0.12 ML C$_2$D$_2$ and 0.70 ML D. data from Figure 26

Figure 32 Rates and activation energy determination for 0.17 ML C$_2$D$_2$ and 0.57 ML D. data from Figure 27

Figure 33 Rates and activation energy determination for 0.06 ML C$_2$D$_2$, 0.57 ML D, and 0.29 ML empty sites. Jul2098.e06-.e12 and Jul2198.e01-.e12 and Jul2498.e01-.e06

Figure 34 Trends in measured E$_a$ values from data in Figure 28-33.

Chapter 4

Figure 1 HREEL spectra of bulk H and C$_2$H$_2$. (a)Feb2197.e02 (b)Feb2797.e03

Figure 2 bulk H and C$_2$H$_2$ TDS Apr2095.003

Figure 3 bulk H and C$_2$H$_2$ TDS w/SBH Mar2595.004

Figure 4 corrected TDS 1.8 ML and 3.1 ML bulk H with C$_2$H$_2$, Apr2095.003 and Apr2095.008

Figure 5 corrected TDS 1.8 ML bulk H and C$_2$H$_2$, and 1.7 ML bulk H and C$_2$H$_4$, Apr2095.003 and Apr1392.004